Department of Mechanical Engineering

Self-Synchronisation of Vibrating Screen Unbalanced Mechanisms as Function of Location, Unbalanced Moment and Operating Frequency

Ziggy Gregory

This thesis is presented for the Degree of Doctor of Philosophy of Curtin University

March 2018

Declaration

To the best of my knowledge and belief this thesis contains no material previously published by any other person except where due acknowledgment has been made.

This thesis contains no material which has been accepted for the award of any other degree or diploma in any university.

Signature :.....

Date: 3 March 2018

Abstract

Most of the vibrating feeder equipment operate with two vibrators where the synchronisation is obtained either by electronically controlling phases of driving electric motors or using kinematic couplings like gears, v-belts or toothed belts. In many cases kinematic couplings can be replaced with self-synchronisation phenomenon which is simpler, cheaper, more reliable and also allows for better design of lubrication systems improving the life of the bearings and allowing for higher loads.

The main objective of the research was to confirm if two vibrators on the same testing rig will self–synchronise when operating in the same and opposite directions. Tests were also done for two vibrators running with different frequencies in the same and opposite directions with ratio of frequencies being a common fraction.

Multiple vibrators are often used because of the size of vibrating equipment with weight exceeding 50t and the required operating speed puts a limit on the size of the bearings that can be used. Big bearings with a low speed limit are unsuitable for applications from a proven design point of view and for that reason several vibrators have to be used to achieve the required vibrating force and frequency.

Several laboratory scale testings have been done with selected cases presented in this thesis. The vibrators self-synchronised in all cases even when working close to the natural frequency of the testing rig. In the case of vibrators working in the same and in opposite directions both of them kept working even when power was cut off to one of them. For dual frequency tests, if the power was cut off to the vibrator with higher speed then it would slow down and then synchronise with the powered one when it reached the same speed. With power cut off to the slower moving vibrator – it would stop.

Additional testing was done on two gearless exciters sitting on two independent, larger scale, (more than 1000 kg), testing rigs, with both exciters driven by two electric motors positioned outside the rigs. Both exciters self-synchronized even though the counterweights on both rigs were arranged to operate with phase differences of 180 degrees, which resulted in vibrations canceling and reduced the static moment required to start the vibrator counterweights.

It was planned to demonstrate conditions having two vibrators running in the same direction, operating at 0 degrees phase difference, which would create circular motion of the testing rig body. The theoretical calculations showed that this configuration should be possible, however physical testing proved to be impractical.

The novelty of the research is that it presents the most comprehensive testing of the self-synchronisation of two vibrators for the application in the vibrating screen industry.

Acknowledgement

I would like to express my gratitude to my supervisor Prof. Ian Howard for his excellent support, patience, and continuous encouragement throughout my doctoral study.

I would also like to say thank you to Berli Kamiel for his Matlab support.

Table of Contents

List of Figures

List of Tables

Chapter 1
General Introduction

1.1 Introduction

Vibration is applied in various processes including material selection processes using vibrating screens. In many cases the vibrating screens are driven by several vibrators because of the size of the screen or stroke shape requirements (elliptical shape, etc.) and then there is a need to synchronise the revolutions and phase. In most cases that is done using kinematic transmissions (gears, toothed belts, etc.) which results in high wear and additional noise. It also requires extra energy and decreases the reliability of the system.

Kinematic couplings can in many cases be replaced with self-synchronisation phenomenon which is simpler, cheaper and more reliable. Gearing options often leads to vibrating screen failure when not re-coupled correctly after maintenance – gears are used in the case of three shaft vibrator arrangements. Gears are also a source of extra noise, heat generations and metal particles contaminating the lubricating oil and significantly reducing the life of the bearings.

Multiple vibrators are often used because of the size of vibrating equipment with weight exceeding 50 t, which puts a limit on the size of the bearings that can be used. Big bearings with a low speed limit become at one stage unsuitable for the application and for that reason several vibrators have to be used to achieve the required vibrating force and frequency. Multiple vibrators are therefore used for all types of vibrating screens.

Using self-synchronisation of mechanisms running at different frequencies would allow the creation of various stroke shapes that would increase screening efficiency without increasing the acceleration of the screen structure. It would also allow for the simplification of the unbalanced mechanism arrangement on vibrating equipment.

Sychronisation effect will happen when several vibrating or oscillating bodies will start moving with the same or multiple frequencies and phase correlations can be established. With changing conditions the synchronization may also change i.e. the phase may change from 180 degrees to 0 degrees.

The first description of synchronisation was reported by Christian Hyugens in the second half of the 17th century. He observed two clocks positioned on light beams whose pendulums always synchronised after being disturbed and the pendulums moved in the opposite direction, (Huygens, 1673). The experiment was conducted with two clocks at the 'Mekhanobr' Institute in Leningrad which proved that the pendulums of the clocks will synchronise not only in opposite phases, but also in the same phases.

Self-synchronisation of vibrators was discovered (or rather rediscovered) in 1947 in 'Mekhanobr' Institute in Leningrad when during experiments with two vibrators, operating on the same isolated supporting structure, both vibrators kept working even though a cable connecting one of the electric motors was damaged. This 'power transfer' fact has been confirmed experimentally and it adds extra redundancy to the system i.e. even with electric motor failure, the vibrating screen will continue working with required power being transferred through the structure from the powered vibrator(s). Experiments confirmed powers in excess of 1000 kW being transmitted between vibrators, (Blekhman 1988).

The self-synchronisation effect is now used in several types of industrial equipment such as; vibrating screens, feeders, mills, breakers, etc.

Combining of data from the existing research and filling in the knowledge gaps would create a consistent study that could lead to further developments of new types of screens which would be cheaper, more reliable and more efficient. As mentioned before, additional study on the process efficiency improvement would significantly improve the value of the proposed research especially in the field of dual frequency screens. There is a significant amount of research in the field of synchronisation of vibrating motors with most of the work done by I. I. Blekhman. It is however mostly theoretical work including up to 4 vibrators, which would not be considered practical from a design and operation point of view. When looking closer at the study, they primarily are combinations of the multiple of two vibrators.

One of the objectives of this research project is to investigate the research with the purpose of practical application of the results. Very often the position of the unbalanced mechanisms is dictated by the screen design and there has to be a clear understanding of operating parameters of the screen before the vibrating screen could be properly designed and built. Currently the majority of mechanisms on vibrating screens are using kinematic couplings by the means of

gears, toothed belts or shafts. Some of the solutions involve controlling the motor phases electronically, which is expensive and also allows the mine personnel to try to 'improve' the process by changing the frequencies, which in many cases leads to the screen running very close to its natural frequency.

Being able to determine the shape of a stroke with mathematical modeling would allow for different screen designs with improved efficiency to combine research results with industrial practice. The industry will benefit from increased efficiency and cost reduction which shall in turn bring more interest in research and provide increased funding. An additional outcome of this investigation will be experimental data supporting future research and numerical models highlighting areas where these models are not applicable. It shall provide a stimulus for study into new or improved mathematical models for screen dynamic behavior that would better represent the physical reality.

There is a significant difference between self-synchronisation which happens by natural phenomenon and forced synchronisation which requires the use of mechanical means like toothed belts, gears, etc., or electronic motor phase control which is expensive and not always reliable.

This thesis will concentrate on self-synchronisation only, however some examples of forced synchronisation will be used to show the difference and advantages of replacing forced synchronisation with simpler, more reliable and cheaper vibrating mechanisms that use self-synchronisation phenomenon. Dual frequency screens offer several advantages in the process which are not available with currently manufactured vibrating screens.

1.2 Objective of the Dissertation

The objective of this thesis is to confirm the suitability of the application of vibrators having the self-sychronisation phenomenon for practical applications for the purpose of excitation of vibrating equipment. Currently used drive arrangements are very often expensive, are not reliable and are difficult to maintain and service.

For screening different materials, various stroke shapes and acceleration values can be used and self-synchronisation would allow for simple changes to the operating parameters of the vibrating screen including stroke shape which is not possible with 'traditional' vibrator drive

arrangements, so the research is needed to confirm the validity of mathematical calculations and the stability of self-synchronisation of vibrators working with different parameters and at different positions on the testing rig.

This dissertation contains a number of chapters and each chapter presents results of the testing of vibrators. Vibrating screens have usually one, two or three vibrators and because two vibrator screens are the most common in industry, the research will concentrate on two vibrator screens. A gearless box type exciter, which has been developed during the research, is a version of two single vibrators and it will also be used in some tests.

1.3 Significance and Innovation

The significant innovation of this research shows the modifications that can be used in vibrating screen design which would increase reliability, improve efficiency of screening, reduce fabrication and operating cost. A direct result of this research is the patent for a gearless exciter design which has already been built and tested.

1.4 Research Method of the Dissertation

This research investigates the self-synchronisation between two vibrators. Two vibrators have been chosen as it is the most common combination used in excitation of vibrating screens. The analytical solution was based on the Hamiltonian principle. Several different experiments were performed for each of the combination of rotation of vibrators i.e. same direction of rotation and opposite directions of rotation for the same frequency and same direction of rotation and opposite directions of rotation for different frequencies of operation for both vibrators. MATLAB software was used for the data acquisition and to transform the accelerometer signals into graphs to show the movement of the testing rig and to validate the analytical solution. Strand 7 Finite Element Analysis software was used for simulation of the stroke and vibration of the testing rig and to confirm FEA suitability for simulation of testing rig movement without the need to use a physical model. In the late stage of the research, a gearless exciter has been designed and built (commercial size) and testing performed to confirm the correctness of the laboratory results.

1.5 Layout of the Dissertation

This dissertation is divided into 10 chapters presenting testing results for different testing parameters using a rig in the University Lab. Some testing has also been done using a gearless exciter which is a redesign of a standard geared exciter commonly used in the mining industry for vibrating screens.

Chapter 1 contains the introduction, objective and innovation of the research, method of the research, research method and layout of the dissertation.

Chapter 2 presents the literature review commencing with the work by Christian Huygens in the 17th century, until today, making observations of the self-synchronisation phenomenon. It discusses the reduction of vibrations using the self-synchronisation phenomenon and the development of dual frequency screens with improved screening efficiency and mechanical reliability.

Chapter 3 discusses theoretical calculations for the vibrators operating with the same frequency, rotating in the same and in opposite directions.

Chapter 4 shows the results of testing for two vibrators rotating in the same and opposite direction, working with different settings but with the same operating frequency. Parameters that were changed included the location of motors, frequency and direction of revolutions. The testing rig was also modified during testing which changed the moment of inertia of the system and the mass of the setup.

Chapter 5 demonstrates the results of testing for two vibrators rotating in the same and opposite direction, working with different settings and with different operating frequencies. Parameters that changed in the testing included the location of motors, frequency and direction of revolutions. The testing rig was also modified during testing which changed the moment of inertia of the system and the mass of the setup.

Chapter 6 evaluates FEA as a method which could replace the physical testing. There are only 3 cases when the screen will have the same stroke shape in every point of the vibrating screen.

Case 1 - Linear motion when the line of force of vibrators rotating in the opposite direction is going through the centre of mass of the vibrating screen and then will obtain linear motion of the screen with all points moving with the same amplitude, phase and trajectory.

Case 2 - Elliptical motion when the line of force of vibrators rotating in the opposite direction is going through the centre of mass of the vibrating screen but the vibrators have different static moment and then will obtain elliptical motion of the screen with all points moving with the same amplitude, phase and trajectory.

Case 3 - Circular motion when the vibrators are rotating in the same direction and they are located symmetrically about the centre of mass and then will obtain circular motion of the screen with all points moving with the same amplitude, phase and trajectory.

In all other cases every point on the screen will move with different trajectory and the best method to determine the orbit in the required position is with FEA using natural frequency analysis and harmonic response. Every screen design process requires the finite element analysis to determine natural frequencies location and static stress so using the FEA model is a logical choice to use for subsequent analysis like determining the shape of the orbit.

Chapter 7 presents an example of an application of this research in practice and discusses advantages and disadvantages of a gearless box type exciter which uses the self-synchronisation phenomenon in comparison to the commonly used geared exciter version which uses gears for synchronisation purposes. The exciter was designed, built and tested and it is working in the field. The FEA model of a screen with a gearless exciter illustrates the possibilities of having various orbit shapes that can be used and easily changed to test and improve the efficiency of the screening process which is not possible with a standard geared exciter.

Chapter 8 presents a discussion on the self-synchronisation testing and results from previous chapters.

Chapter 9 draws conclusions from the obtained results and outlines how the objectives of the research have or not have been met.

Chapter 10 presents options for future research with some brief discussion on the existing vibrating equipment and possibilities of application of self-synchronisation of vibrators in current and future applications, including reductions of vibration using the self-synchronisation phenomenon. It also discusses resonance screens and feeders with application and advantages in comparison to standard 'brute force' vibrating equipment in specific processes.

Chapter 2
Literature Review

The synchronisation phenomenon is described by Blekhman as (Blekhman 1988) - 'several man-made or natural objects performing in the absence of interaction oscillations or rotational motions with different frequencies (angular velocities); they start moving with the same multiple or commensurable frequencies (angular velocities) in the presence of even very weak interactions. In such cases, definite phase correlations between oscillations and rotations are being established.'

This has been further described as coincidence of any scalar characteristics of the subsystem i.e. amplitude, energy, power, frequency, etc. from which synchronisation phenomenon can be established, (Blekhman, Fradkov, Nijmeijer and Pogromsku, 1997).

First observation and description of the self-synchronisation effect was made by Christian Huygens in the second half of the 17th century and published in 1673. He observed two clocks positioned on a light beam when sailing and noticed that they always became synchronised after a disturbance and were working in the opposite phases, (Blekhman 1988).

The experiment with clocks was repeated at the 'Mekhanobr' Institute in Leningrad and it showed that both opposite and syn-phased motion of the clock can be stable. Work on self-synchronisation started in 'Mekhanobr' Institute and the theory of self-synchronisations of pendulums was developed in publications by N. Minorsky, I. I. Blekhman and Y. I. Marchenko.

First theoretical explanation and study of the self-synchronisation effect in vibrators was reported in 1953 which is about 5 years after the self-synchronisation of mechanical vibro-exciters was discovered.

2.1 General Self-Synchronisation

Closed physical systems where the vibrating machines are transferring energy between each other are defined as synchronisation.

Vibrating machines in many cases are driven by several vibrators located in the same platform. In many cases the requirement is to synchronise rotating speed and phase which is very often done using kinematic couplings (gears, toothed belts, etc.). All these means create noise, need to be serviced and require also extra energy to operate.

In laboratories the self-synchronisation phenomenon has been noticed when the vibrators will match the running speed without any kinematic or electrical connection in between them. Practical research in self-synchronization encountered problems though because there was no understanding as to why this happened.

Self-synchronisation effect is positive when used on cases having several vibrators because it can be used to obtain stable and reliable work parameters with simple design. In other cases, when the phenomenon is not taken into account, it can cause serious damage to the plant and equipment. This situation can happen when several vibrators working on the same foundation or structure self-synchronise and work in the same frequency and phase, which will sum up the vibration forces. If however there is a correct understanding of the system and self-synchronisation is taken into account during the design phase, then it can be quite advantageous. When the self-synchronisation will take place with parameters selected so the phase between vibrators will be 180˚, then in this case, the phenomena can be used to cancel or reduce the vibration signal transferred to the supporting structure or foundation.

The self-synchronisation phenomenon was noticed for the first time in the 17^{th} century by Hyugens, where he described two clocks sitting on a light suspended beam working in counter-phase synchronisation.

In the 19^{th} century, Rayleigh researched synchronisation in acoustic and electro-acoustic systems and one of the observations was that two organ tubes would resonate with the same frequency if the out of tune difference between them was small.

Self-synchronisation of vibrators was discovered (or rather rediscovered) by accident in 1947 at the 'Mekhanobr' Institute in Leningrad when during experiments with two vibrators, operating on the same isolated supporting structure, they both kept working even though a cable connecting one of electric motors was damaged, as noted in the 'Mekhanobr' internal report in 1948, (Blekhman 2015, 52). Vibrators were driven with asynchronous motors however it was later confirmed that is some conditions the vibrator powered with synchronous motors will also synchronise.

Several vibrators positioned on the same structure and not connected electrically or kinematically will rotate synchronously with the same phase under certain circumstances, (Blekhman 1988, 240). Under the same phase is to be understood that they will not necessarily have the same phase angle. For two vibrators it would be 0˚ or 180˚, however for systems with several vibrators it will be a function of the vibrator's location about the centre of gravity of the system, direction of rotation and static moment of vibrators.

Accordingly to Blekhman (1988, 190), the total power supplied to the motors equals the total power of the friction of rotation and that the vibrational torques in the system don't participate in the general energy balance but only redistribute the energy between vibrators. It is described as the process of adding energy to 'slower' motors and subtracting it from the 'faster' ones which results in the equalisation of rotating frequencies which means self-synchronisation.

It has been noticed in some of the experiments done during this research that it is correct in some circumstances i.e. the rotational speed of one of the exciters was reduced when the power supply of the other exciter was switched off, but in other cases the rotating frequency has not changed. It was found to be a function of static moment, moment of the inertia of the system and rotating frequency.

That agrees well with the Blekhman (2015, 53), that the number of effects in the self-synchronisation cannot be predicted on intuitive considerations or be discovered without specifically designed experimentation.

Blekhman (1988, 94) also presented calculation for cases with three and four of vibrators and defined conditions for self-synchronisation. A similar subject was presented in an article, (ZHAO, ChunYu, WEN BangChun, ZHANG XueLiang, 2009) on four vibrators working in

the same plane. Vibrating screens need enough force to excite the vibration level required for the screening process and with bigger screens more force is required but the force is limited by the bearing and required operating speed for the process with fine screening requiring higher frequency. Using several vibrators for big screens would make the screen operate with the required high frequency and using several vibrators which are positioned equally spaced on the screen structure would result in the low stress in the screen structure and therefore long fatigue life.

One of the interesting research findings was when the theoretical results were compared to results obtained from physical testing and the position of vibrators was changed several times in respect to the centre of gravity of the screen (Banaszewski T., 2000) where the axis of symmetry was not going through the centre of gravity of the vibrating screen. The exciters still self-synchronised themselves, through the centre of gravity, though the vibration shape was different for each point of the screen (on a single plane).

Chunyu Zhao, Qinghua Zhao, Yimin Zhang, Bangchun Wen (2010) investigated the case of synchronisation of two non-identical exciters and concluded that the stability of synchronisation depended on the ratio of the mass of vibrators and the mass of the vibrating system and also the ratio of the distance between one vibrator and the centre of mass of the vibrating body to the equivalent of the rotating radius of the vibrating system about its centre of mass, and it wasn't dependent on the parameters of the motors.

Another research paper examined instabilities in self-synchronisation of vibrators in vibrating equipment (Michalczyk J., Cieplok G., 2014). The subject of the research was on the influence of elastic support element arrangement, ratios of elasticity and damping ratios. The research concluded that to obtain the self-sychronisation, the elastic elements should be symmetrically arranged about the centre of gravity of the vibrating equipment in vertical and horizontal directions and also the values of elasticity and damping constants should be the same in both directions.

The problem of having insufficient stiffness of the vibrators mounting resulting in inaccuracy of self-synchronisation was scrutinised by Michalczyk (2012) and he concluded that the elasticity of the individual mounting does not influence the synchronisation.

2.2 Self-synchronisation in reduction of vibration level

Self-synchronisation application is also being used in reduction of vibration which can be done by using vibrators working in the opposite phase or additional mass, with properly selected spring characteristic reducing the vibration.

Systems based on synchronisation of an additional sprung mass will be preferable to dynamic systems with additional vibrators which also would use the synchronisation principle to reduce vibration level. The device working on this principle is called a Frahm eliminator and allows the reduction of the vibration level by the magnitude order of 1. It does work very well in the steady state of vibrations but it would reduce the resonance by about 20% only so it is not recommended when the transient resonance could cause a significant problem (Michalczyk, Banaszewski 2006, 135).

Research in minimisation of dynamic forces transmitted by vibrating conveyors into foundations, (Czubak, 2012) proved that if a conveyor is operating based on Frahm's principle, the dynamic forces transmitted to the support structure or foundations can be very low and the heavy isolating frame is not necessary. This is another case where using proper design of equipment can result in significant material saving, meaning lower price and better operation of equipment, with lower vibration level.

2.3 Dual frequency vibrating screens

Self-synchronisation is not limited to vibrators working with the same frequencies; it also applies to exciters working with a slower vibrator being a proper fraction of the operating frequency of the faster vibrator, (Modrzewski, Wodzinski, 2009).

The combination of two frequencies allows for cyclical higher operating acceleration of the screen which allows for recurring operation with 7 g when the standard design of the operating screen is normally 5 g, (Fischer, 1982). The variable shape and amplitude allows for better screening efficiency by increasing the acceleration and randomisation of the screened material. It has a significant advantage in screening of difficult to screen materials in comparison to traditional screens and test work has shown clear efficiency gains which can be very substantial in commercial terms. By taking into account the production value, of more than $100 k per hour for some screens, in this case each percent of increased efficiency has very

significant long term economic benefit. The dual frequency screen is not as efficient in screening of fine materials, as for example flip-flow type screens, but it can work where the flip-flow screen can't which is for high temperature screening.

2.4 Concluding statement

There has been only limited research in the field of self and forced synchronization of vibrating screens. There are several options for self-sychronisation for the same systems and the parameters will be selected based on the system parameters i.e. operating speed, static moment required and also process requirements which should be selected based on screening efficiency trials.

Most of the early work done in the field on self-sychronisation was conducted at the Mekhanobr Institute in Leningrad (now Sankt Petersburg) and the research which followed was based on the fundamentals that had been established there. Most of the research work is very theoretical with no conclusion or suggestion of practical application in the industry, not to mention that the understanding of self-synchronisation of vibrators in the industry is very limited and it is not going to change without the academic/theoretical/technical support from universities. It would also require higher maintenance standards in the mines and quarries.

All research in synchronisation looks into self-synchronisation in one plane only. No research articles were found on synchronisation of vibrators in planes intersecting at different angles. Probably the most common would be 90 degrees, which could be for example manufactured vibrating screens that combine linear vertical and horizontal circular motions. It would be interesting to check if they could also self-synchronise.

Chapter 3
Vibrating screen with two vibrators rotating with the same frequency

3.1 Introduction

Most of the vibrating screens operate with linear or elliptical strokes, though for flaky material elliptical motion is recommended, which is obtained either by controlling phases of the driving electric motors or very often through a triple-vibrator mechanism coupled through a set of gears. Both solutions are expensive and the triple gear option often leads to vibrating screen failure when the assembly is not reconnected correctly after maintenance. On many occasions, even double mechanisms will be coupled by toothed belts or gears even when not required and if not re-assembled/aligned correctly can lead to catastrophic failure of the equipment.

Using self-synchronisation of mechanism running at the same frequencies would allow for the creation of various stroke shapes that would increase screening efficiency without increasing acceleration of the screen structure. It would also allow the simplification of the unbalanced mechanism arrangement on vibrating equipment and therefore improve reliability and reduce cost.

This chapter will present results of testing of a model of a vibrating screen to investigate if the option is feasible.

3.2 Theoretical considerations

The analytical development presented here follows the work according to Banaszewski (1990). Figure 3.1 presents a model of two vibrators on a soft-suspended solid body performing planar vibrations. There are two counterweights with masses m_0 with distance r_0 to the centres of the driving shafts and with a distance b from the centre of mass S to the shaft centres. The mass of the testing rig m_1 is sitting on a spring with constants k_x and k_y in the x and y directions respectively.

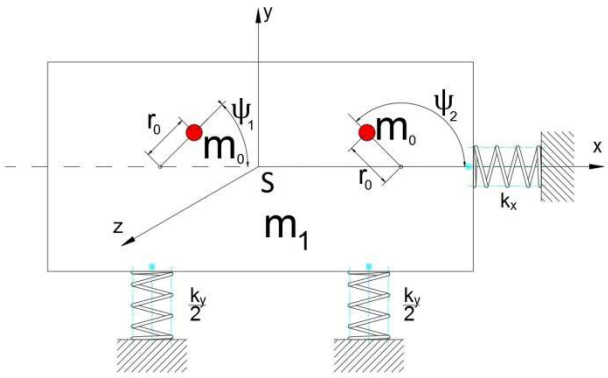

Figure 3.1 Model of a vibrating screen with two vibrators

The direction of rotation of the counterweights can be the same or opposite and will be defined by the coefficient $\gamma = \pm 1$. The positive sign is presumed for the direction of revolution of vibrator 1 when the direction is counter clockwise. The phase difference between the two counterweights will be described with angle λ.

The angular position of the counterweight of vibrator 1 can be described as

$$\psi_1 = \omega t \tag{3.1}$$

and the angular position of the counterweight of vibrator 2 will be given by

$$\psi_2 = \gamma \omega t + \lambda \tag{3.2}$$

To check when the self-synchronization will exist and the value of λ, Hamilton's principle can be used, given by

$$\int (T - U) dt = 0 \tag{3.3}$$

with T being the kinetic energy of the system and U representing the spring dynamic energy.

The kinetic energy of the system T will be equal to the kinetic energy T_s of the system mass m_1 and the energy of rotational components T_r about the centre of gravity S,

$$T = T_s + T_r \tag{3.4}$$

Potential energy U is the energy stored in springs and represented by the equation

$$U = k_x x + k_y y \tag{3.5}$$

Similarly the kinetic energy of the centre of gravity is given by

$$T_s = \frac{m}{2}(\dot{x}^2 + \dot{y}^2) \tag{3.6}$$

Velocities in equation (3.6) can be derived from equations of motion of the centre of gravity and are described as

$$m\ddot{x} + k_x x = m_0 r_0 \omega^2 (\cos\psi_1 + \cos\psi_2) \tag{3.7}$$

$$m\ddot{y} + k_y y = m_0 r_0 \omega^2 (\sin\psi_1 + \sin\psi_2) \tag{3.8}$$

for mass $m = m_1 + 2m_0$.

Using equations (3.1) and (3.2) the formula (3.7) will take the form

$$\cos\psi_1 + \cos\psi_2 = 2\cos\frac{\lambda}{2}\cos\left(\omega t + \gamma\frac{\lambda}{2}\right) \tag{3.9}$$

similarly equation (3.8) can be written,

for $\gamma = +1$,

$$\sin\psi_1 + \sin\psi_2 = 2\cos\frac{\lambda}{2}\sin\left(\omega t + \gamma\frac{\lambda}{2}\right) \tag{3.10}$$

And this will take the form (3.11) for $\gamma = -1$,

$$\sin\psi_1 + \sin\psi_2 = 2\cos\frac{\lambda}{2}\sin\left(\omega t - \gamma\frac{\lambda}{2}\right) \tag{3.11}$$

The solution for equations (3.7) and (3.8) will therefore result in

$$x = A_x \cos\left(\omega t + \gamma\frac{\lambda}{2}\right) \tag{3.12}$$

$$y = A_y(\sin\psi_1 + \sin\psi_2) \tag{3.13}$$

where

$$A_x = \frac{2m_0 r_0 \omega^2 \cos\frac{\lambda}{2}}{k_x - m\omega^2} \tag{3.14}$$

With A_x depending on γ, and taking forms,

for $\gamma = +1$,

$$A_y = \frac{2m_0 r_0 \omega^2 \cos\frac{\lambda}{2}}{k_y - m\omega^2} \tag{3.15}$$

and for $\gamma = -1$

$$A_y = \frac{2m_0 r_0 \omega^2 \sin\frac{\lambda}{2}}{k_y - m\omega^2} \tag{3.16}$$

When the unbalanced masses are rotating in the same direction for $\gamma=+1$, velocities in equation (3.6) will be equal, as given by

$$\dot{x} = -A_x \sin\left(\omega t + \gamma\frac{\lambda}{2}\right) \tag{3.17}$$

$$\dot{y} = A_y \cos\left(\omega t + \gamma\frac{\lambda}{2}\right) \tag{3.18}$$

Substituting equations (3.16) and (3.17) into (3.5) will result in

$$T_s = \frac{m_0^2 r_0^2 \omega^6}{m}\left[A_x^2\omega^2\sin^2\left(\omega t + \gamma\frac{\lambda}{2}\right) + A_y^2\omega^2\cos^2\left(\omega t + \gamma\frac{\lambda}{2}\right)\right] \tag{3.19}$$

Because in equation (3.3) the interest is in the average value of kinetic energy, it can be calculated from equation (3.19) and taking into account equations (3.14) and (3.15), it can be shown to be given by

$$T_s = \frac{m_0^2 r_0^2 \omega^6}{m} \cos^2 \frac{\lambda}{2} \left[\frac{1}{\left(\omega^2 - \omega_{0x}^2\right)^2} + \frac{1}{\left(\omega^2 - \omega_0^2\right)^2} \right] \tag{3.20}$$

where ω_{0x} and ω_0 are the natural frequencies of the system in directions x and y as is shown in (3.21) and (3.22)

$$\omega_{0x} = \sqrt{\frac{k_x}{m}} \tag{3.21}$$

$$\omega_0 = \sqrt{\frac{k_y}{m}} \tag{3.22}$$

Calculating average energy in the same way for the vibrators rotating in the opposite directions, $\gamma = -1$, obtains

$$T_s = \frac{m_0^2 r_0^2 \omega^6}{m} \left[\frac{\cos^2 \frac{\lambda}{2}}{\left(\omega^2 - \omega_{0x}^2\right)^2} + \frac{\sin^2 \frac{\lambda}{2}}{\left(\omega^2 - \omega_0^2\right)^2} \right] \tag{3.23}$$

Equations (19) and (22) can then be brought to a single expression

$$T_s = \frac{m_0^2 r_0^2 \omega^6}{2m} \left[\frac{1 + \cos\lambda}{\left(\omega^2 - \omega_{0x}^2\right)^2} + \frac{1 + \gamma \cos\lambda}{\left(\omega^2 - \omega_0^2\right)^2} \right] \tag{3.24}$$

with the kinetic energy of rotational vibrations described by

$$T_r = \frac{1}{2} I \dot{\varphi}^2 \tag{3.25}$$

where, I is the moment of inertia of the system about the z axis and ϕ represents the angle between the y axis and the centre line of the counterweight (swing).

A constant moment of inertia will be used without taking into account small changes in rotation and related to changes to the mass moment of inertia of the system and required velocity of the swing will be determined from the moment equation

$$I\ddot{\varphi} = m_0 r_0 \omega^2 b(\sin\psi_1 - \sin\psi_2) \tag{3.26}$$

which after double integration and taking into account equations (3.1) and (3.2) will take the form

$$\varphi = \frac{m_0 r_0 b}{I}(\sin\psi_1 - \sin\psi_2) \tag{3.27}$$

where the angular velocity is given by

$$\dot{\varphi} = \frac{m_0 r_0 b\omega}{I}(\gamma\sin\psi_2 - \cos\psi_1) \tag{3.28}$$

After substitution of equation (3.27) into (3.24)

$$T_r = \frac{m_0^2 r_0^2 b^2 \omega^2}{2I}(\cos^2\psi_2 + \cos^2\psi_1 - 2\gamma\cos\psi_1\cos\psi_2) \tag{3.29}$$

the average value of the energy will take the form

$$T_r = \frac{m_0^2 r_0^2 b^2 \omega^2}{2I}(1 - \gamma\cos\lambda) \tag{3.30}$$

and the potential energy stored in springs will be represented by equation (3.31)

$$U = (\frac{1}{2}k_y y^2 + \frac{1}{2}k_x x^2) \tag{3.31}$$

After substituting into equation (3.30) equations (3.11) and (3.12) and taking into account equations (3.13), (3.14), (3.15) and (3.20) and (3.21) the equation for system energy will appear as

$$U = \frac{m_0^2 r_0^2 \omega^4}{2m}\left[\frac{\omega_0^2}{(\omega_0^2-\omega^2)^2}(\sin\psi_1 + \sin\psi_2)^2 + \frac{4\omega_{0x}^2}{(\omega_{0x}^2-\omega^2)^2}\cos^2\frac{\lambda}{2}\cos^2\left(\omega t + \gamma\frac{\lambda}{2}\right)\right] \tag{3.32}$$

with an average value of this energy being

$$U = \frac{m_0^2 r_0^2 \omega^4}{2m}\left[\frac{\omega_0^2}{(\omega_0^2-\omega^2)^2}(1 + \gamma\cos\lambda)^2 + \frac{2\omega_{0x}^2}{(\omega_{0x}^2-\omega^2)^2}\cos^2\frac{\lambda}{2}\right] \tag{3.33}$$

Inserting the equations of all the energies, (3.24), (3.30), and (3.33) into equation (3.3), the equation for the total energy of the system can be reformulated to yield

$$\int (T-U)dt = \frac{m_0^2 r_0^2 \omega^4}{2m}\left[\frac{(1+\cos\lambda)\omega^2}{(\omega^2-\omega_{0x}^2)^2} + \frac{(1+\gamma\cos\lambda)\omega^2}{(\omega^2-\omega_0^2)^2} + \frac{mb^2(1-\gamma\cos\lambda)}{I\omega^2} - \frac{\omega_0^2(1+\gamma\cos\lambda)}{(\omega^2-\omega_0^2)^2} - \frac{\omega_{0x}^2(1+\cos\lambda)}{(\omega^2-\omega_{0x}^2)^2}\right] \quad (3.34)$$

with the variable of this function being the angle λ.

A simpler version of the function can be shown to be given by

$$f(\lambda) = \frac{2m}{m_0^2 r_0^2 \omega^4}\int (T-U)dt = \frac{1+\cos\lambda}{\omega^2-\omega_{0x}^2} + \frac{1+\gamma\cos\lambda}{\omega^2-\omega_0^2} + \frac{mb^2(1-\gamma\cos\lambda)}{I\omega^2} \quad (3.35)$$

and the function should reduce to 0. By understanding when the first derivative goes to zero, conditions can be defined when it will happen. This shows

$$\frac{d\gamma}{d\lambda} = \left(\frac{-1}{\omega^2-\omega_{0x}^2} - \frac{\gamma}{\omega^2-\omega_0^2} + \frac{\gamma mb^2}{I\omega^2}\right)\sin\lambda = 0 \quad (3.36)$$

if

$$\frac{\gamma mb^2}{I\omega^2} - \frac{-1}{\omega^2-\omega_{0x}^2} - \frac{\gamma}{\omega^2-\omega_0^2} = 0 \quad (3.37)$$

and then condition (3.36) is fulfilled for any value of λ. This means that no interaction between vibrators occurs and the vibrations will be constant and stable for any value of λ. It also means that if parameters are selected to satisfy equation (3.37) then the vibrators don't interact and they will be working in all conditions without any interaction.

The first part of equation (3.37) is proportional to rotational energy and if vibrators are close to each other or if the moment of inertia is big enough ($\frac{b^2}{I} \rightarrow 0$) then this part of the equation can be omitted. The equation will then be satisfied for $\omega \rightarrow \infty$ or $\omega_{0x} \approx \omega_0 \rightarrow \infty$.

In practical terms, this means that self-synchronisation will always happen for rotation of vibrators in the same direction.

For rotation of vibrators in opposite directions ($\gamma = -1$) equation (3.37) will be fulfilled (with first part of the equation omitted) when,

$$\omega_{0x} = \omega_0, \text{ i.e. } k_x = k_y$$

This means that self-synchronisation will happen when the stiffnesses in the x and y directions are different. If the conditions of the equation (3.37) are not fulfilled, then from equation (3.36) we receive,

$$\sin\lambda = 0, \text{ so } \lambda = 0° \text{ or } 180°$$

For the Hamilton principle to be fulfilled for $\lambda = 0°$, equation (3.35) for γ=-1 and $\lambda = 0°$ will take the form,

$$f(\lambda = 0°) = \frac{2}{\omega^2 - \omega_{0x}^2} + \frac{2}{\omega^2 - \omega_0^2} \qquad (3.38)$$

and then from equations (3.11) and (3.12), circular motion of the model will be obtained, including the centre of gravity as shown on Fig. 3.2.

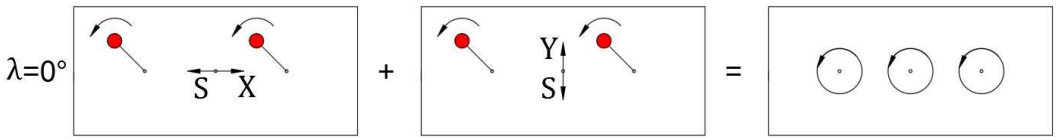

Figure 3.2 Circular motion of the model with two vibrators

For $\lambda = 180°$, equation (3.34) will be

$$f(\lambda = 180°) = \frac{2mb^2}{I\omega^2} \qquad (3.39)$$

and then rotational motion with a stationary centre of gravity will occur because the amplitudes of vibration (equations 3.14 and 3.15) equal zero for cos 180˚/2, as is shown in Figure 3.3.

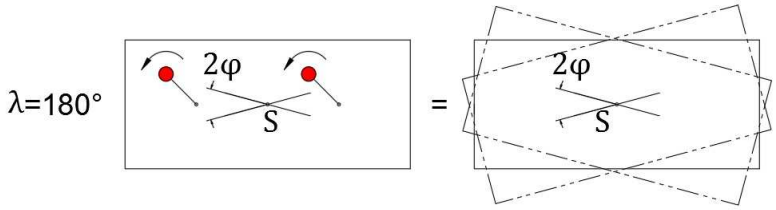

Figure 3.3 Rocking motion of the vibrating model

The stroke shape of the vibrating model depends on ω, I, m and on the natural frequency of the system.

From comparison of equations (3.37) and (3.38), the results show that for the most often used system parameters, vibrations as shown on Figure 3.2 require less energy and therefore are more common,

$$\frac{b^2}{I} < \frac{2\omega^4 - (\omega_0^2 + \omega_{0x}^2)\omega^2}{m(\omega^2 - \omega_0^2)(\omega^2 - \omega_{0x}^2)} \qquad (3.40)$$

For the opposite direction of rotation of vibrators, γ=-1 and λ = 0°, equation (3.34) shows that the resultant trajectory will be a combination of linear motion about the x axis and rotation about the centre of gravity as presented in Figure 3.4,

$$f(\lambda = 0°) = \frac{2}{\omega^2 - \omega_{0x}^2} + \frac{2mb^2}{I\omega^2}. \qquad (3.41)$$

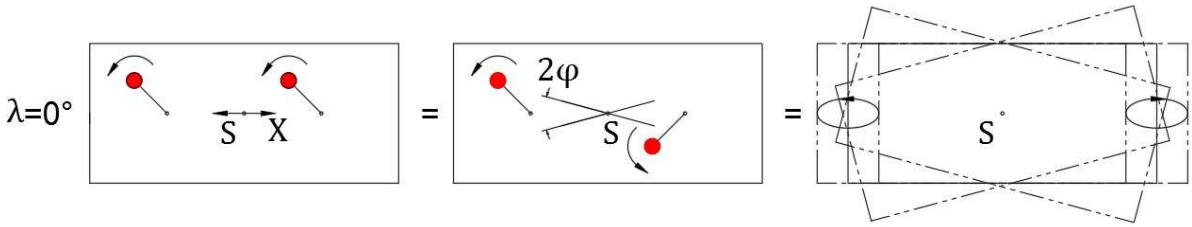

Figure 3.4 Combination of rocking and linear motion of the screen

For γ = -1 and λ = 180° the result will be linear motion perpendicular to the line connecting the vibrators as is shown in Figure 3.5, where

$$f(\lambda = 180°) = \frac{2}{\omega^2 - \omega_0^2}. \qquad (3.42)$$

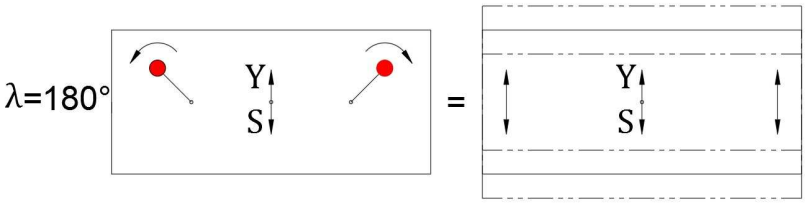

Figure 3.5 Linear motion of the model

This case requires less energy and therefore in the majority of cases the movement will be linear.

3.3 Vibrators rotating in the same direction

The majority of vibrating screens operating in the aggregate industry operate with circular stroke shape, because the process operating with circular motion has lower cost rather than being efficiency driven when it comes to screening aggregate as is shown in Figure 3.6. Bigger screens typically operate with two circular motion unbalanced eccentric shafts and have the phase controlled by the toothed belt and with one electric motor driving the vibrators' arrangement.

Figure 3.6 Toothed belt transferring power and controlling phase between two vibrators

There are also a small numbers of designs with vibrators positioned far apart from each other as presented in Figure 3.7. This design, Fig 3.7, is advantageous from the structural point of view, because by dividing the screen into 3 parts it offers uniform loading on the screen structure and therefore it would reduce stress levels and make the distribution of stress more homogenous. The distance between vibrators prevents the use of toothed belts to control phases and that is the reason the phases have to be controlled electronically. It is more expensive and doesn't offer benefits to the process and that is the reason the drive as presented in Figure 3.6 is mostly used. If self-synchronisation in revolutions and phase of vibrator arrangement as shown in Figure 3.6 could be achieved, that would improve reliability and reduce the cost of fabrication and maintenance of vibrating screens.

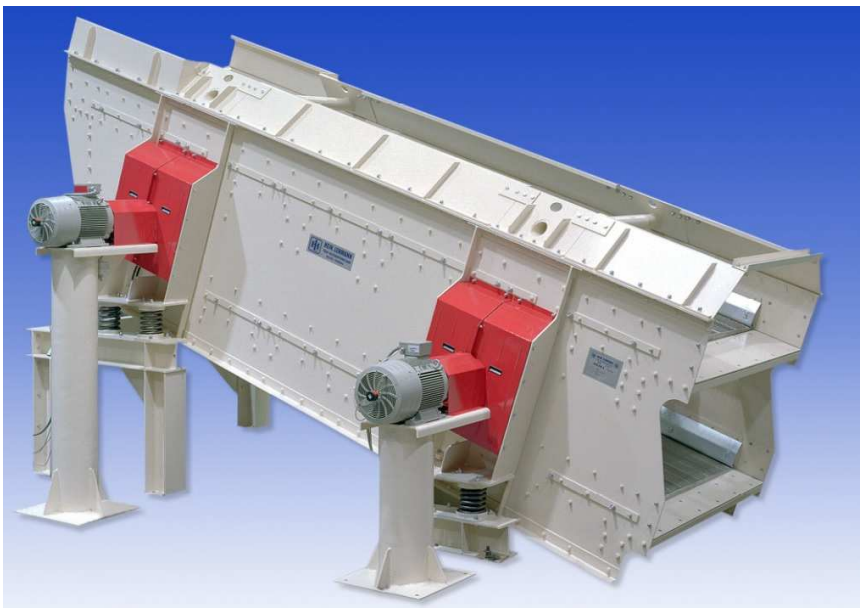

Figure 3.7 Hein Lehman two electric motors with phase controlled electronically (HEIN, LEHMANN GmbH)

3.4 Vibrators rotating in the opposite directions

There are a wide range of screens that have linear or elliptical stroke shape. Figure 3.8 presents a screen that uses the self-synchronisation phenomenon with no kinematic connection between the two unbalanced shafts driven by separate electric motors. This type of screen is discussed further in chapter 4. The drive combination does not take much space on the structure, so the screen can be lower and more compact in comparison to the screen presented in Figure 3.9.

Figure 3.8 Vibrating screen with two unbalanced shafts driven by two separate electric motors

Because of the orientation of the mechanisms, the stroke shape is elliptical at feed and discharge ends and linear in the middle. Having elliptical and linear strokes it will in many cases improve the screening efficiency if compared only to the screen from Figure 3.9 which offers only linear motion, unless shafts are electronically controlled and then all points of the screen move in the same elliptical shape. It comes however at significant extra cost and makes the installation less reliable. Figure 3.9 shows a similar screen to that previously discussed which is also using the self-synchronisation principle but with linear stroke shape because of the different position of the unbalanced shaft mechanisms about the centre of mass.

Figure 3.9 Two unbalanced shafts driven by two separate electric motors (Metso Minerals)

Figure 3.10 shows a typical vibrating screen that uses two box type vibrators with one shaft driven and the power transferred to the second shaft through a pair of gears. It is a typical case of forced synchronization. Gears are also a means of splashing the oil for the lubrication purposes in this design. Splash lubrication is unreliable and the reliability is lower with larger mechanisms and bigger bearings where the problem is with correct lubrication of the external bearing races. Gears generate extra heat, noise and are the main source of metal contamination of lubricating oil. Vibrators presented in Figures 3.8 and 3.9 are operating with a proper oil bath or smaller screens use grease lubricated bearings which works satisfactorily because of the improved heat exchange than in the case of box type vibrators.

Figure 3.10 Typical vibrating screen with two geared box type exciters

Figure 3.11 presents a small screen with two electric unbalanced motors. The motors self-synchronise about themselves and about the centre of mass. It is a cost effective option for small screens, however the cost of bigger vibrators is high and with bigger screens, the natural frequencies are more difficult to control and the set speed electric unbalanced motors require frequency controllers. They are also grease lubricated and it limits the forces that can be created using this type of vibrators.

Figure 3.11 Vibrating screen with two electric vibrators operating in counter-directions

Chapter 4
Experimental Tests for vibrators operating with the same frequency

Test were performed in a laboratory with a testing rig simulating a vibrating screen, complete with springs, 2 vibrating motors with frequency controllers and accelerometers. Originally used urethane springs were found not to be suitable for the purpose and have been replaced with steel springs. Because of the low static moment, new counterweights were designed and fabricated with suitable guards. Initial tests with 16 counterweight segments per vibrator and speed reduced to 1000 rpm showed that the static moment was too large and for extreme positions of vibrators, the springs were bottoming out which could damage both springs and the testing rig. Additionally the static moment was too high for the electric motors and they were not able to start without a 'push', which initially resulted in damage to one of the electric motors. Counterweight segments were reduced to 8 per vibrator and the max rpm increased to 1500 rpm. It was decided to use two motors for the experiments because it is the most common configuration used in the industry and for the sake of simplicity. Testing with three and four vibrators could be planned to be done in the future work.

The testing rig weight without vibrators was 15.8 kg. The electric vibrators used for the testing were TO 1000 series ATA vibrators, (single phase vibrators, 240 V, 70 W, with frequency controllers, TBe-028. Each of the vibrators weighed 3.3 kg. Counterweights were modified to achieve the required static moment. Maximum rotating speed was chosen to take the increased static moment into account and new guards were fabricated to make the testing safe. Shaft sizing was recalculated based on manufacturer's data, and was suitable for centrifugal forces of 500 N and 3000 rpm. Figures 4.1 and 4.2 show the parameters of the vibrators used for testing.

TO1000 SERIES VIBRATORS

FEATURE

- ◆Efficient vibration, slight weight, small volume
- ◆H-grade insulation
- ◆Stable amplitude
- ◆No noise problem
- ◆Easy assemble, operation, and maintenance

APPLICATION

PCB plating, Bin Activation, Compaction, Feeding, Screening, chemical industry

DIMENSION

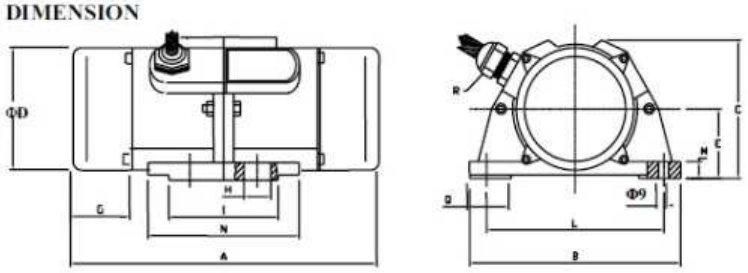

MODEL	A	B	C	D	E	G	H	I	L	M	N	R	Q
TO/Tb	145	112	67	61	33	29	14.5	28-38	92	9	55	M-16	21
TB/TBe/TY	192	121	72	66	35	38	14.5	28-38	92	13	58	M-16	24

SPECTIFICATION

MODEL	VOLT	Hz	CURRENT	PHASE	CENTRIGUGAL FORCE(KG)	WATT	RPM
TO-0.1	220	50/60	0.13	1	30	30	3000/3600
Tb-0.1	110	50/60	0.30	1	30	30	3000/3600
TO-0.1a	220	50/60	0.11	3	30	42	3000/3600
TBe-0.28	220	50/60	0.31	1	50	70	3000/3600
TBe-1	110	50/60	0.64	1	50	70	3000/3600
TBe-2-3	220	50/60	0.18	3	50	70	3000/3600
TY-2	220	50/60	0.41	1	55	90	3000/3600
TY-1	110	50/60	0.82	1	55	90	3000/3600
TY-2-3	220	50/60	0.24	3	55	90	3000/3600

Figure 4.1 Vibrators selection

4.	**TO1000 series** **TBe-0.28S** **2P AC adjustable speed vibrators with controller**	**220V 1phase 70W** **50/60Hz,** **3000/3600RPM** (approx. 3.6kg)	**1**	**US$135**	

Figure 4.2 Parameters of the vibrator's selected – shown with a frequency controller

Figure 4.3 shows a photo of the initial setup of the testing rig with original counterweights and urethane springs.

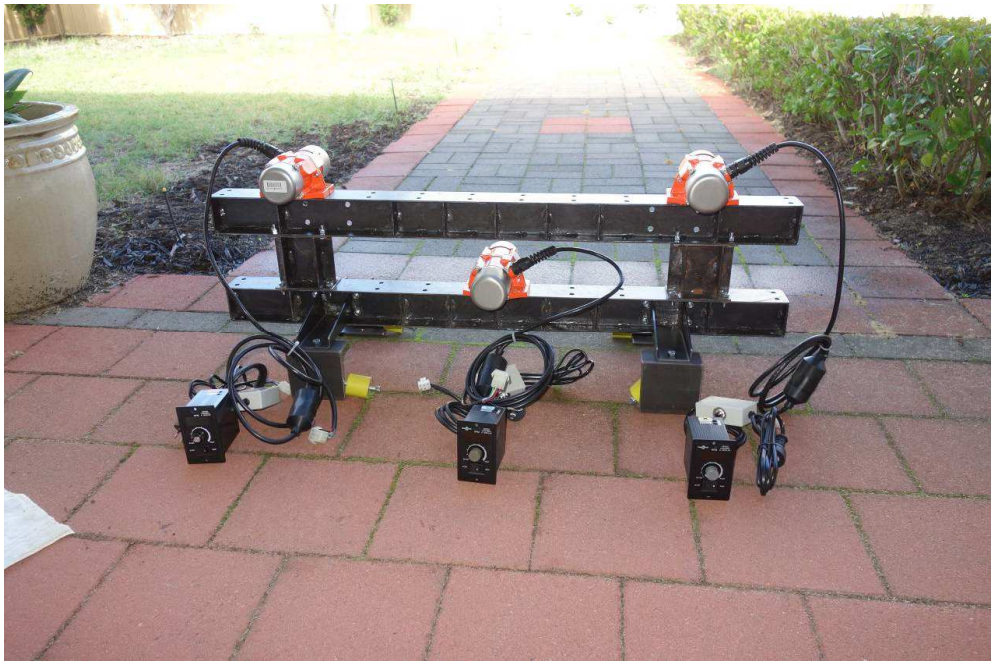

Figure 4.3 Initial setup of the testing rig with original counterweights and urethane springs

This setup was later changed to the new arrangement as per Figure 4.4 with three vibrators and metal springs. Figure 4.5 shows the final setup with two vibrators and two frequency controllers which was used for the experimental research of this thesis.

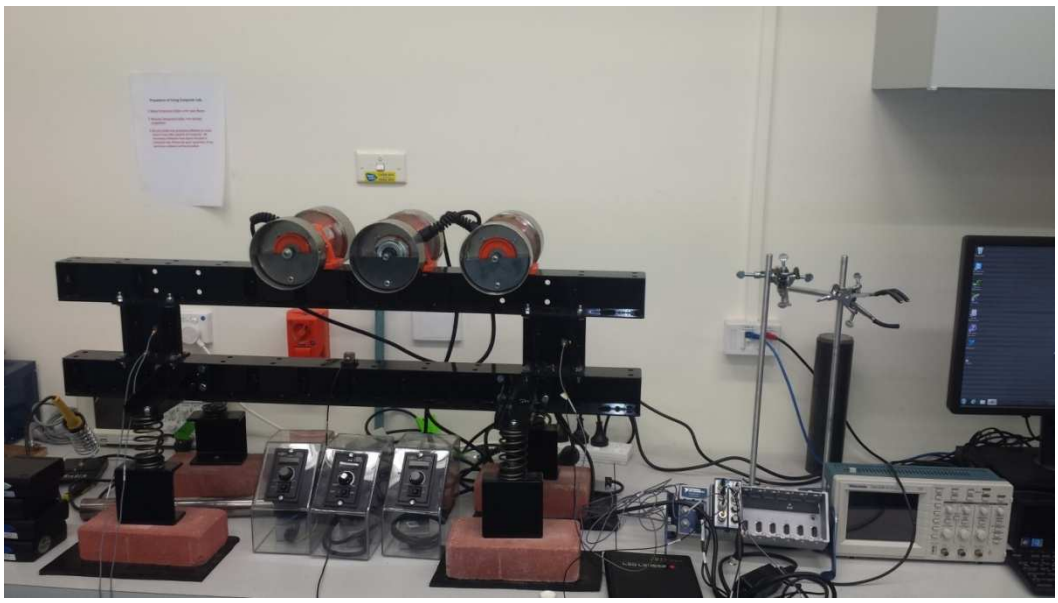

Figure 4.4 Testing rig setup with steel springs – 3 vibrators with modified counterweights shown

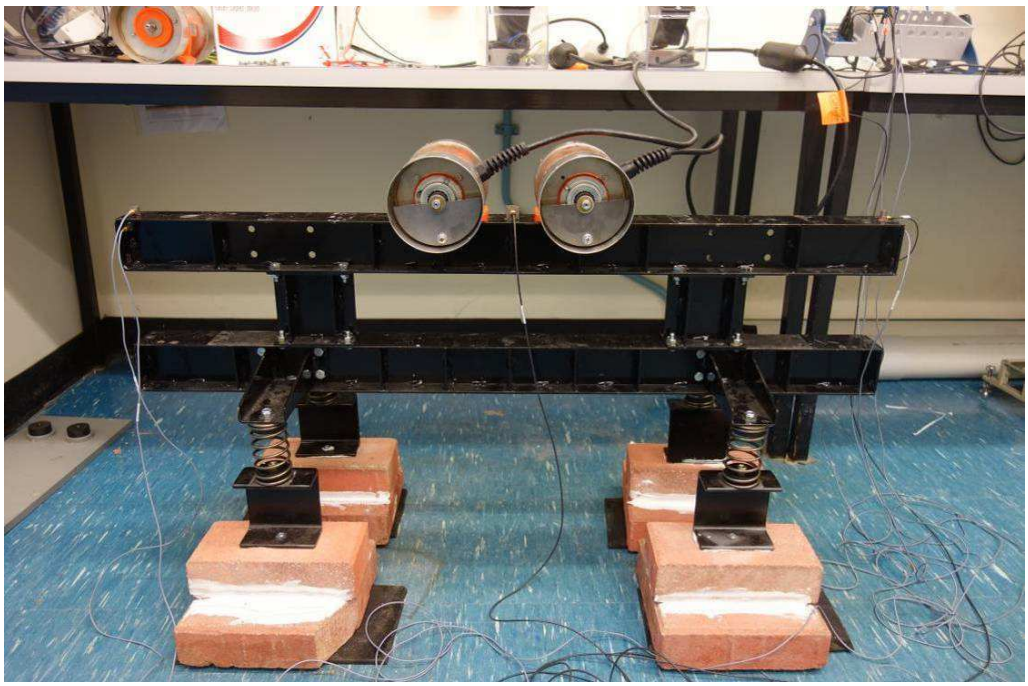

Figure 4.5 Testing rig setup in configuration used for testing – two vibrators modified counterweights

The National Instruments NI cDAQ-9178 8-Slot USB Chassis with 2 off NI 9234 four-channel dynamic signal acquisition modules was used for the experimental vibration measurement and is shown in Figure 4.6.

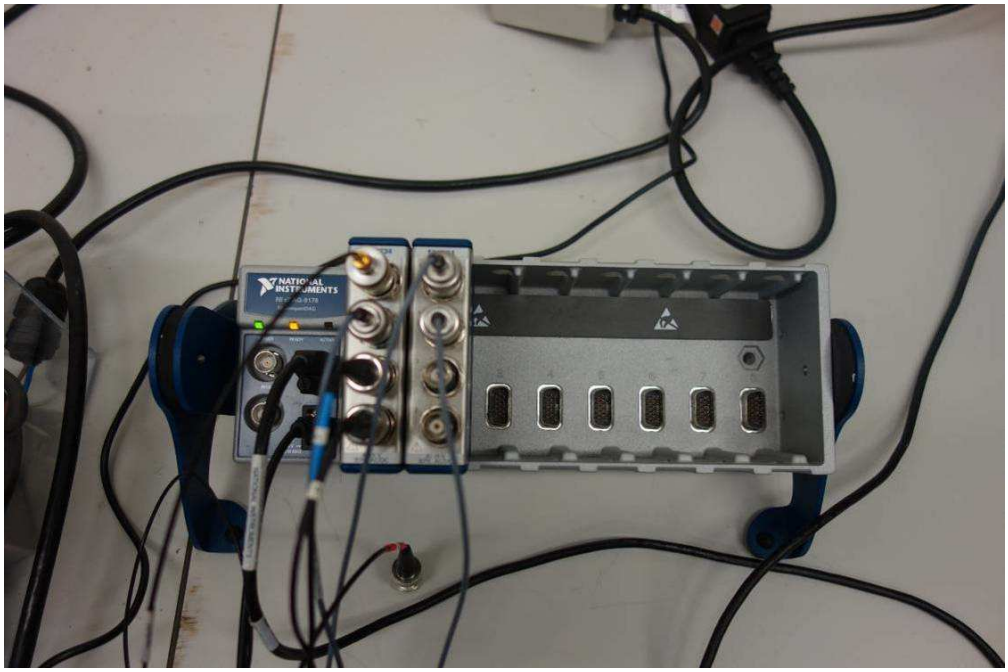

Figure 4.6 NI cDAQ-9178 8-Slot USB Chassis with 2 off NI 9234 four-channel dynamic signal acquisition modules

Frequency controllers and motors were marked with the isolating tape for ease of identification as to which controller belonged to which vibrator as is shown in Figure 4.7.

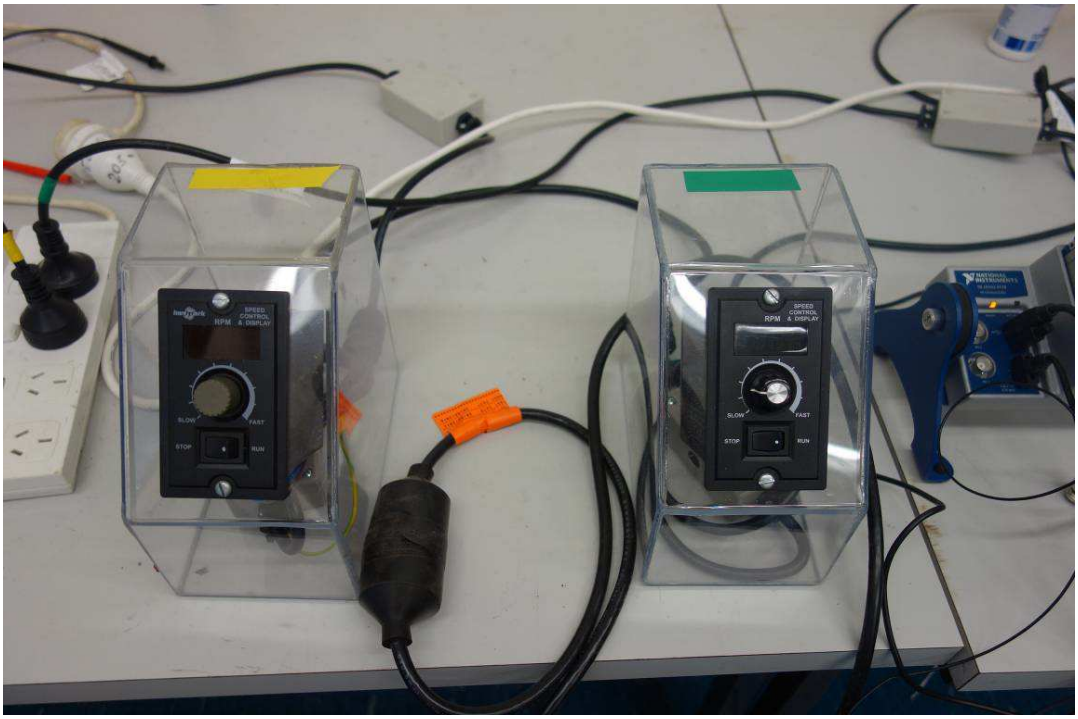

Figure 4.7 Two Frequency controllers

Four single axis B&K accelerometers and 1 triaxial (two outputs used only) have been used to simultaneously record the X-Y vibration data from 3 positions on the testing rig. 4 off compression springs were used for isolation; ASI springs C1937-158-4000 with spring rate 5.08 N/mm. All the vibration data was recorded and analysed using PC and Matlab software and all pictures and movies were taken using a Sony Cybershot RX100 Compact Digital Camera. Figure 4.8 illustrates the positions of the vibrating motors and the location of accelerometers that were used to record the orbit trajectories. Accelerometers were located in three positions for measuring acceleration in two axes (X – horizontal and Y – vertical) so the stroke shape and acceleration could be recorded.

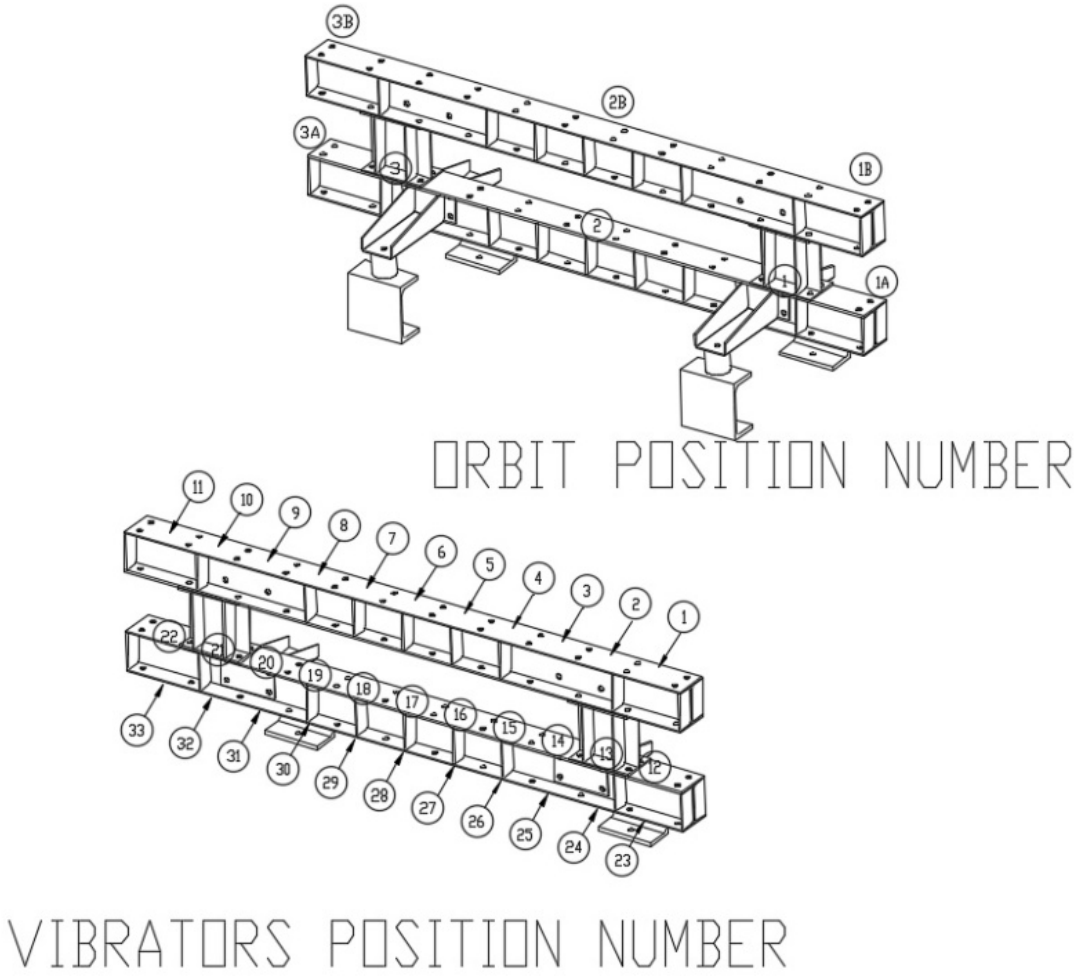

Figure 4.8 Vibrators position number and orbits (accelerometers) position number

Figure 4.9 shows an FEA Strand 7 model which was used for the purpose of defining moments of inertia for different setups of the testing rig. Strand 7 Finite Element Analysis software harmonic analysis solver was used to check if the physical results can be simulated using finite element analysis software which later if successful would be used to visualise trajectories at any point of interest on the designed screen in a fast and effective way. The plate FEA model was tested against the beam only FEA model and it was found that in both cases the results were the same, but with the plate model the computational time of several seconds was required while the beam model yielded results almost instantaneously and therefore in the simulations the beam model was used. Of particular interest were trajectories obtained for dual frequency testing.

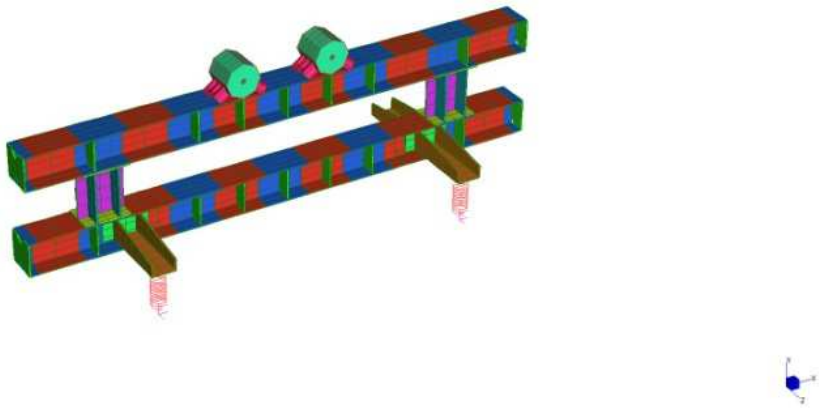

Figure 4.9 Strand 7 FEA testing rig model - plates

Figure 4.10 illustrates the FEA Strand 7 model which was built using beam elements, which provided for faster solution times.

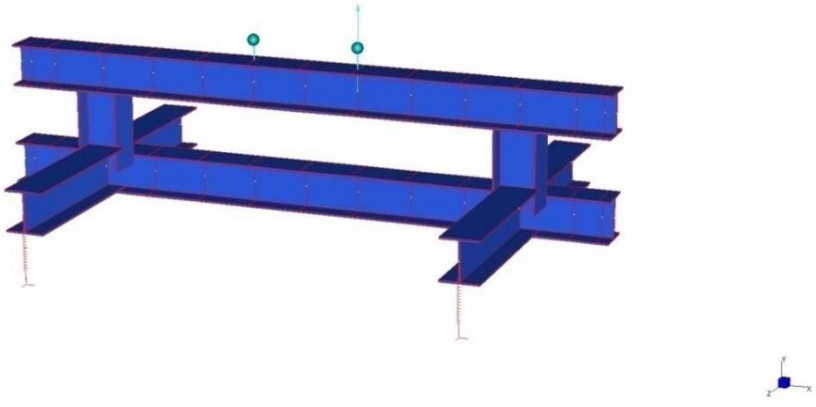

Figure 4.10 Strand 7 FEA testing rig model – beams

The overall laboratory setup is shown in Figure 4.11. To enable the taking of photographic images of the vibrator counterweights and to determine their phase angles, a stroboscope was used. Two unbalanced vibrating motors with adjustable counterweights (static moment) and frequency controllers (rpm) were used in the experiments.

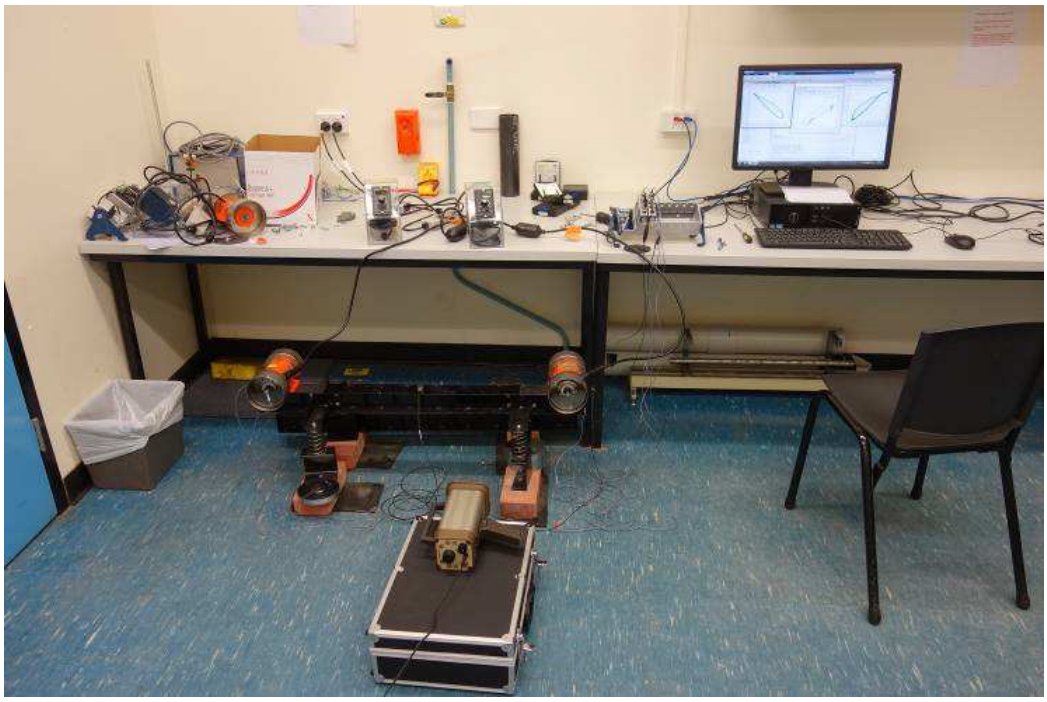

Figure 4.11 Setup of the testing rig with accelerometers, frequency controllers, stroboscope, etc.

4.1 Experimental testing for the two vibrators rotating in the same direction

Chapter 4.1 presents the test results of two vibrators operating with the same frequency, rotating in the same direction at different locations on the testing rig. Table 4-1 shows the detail of the case study parameters for each of the 15 test cases that were studied in detail.

Table 4.1 Positions of orbits and vibrators for screen tests with both vibrators rotating in the same direction

Case No	Left Vibrator position rpm/Hz	Right Vibrator position rpm/Hz	Orbit Pos 1	Orbit Pos 2	Orbit Pos 3
4.1.1	7 1035/17.25	5 1035/17.25	1B	2B	3B
4.1.1a	7 1545/23.75	5 1545/23.75	1B	2B	3B
4.1.1b	7 570/9.5	5 570/9.5	1B	2B	3B
4.1.2	10 570/9.5	2 570/9.5	1B	2B	3B
4.1.3	11 1060/19.08	1 1060/19.08	1B	2B	3B
4.1.4	18 1450/24.2	16 1450/24.2	1B	2B	3B
4.1.5	22 1460/24.3	12 1460/24.3	1B	2B	3B
4.1.5a	22 1460/24.3	12 Vibrator Off	1A	2	3A
4.1.6	4 1300/20.66	2 1300/20.66	1B	2B	3B
4.1.7	9 1060/17.66	25 1060/17.66	1B	2B	3B
4.1.8	18 1550/25.8	16 1550/25.8	1A	2	3A
4.1.9	20 1550/25.88	14 1550/25.88	1A	2	3A
4.1.9a	20 1550/25.8	14 Vibrator Off	1A	2	3A
4.1.10	22 1200/20	12 1200/20	1B	2B	3B
4.1.11	22 1060/17.66	12 1060/17.66	1B	2B	3B

Figures 4.12 to 4.41 show the rig setup with the position of vibrators and location of accelerometers and also presents the trajectories and magnitudes of the strokes (orbits) plotted in an X-Y graph and the corresponding acceleration time histories in X (lower graphs) and Y (upper graphs) directions.

Photographic pictures were taken during testing rig operation using the stroboscope to show the location of the vibrators and the operational position and phase difference of the two counterweights.

Tables from 4.1 to 4.16 demonstrate the parameters used for each testing case for both vibrators rotating in the same direction with the conditions for self-synchronisation for each case assessed based on the work by Blekhman (1988).

$$\frac{\mathrm{Mr}^2}{\mathrm{I}} > 2 \; conditions\; for\; sychronised\; motion\; of\; two\; exciters\; in\; circular\; motion$$

M - mass of the testing rig [kg]

R – distance of the centre of vibrators from the centre of gravity [m]

I - moment of inertia [kgm^2]

Distances of centres of exciters and moments of inertia were calculated using the Strand 7 finite element models which allowed for quick and precise calculation and the models were later used for simulation and comparison of results obtained with physical and mathematical calculations.

The use of the Strand 7 FEA model provided the functionality for checking on new model parameters after changes of vibrators positions i.e.:

- Moment of Inertia
- Distance of exciters' centres to the centre of mass

Testing results are presented in the Figures showing the position of vibrators and counterweights. The Figures show the shape and size of orbits, and acceleration signal shape in the Y direction (upper graph) and X direction (lower graph).

Table 4.2 Test parameters of screen test Case 4.1.1 with both vibrators rotating in the same direction

	Unit	Value
Moment of Inertia	kgm^2	1.9544
Vibrator Static Moment (each)	kgm	$1387.8e^{-5}$
The phase difference of	deg	180
Distance of left exciter centre to the centre of mass	m	0.162779
Distance of right exciter centre to the centre of mass	m	0.162779
Vibrator rotational speed	rpm/Hz	1035/17.25
Mass of the setup	kg	24.7

$$\frac{Mr^2}{I} = 0.33 < 2 \; - \; \text{conditions for self} - \text{sychronised circular motion not met}$$

Table 4.3 Orbit Plots and Acceleration Amplitude results for test Case 4.1.1 with both vibrators rotating in the same direction

Value	Unit	Position 3	Position 2	Position 1
Acceleration in Y Direction	mm/s^2	10	1	10
Acceleration in X Direction	mm/s^2	1	2	2

Case 4.1.1 shown in Figure 4.12 has both vibrators rotating in the same direction at 17.25 Hz. The phase difference of 180 degrees is clearly shown on the Figure 4.12 and also on the graphs showing the sinusoidal signal with acceleration, where it is better presented on graphs with shorter signal measurement time where the start of the signal from time '0' can be easily observed. Orbit plots and acceleration values are presented in Figure 4.13. The results clearly show that the testing rig was moving in a rocking motion with a pivot point at the centre of mass. The centre of mass is outside of the physical body of the testing rig and therefore the results presenting the acceleration in position 2 is not located at the centre of mass. A simple bracket could be fabricated to enable positioning of the accelerometer 2 exactly at the centre of mass but because the centre of mass is changing location with different positions of the vibrators during testing several brackets would have to be fabricated to suit different cases,

therefore the decision was made to abandon this idea. Some small irregularities can be observed on the graphs in the X direction which related to the slight movement of the testing rig. Like most of the live equipment there is some looseness and misalignment. More elaboration will be done in descriptions of the next cases with higher operating frequency or with the testing rig running close to the natural frequency where the unwanted movement is more pronounced. When one of the vibrators was turned off, both vibrators kept running with no difference to the movement of the testing rig.

Figure 4.12 Case 4.1.1 Setup

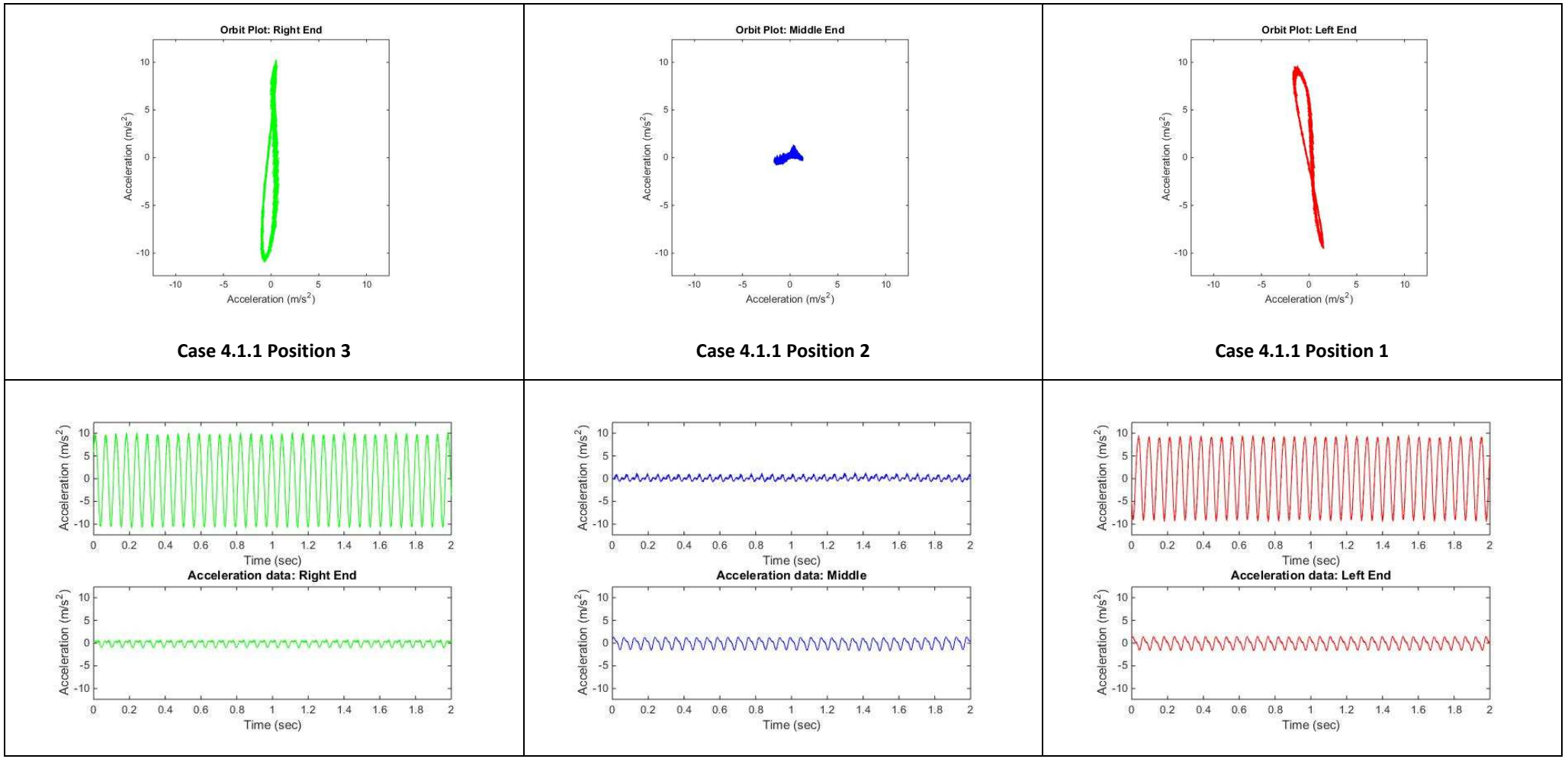

Figure 4.13 Orbit plots and acceleration graphs (X – lower graph, Y-upper graph) for case 4.1.1

Table 4.4 Test parameters of screen test Case 4.1.1a with both vibrators rotating in the same direction

	Unit	Value
Moment of Inertia	kgm^2	1.9544
Vibrator Static Moment (each)]	kgm	$1387.8e^{-5}$
The phase difference of	deg	180
Distance of left exciter centre to the centre of mass	m	0.162779
Distance of right exciter centre to the centre of mass	m	0.162779
Vibrator rotational speed	rpm/Hz	1545/23.75
Mass of the setup	kg	24.7

$$\frac{Mr^2}{I} = 0.33 < 2 \; - \; \text{conditions for self} - \text{sychronised circular motion not met}$$

Table 4.5 Orbit Plots and Acceleration Amplitude results for test Case 4.1.1a with both vibrators rotating in the same direction

Value	Unit	Position 3	Position 2	Position 1
Acceleration in Y Direction	mm/s^2	20	4	17
Acceleration in X Direction	mm/s^2	1	2	2

Case 4.1.1a is shown in Figure 4.14 with both vibrators rotating in the same direction at 23.75 Hz. The difference between cases 4.1.1 and 4.1.1a is only the vibrators rotating speed. The phase difference of 180 degrees is also clearly shown on the Figure 4.14 and also on the graphs showing the sinusoidal signal with acceleration in Figure 4.15. The orbit plots and acceleration values are presented in Figure 4.15. The difference between the acceleration results in the Y direction is most likely a result of the spring stiffness difference and also a function of direction of revolutions. The testing rig was again moving in a rocking motion with the pivot point at the centre of mass. One of the vibrators was turned off and both vibrators kept running with no difference to the movement of the testing rig.

Figure 4.14 Case 4.1.1a Setup

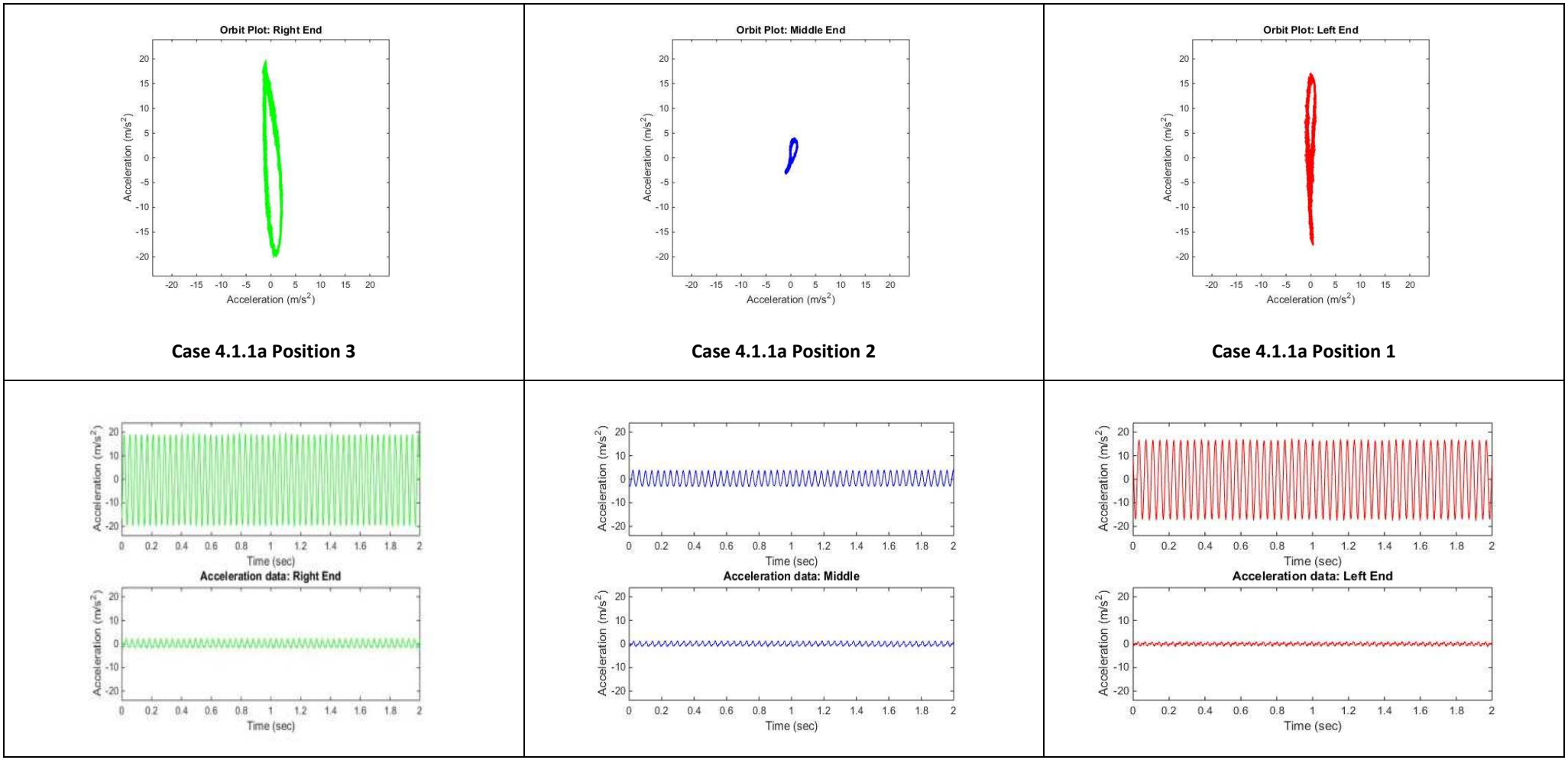

Figure 4.15 Orbit plots and acceleration graphs (X – lower graph, Y-upper graph) 4.1.1a

Table 4.6 Test parameters of screen test Case 4.1.1b with both vibrators rotating in the same direction

	Unit	Value
Moment of Inertia	kgm^2	1.9544
Vibrator Static Moment (each)]	kgm	$1387.8e^{-5}$
The phase difference of	deg	180
Distance of left exciter centre to the centre of mass	m	0.162779
Distance of right exciter centre to the centre of mass	m	0.162779
Vibrator rotational speed	rpm/Hz	570/9.5
Mass of the setup	kg	24.7

$$\frac{\mathrm{Mr}^2}{\mathrm{I}} = 0.33 < 2 \; - \; \text{conditions for self} - \text{sychronised circular motion not met}$$

Table 4.7 Orbit Plots and Acceleration Amplitude results for test Case 4.1.1b with both vibrators rotating in the same direction

Value	Unit	Position 3	Position 2	Position 1
Acceleration in Y Direction	mm/s^2	5	2	5
Acceleration in X Direction	mm/s^2	2	1.5	1.5

Case 4.1.1b is shown in Figure 4.16 with both vibrators rotating in the same direction at the reduced speed of 9.5 Hz. Difference between cases 4.1.1 and 4.1.1a and 4.1.b was the vibrators rotating speed only. The phase difference of 180 degrees was clearly shown on the Figure 4.16 and also on the graphs showing the sinusoidal response. The testing rig was moving in a rocking motion with the pivot point again at the centre of mass outside the physical body of the testing rig. The running speed very close to one of the natural frequencies of the testing rig was selected on purpose to check the influence of the resonance on the self-synchronisation. After the test, the conclusion was that it doesn't make any difference. To be more precise, the resonance region is where the equipment can still operate. Even with power to one of the vibrators turned off, both vibrators were operating without any noticeable difference in

behaviour. Most likely the current draw increased in the vibrator which was still powered and possibly there was a small change in phase. The vibration originating from the testing rig working in the resonance region is clearly visible on the graphs in the Figure 4.17, especially on the orbit plots.

Resonance can be induced by low or high frequency excitation, namely subharmonic and superharmonic resonance phenomena. 'Traditional' vibrational resonance appears in a continuous region when the subharmonic and superharmonic resonances occur in some discrete regions only. Some research is showing that both subharmonic and superharmonic resonance are not only integer multiples of the low frequency (Yang et al., 2016, and Mi Han et al., 2002).

Taking also into account that the waveforms are very rarely a pure sine wave, there are many more reasons why extra harmonics appear on the spectrum, including, looseness, misalignment, bearing wear, gear faults, nonlinearity.

There will therefore be harmonics visible on other graphs in different testing cases but they will not be taken into account unless it would affect the self-synchronisation of the vibrators.

Vibrating screens should never work at/or very close to the natural frequency as it can result in structural damage to the vibrating screen and therefore operating close to the resonance condition will not be considered in the research. During the startup the screen will go through the natural frequencies but because of the short time the frequencies don't get excited. Similar process happens during a rundown where normally only some of the rigid body motion frequencies will create excessive screen movement but again it doesn't make any difference to the self-synchronisation of vibrators.

Figure 4.16 Case 4.1.1b Setup

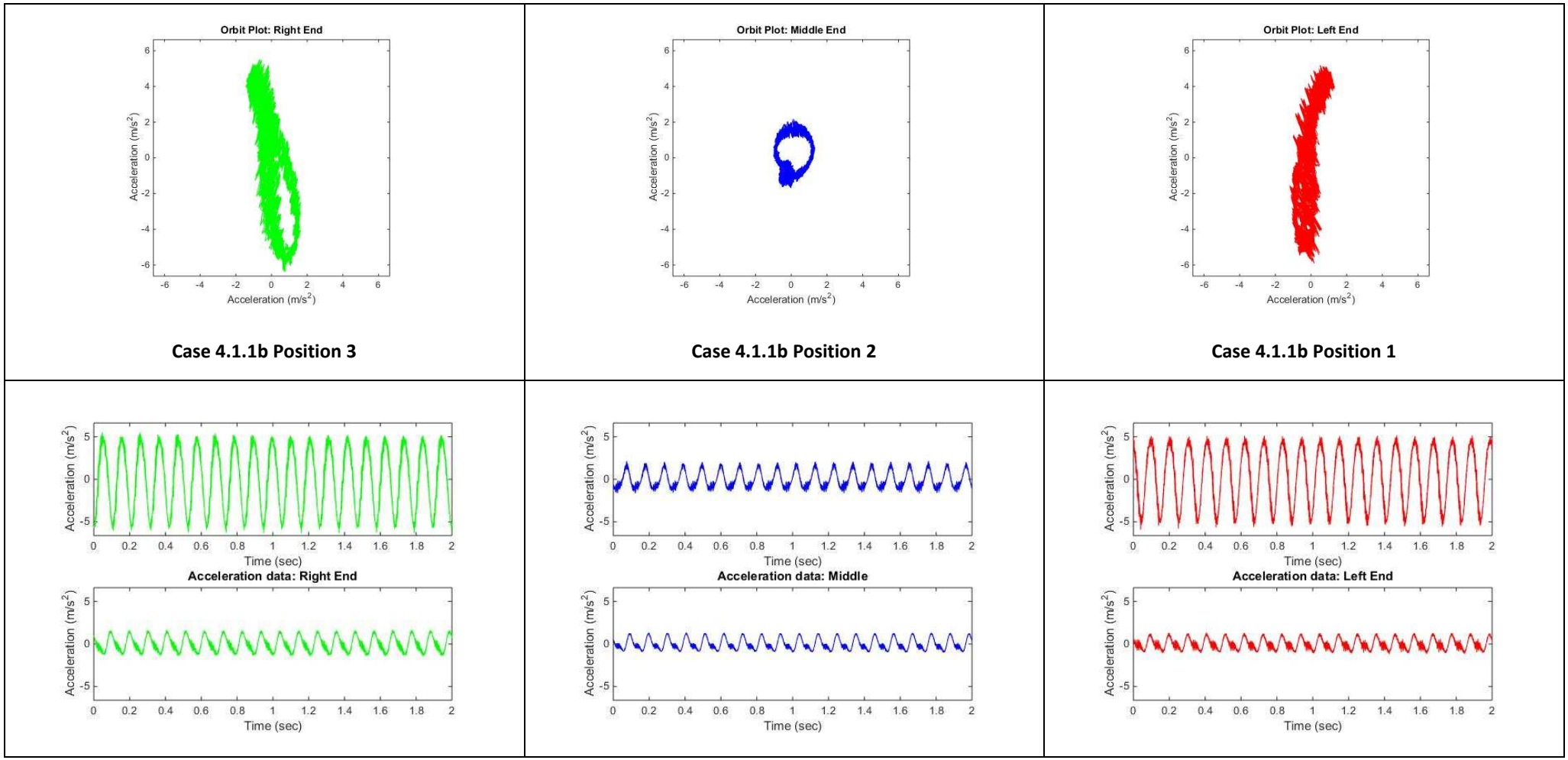

Figure 4.17 Orbit plots and acceleration graphs (X – lower graph, Y-upper graph) for case 4.1.1b

Table 4.8 Test parameters of screen test Case 4.1.2 with both vibrators rotating in the same direction

	Unit	Value
Moment of Inertia	kgm^2	1.9544
Vibrator Static Moment (each)]	kgm	$1387.8e^{-5}$
The phase difference of	deg	180
Distance of left exciter centre to the centre of mass	m	0.162779
Distance of right exciter centre to the centre of mass	m	0.162779
Vibrator rotational speed	rpm/Hz	570/9.5
Mass of the setup	kg	24.7

$$\frac{Mr^2}{I} = 0.33 < 2 \; - \; \text{conditions for self} - \text{sychronised circular motion not met}$$

Table 4.9 Orbit Plots and Acceleration Amplitude results for test Case 4.1.2 with both vibrators rotating in the same direction

Value	Unit	Position 3	Position 2	Position 1
Acceleration in Y Direction	mm/s^2	25	5	25
Acceleration in X Direction	mm/s^2	2	2	8

Case 4.1.2 is shown in Figure 4.18 with both vibrators rotating in the same direction at 9.5 Hz. Difference between cases 4.1.1, 4.1.1a and 4.1.b was the vibrators rotating speed only. Case 4.1.2 has the vibrators shifted outwards from the centre of mass. The resulting phase difference of 180 degrees was also clearly shown on Figure 4.18 and also on the graphs showing the sinusoidal response. Again the testing rig was moving in a rocking motion with pivot point at the centre of mass outside the physical body of the testing rig. The running speed very close to one of the natural frequencies of the testing rig was again selected on purpose to check the influence of the resonance on self-synchronisation. Again the test conclusion was that it doesn't make any difference.

Even with power to one of the vibrators turned off, both vibrators remained operating without any noticeable difference. Most likely the current draw increased in the vibrator which was still powered and possibly there was a small change in phase. The vibration from the testing rig working in the resonance region is clearly visible on the graphs on the Figure 4.19, especially on the orbit plots.

Figure 4.18 Case 4.1.2 Setup

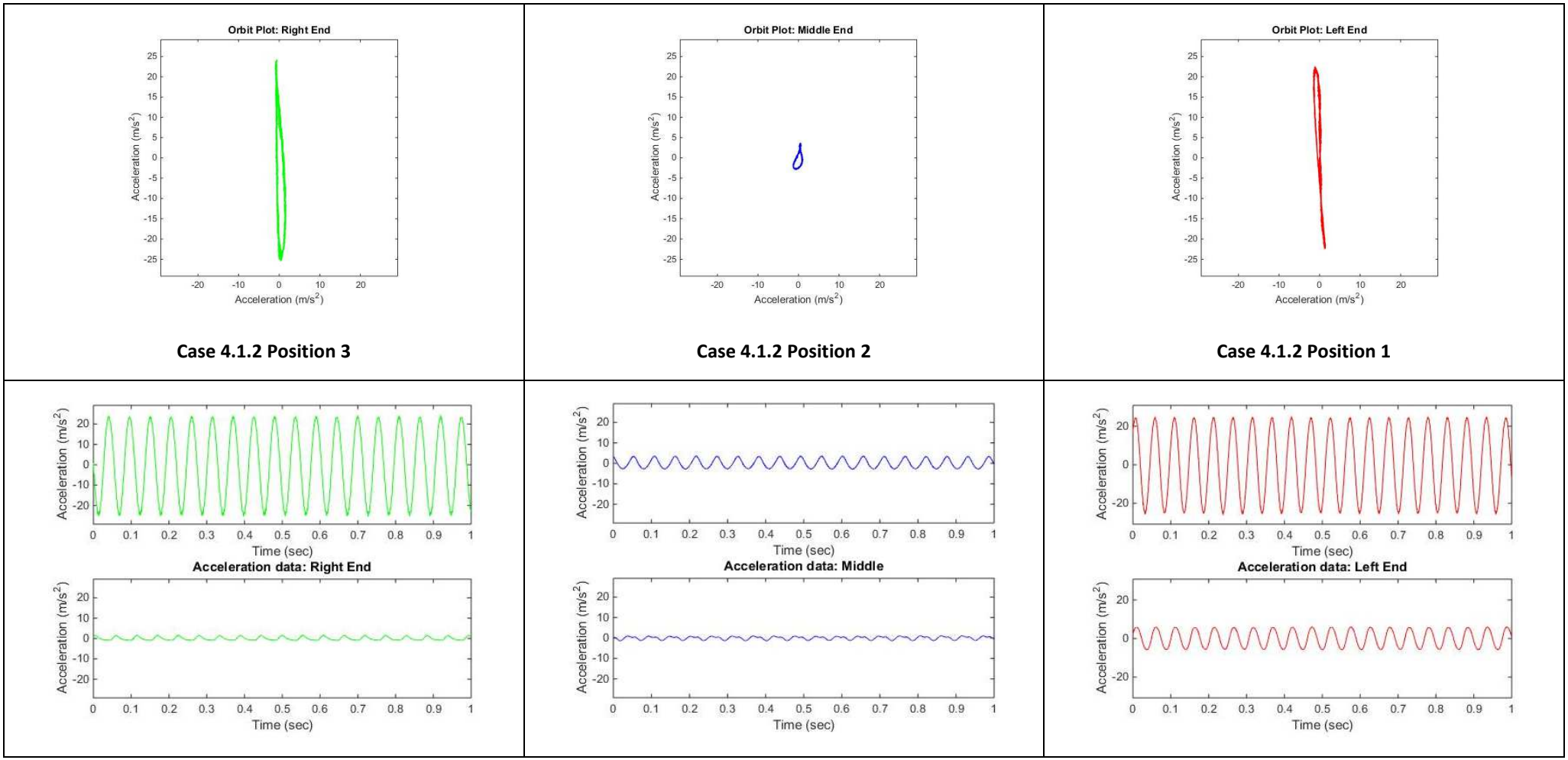

Figure 4.19 Orbit plots and acceleration graphs (X – lower graph, Y-upper graph) for case 4.1.2

Table 4.10 Test parameters of screen test Case 4.1.3 with both vibrators rotating in the same direction

	Unit	Value
Moment of Inertia	kgm^2	3.977
Vibrator Static Moment (each)	kgm	$1387.8e^{-5}$
The phase difference of	deg	180
Distance of left exciter centre to the centre of mass	m	0.523516
Distance of right exciter centre to the centre of mass	m	0.523516
Vibrator rotational speed	rpm/Hz	1060/19.08
Mass of the setup	kg	24.7

$$\frac{Mr^2}{I} = 1.68 < 2 \; - \; \text{conditions for self} - \text{sychronised circular motion not met}$$

Table 4.11 Orbit Plots and Acceleration Amplitude results for test Case 4.1.3 with both vibrators rotating in the same direction

Value	Unit	Position 3	Position 2	Position 1
Acceleration in Y Direction	mm/s^2	23	10	22
Acceleration in X Direction	mm/s^2	10	8	7

Case 4.1.3 is shown in Figure 4.20 with both vibrators rotating in the same direction at 19.08 Hz. For this case study, the vibrators have been repositioned to the outer side of the beam. The phase difference of 180 degrees was clearly shown on the Figure 4.20 and also on the graphs showing the sinusoidal signal with acceleration in Figure 4.21. The orbit plots and acceleration values are also shown in Figure 4.21. The testing rig was again moving in a rocking motion with pivot point at the centre of mass outside the physical body of the testing rig. It is interesting to see the comparison between cases 4.1.2 and 4.1.3, as even though the latter is running with higher frequency, the acceleration amplitude in the Y direction dropped down for positions 1 and 3 but the acceleration in X direction increased significantly in all locations. Acceleration at position 2 increased 4 times just by changing the locations of the vibrators from 10-2 to 11-1. One of the vibrators was turned off and both vibrators kept running with no discernible difference to the movement of the testing rig.

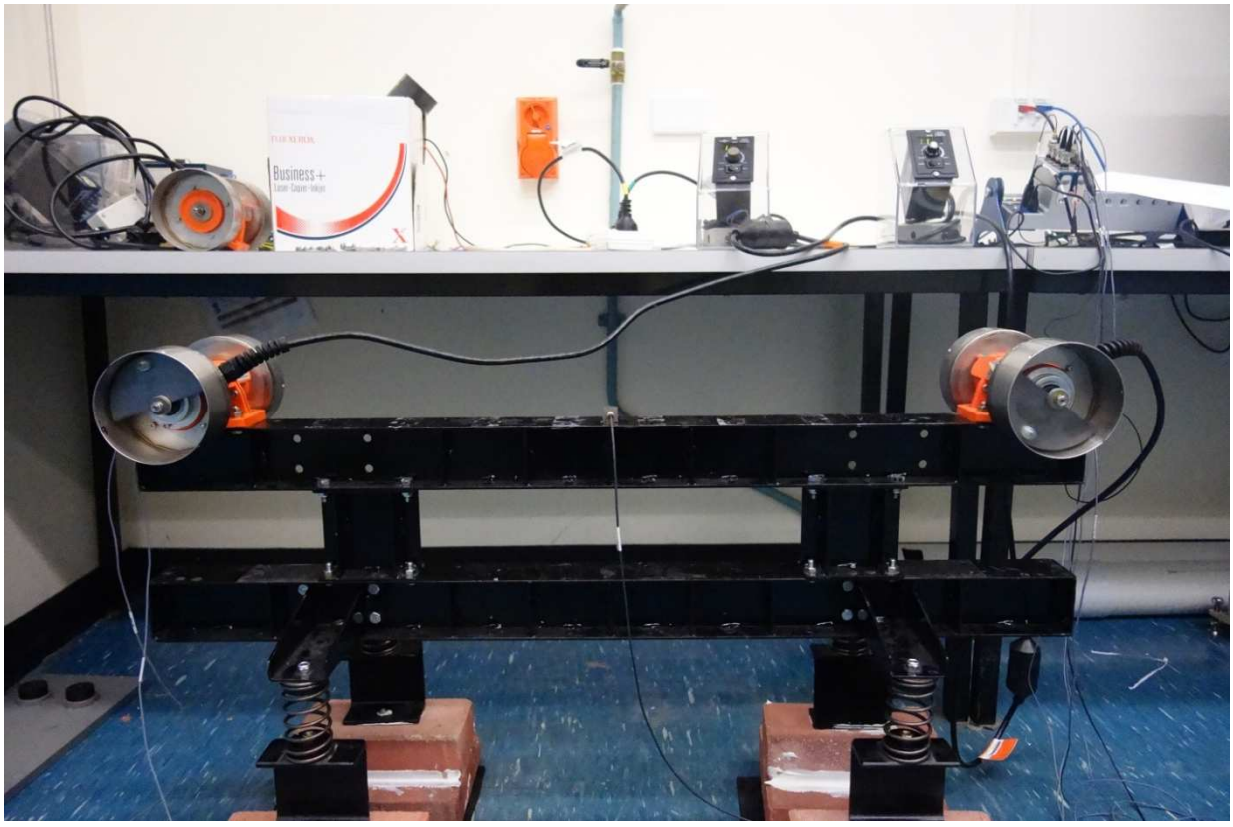

Figure 4.20 Case 4.1.3 Setup

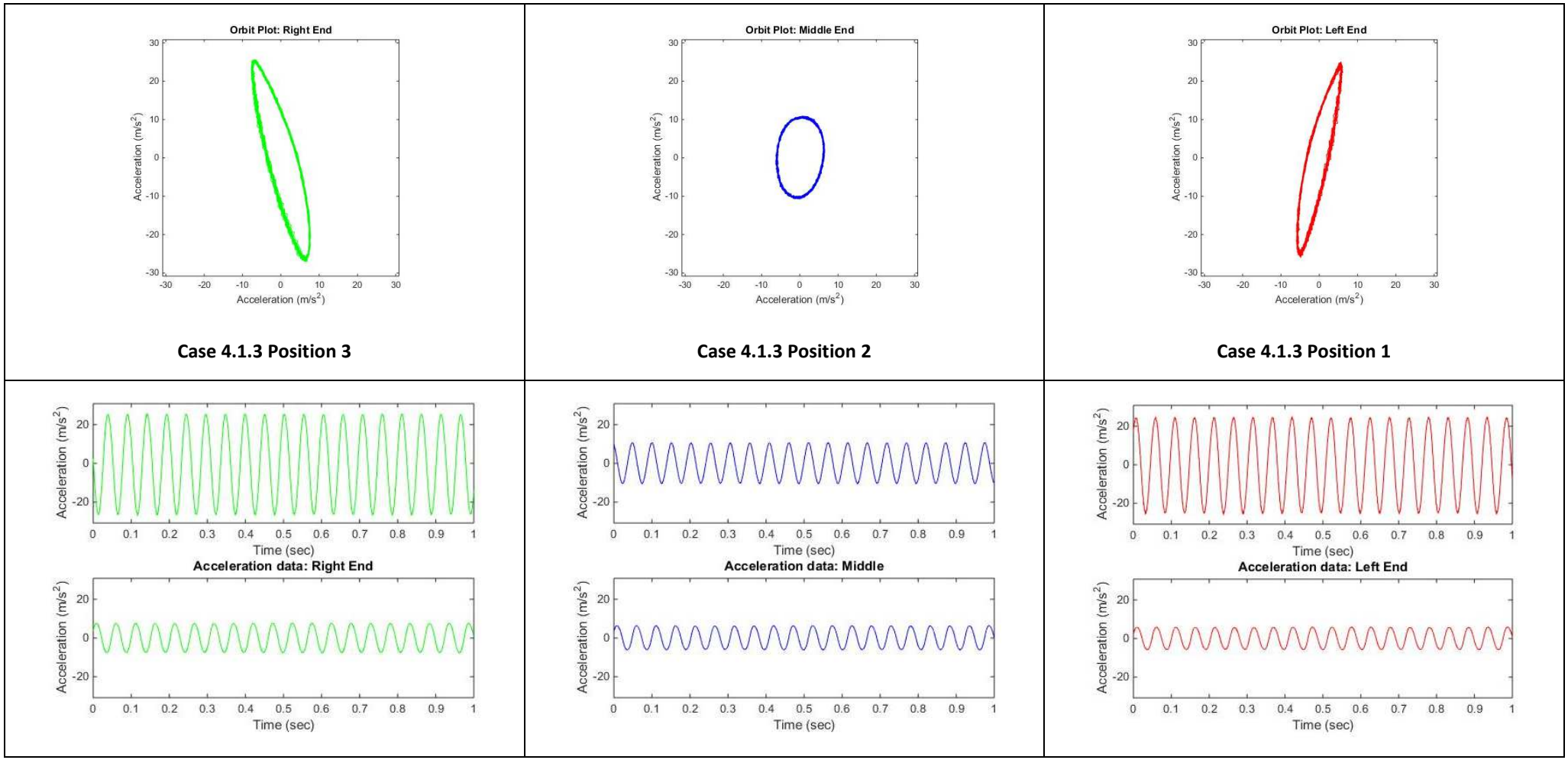

Figure 4.21 Orbit plots and acceleration graphs (X – lower graph, Y-upper graph) for case 4.1.3

Table 4.12 Test parameters of screen test Case 4.1.4 with both vibrators rotating in the same direction

	Unit	Value
Moment of Inertia	kgm^2	2.165
Vibrator Static Moment (each)]	kgm	$1387.8e^{-5}$
The phase difference of	deg	180
Distance of left exciter centre to the centre of mass	m	0.092465
Distance of right exciter centre to the centre of mass	m	0.092465
Vibrator rotational speed	rpm/Hz	1450/24.2
Mass of the setup	kg	24.7

$$\frac{Mr^2}{I} = 0.1 < 2 \; - \; \text{conditions for self} - \text{sychronised circular motion not met}$$

Table 4.13 Orbit Plots and Acceleration Amplitude results for test Case 4.1.4 with both vibrators rotating in the same direction

Value	Unit	Position 3	Position 2	Position 1
Acceleration in Y Direction	mm/s^2	20	3	20
Acceleration in X Direction	mm/s^2	4	7	3

Case 4.1.4 is shown in Figure 4.22 with both vibrators rotating in the same direction at 24.2 Hz. The vibrators here are located on the lower beam. Again the phase difference of 180 degrees was clearly shown on the Figure 4.22 and also on the graphs showing the sinusoidal signal with acceleration and orbit plots in Figure 4.23. The testing rig was moving in a rocking motion with the pivot point at the centre of mass outside the physical body of the testing rig. Moving the vibrators closer to the centre of mass made the acceleration in position 2 bigger than in cases with vibrators moved to the outside of the testing rig. One of the vibrators was turned off and both vibrators still kept running with no difference to the movement of the testing rig.

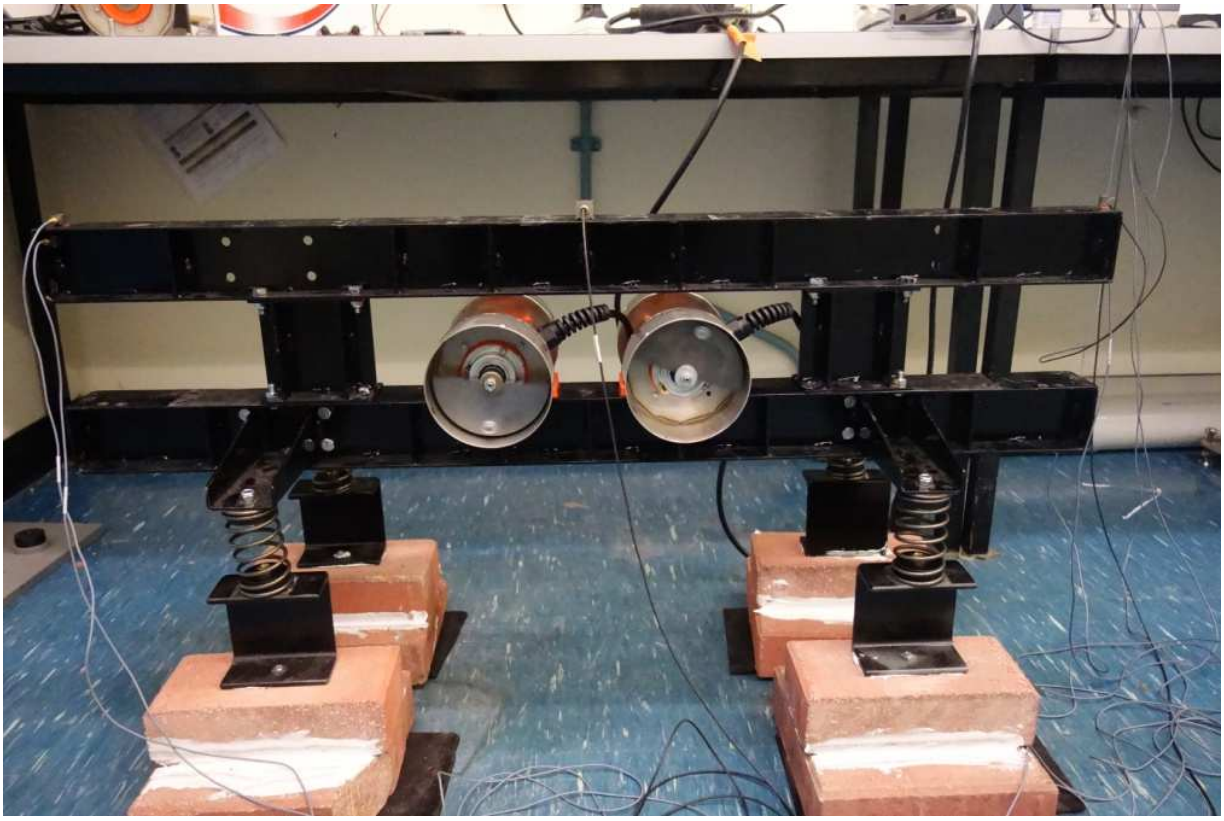

Figure 4.22 Case 4.1.4 Setup

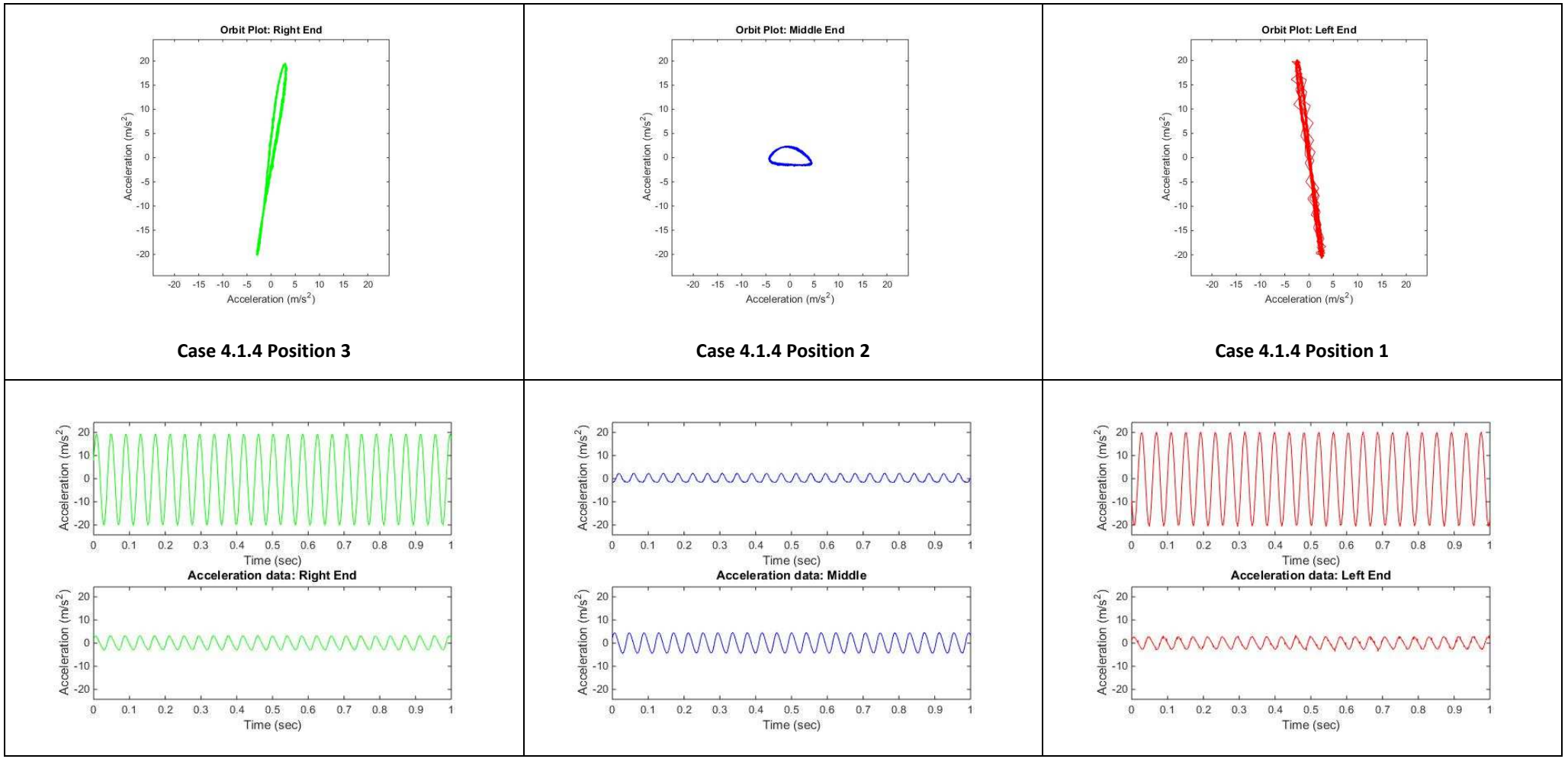

Figure 4.23 Orbit plots and acceleration graphs (X – lower graph, Y-upper graph) for case 4.1.4

Table 4.14 Test parameters of screen test Case 4.1.5 with both vibrators rotating in the same direction

	Unit	Value
Moment of Inertia	kgm^2	3.813
Vibrator Static Moment (each)]	kgm	$1387.8e^{-5}$
The phase difference of	deg	180
Distance of left exciter centre to the centre of mass	m	0.506085
Distance of right exciter centre to the centre of mass	m	0.506085
Vibrators rotational speed	rpm/Hz	1460/24.3
Mass of the setup	kg	24.7

$$\frac{Mr^2}{I} = 1.66 < 2 \; - \; \text{conditions for self} - \text{sychronised circular motion not met}$$

Table 4.15 Orbit Plots and Acceleration Amplitude results for test Case 4.1.5 with both vibrators rotating in the same direction

Value	Unit	Position 3	Position 2	Position 1
Acceleration in Y Direction	mm/s^2	50	5	50
Acceleration in X Direction	mm/s^2	15	10	15

Case 4.1.5 is shown in Figure 4.24 with both vibrators rotating in the same direction at 24.3 Hz. The vibrators were located on the lower beam at the extreme ends. The phase difference of 180 degrees was clearly shown in Figure 4.24 and also on the graphs showing the sinusoidal signal with acceleration and orbit plots presented in Figure 4.25. Again, the testing rig was moving in a rocking motion with pivot point at the centre of mass outside the physical body of the testing rig.

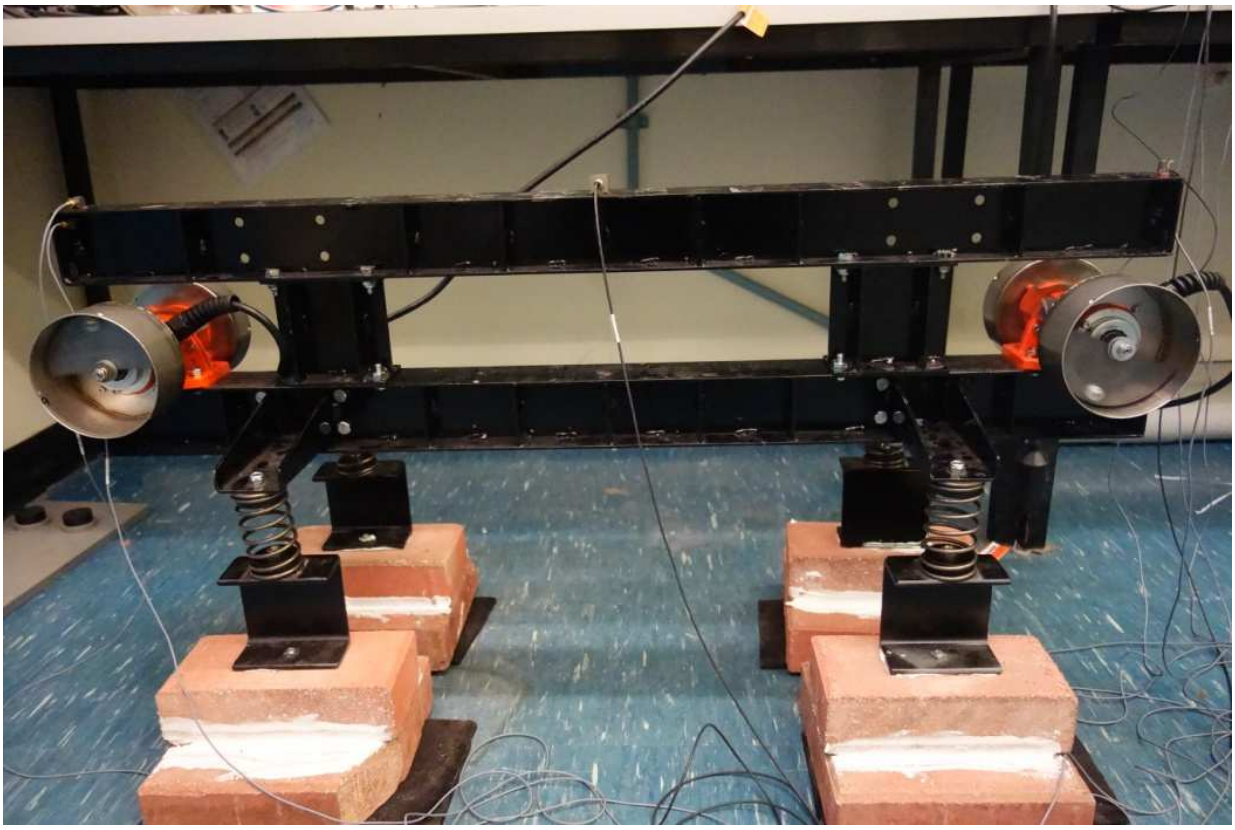

Figure 4.24 Case 4.1.5 Setup

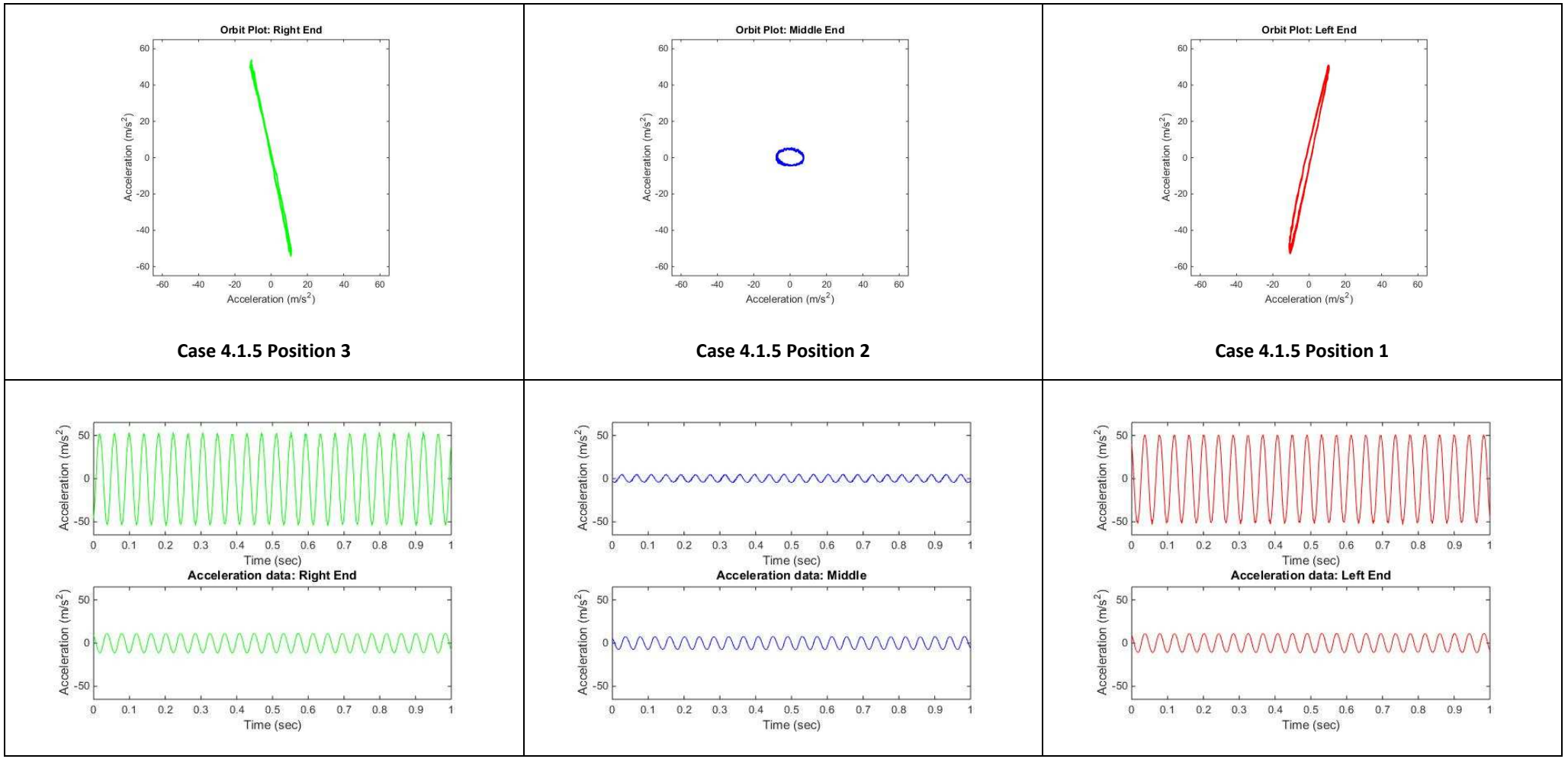

Figure 4.25 Orbit plots and acceleration graphs (X – lower graph, Y-upper graph) for case 4.1.5

Table 4.16 Test parameters of screen test Case 4.1.5a with both vibrators rotating in the same direction

	Unit	Value
Moment of Inertia	kgm^2	3.813
Vibrator Static Moment (each)]	kgm	$1387.8e^{-5}$
The phase difference of	deg	180
Distance of left exciter centre to the centre of mass	m	0.506085
Distance of right exciter centre to the centre of mass	m	0.506085
Vibrators rotational speed	rpm/Hz	1460/24.3
Mass of the setup	kg	24.7

$$\frac{\mathrm{Mr}^2}{\mathrm{I}} = 1.66 < 2 \; - \; \text{conditions for self} - \text{sychronised circular motion not met}$$

Table 4.17 Orbit Plots and Acceleration Amplitude results for test Case 4.1.5a with both vibrators rotating in the same direction

Value	Unit	Position 3	Position 2	Position 1
Acceleration in Y Direction	mm/s^2	50	5	50
Acceleration in X Direction	mm/s^2	8	12	8

Case 4.1.5a is shown in Figure 4.26 with both vibrators rotating in the same direction at 24.3 Hz. The vibrators were located on the lower beam at extreme ends. The difference between cases 4.1.5 and 4.1.5a is that the power supply to one of the vibrators was turned off. The phase difference of 180 degrees was clearly shown in Figure 4.26 and also on the graphs showing the sinusoidal signal with acceleration in Figure 4.27. Orbit plots and acceleration values are shown in Figure 4.27. Amplitude of acceleration remained the same in Y direction, it got reduced in X direction at positions 1 and 3 but slightly increased in position 2. The testing rig was moving in a rocking motion with the pivot point at the centre of mass outside the physical body of the testing rig. With one of the vibrators turned off, both vibrators kept running with only minimal difference to the movement of the testing rig. There were no changes in the amplitudes, however the angle of the stroke at positions 1 and 3 have changed.

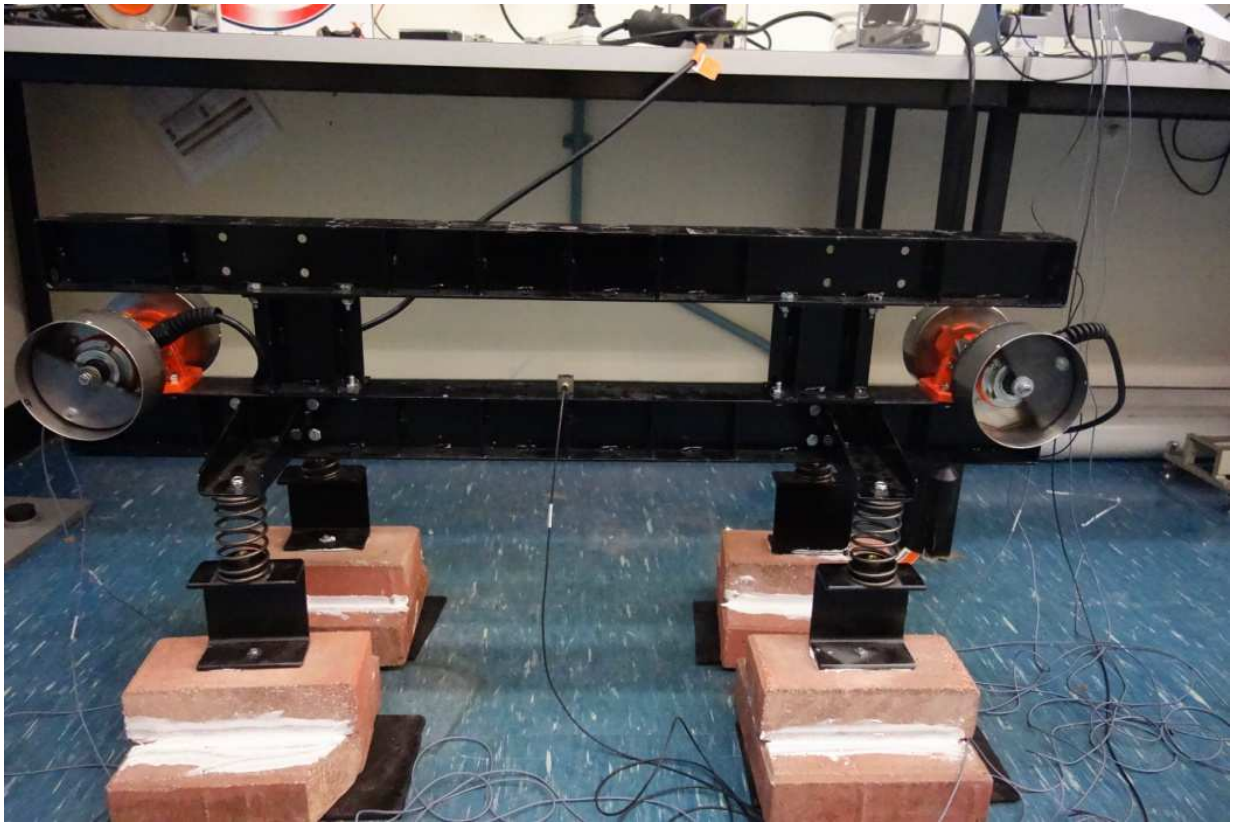

Figure 4.26 Case 4.1.5a Setup

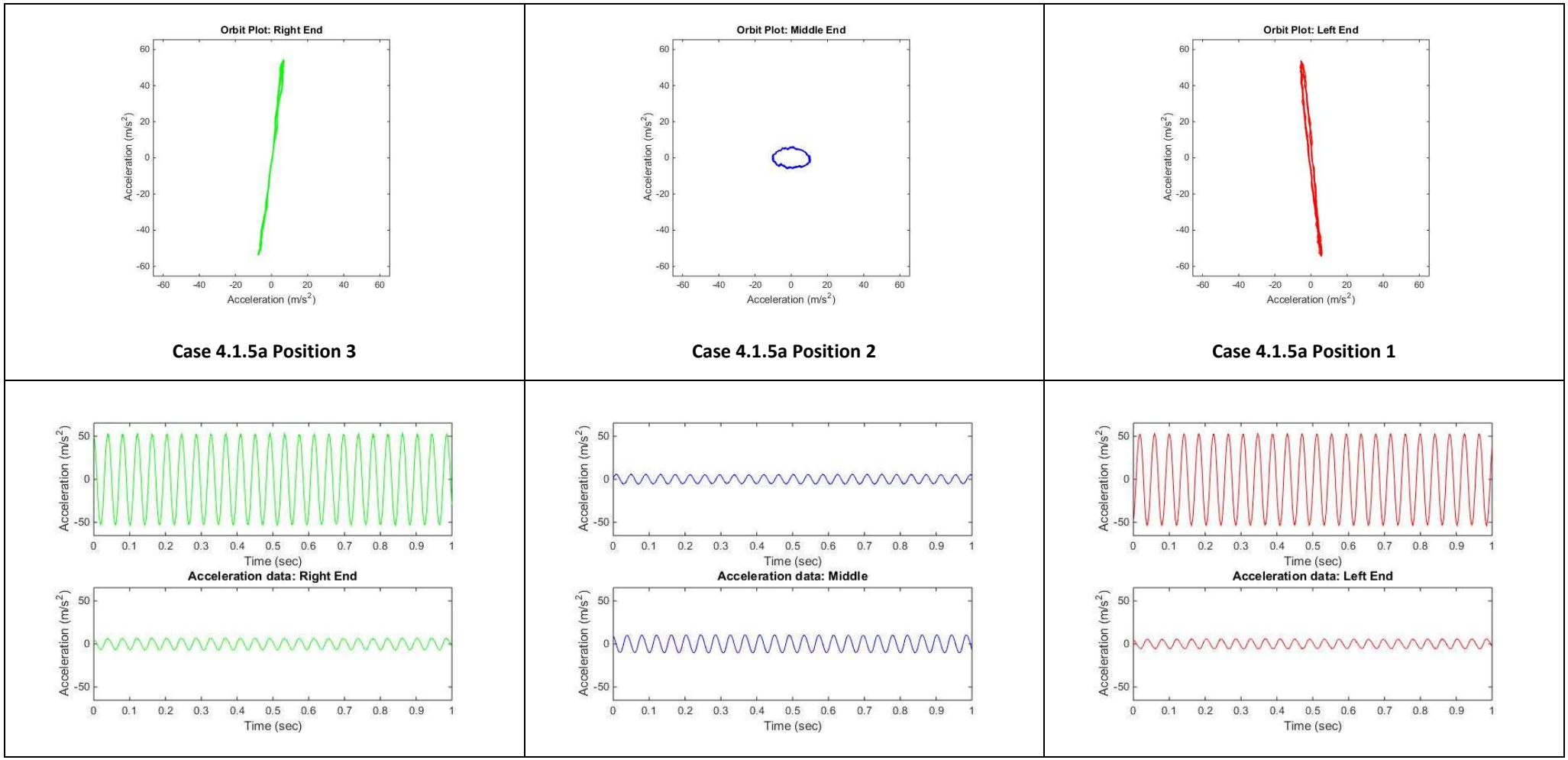

Figure 4.27 Orbit plots and acceleration graphs (X – lower graph, Y-upper graph) for case 4.1.5a

Table 4.18 Test parameters of screen test Case 4.1.6 with both vibrators rotating in the same direction

	Unit	Value
Moment of Inertia	kgm^2	2.791
Vibrator Static Moment (each)]	kgm	1387.8e-5
The phase difference of	deg	180
Distance of left exciter centre to the centre of mass	m	0.173456
Distance of right exciter centre to the centre of mass	m	0.323026
Vibrators rotational speed	rpm/Hz	1300/20.66
Mass of the setup	kg	24.7

$$\frac{\mathrm{Mr}^2}{\mathrm{I}} = 0.55 < 2 \; - \; \text{conditions for self} - \text{sychronised circular motion not met}$$

Table 4.19 Orbit Plots and Acceleration Amplitude results for test Case 4.1.6 with both vibrators rotating in the same direction

Value	Unit	Position 3	Position 2	Position 1
Acceleration in Y Direction	mm/s^2	12	3	10
Acceleration in X Direction	mm/s^2	2	2	3

Case 4.1.6 is shown in Figure 4.28 with both vibrators rotating in the same direction at 20.66 Hz. The difference to the previously presented cases is the asymmetric position of the vibrators about the axis of symmetry of the testing rig. The vibrators here are positioned on the upper beam with both vibrators on the right of the centre of the testing rig. The phase difference of 180 degrees is clearly shown in the Figure 4.28 and also on the graphs showing the sinusoidal signal with acceleration in Figure 4.29. The orbit plots and acceleration values are shown in Figure 4.29. Amplitude of acceleration is similar for the positions of accelerometers 1 and 3. The shape of the orbit in the position 2 changed from an elliptical shape to a figure eight shape. Testing rig was moving in a rocking motion with pivot point at the centre of mass outside the physical body of the testing rig. This confirmed that symmetry about the centre of mass or body of the testing rig is not a condition required for the synchronization.

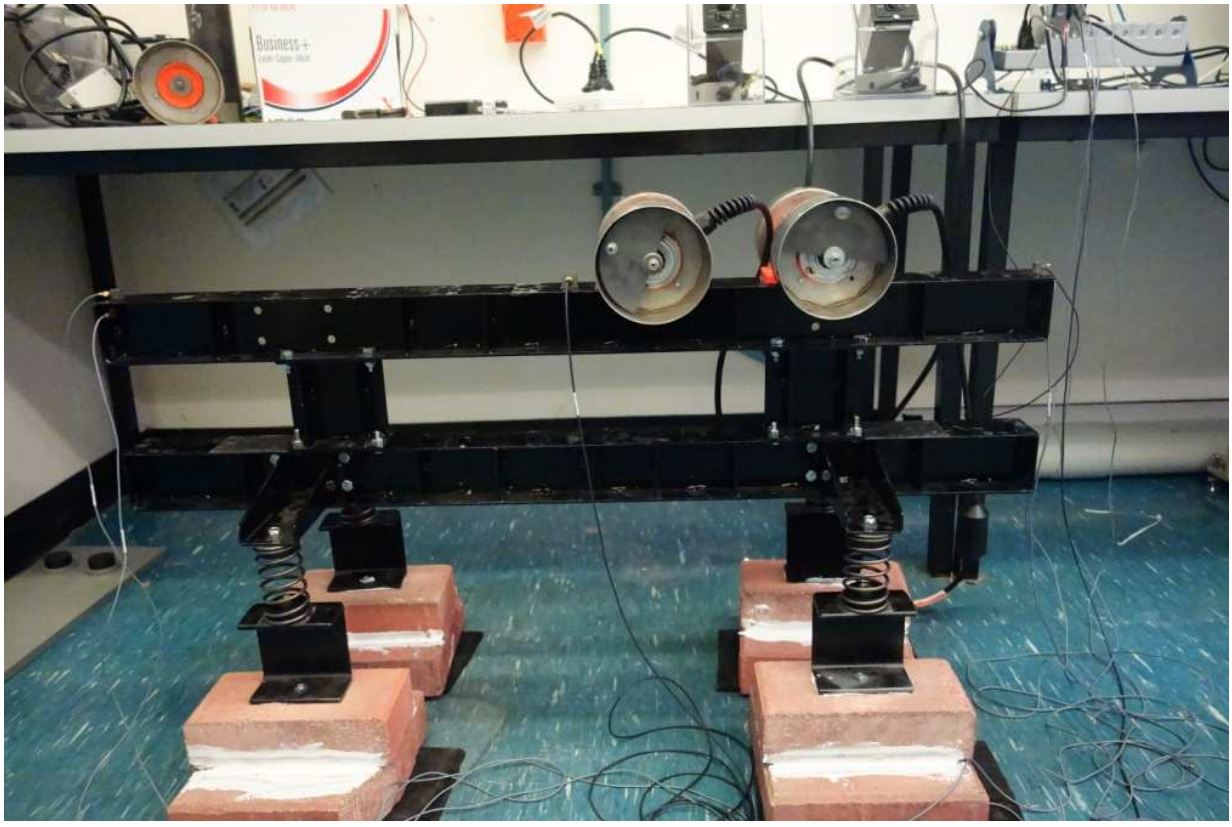

Figure 4.28 Case 4.1.6 Setup

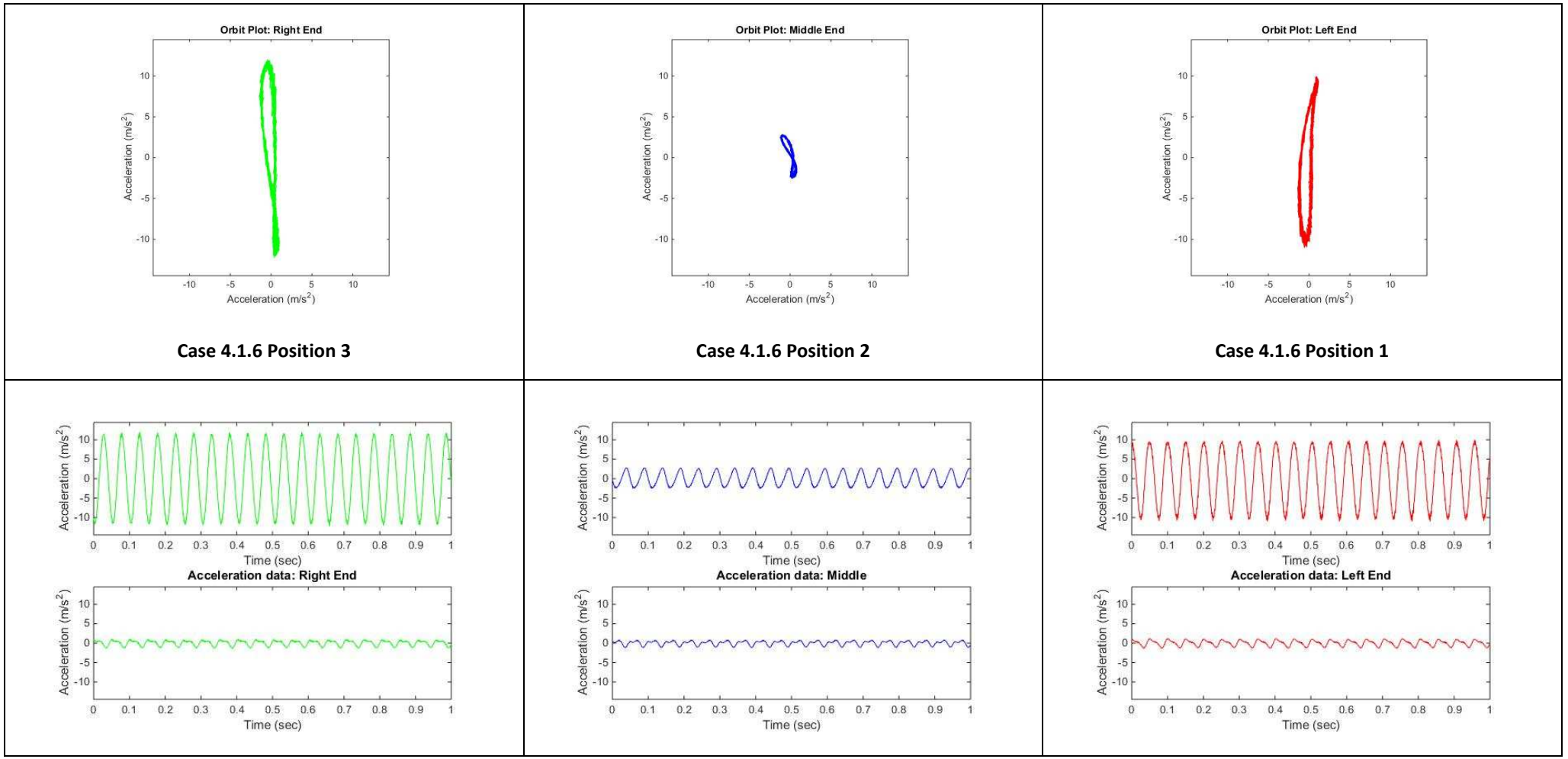

Figure 4.29 Orbit plots and acceleration graphs (X – lower graph, Y-upper graph) for case 4.1.6

Table 4.20 Test parameters of screen test Case 4.1.7 with both vibrators rotating in the same direction

	Unit	Value
Moment of Inertia	kgm^2	2.780
Vibrator Static Moment (each)]	kgm	1387.8e-5
The phase difference of	deg	180
Distance of left exciter centre to the centre of mass	m	0.327393
Distance of right exciter centre to the centre of mass	m	0.307205
Vibrators rotational speed	rpm/Hz	1060/17.66
Mass of the setup	kg	24.7

$$\frac{\mathrm{Mr}^2}{\mathrm{I}} = 0.89 < 2 \; - \; \text{conditions for self} - \text{sychronised circular motion not met}$$

Table 4.21 Orbit Plots and Acceleration Amplitude results for test Case 4.1.7 with both vibrators rotating in the same direction

Value	Unit	Position 3	Position 2	Position 1
Acceleration in Y Direction	mm/s^2	35	3	35
Acceleration in X Direction	mm/s^2	10	10	10

Case 4.1.7 is shown in Figure 4.30 with both vibrators rotating in the same direction at 17.66 Hz. For this case study, the vibrators have been positioned at an angle of 45 to the horizontal plane going through the centre of mass of the testing rig which is common for the vibrating drives of the vibrating screens. The phase difference of 180 degrees is clearly shown in Figure 4.30 and also on the graphs showing the sinusoidal signal with acceleration in Figure 4.31. The orbit plots and acceleration values are presented in Figure 4.31. The amplitude of acceleration in the X direction was the same for all positions. The same amplitude size for the accelerometers at positions 1 and 3 was observed, but with smaller amplitude in position 2. The testing rig was moving in a rocking motion with pivot point at the centre of mass outside the physical body of the testing rig.

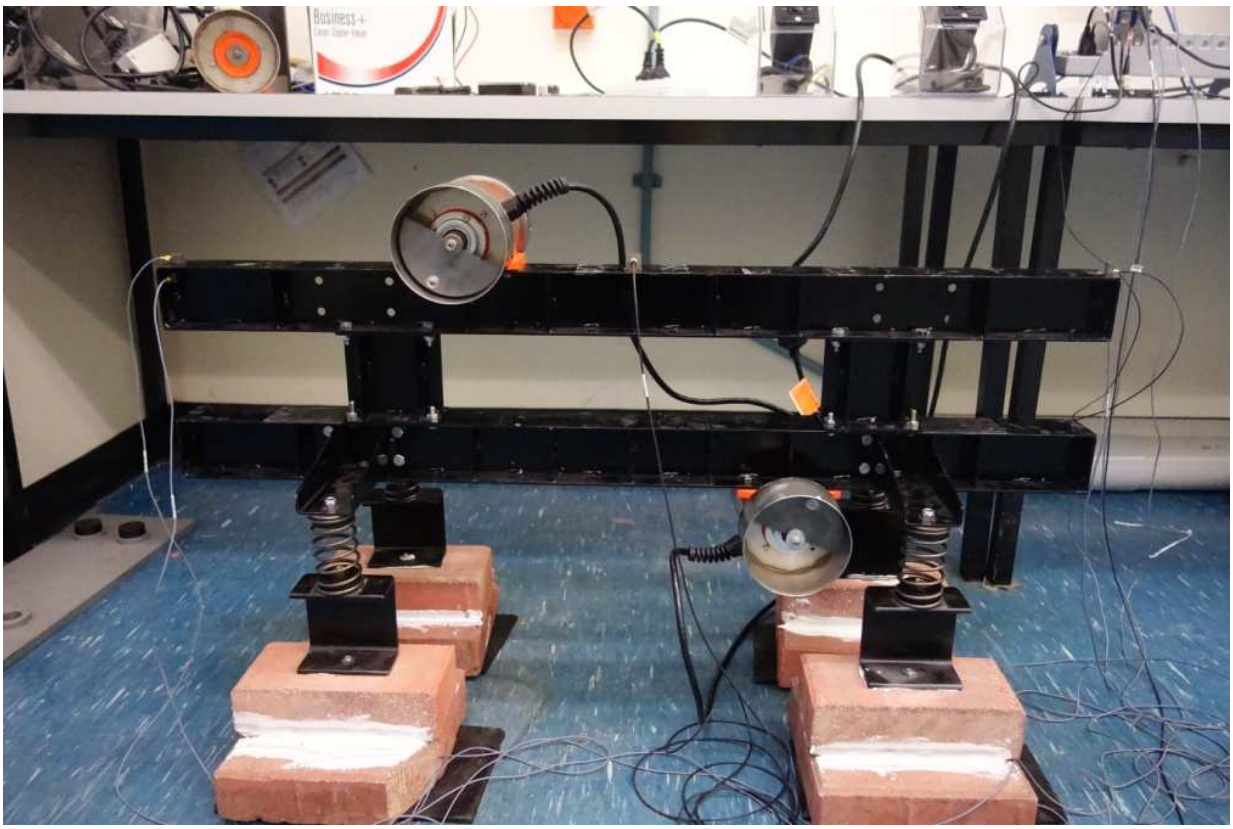

Figure 4.30 Case 4.1.7 Setup

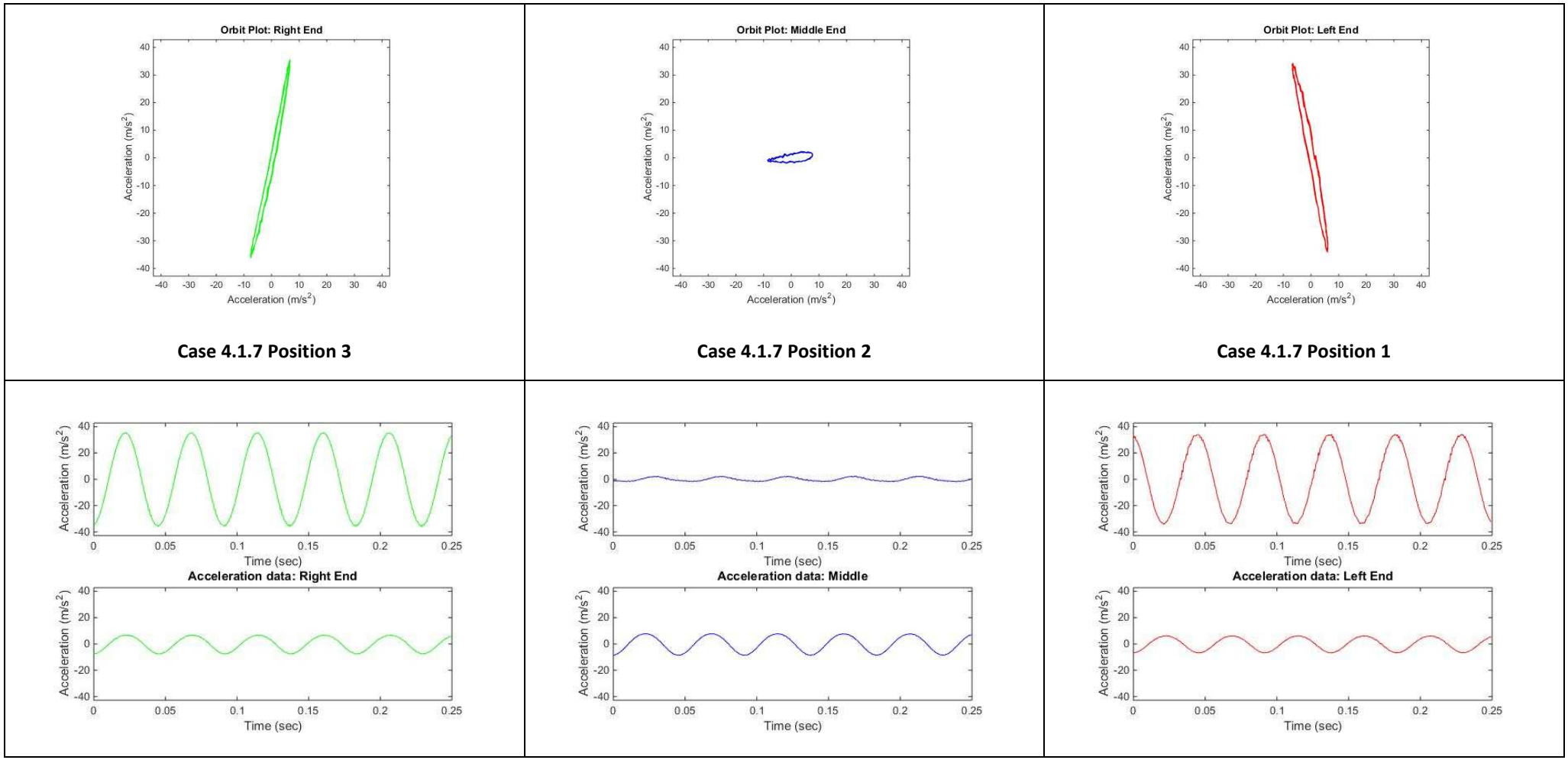

Figure 4.31 Orbit plots and acceleration graphs (X – lower graph, Y-upper graph) for case 4.1.7

Table 4.22 Test parameters of screen test Case 4.1.8 with both vibrators rotating in the same direction

	Unit	Value
Moment of Inertia	kgm^2	1.365
Vibrator Static Moment (each)]	kgm	$1387.8e^{-5}$
The phase difference of	deg	180
Distance of left exciter centre to the centre of mass	m	0.101929
Distance of right exciter centre to the centre of mass	m	0.101929
Vibrators rotational speed	rpm/Hz	1550/25.8
Mass of the setup	kg	17.8

$$\frac{\mathrm{Mr}^2}{\mathrm{I}} = 0.135 < 2 \; - \; \text{conditions for self} - \text{sychronised circular motion not met}$$

Table 4.23 Orbit Plots and Acceleration Amplitude results for test Case 4.1.8 with both vibrators rotating in the same direction

Value	Unit	Position 3	Position 2	Position 1
Acceleration in Y Direction	mm/s^2	45	5	45
Acceleration in X Direction	mm/s^2	5	3	2

Case 4.1.8 is shown in Figure 4.30 with both vibrators rotating in the same direction at 25.88 Hz. The testing rig was modified with upper and vertical supports removed which reduced the mass by about 30%. Vibrators were repositioned to the centre of the beam. The phase difference of 180 degrees is clearly shown on the Figure 4.32 and also on the graphs showing the sinusoidal signal with acceleration in Figure 4.33. The orbit plots and acceleration values are shown in Figure 4.33. The amplitudes for accelerometers' positions 1 and 3 had the same value, with smaller amplitude for position 2. Again, the testing rig was moving in a rocking motion with pivot point at the centre of mass outside the physical body of the testing rig.

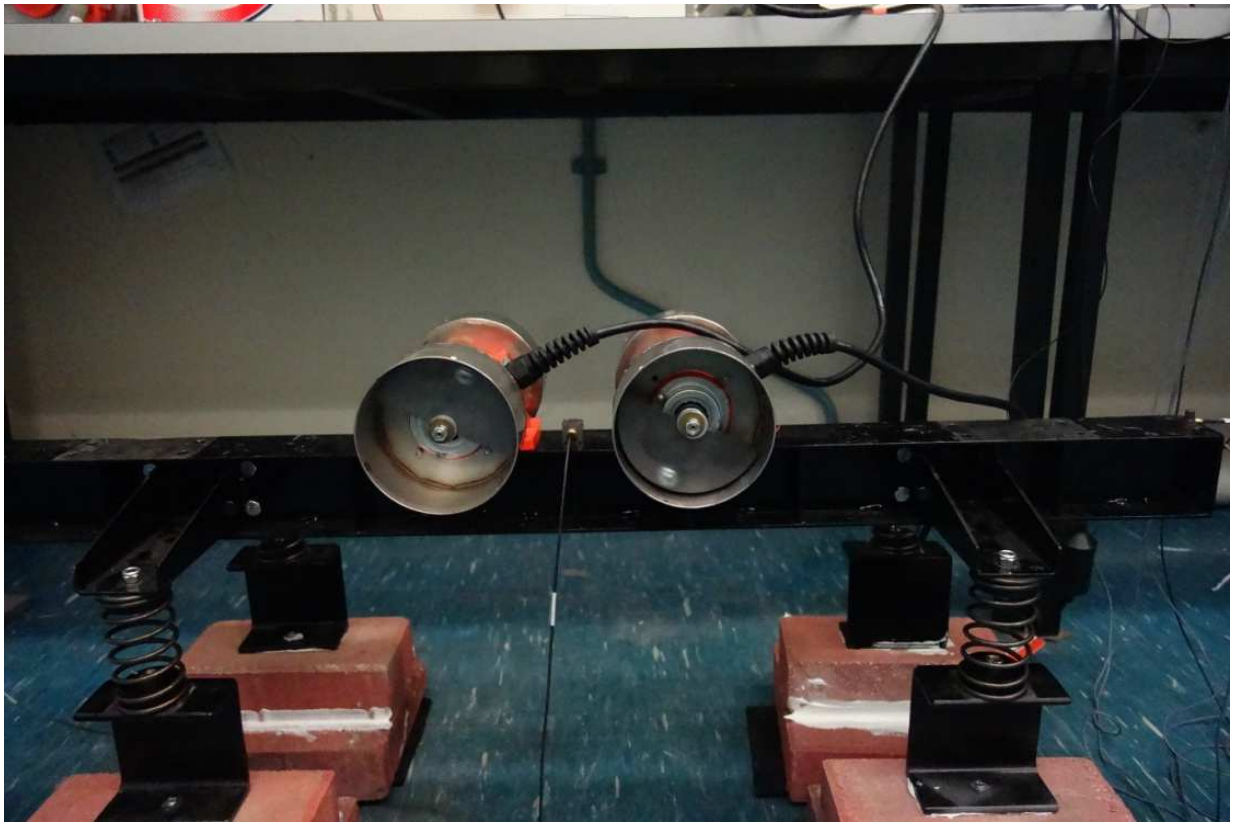

Figure 4.32 Case 4.1.8 Setup

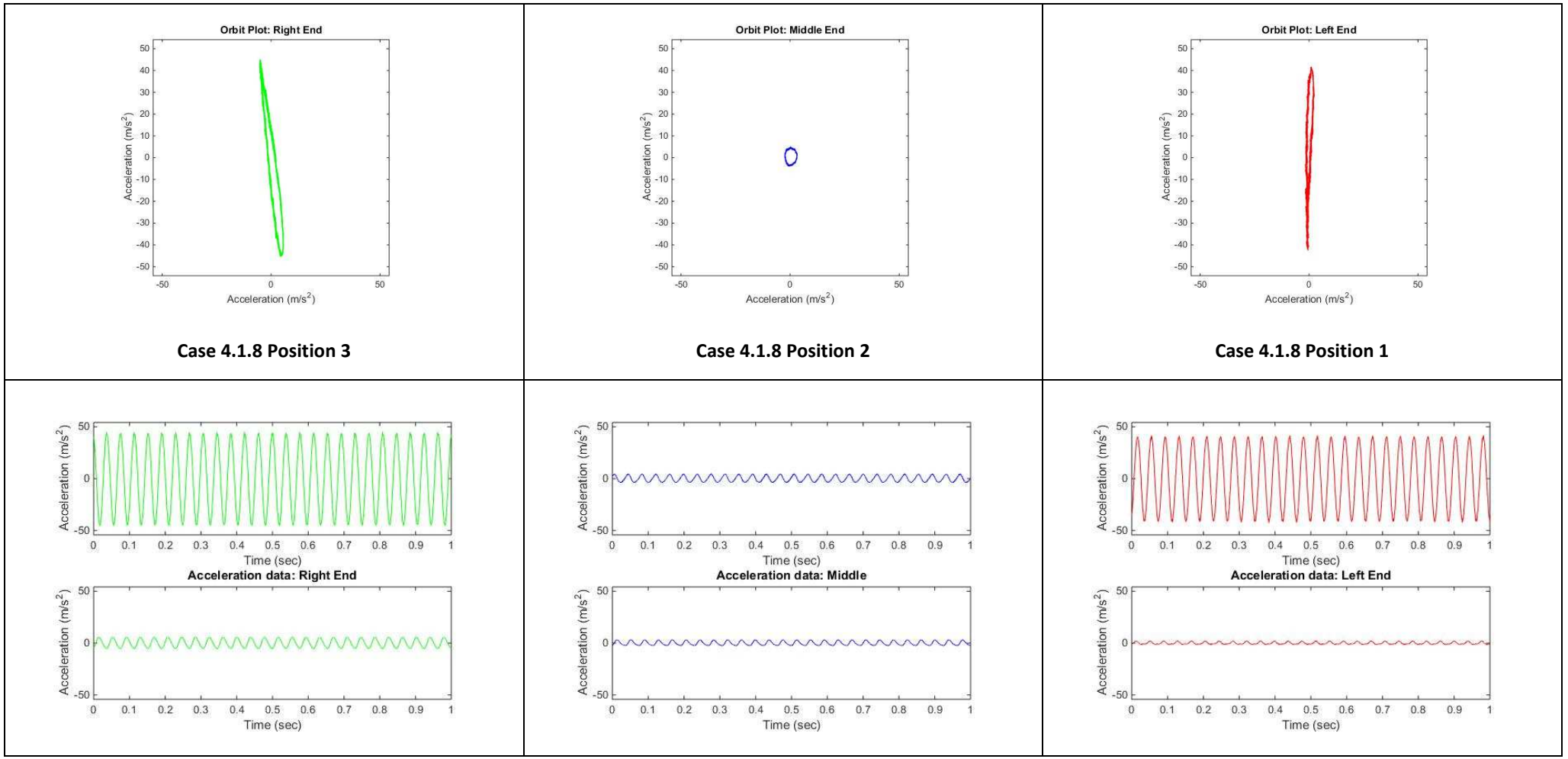

Figure 4.33 Orbit plots and acceleration graphs (X – lower graph, Y-upper graph) for case 4.1.8

Table 4.24 Test parameters of screen test Case 4.1.9 with both vibrators rotating in the same direction

	Unit	Value
Moment of Inertia	kgm^2	1.816
Vibrator Static Moment (each)	kgm	$1387.8e^{-5}$
The phase difference of	deg	180
Distance of left exciter centre to the centre of mass	m	0.279466
Distance of right exciter centre to the centre of mass	m	0.279466
Vibrators rotational speed	rpm/Hz	1550/25.88
Mass of the setup	kg	17.8

$$\frac{\mathrm{Mr}^2}{\mathrm{I}} = 0.76 < 2 \; - \; \text{conditions for self} - \text{sychronised circular motion not met}$$

Table 4.25 Orbit Plots and Acceleration Amplitude results for test Case 4.1.9 with both vibrators rotating in the same direction

Value	Unit	Position 3	Position 2	Position 1
Acceleration in Y Direction	mm/s^2	75	10	70
Acceleration in X Direction	mm/s^2	10	5	3

Case 4.1.9 is shown in Figure 4.34 with both vibrators rotating in the same direction at 25.88 Hz. Vibrating motors were spaced one set of holes wider in comparison to the previous case. The phase difference of 180 degrees was clearly shown on the Figure 4.34 and also on the graphs showing the sinusoidal signal with acceleration in Figure 4.35. The orbit plots and acceleration values are shown in Figure 4.35. Testing rig was moving in a rocking motion with pivot point at the centre of mass outside the physical body of the testing rig.

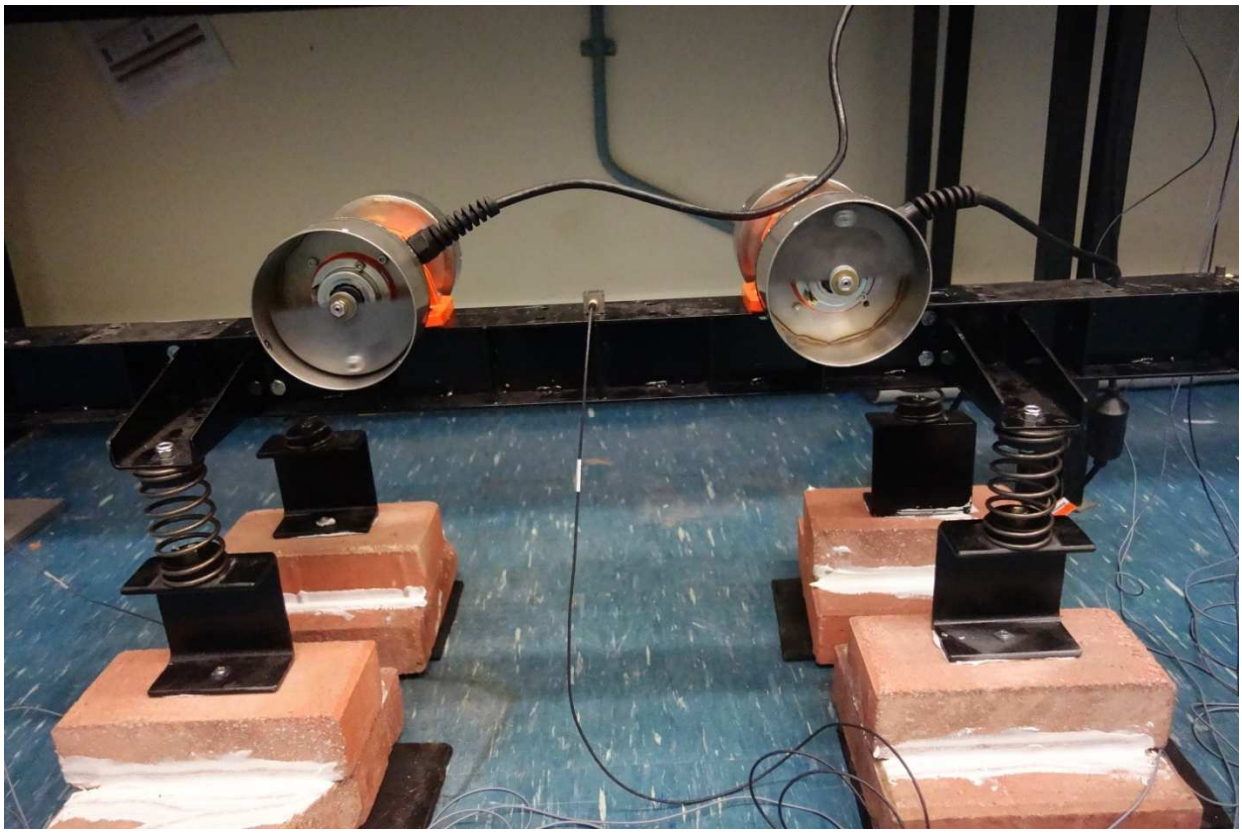

Figure 4.34 Case 4.1.9 Setup

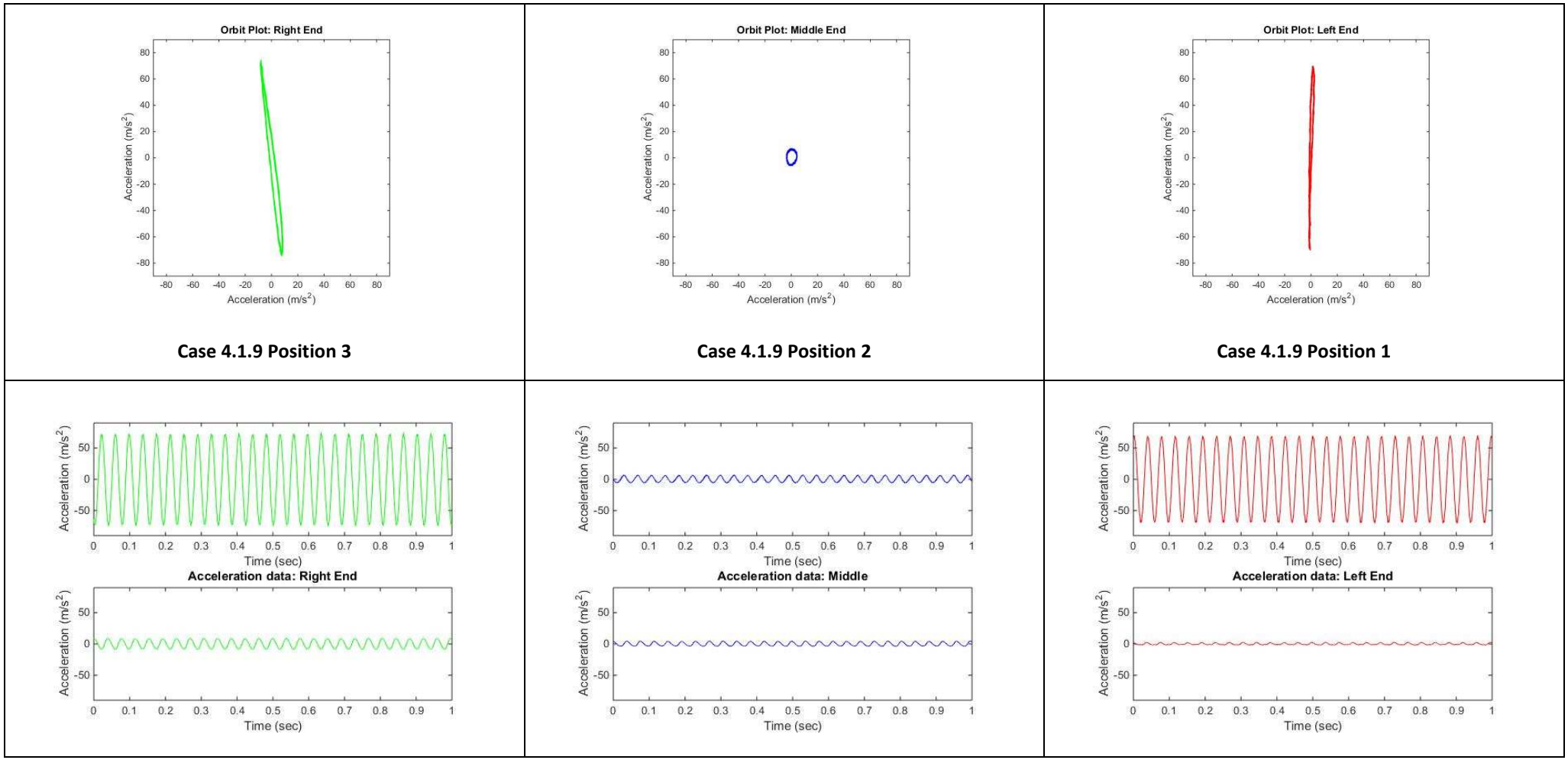

Figure 4.35 Orbit plots and acceleration graphs (X – lower graph, Y-upper graph) for case 4.1.9

Table 4.26 Test parameters of screen test Case 4.1.9a with both vibrators rotating in the same direction

	Unit	Value
Moment of Inertia	kgm^2	1.816
Vibrator Static Moment (each)]	kgm	$1387.8e^{-5}$
The phase difference of	deg	180
Distance of left exciter centre to the centre of mass	m	0.279466
Distance of right exciter centre to the centre of mass	m	0.279466
Vibrators rotational speed	rpm/Hz	1550/25.8
Mass of the setup	kg	17.8

$$\frac{Mr^2}{I} = 0.76 < 2 \; - \; \text{conditions for self} - \text{sychronised circular motion not met}$$

Table 4.27 Orbit Plots and Acceleration Amplitude results for test Case 4.1.9a with both vibrators rotating in the same direction

Value	Unit	Position 3	Position 2	Position 1
Acceleration in Y Direction	mm/s^2	75	10	70
Acceleration in X Direction	mm/s^2	10	5	3

Case 4.1.9a is shown in Figure 4.36 with both vibrators rotating in the same direction at 25.88 Hz. Operating parameters of Case 4.1.9a are the same as of Case 4.1.9 though amplitudes were recorded with one vibrator operating without power and relying only on self-synchronisation phenomenon. The phase difference of 180 degrees was clearly shown in the Figure 4.37 and also on the graphs showing the sinusoidal signal with acceleration in Figure 4.37. The orbit plots and acceleration values are shown in Figure 4.35. Testing rig was moving in a rocking motion with pivot point at the centre of mass outside the physical body of the testing.

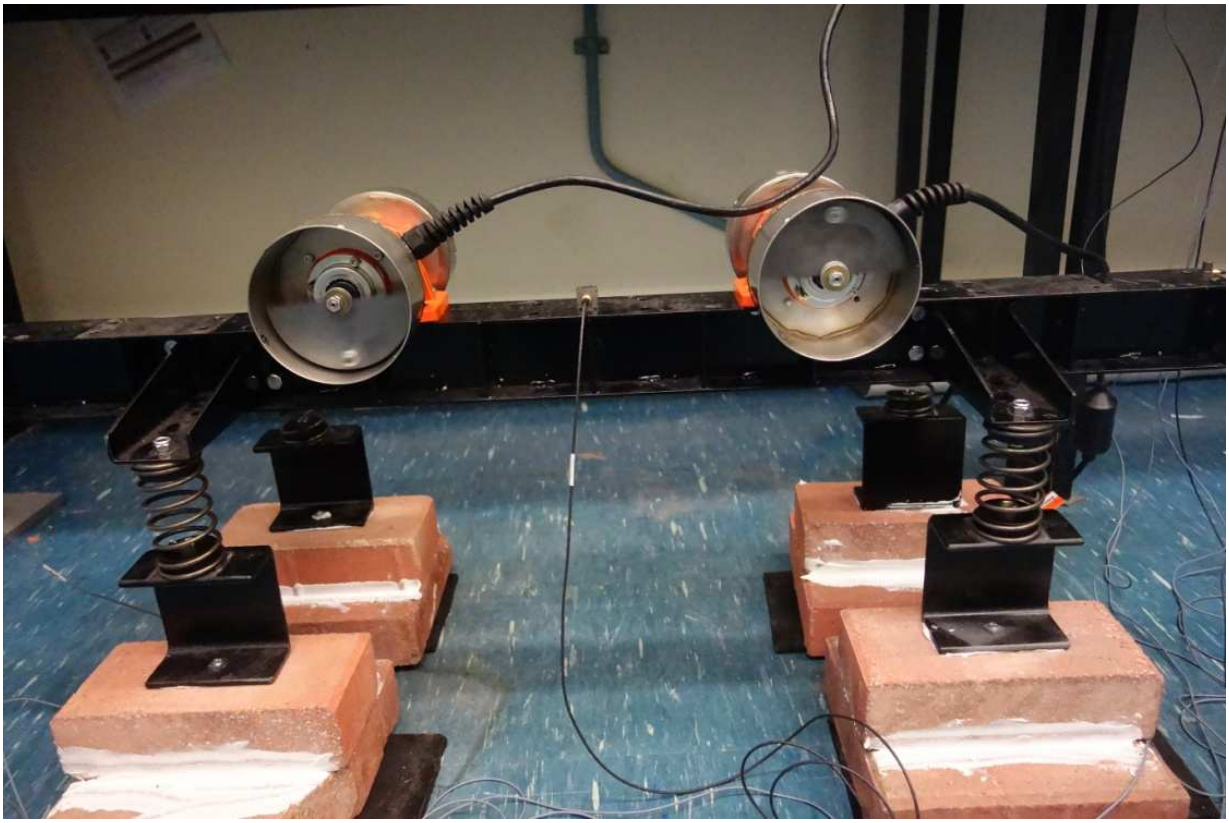

Figure 4.36 Case 4.1.9a Setup

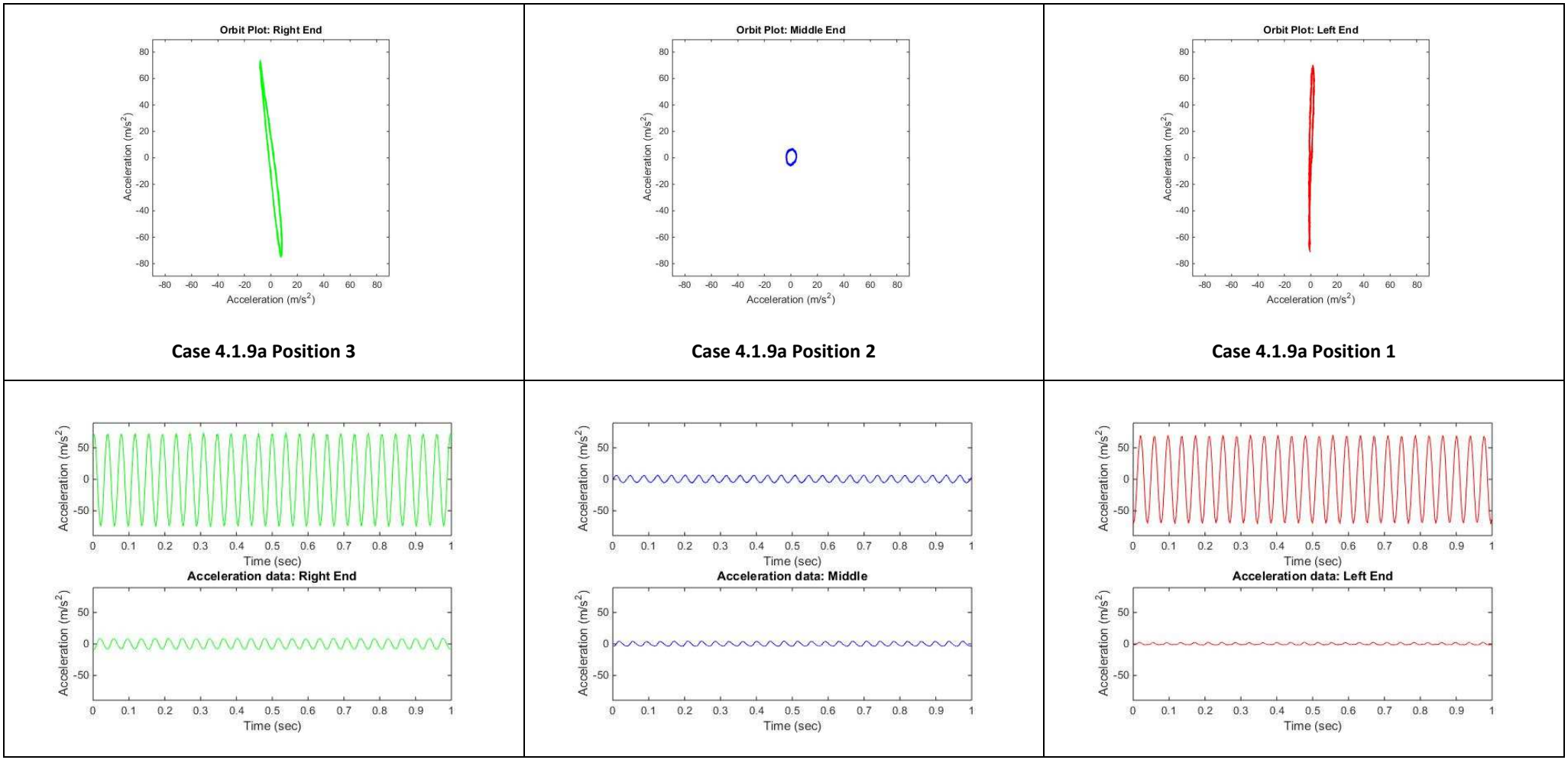

Figure 4.37 Orbit plots and acceleration graphs (X – lower graph, Y-upper graph) for case 4.1.9a

Table 4.28 Test parameters of screen test Case 4.1.10 with both vibrators rotating in the same direction

	Unit	Value
Moment of Inertia	kgm^2	3.013
Vibrator Static Moment (each)]	kgm	$1387.8e^{-5}$
The phase difference of	deg	180
Distance of left exciter centre to the centre of mass	m	0.527899
Distance of right exciter centre to the centre of mass	m	0.507899
Vibrators rotational speed	rpm/Hz	1200/20
Mass of the setup	kg	17.8

$$\frac{\mathrm{Mr}^2}{\mathrm{I}} = 1.52 < 2 \; - \; \text{conditions for self} - \text{sychronised circular motion not met}$$

Table 4.29 Orbit Plots and Acceleration Amplitude results for test Case 4.1.10 with both vibrators rotating in the same direction

Value	Unit	Position 3	Position 2	Position 1
Acceleration in Y Direction	mm/s^2	50	1	50
Acceleration in X Direction	mm/s^2	3	1	3

Case 4.1.10 is shown in Figure 4.38 with both vibrators rotating in the same direction at 20 Hz. The vibrators were repositioned to the outer side of the beam. The phase difference of 180 degrees was clearly shown on the Figure 4.39 and also on the graphs showing the sinusoidal signal with acceleration in Figure 4.39. Orbit plots and acceleration values are shown in Figure 4.35. The testing rig was moving in a rocking motion with pivot point at the centre of mass outside the physical body of the testing rig, however the acceleration in Y and X directions in position 2 is very low which would suggest the accelerometer at position 2 is very close to the pivot point. The testing rig was moving in a rocking motion with pivot point at the centre of mass.

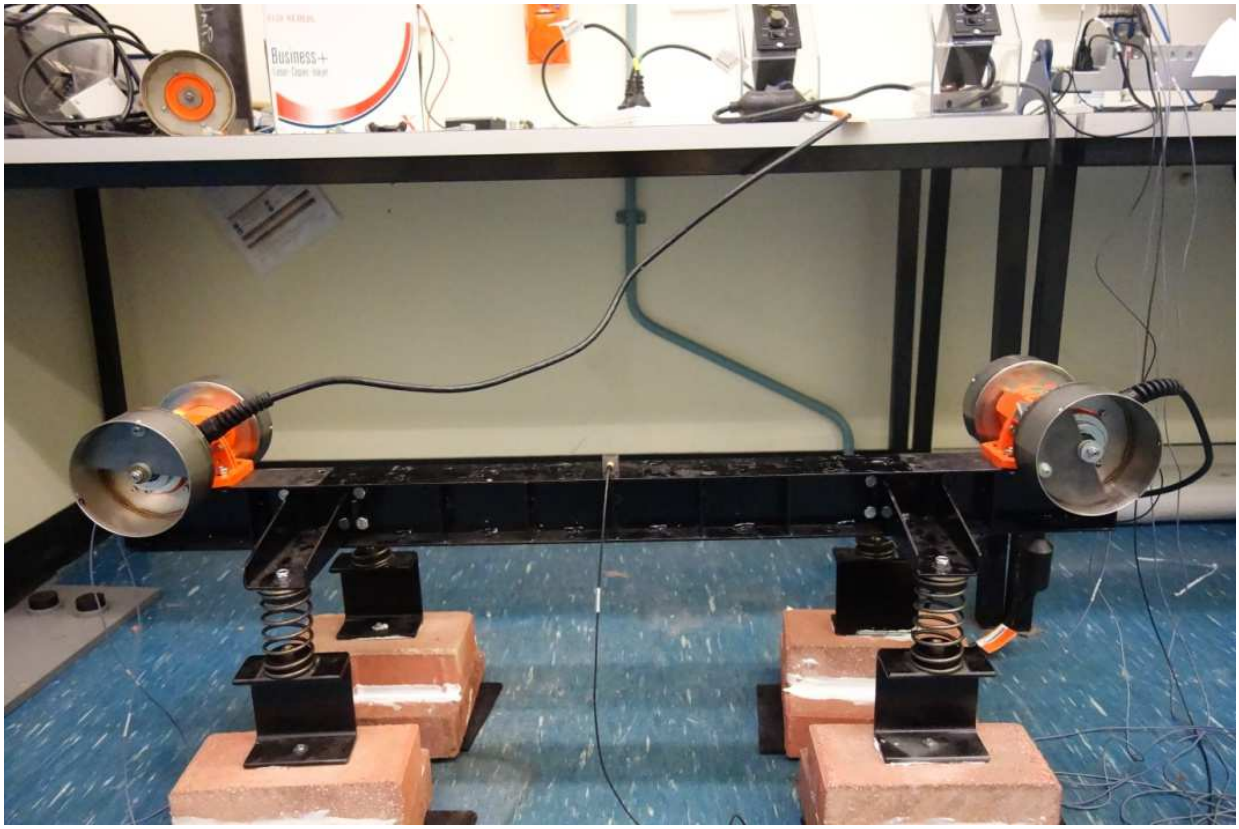

Figure 4.38 Case 4.1.10 Setup

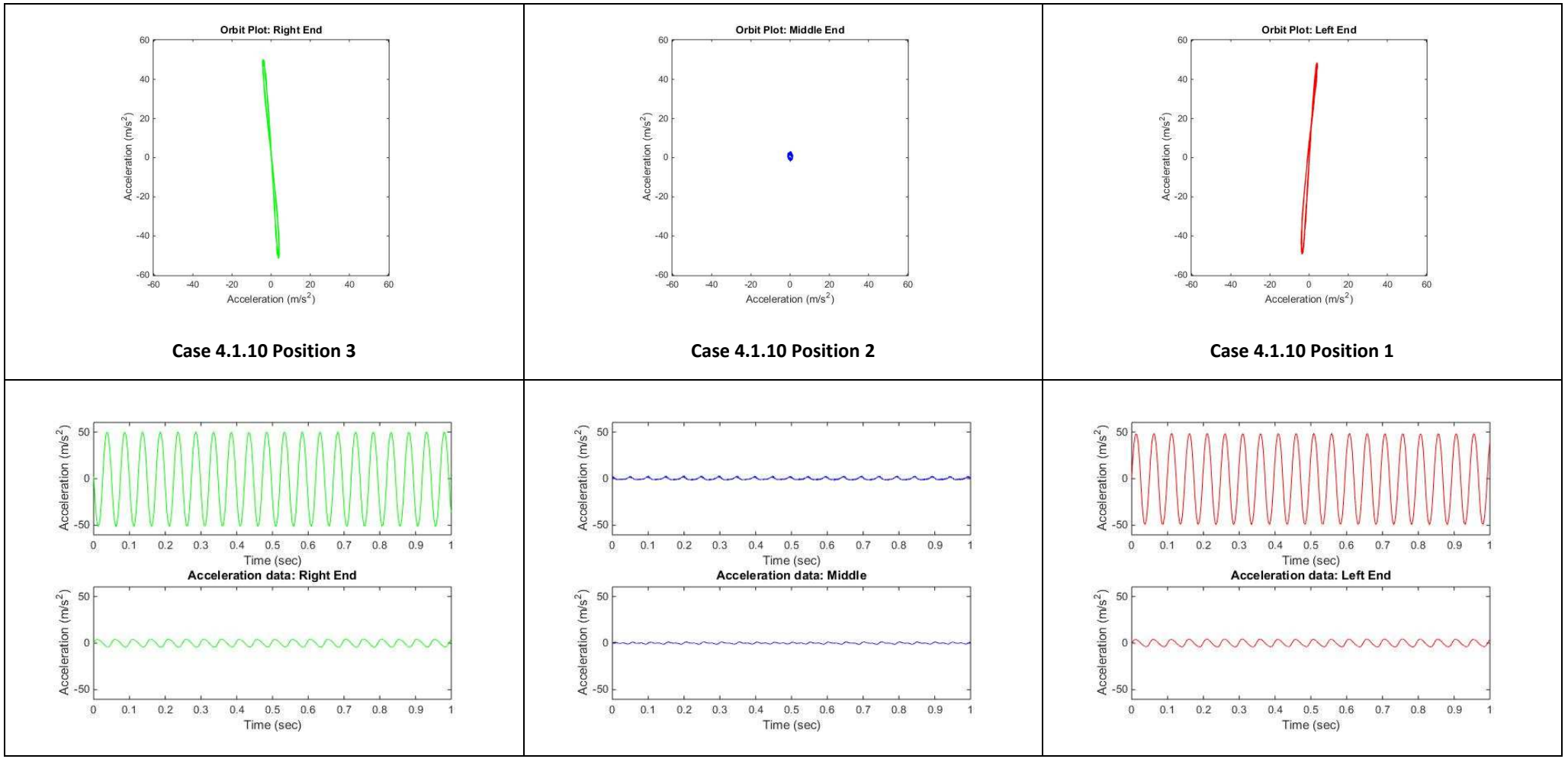

Figure 4.39 Orbit plots and acceleration graphs (X – lower graph, Y-upper graph) for case 4.1.10

Table 4.30 Test parameters of screen test Case 4.1.11 with both vibrators rotating in the same direction

	Unit	Value
Moment of Inertia	kgm^2	3.013
Vibrator Static Moment (each)]	kgm	$1387.8e^{-5}$
The phase difference of	deg	180
Distance of left exciter centre to the centre of mass	m	0.507899
Distance of right exciter centre to the centre of mass	m	0.507899
Vibrators rotational speed	rpm/Hz	1060/17.66
Mass of the setup	kg	17.8

$$\frac{\mathrm{Mr}^2}{\mathrm{I}} = 1.52 < 2 \; - \; \text{conditions for self} - \text{sychronised circular motion not met}$$

Table 4.31 Orbit Plots and Acceleration Amplitude results for test Case 4.1.11 with both vibrators rotating in the same direction

Value	Unit	Position 3	Position 2	Position 1
Acceleration in Y Direction	mm/s^2	20	5	20
Acceleration in X Direction	mm/s^2	8	5	8

Case 4.1.11 is shown in Figure 4.40 with both vibrators rotating in the same direction at 17.8 Hz. The case setup was the same as in case 4.1.10 with operating frequency changed from 20 Hz to 17.8Hz. The phase difference of 180 degrees is shown in the Figure 4.40 and also on the graphs showing the sinusoidal signal with acceleration in Figure 4.41. The orbit plots and acceleration values are shown in Figure 4.41. Reduced operating frequency resulted in increased acceleration in X direction in all accelerometer positions. Magnitude of acceleration orbit at location 2 increased by factor of 5 in both X and Y direction which is interesting and goes against the intuitive feeling that increasing the frequency and therefore the rotating force would create better conditions to create circular motion in all points of the testing rig. The testing rig was moving in a rocking motion with pivot point at the centre of mass outside the physical body of the testing.

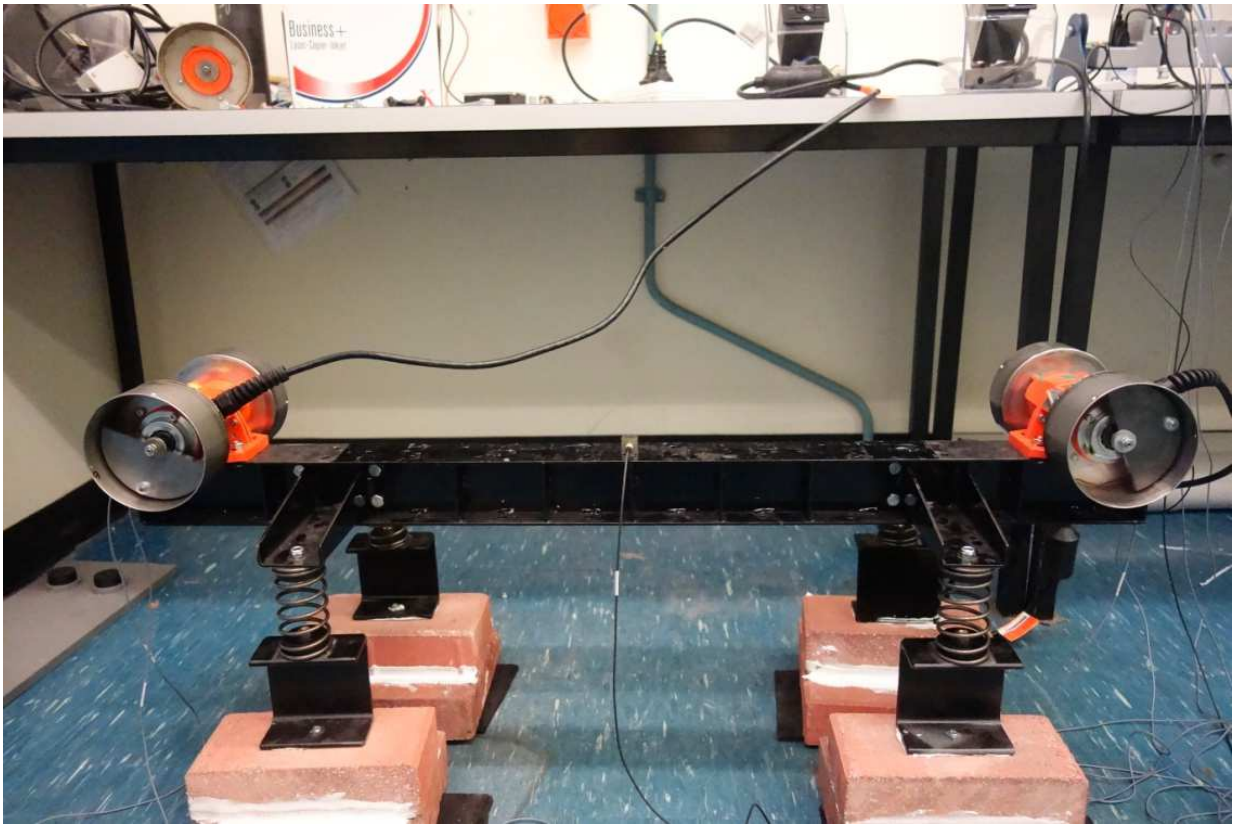

Figure 4.40 Case 4.1.11 Setup

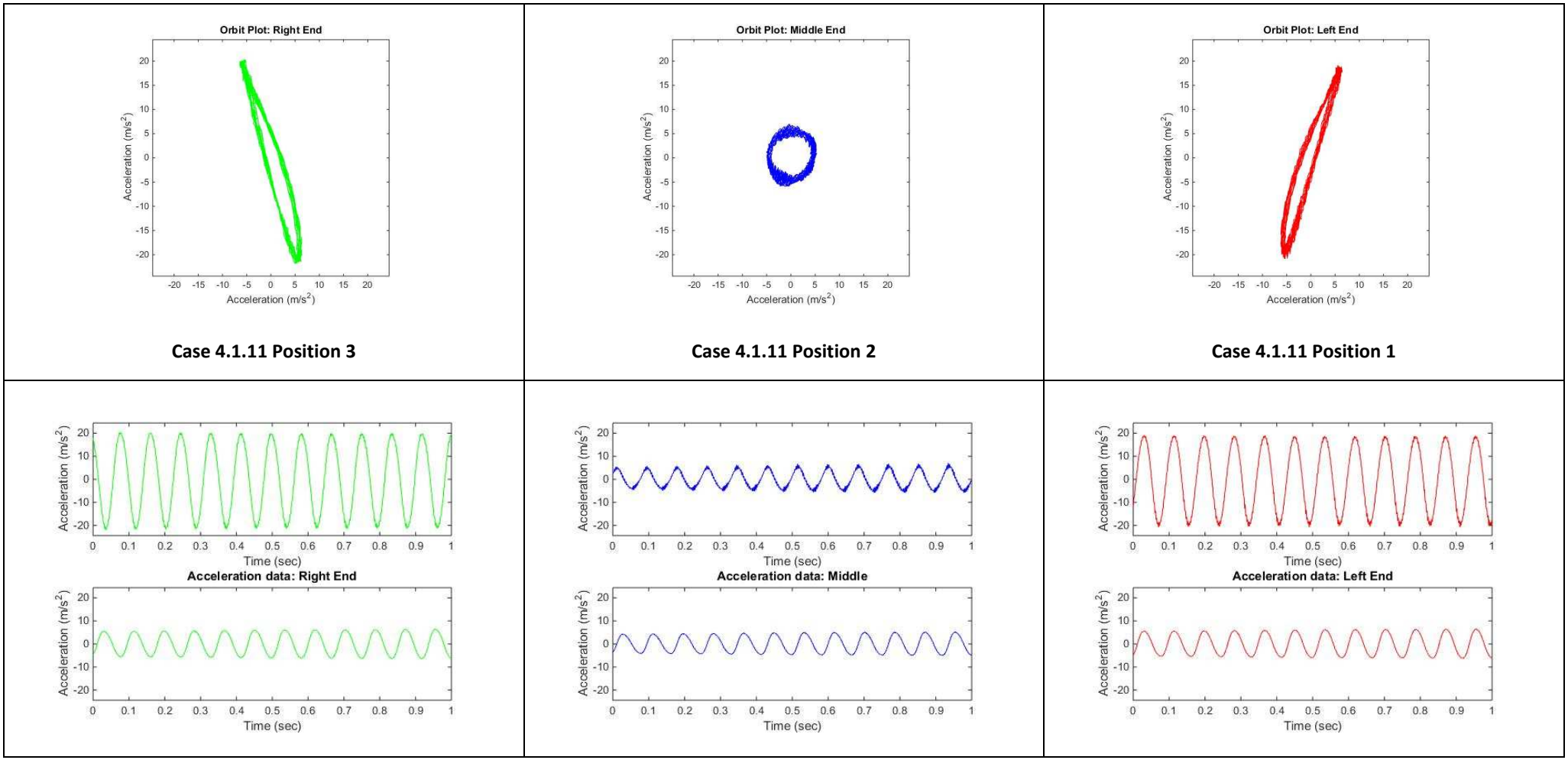

Figure 4.41 Orbit plots and acceleration graphs (X – lower graph, Y-upper graph) for case 4.1.11

4.2 Critical analysis of experimental results with vibrators operating in the same direction - results

Several different combinations of ω, moment of inertia, and vibrator positions were tried with the 15 analysed case studies as is shown in section 4.1. In all cases, the vibrators self-synchronised with counterweights at 180˚ phase difference.

The synchronisation was shown to be very stable and both vibrators remained rotating even when power was disconnected to one of them with no or minimal difference to the stroke shape, with the vibration magnitude remaining the same as in equivalent cases with both vibrators powered.

The counterweight position was always the 180˚ phase difference and that created a rocking motion of the testing rig. This type of motion cannot be used as a primary movement of the screen but could possibly be used though as a secondary vibration to create 3D movement of the screen.

The further the vibrators were located from the centre of gravity, the smaller the stroke amplitude at the centre of mass or near the CoM location and then the larger the motion at the test rig ends.

In theoretical calculation, there is a case when both counterweights would start rotating with 0˚ of the phase difference and the whole testing rig would then operate with circular stroke at any point of the testing rig.

Even circular motion in all points of the testing rig with 0˚ phase difference was not achieved in any of the testing cases. The testing rig designed to confirm the conditions required to achieve self-synchronisation with circular motion of the rig with zero degrees of the phase difference would have to be custom designed with special spring arrangement as high magnitude of rocking motion would be expected before the transition into regular circular motion could be expected.

Blekhman (1988) theoretically calculated the conditions of stable synchronous circular motion which would be necessary for practical use of self-synchronisation of vibrators rotating in the same direction as a main source of screen vibration, where,

$$\frac{Mr^2}{I} > 2$$

M - mass of screen

r - distance of vibrating motors from the centre of gravity

I - moment of inertia

None of the tests conditions as shown in section 4.1 fulfilled the required conditions. One of the experiments was done with double counterweights but because the testing rig was rocking about the centre of gravity with very high amplitude and the isolating springs were closing, the test case was not completed.

It was concluded from the above experiments that to obtain self-synchronisation and stable circular motion is difficult to achieve and impractical from the design point of view. It would require a screen to work with high acceleration (probably 10 g which is double of the standard for the vibrating screen design of 5 g) which would make the screen very heavy because of the structural requirements.

Special arrangement with springs and impact dampers would have to be designed to let the screen/testing rig to go through excessive rocking motion and simultaneously to be able to operate with correct isolation during standard operation of the screen. The screen would be susceptible to overload and would change from circular motion to rocking in case of overload or impact feed to the screen and then the screen would be buried because it would not be discharging the oversize material but transporting it to the centre of gravity or in this case, the centre of the screen.

A significant safety margin would have to be employed to prevent the possibility of screen ‘rocking motion’ which results in material building to the ‘pivot centre’ and burying the screen under load.

The current practice of coupling the vibrating motors with a toothed belt or controlling the phases electronically is the best solution in this case.

4.3 Experimental Tests - Vibrators rotating in the opposite directions

Chapter 4.3 presents the test results of two vibrators operating with the same frequency and rotating in opposite directions at different locations on the testing rig. Table 4-32 shows the parameters for each of 10 test cases.

Table 4.32 Positions of orbits and vibrators for screen tests with vibrators rotating in the opposite directions

Case No	Vibrator 1 position No rpm/Hz	Vibrator 2 position No rpm/Hz	Orbit Pos 1	Orbit Pos 2	Orbit Pos 3
4.2.1	4 1360/22.66	2 1360/22.66	1B	2B	3B
4.2.2	9 1300/21.66	25 1300/21.66	1B	2B	3B
4.2.3	11 1100/18.33	23 1100/18.33	1B	2B	3B
4.2.4	11 1660/25.8	23 1660/25.8	1B	2B	3B
4.2.5	11 2000/20.33	23 2000/20.33	1B	2B	3B
4.2.6	22 1200/20	12 1200/20	1B	2B	3B
4.2.7	22 OFF	12 1200/20	1B	2B	3B
4.2.8	22 1500/26	12 1500/26	1B	2B	3B
4.2.9	18 1200/20	16 1200/20	1A	2	3A
4.2.10	22 1500/25	12 1500/25	1A	2	3A

Figures 4.42 to 4.61 show the test rig setup with the positions of vibrators and location of accelerometers. Photographic pictures were taken during the testing rig operation to show the physical setup and also show the phase of counterweights using the stroboscope.

Tables 4.33 to 4.52 present the trajectory and magnitude of the stroke plotted in X-Y graphs and the acceleration in X and Y directions.

Table 4.33 Test parameters of screen test Case 4.2.1 with vibrators rotating in the opposite directions

	Unit	Value
Moment of Inertia	kgm^2	2.699
Vibrator Static Moment (each)	kgm	$1387.8e^{-5}$
The phase difference of	deg	180
Distance of left exciter centre to the centre of mass	m	0.173456
Distance of right exciter centre to the centre of mass	m	0.323026
Vibrators rotational speed	rpm/Hz	1360/22.66
Mass of the setup	kg	24.7

Table 4.34 Orbit Plots and Acceleration Amplitude results for test Case 4.2.1 with both vibrators rotating in opposite directions

Value	Unit	Position 3	Position 2	Position 1
Acceleration in Y Direction	mm/s^2	18	22	25
Acceleration in X Direction	mm/s^2	10	10	10

Case 4.2.1 is shown in Figure 4.42 with both vibrators rotating in opposite directions at 22.66 Hz frequency. The phase difference of 180 degrees is shown on the Figure 4.42 and also on the graphs showing the sinusoidal signal with acceleration and orbit plots and acceleration values are shown in Figure 4.43. The testing rig was shown to be moving with an elliptical motion at each location with different amplitude and stroke shape.

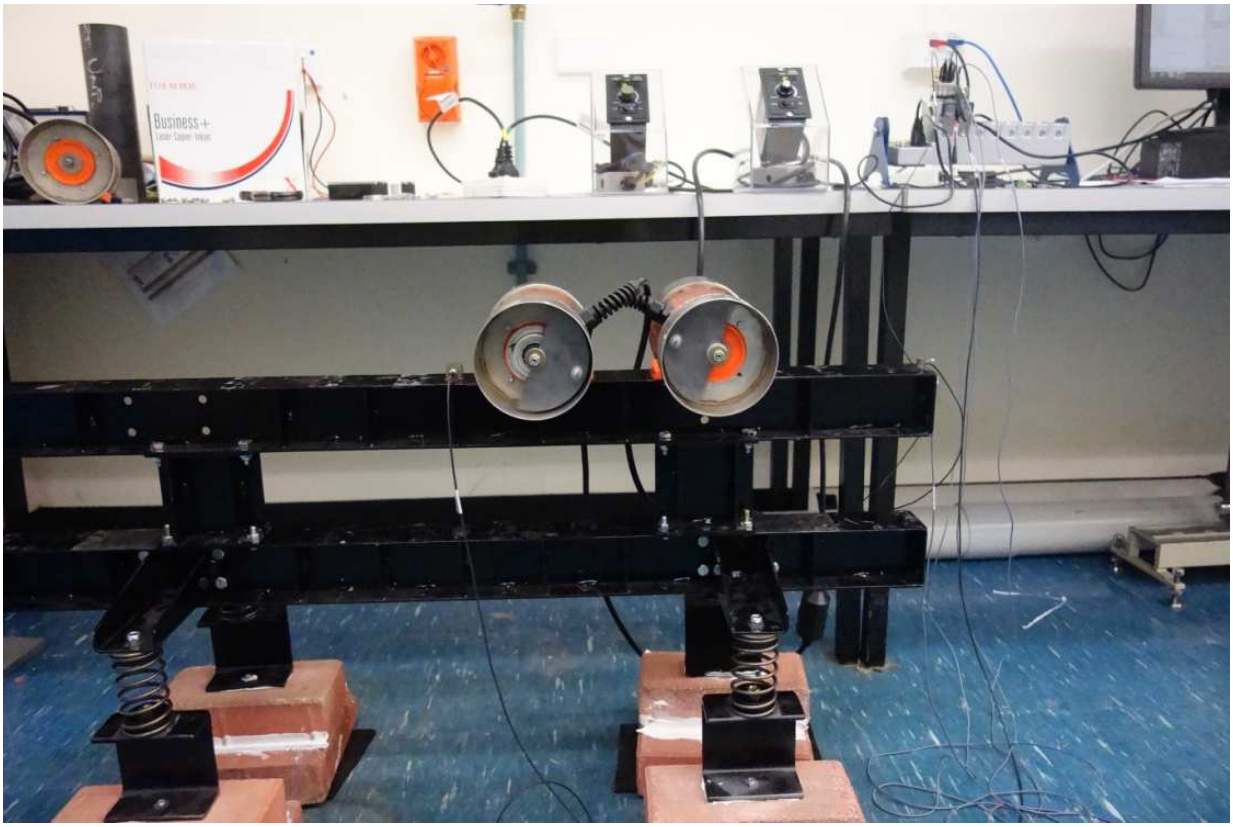

Figure 4.42 Case 4.2.1 Setup

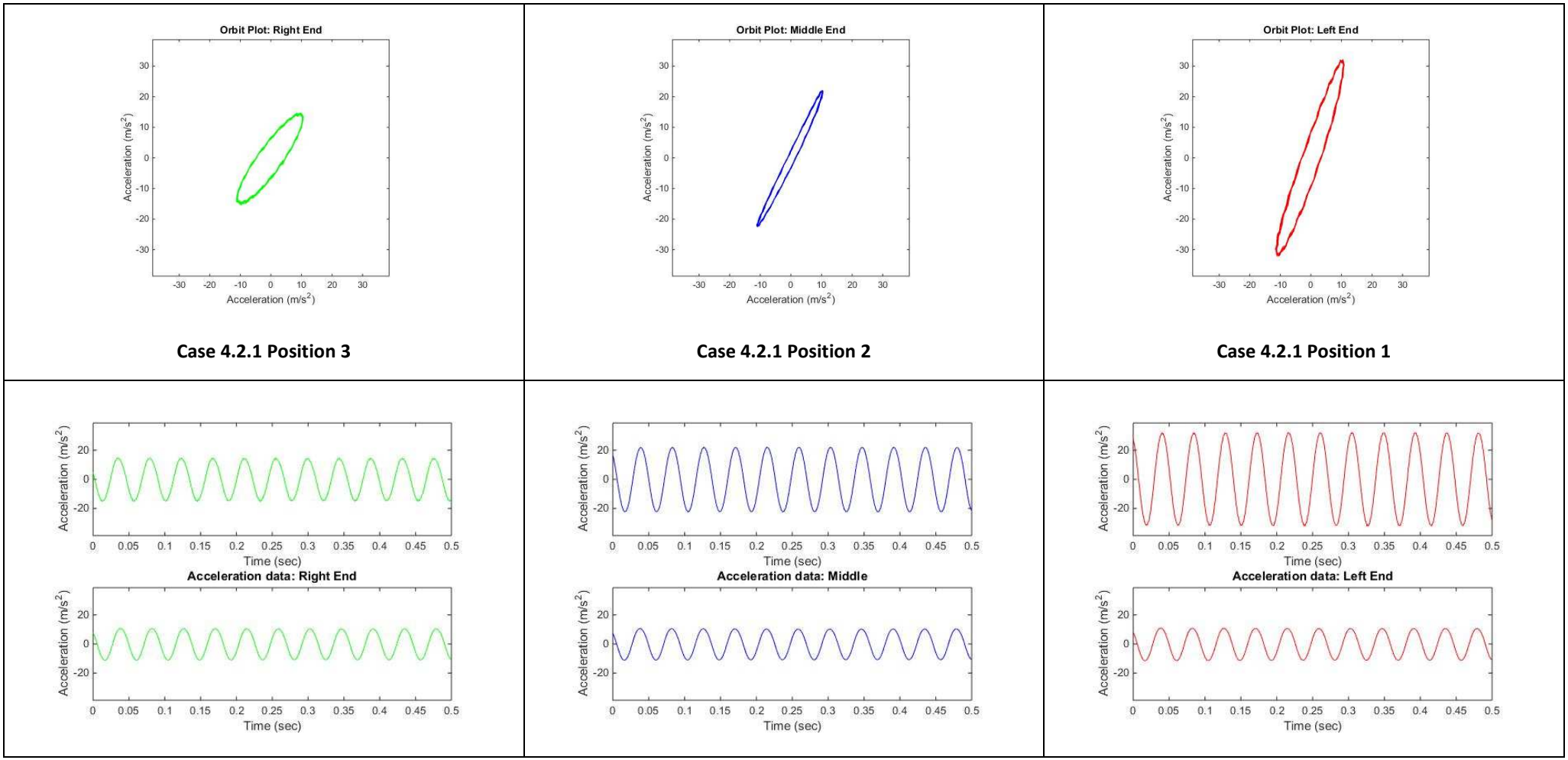

Figure 4.43 Orbit plots and acceleration graphs (X – lower graph, Y-upper graph) for case 4.2.1

Table 4.35 Test parameters of screen test Case 4.2.2 with vibrators rotating in the opposite directions

	Unit	Value
Moment of Inertia	kgm^2	3.057
Vibrator Static Moment (each)	kgm	$1387.8e^{-5}$
The phase difference of	deg	180
Distance of left exciter centre to the centre of mass	m	0.327393
Distance of right exciter centre to the centre of mass	m	0.307505
Vibrators rotational speed	rpm/Hz	1300/21.66
Mass of the setup	kg	24.7

Table 4.36 Orbit Plots and Acceleration Amplitude results for test Case 4.2.2 with both vibrators rotating in opposite directions

Value	Unit	Position 3	Position 2	Position 1
Acceleration in Y Direction	mm/s^2	26	26	26
Acceleration in X Direction	mm/s^2	24	24	24

Case 4.2.2 is shown in Figure 4.44 with both vibrators rotating in opposite directions at 21.66 Hz frequency. The phase difference of 180 degrees is shown on the Figure 4.44 and also on the graphs showing the sinusoidal signal with acceleration and orbit plots presented in Figure 4.45. The testing rig was moving in an elliptical motion at each location with the same amplitude but different stroke shape. No stroke or movement changed when the power to one of the vibrators was cut off.

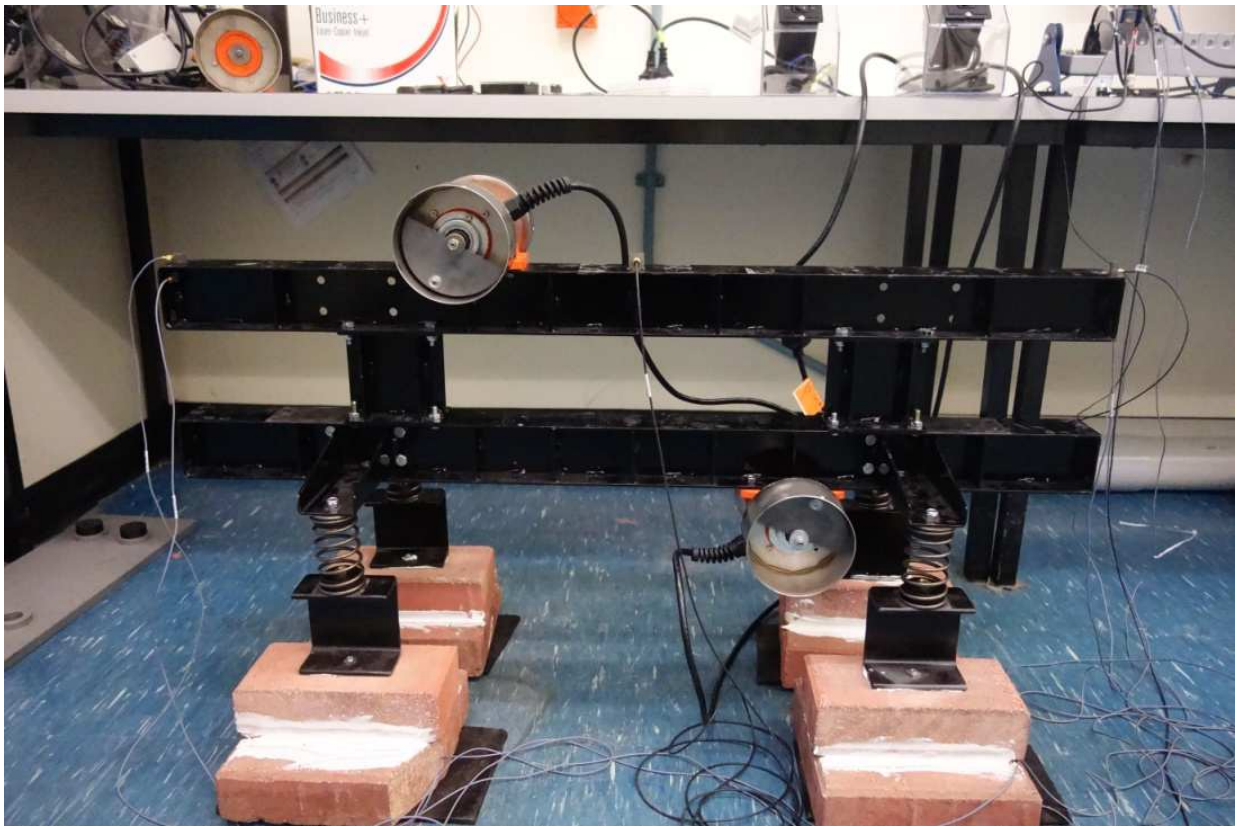

Figure 4.44 Case 4.2.2 Setup

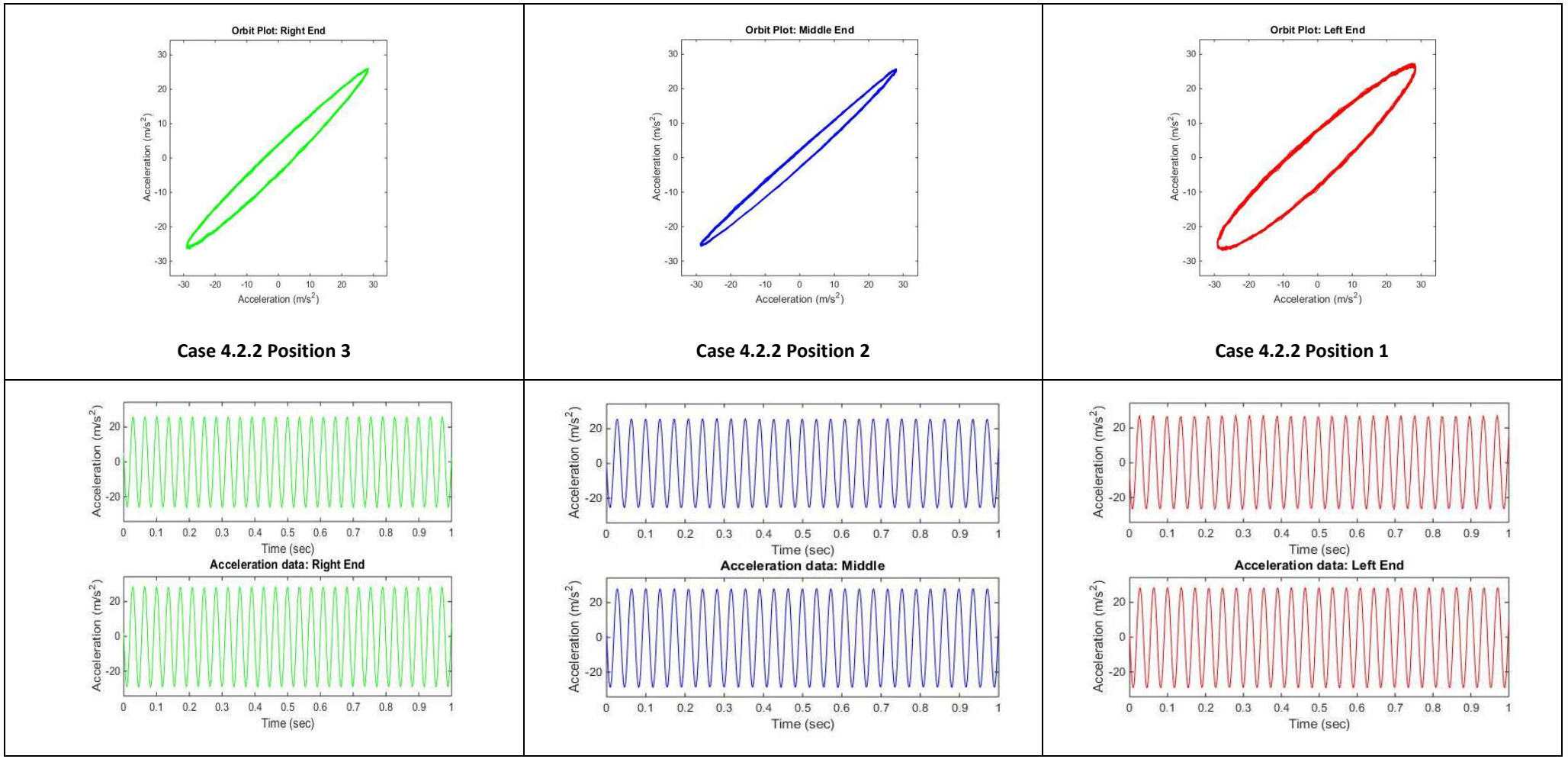

Figure 4.45 Orbit plots and acceleration graphs (X – lower graph, Y-upper graph) for case 4.2.2

Table 4.37 Test parameters of screen test Case 4.2.3 with vibrators rotating in the opposite directions

	Unit	Value
Moment of Inertia	kgm^2	4.783
Vibrator Static Moment (each)	kgm	$1387.8e^{-5}$
The phase difference of	deg	180
Distance of left exciter centre to the centre of mass	m	0.535767
Distance of right exciter centre to the centre of mass	m	0.523674
Vibrators rotational speed	rpm/Hz	1100/18.33
Mass of the setup	kg	24.7

Table 4.38 Orbit Plots and Acceleration Amplitude results for test Case 4.2.3 with both vibrators rotating in opposite directions

Value	Unit	Position 3	Position 2	Position 1
Acceleration in Y Direction	mm/s^2	18	18	18
Acceleration in X Direction	mm/s^2	8	8	8

Case 4.2.3 is shown in Figure 4.46 with both vibrators rotating in opposite directions at 18.33 Hz frequency. The phase difference of 180 degrees is shown on the Figure 4.46 and also on the graphs showing the sinusoidal signal with acceleration and orbit plots presented in Figure 4.47. Testing rig was moving in an elliptical motion at all locations with the same amplitude and different stroke shape. With vibrators positioned wider on the testing rig the angle from the vertical decreased as expected. No stroke or movement changed when the power to one of the vibrators was cut off.

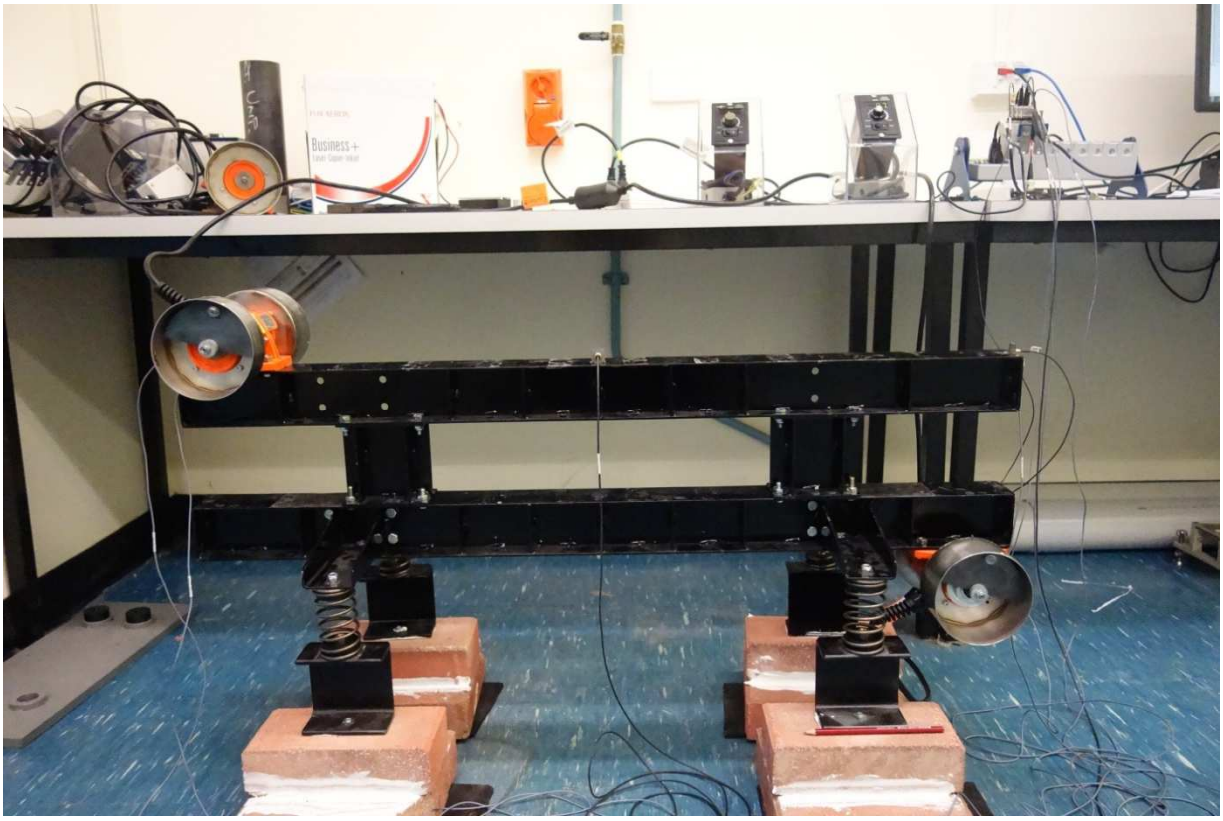

Figure 4.46 Case 4.2.3 Setup

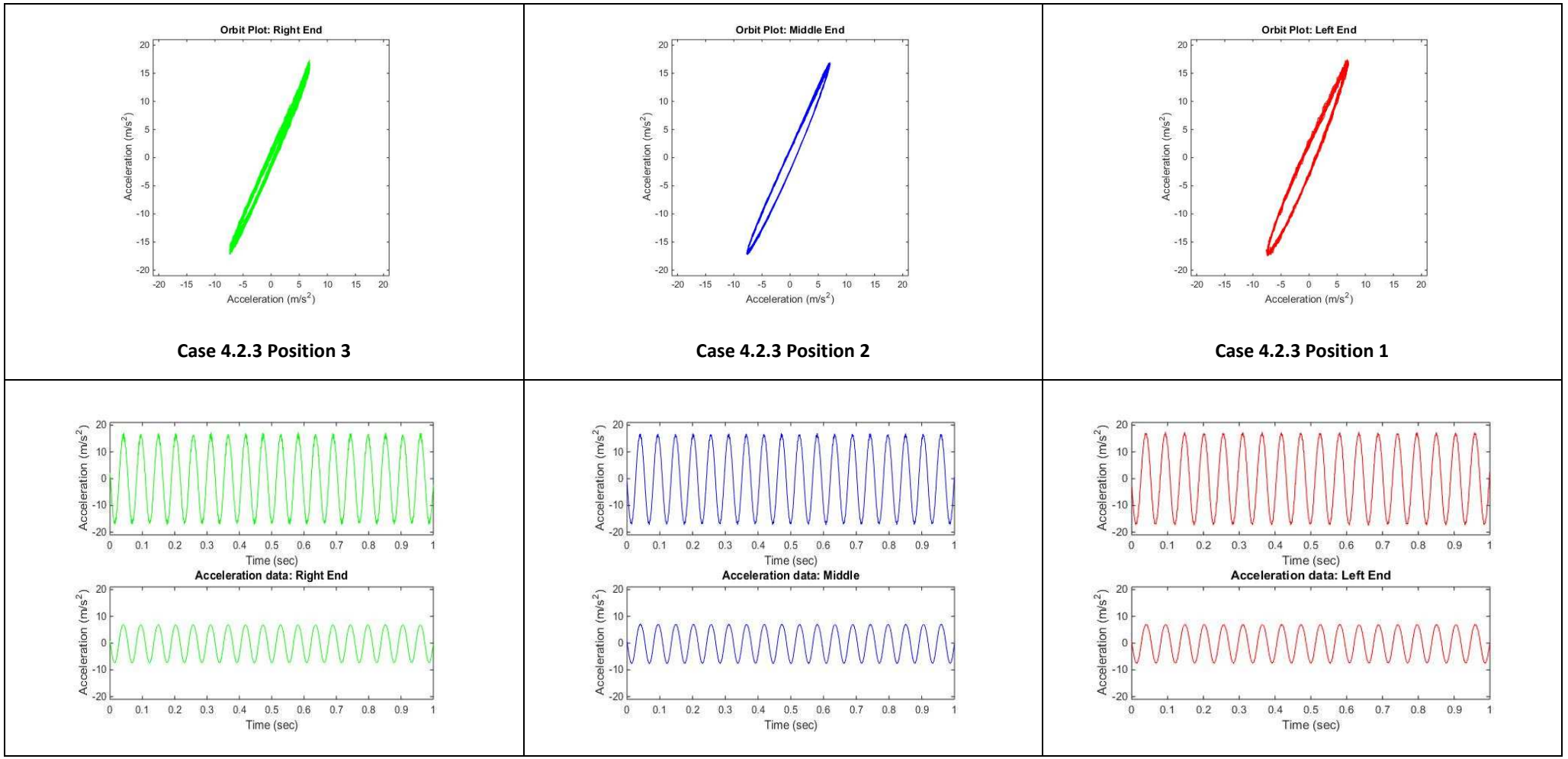

Figure 4.47 Orbit plots and acceleration graphs (X – lower graph, Y-upper graph) for case 4.2.3

Table 4.39 Test parameters of screen test Case 4.2.4 with vibrators rotating in the opposite directions

	Unit	Value
Moment of Inertia	kgm^2	4.783
Vibrator Static Moment (each)	kgm	$1387.8e^{-5}$
The phase difference of	deg	180
Distance of left exciter centre to the centre of mass	m	0.535767
Distance of right exciter centre to the centre of mass	m	0.523674
Vibrators rotational speed	rpm/Hz	1660/25.8
Mass of the setup	kg	24.7

Table 4.40 Orbit Plots and Acceleration Amplitude results for test Case 4.2.4 with both vibrators rotating in opposite directions

Value	Unit	Position 3	Position 2	Position 1
Acceleration in Y Direction	mm/s^2	38	38	38
Acceleration in X Direction	mm/s^2	18	18	18

Case 4.2.4 is shown in Figure 4.48 with both vibrators rotating in opposite directions at 25.8 Hz frequency. The phase difference of 180 degrees is shown on the Figure 4.48 and also on the graphs showing the sinusoidal signal with acceleration and orbit plots presented in Figure 4.49. The testing rig was moving in an elliptical motion at all locations with the same amplitude but slightly different stroke shapes. Vibrators were positioned as in case 4.2.3 with different operating frequency. Stroke shapes are the same with a change in amplitude magnitude because of the higher running speed. No stroke or movement changed when the power to one of the vibrators was cut off.

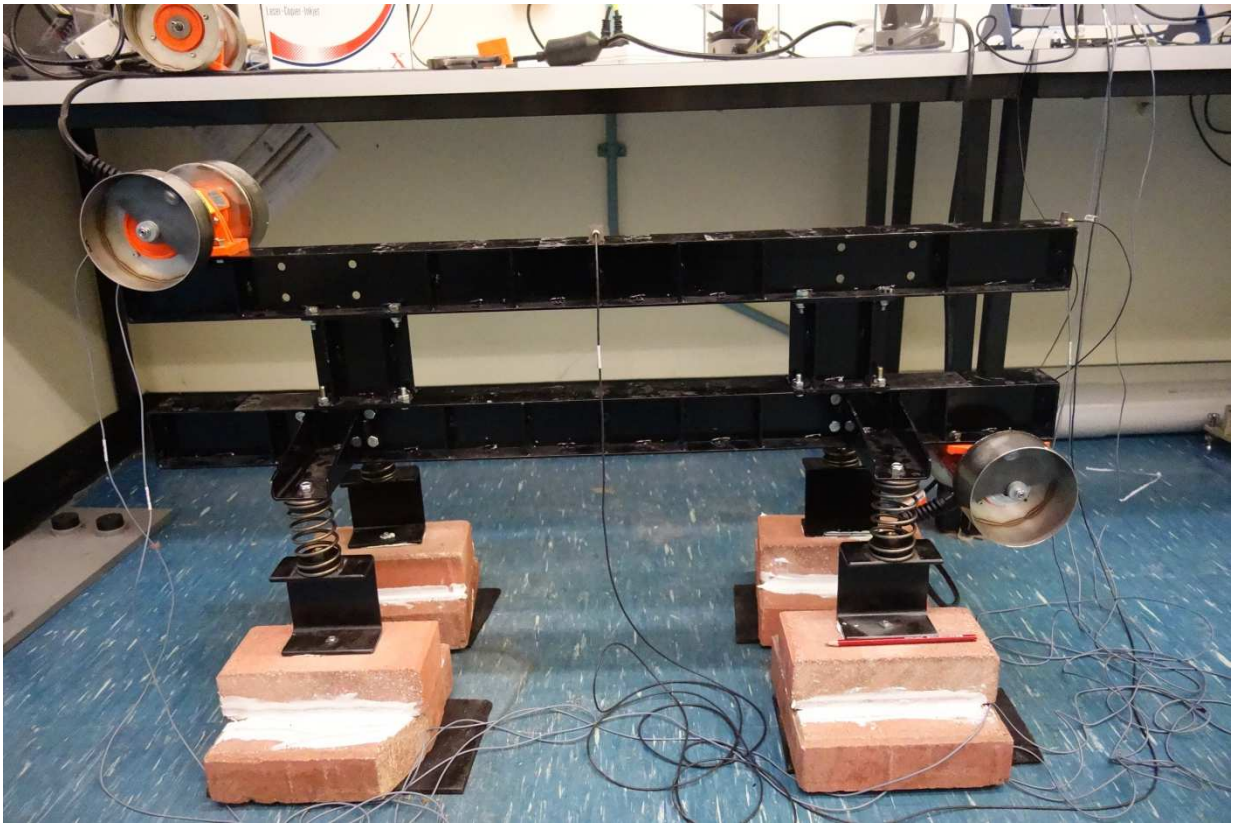

Figure 4.48 Case 4.2.4 Setup

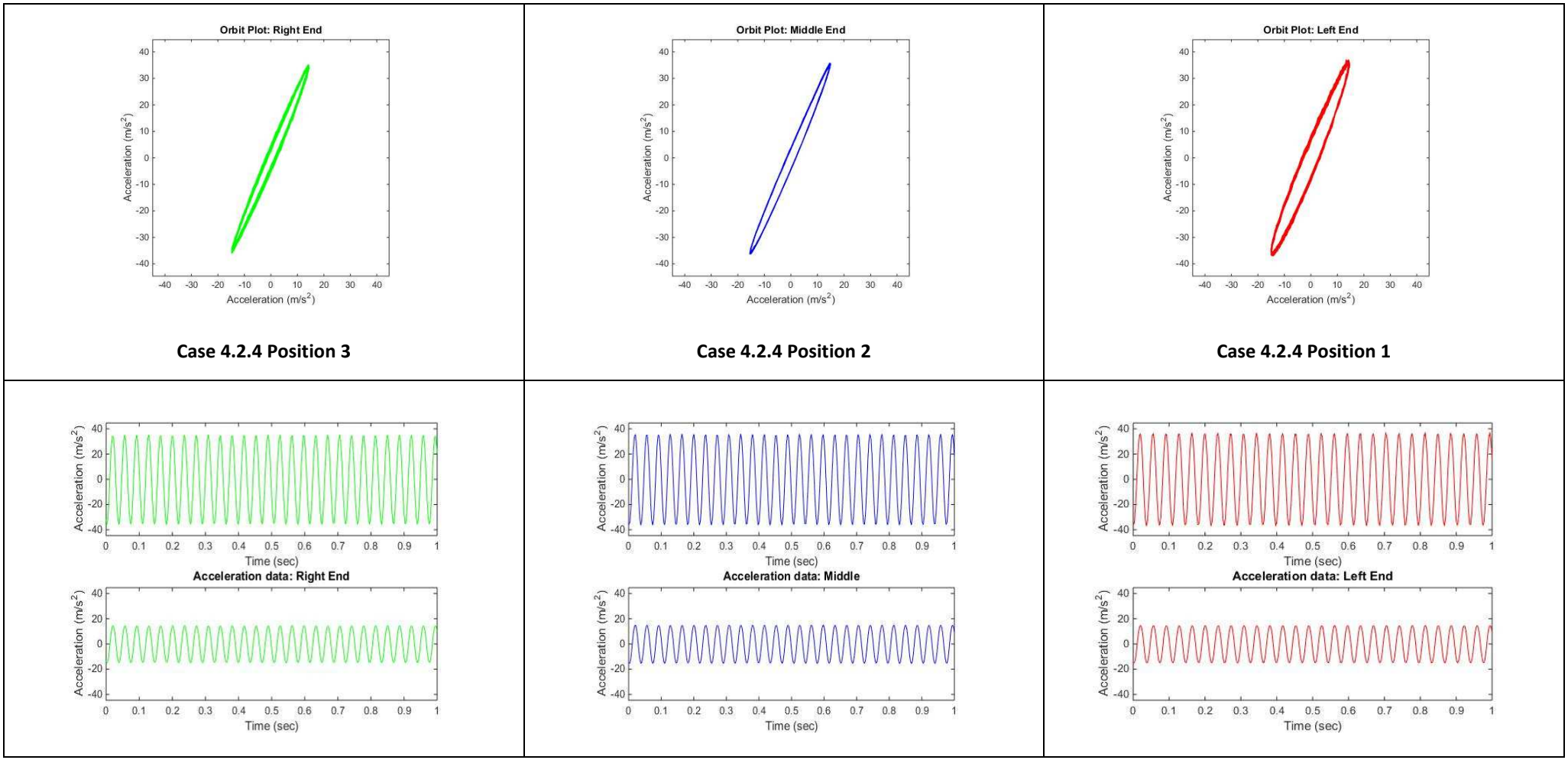

Figure 4.49 Orbit plots and acceleration graphs (X – lower graph, Y-upper graph) for case 4.2.4

Table 4.41 Test parameters of screen test Case 4.2.5 with vibrators rotating in the opposite directions

	Unit	Value
Moment of Inertia	kgm^2	4.783
Vibrator Static Moment (each)	kgm	$1387.8e^{-5}$
The phase difference of	deg	180
Distance of left exciter centre to the centre of mass	m	0.535767
Distance of right exciter centre to the centre of mass	m	0.523674
Vibrators rotational speed	rpm/Hz	2000/20.33
Mass of the setup	kg	24.7

Table 4.42 Orbit Plots and Acceleration Amplitude results for test Case 4.2.5 with both vibrators rotating in opposite directions

Value	Unit	Position 3	Position 2	Position 1
Acceleration in Y Direction	mm/s^2	50	50	50
Acceleration in X Direction	mm/s^2	20	20	20

Case 4.2.5 is shown in Figure 4.50 with both vibrators rotating opposite directions at 20.33 Hz frequency. The phase difference of 180 degrees is shown on the Figure 4.50 and also on the graphs showing the sinusoidal signal with acceleration in Figure 4.51. Testing rig was moving in an elliptical motion at all locations with the same amplitudes but slightly different stroke shapes. Extra vibration which can be observed on orbits at locations 1 and 3 are results of the operation speed being close to a natural frequency which did not affect the self-synchronisation. There was no stroke or testing rig noticeable movement change when the power to one of the vibrators was cut off.

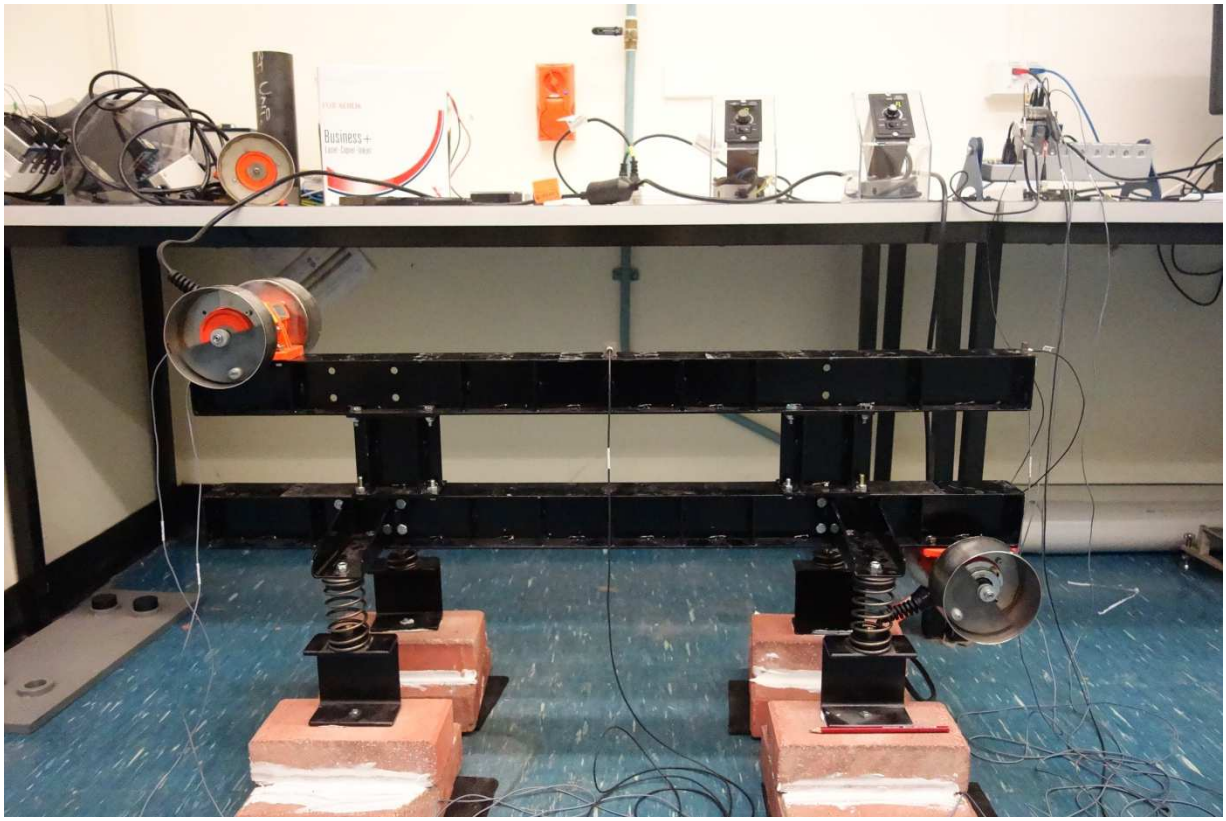

Figure 4.50 Case 4.2.5 Setup

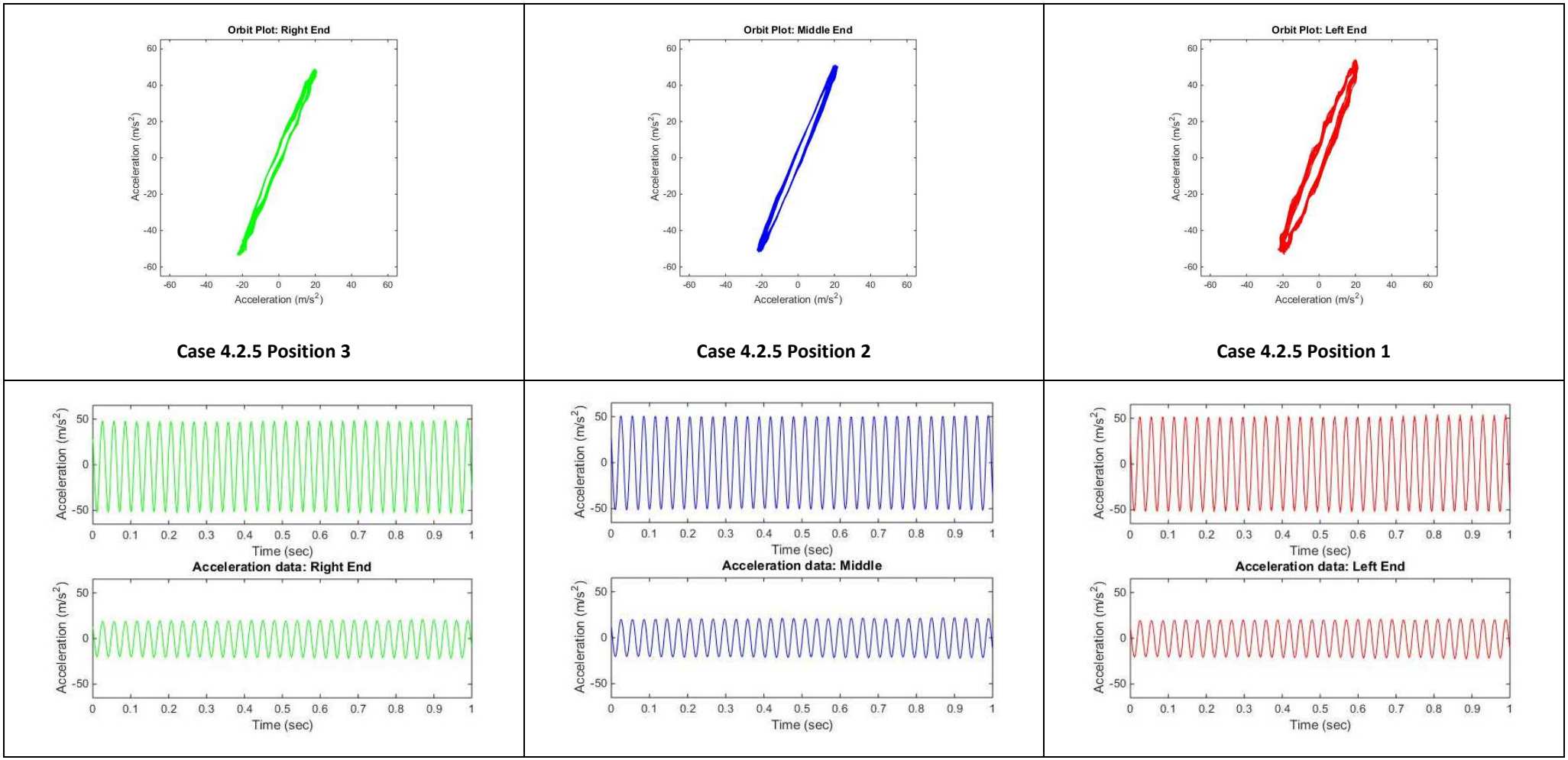

Figure 4.51 Orbit plots and acceleration graphs (X – lower graph, Y-upper graph) for case 4.2.5

Table 4.43 Test parameters of screen test Case 4.2.6 with vibrators rotating in the opposite directions

	Unit	Value
Moment of Inertia	kgm^2	3.813
Vibrator Static Moment (each)	kgm	$1387.8e^{-5}$
The phase difference of	deg	180
Distance of left exciter centre to the centre of mass	m	0.506085
Distance of right exciter centre to the centre of mass	m	0.506085
Vibrators rotational speed	rpm/Hz	1200/20
Mass of the setup	kg	24.7

Table 4.44 Orbit Plots and Acceleration Amplitude results for test Case 4.2.6 with both vibrators rotating in opposite directions

Value	Unit	Position 3	Position 2	Position 1
Acceleration in Y Direction	mm/s^2	21	21	21
Acceleration in X Direction	mm/s^2	1	1	1

Case 4.2.6 is shown in Figure 4.52 with both vibrators rotating in opposite directions at 20 Hz frequency. The phase difference of 180 degrees is shown on the Figure 4.52 and also on the graphs showing the sinusoidal signal with acceleration in Figure 4.53. The orbit plots and acceleration values are shown in Figure 4.53. The testing rig was moving in linear motion at all location with the same amplitudes. No stroke or movement change was observed when the power to one of the vibrators was cut off.

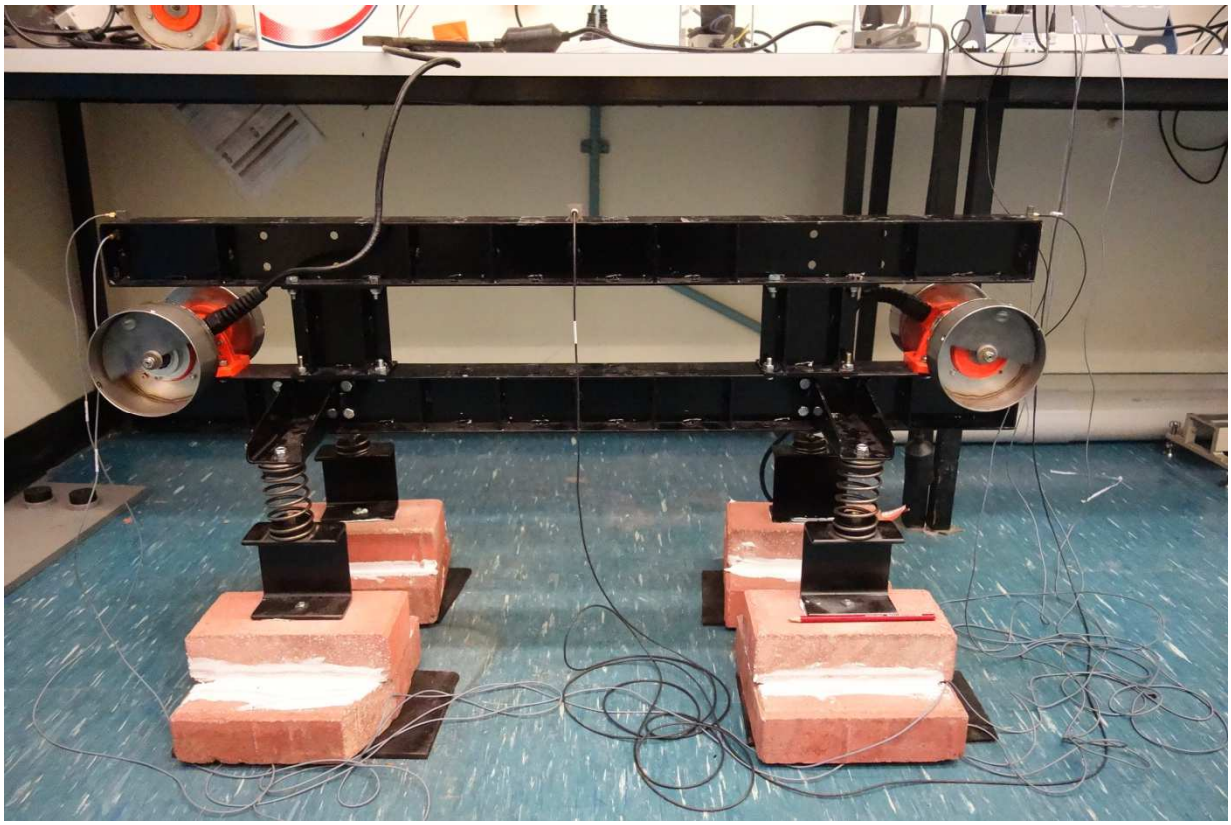

Figure 4.52 Case 4.2.6 Setup

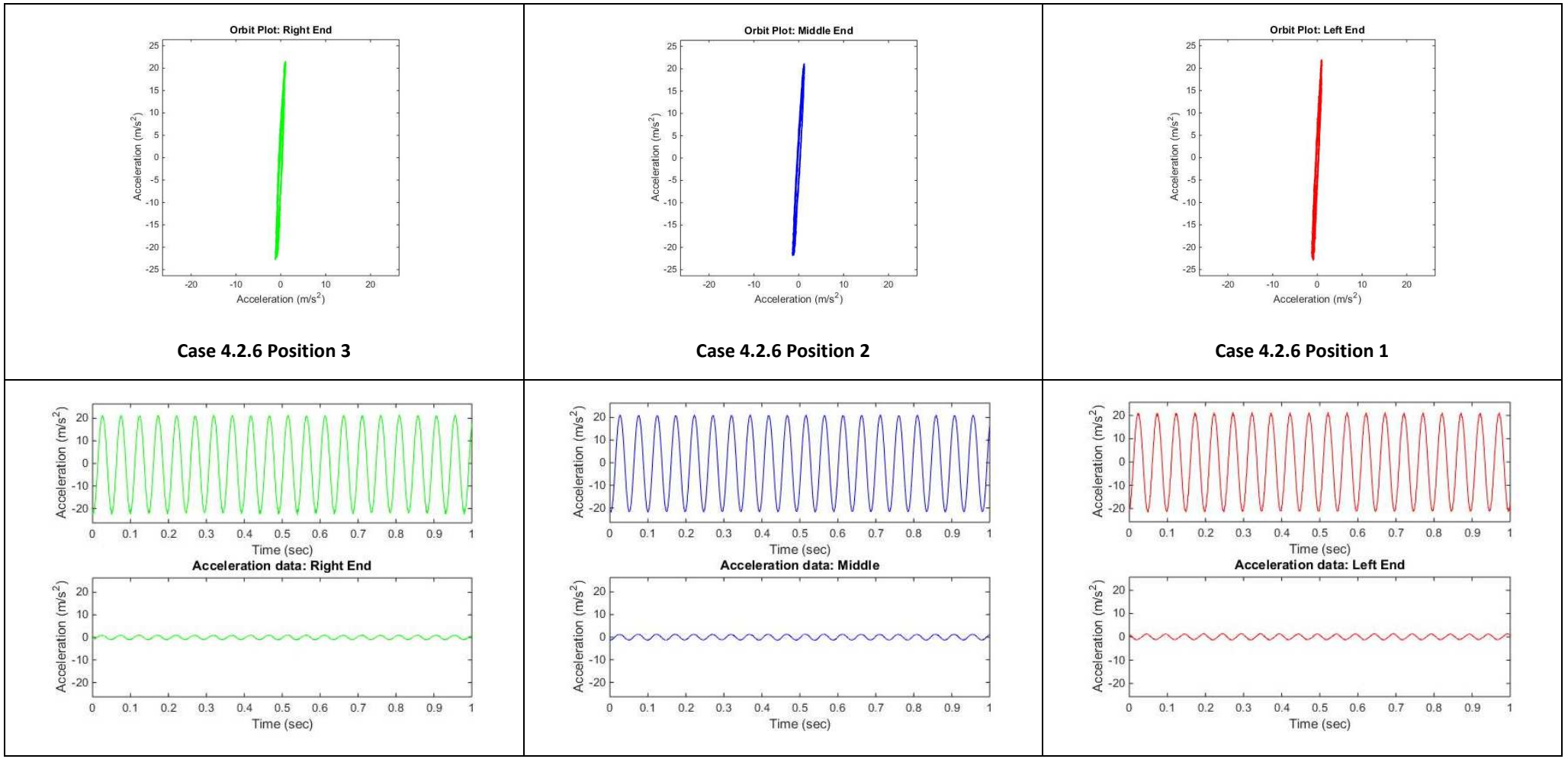

Figure 4.53 Orbit plots and acceleration graphs (X – lower graph, Y-upper graph) for case 4.2.6

Table 4.45 Test parameters of screen test Case 4.2.7 with vibrators rotating in the opposite directions

	Unit	Value
Moment of Inertia	kgm^2	3.813
Vibrator Static Moment (each)	kgm	$1387.8e^{-5}$
The phase difference of	deg	180
Distance of left exciter centre to the centre of mass	m	0.506085
Distance of right exciter centre to the centre of mass	m	0.506085
Vibrators rotational speed	rpm/Hz	1200/20
Mass of the setup	kg	24.7

Table 4.46 Orbit Plots and Acceleration Amplitude results for test Case 4.2.7 with both vibrators rotating in opposite directions

Value	Unit	Position 3	Position 2	Position 1
Acceleration in Y Direction	mm/s^2	21	21	21
Acceleration in X Direction	mm/s^2	1	1	1

Case 4.2.7 is shown in Figure 4.54 and has the same parameters as Case 4.2.6, though all readings were taken with one of the vibrators powered off. The phase difference of 180 degrees is presented on the Figure 4.54 and also on the graphs showing the sinusoidal signal with acceleration in Figure 4.55. The orbit plots and acceleration values are shown in Figure 4.55. Amplitude magnitudes in X and Y directions are the same with slightly elliptical orbit shape when compared to results obtained in Case 4.2.6.

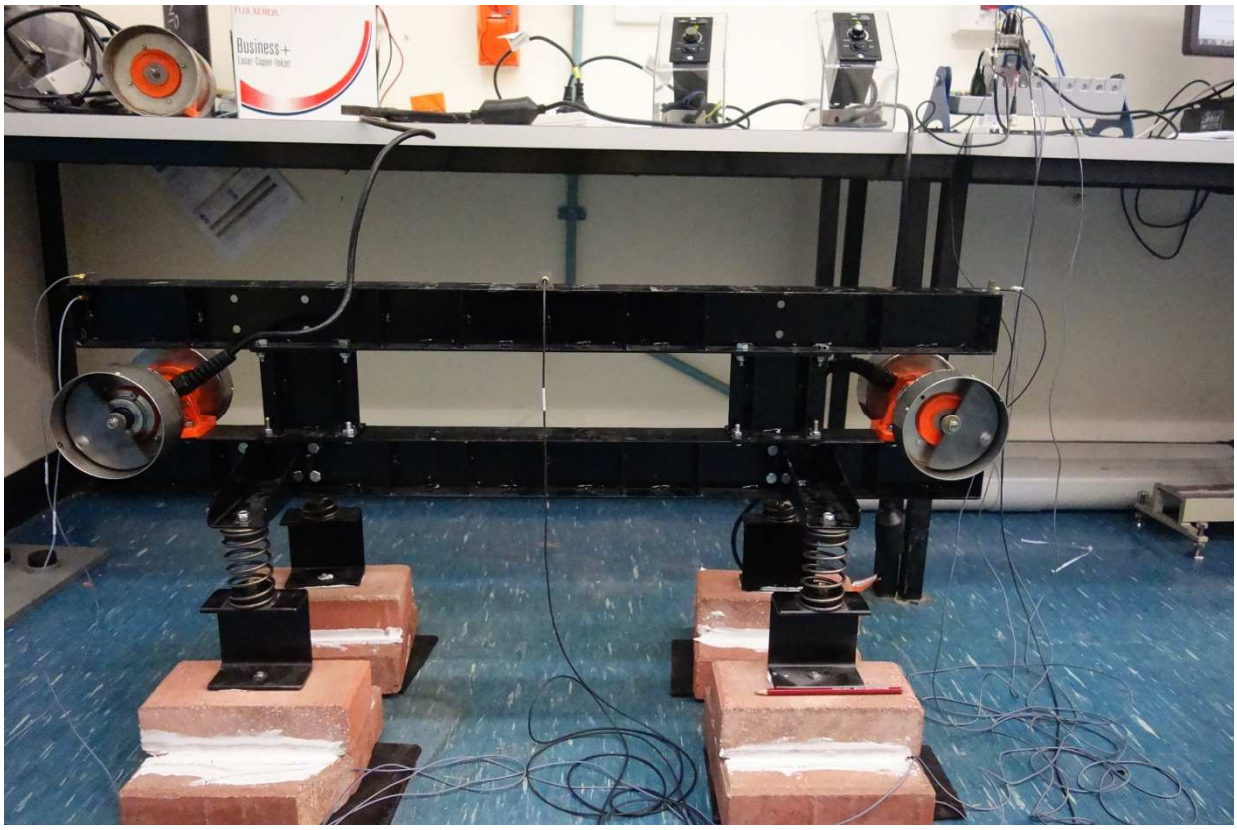

Figure 4.54 Case 4.2.7 Setup

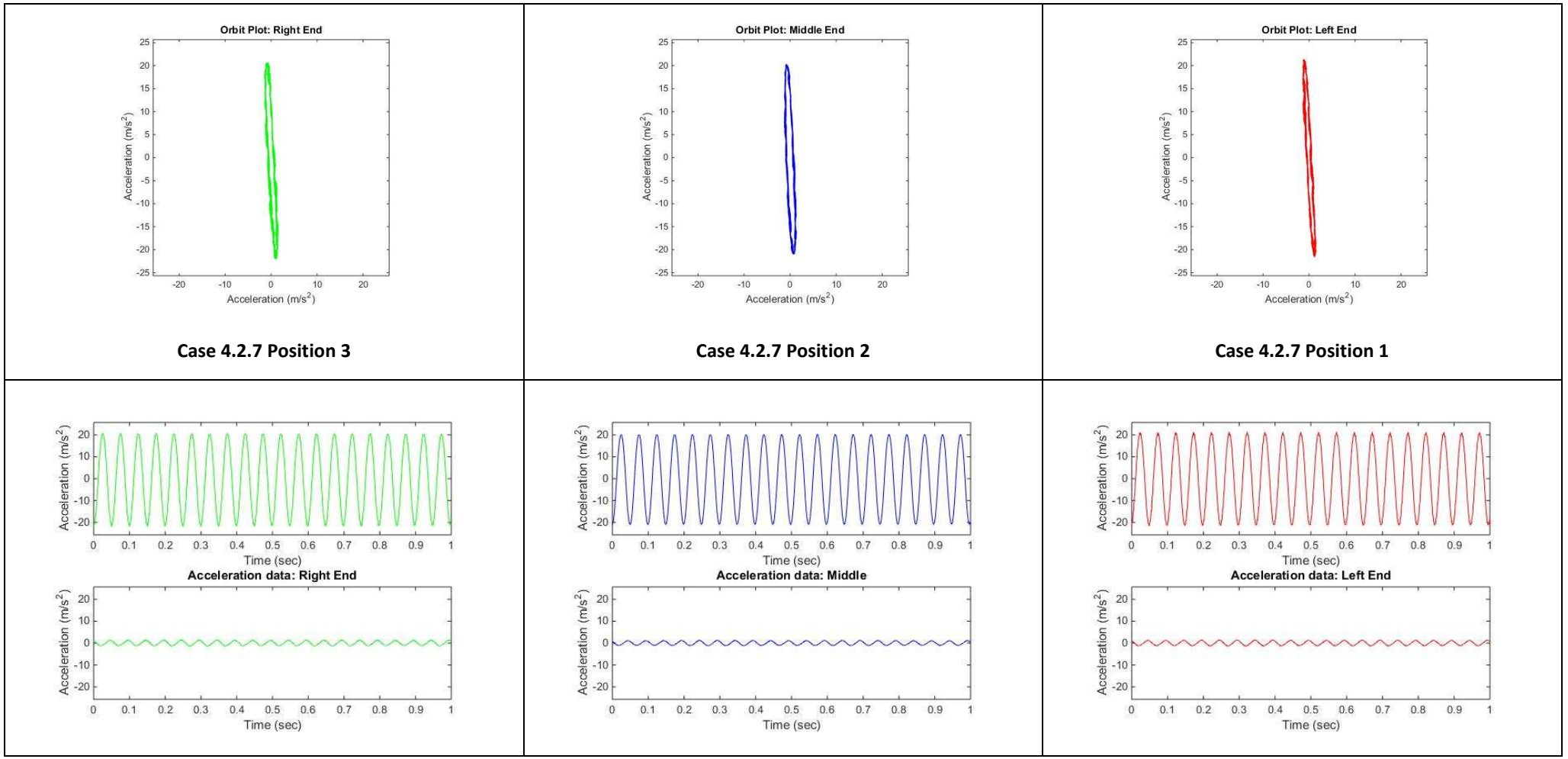

Figure 4.55 Orbit plots and acceleration graphs (X – lower graph, Y-upper graph) for case 4.2.7

Table 4.47 Test parameters of screen test Case 4.2.8 with vibrators rotating in the opposite directions

	Unit	Value
Moment of Inertia	kgm^2	3.813
Vibrator Static Moment (each)	kgm	$1387.8e^{-5}$
The phase difference of	deg	180
Distance of left exciter centre to the centre of mass	m	0.506085
Distance of right exciter centre to the centre of mass	m	0.506085
Vibrators rotational speed	rpm/Hz	1500/26
Mass of the setup	kg	24.7

Table 4.48 Orbit Plots and Acceleration Amplitude results for test Case 4.2.8 with both vibrators rotating in opposite directions

Value	Unit	Position 3	Position 2	Position 1
Acceleration in Y Direction	mm/s^2	32	32	32
Acceleration in X Direction	mm/s^2	3	3	3

Case 4.2.8 is shown in Figure 4.56 with both vibrators rotating in opposite directions at 26 Hz frequency. The phase difference of 180 degrees is presented on the Figure 4.56 and also on the graphs showing the sinusoidal signal with acceleration in Figure 4.57. The orbit plots and acceleration values are shown in Figure 4.57. The testing rig was moving in linear motion with the same amplitude and stroke shape at all locations.

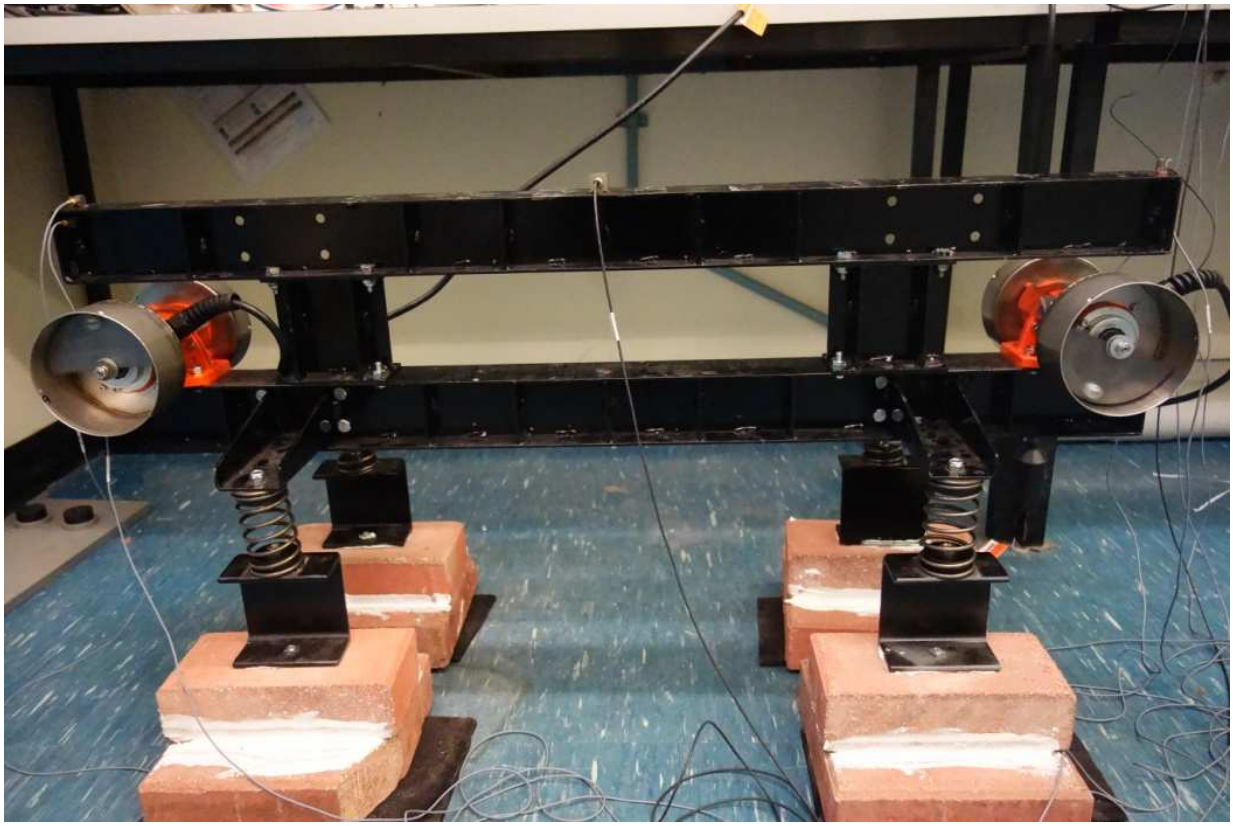

Figure 4.56 Case 4.2.8 Setup

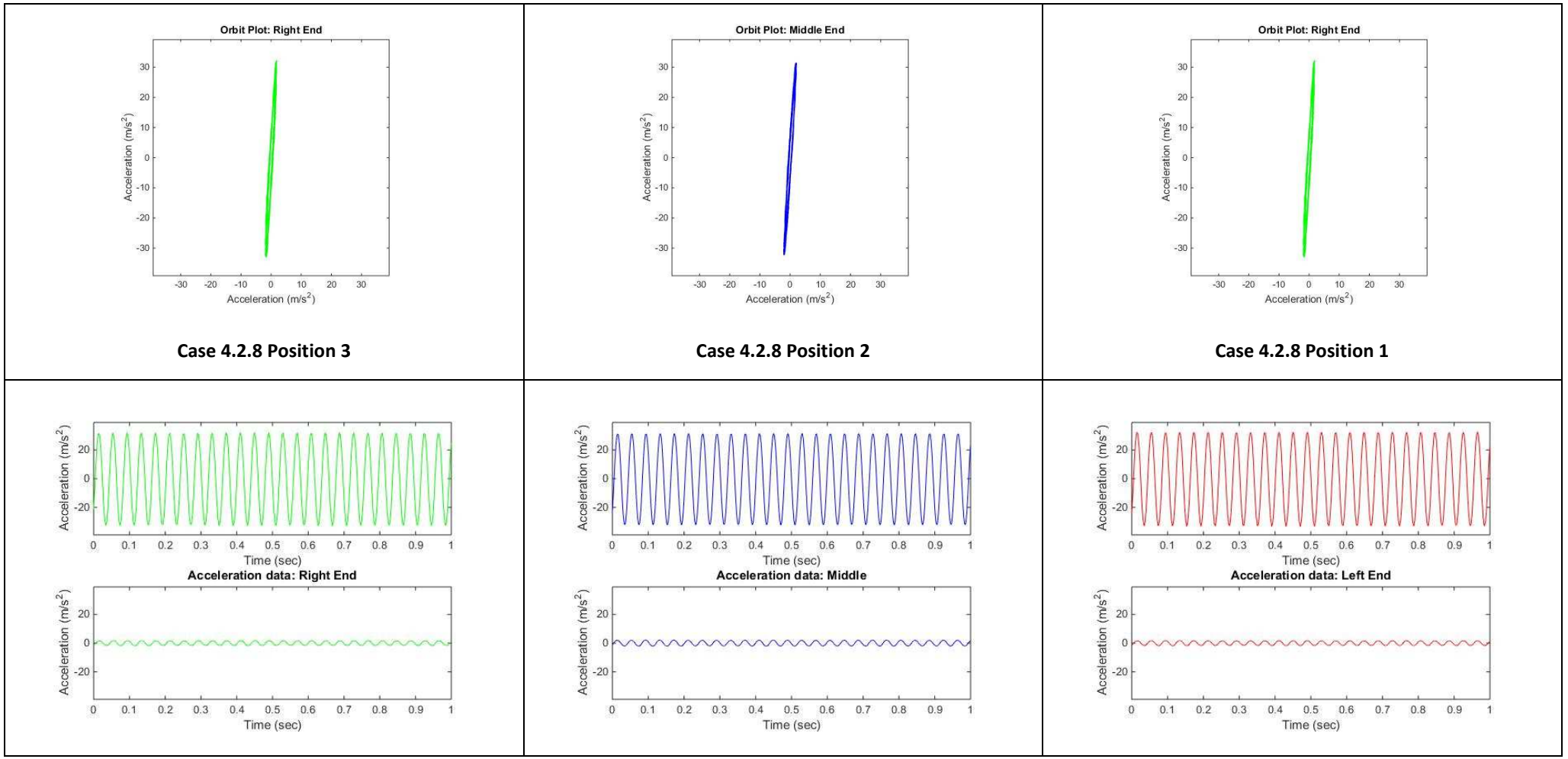

Figure 4.57 Orbit plots and acceleration graphs (X – lower graph, Y-upper graph) for case 4.2.8

Table 4.49 Test parameters of screen test Case 4.2.9 with vibrators rotating in the opposite directions

	Unit	Value
Moment of Inertia	kgm^2	1.365
Vibrator Static Moment (each)	kgm	$1387.8e^{-5}$
The phase difference of	deg	180
Distance of left exciter centre to the centre of mass	m	0.101929
Distance of right exciter centre to the centre of mass	m	0.101929
Vibrators rotational speed	rpm/Hz	1200/20
Mass of the setup	kg	17.8

Table 4.50 Orbit Plots and Acceleration Amplitude results for test Case 4.2.9 with both vibrators rotating in opposite directions

Value	Unit	Position 3	Position 2	Position 1
Acceleration in Y Direction	mm/s^2	38	32	32
Acceleration in X Direction	mm/s^2	10	12	12

Case 4.2.9 is shown in Figure 4.58 with both vibrators rotating in opposite directions at 20 Hz frequency. The phase difference of 180 degrees is presented on the Figure 4.58 and also on the graphs showing the sinusoidal signal with acceleration in Figure 4.59. The orbit plots and acceleration values are shown in Figure 4.59. The top of the testing rig has been removed which changed the rig mass and moment of inertia. The testing rig was moving in slight elliptical motion at locations 1 and 3 and linear motion at location 1. There are different amplitudes in shapes and magnitudes at all positions but it did not affect self-synchronisation in any way. There was no noticeable change in movement when one of the vibrators was turned off.

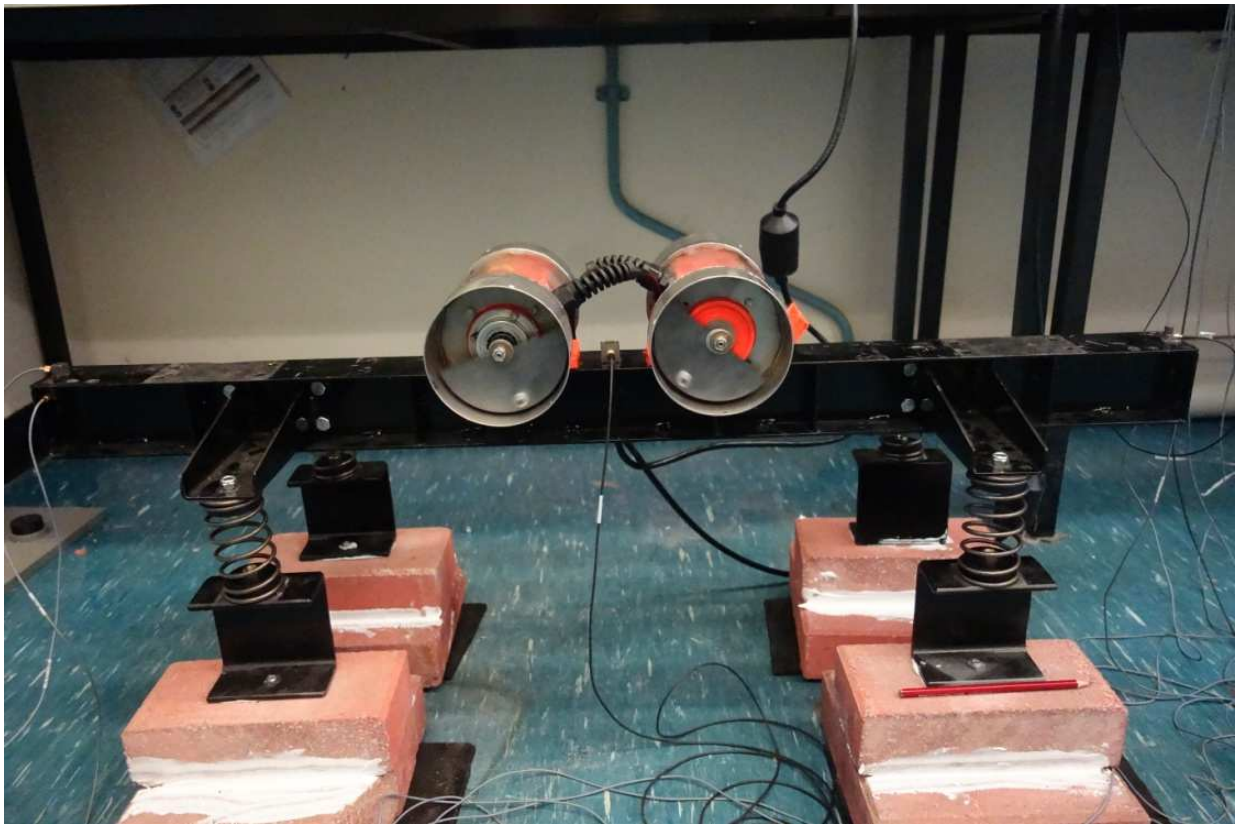

Figure 4.58 Case 4.2.9 Setup

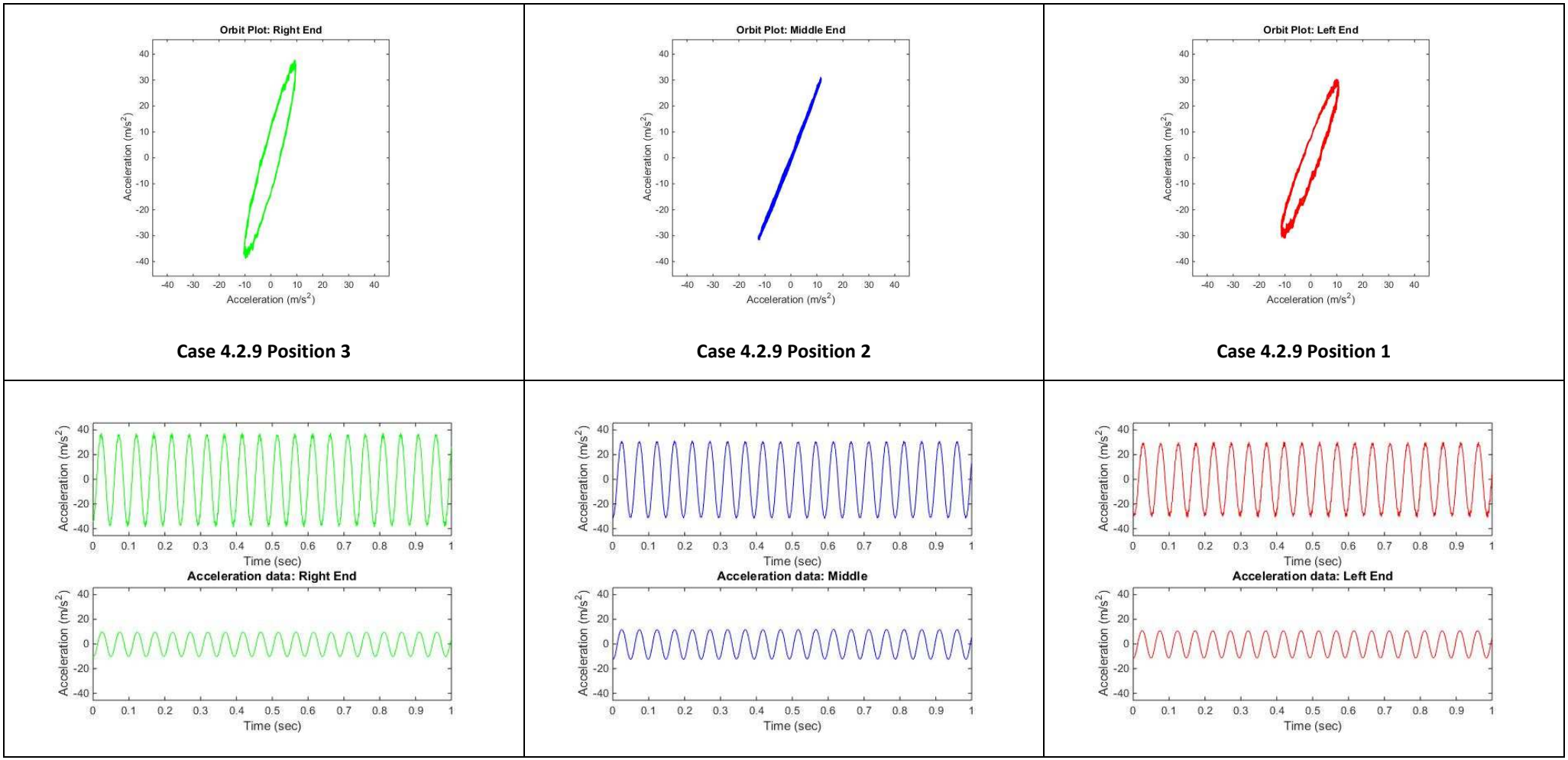

Figure 4.59 Orbit plots and acceleration graphs (X – lower graph, Y-upper graph) for case 4.2.9

Table 4.51 Test parameters of screen test Case 4.2.10 with vibrators rotating in the opposite directions

	Unit	Value
Moment of Inertia	kgm^2	3.013
Vibrator Static Moment (each)	kgm	$1387.8e^{-5}$
The phase difference of	deg	180
Distance of left exciter centre to the centre of mass	m	0.506085
Distance of right exciter centre to the centre of mass	m	0.506085
Vibrators rotational speed	rpm/Hz	1500/25
Mass of the setup	kg	17.8

Table 4.52 Orbit Plots and Acceleration Amplitude results for test Case 4.2.10 with both vibrators rotating in opposite directions

Value	Unit	Position 3	Position 2	Position 1
Acceleration in Y Direction	mm/s^2	50	50	50
Acceleration in X Direction	mm/s^2	1	1	1

Case 4.2.10 is shown in Figure 4.60 with both vibrators rotating in opposite directions at 25 Hz frequency. The phase difference of 180 degrees is presented on the Figure 4.60 and also on the graphs showing the sinusoidal signal with acceleration in Figure 4.61. The orbit plots and acceleration values are shown in Figure 4.61. The testing rig was moving in linear motion at all location with the same amplitudes. Some irregularities in the orbit shapes are related to high acceleration which caused some nonlinearities showing up from the springs.

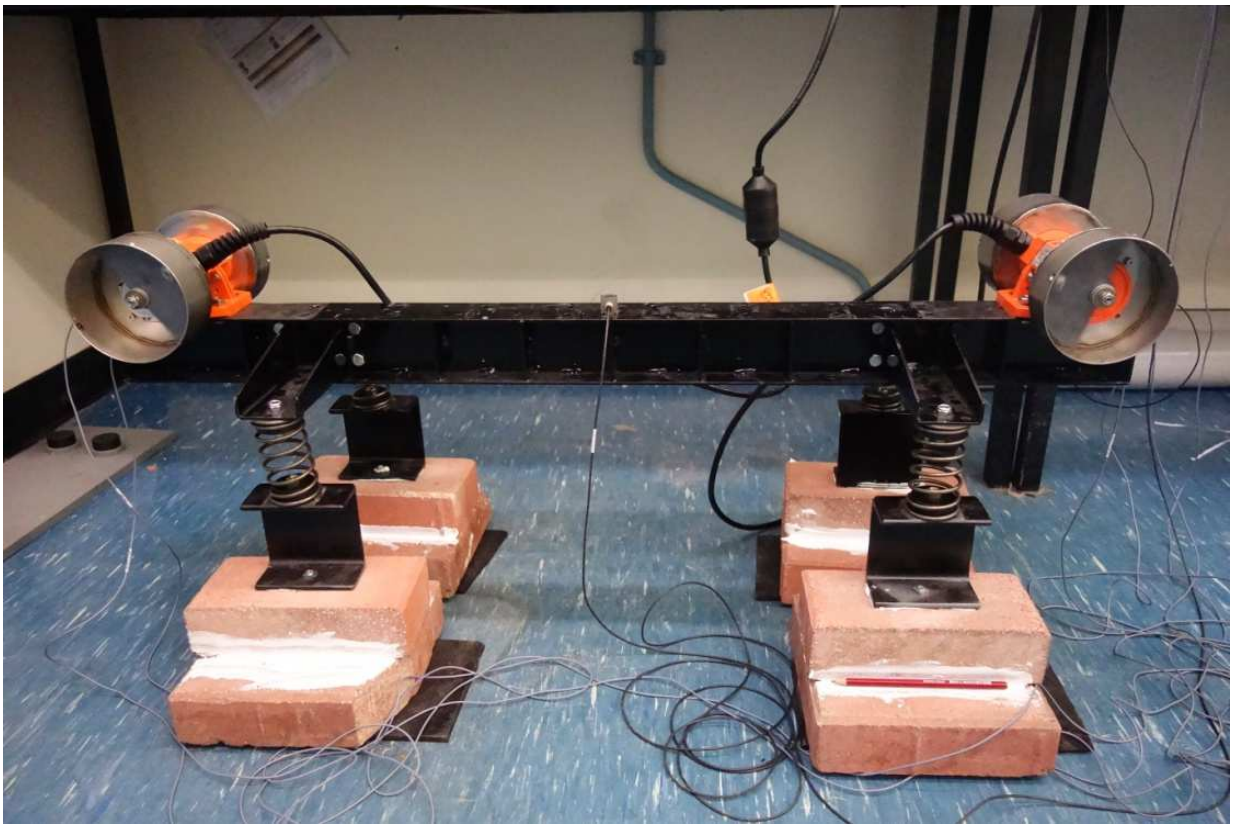

Figure 4.60 Case 4.2.10 Setup

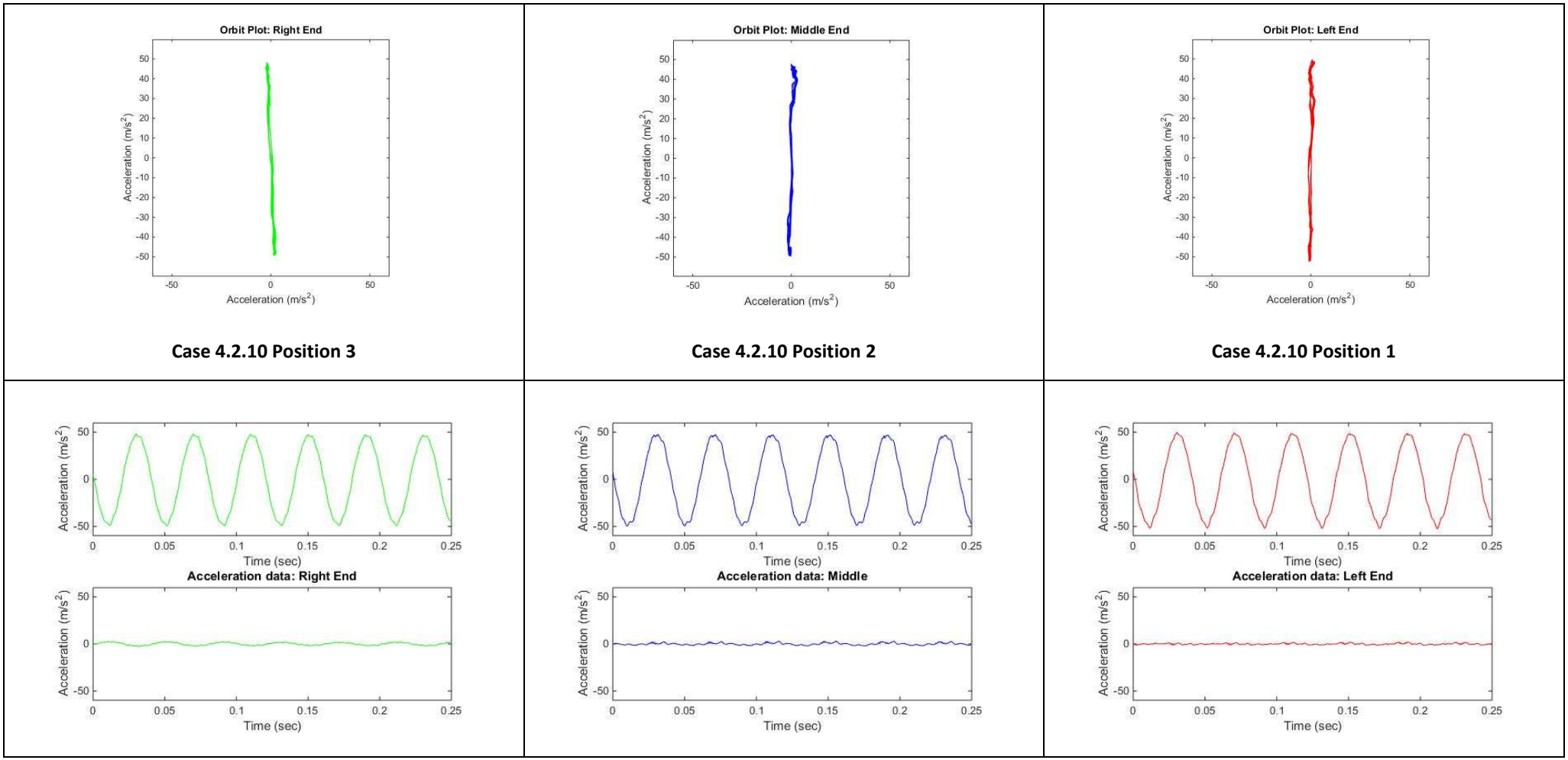

Figure 4.61 Orbit plots and acceleration graphs (X – lower graph, Y-upper graph) for case 4.2.10

4.4 Critical analysis of experimental results with vibrators rotating in opposite directions - results

Several different combinations of ω, moment of inertia, and several vibrating positions were investigated in section 4.3 with 10 case studies being presented.

In all cases, the vibrators self-synchronised with counterweights at 180˚ phase difference. Similarly in all cases on revolutions in the same directions, the phase difference was also 180˚.

Self-synchronisation was very stable in all cases and both vibrators were kept rotating even with power disconnected to one of them.

Stroke shape can be elliptical or linear and can be controlled also without electronic means. The angle of the stroke is always perpendicular to the line connecting both vibrators when it is going through the centre of mass. If the line connecting both motors does not go through the centre of mass, then the angle will be a function of the location of the centre of mass.

Self-synchronisation in the case of revolution in opposite directions always happened but it can be controlled to obtain the required stroke angle and shape (linear or elliptical) by different location of vibrators and adjustable static moment of vibrators.

The testing results confirmed theoretical calculation results accordingly to which vibrators rotating in opposite directions will always self-synchronise. Operation of the testing rig in the resonance region did show some additional vibrations on orbit plots but it did not change the phase between vibrators.

Depending on the position of the vibrators about the centre of gravity, linear or elliptical stroke shape can be obtained, for both vibrators with the same static moment.

Similar results on self-synchronisation was obtained by other researches (Bangchun at al., 2012).

Chapter 5
Vibrators rotating with two different frequencies

There are several manufacturers of dual frequency vibrating screens and an example of this type of screen is shown in Figure 5.1. Little work has been done in comparison to standard vibrating screens, though some research has been done at the Technical University of Lodz, Poland and there are also several articles written by Mr. Fischer, (Fisher, 1982).

Dual frequency screening can achieve better efficiency of screening by improved stratification of screening material. It is caused by superimposed vibration which varies in acceleration and different stroke shape in every point of the vibrating screen.

Variation of stroke and acceleration can create better condition for screening of difficult materials and improved efficiency in comparison to standard single-frequency screening equipment.

There are many options for the location of vibrators and they will determine the trajectories which are possible to achieve.

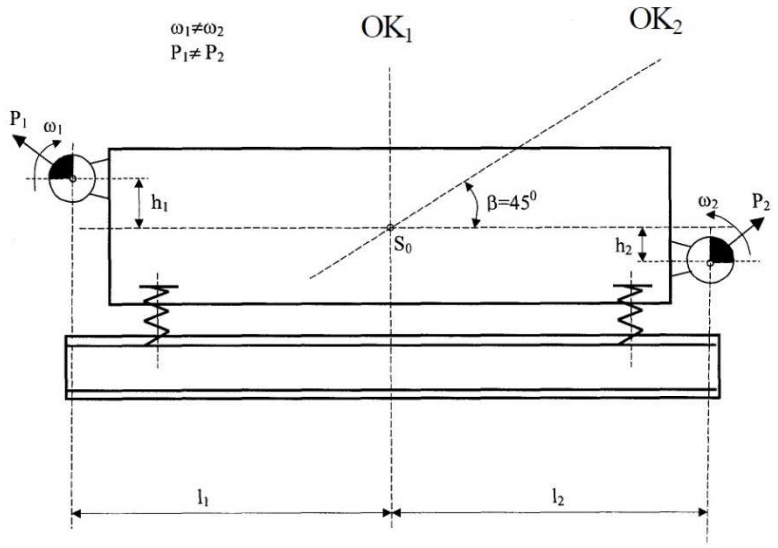

Figure 5.1 Example of a dual frequency screen

5.1 Experimental Tests - Vibrators rotating with different frequencies

Chapter 5.1 presents results from a testing rig with two vibrators running with different frequencies in the same or in opposite directions. Only selected test results are presented. L (left) and R (right) next to rpm/Hz denote the direction of revolutions of vibrators.

The upper beam of the rig and vertical supports were removed for some of the experiments to change the mass and moment of inertia of the testing rig. The location of vibrators, running speed and running vibrators speed ratio was also varied.

Figures 5.2 to 5.29 show the rig setup with position of vibrators, location of accelerometers and present the trajectories and magnitudes of the strokes plotted in X-Y graphs along with the accelerations in X and Y directions. Photos were taken during testing rig operation and the counterweights phase is shown, however the phase between counterweights changes continuously so the pictures are for presentation of the testing rig setup and indication of directions of rotation of vibrators. The power cable direction leaving the housing is also showing the direction of revolution.

The excel spreadsheet has been created (based on calculations done by Modrzewski and Wodzinski (2010)) to compare the analytical and testing results and the correlation is very close. It can only determine the trajectory between the vibrators but it is a very useful tool to quickly check if the settings are correct or what frequencies are required to get a specific trajectory. Some extra options have been added for calculations to be performed later during testing with three vibrators (more vibrators added and an option for a phase difference).

Various testing times were used to better present the orbits and to show repeatability of the movement.

Table 5-1 shows the parameters for each of the 14 presented test cases.

Table 5.1 Testing parameters for vibrators rotating with two different frequencies

Case No	Left Vibrator position rpm/Hz	Right Vibrator position Rpm/Hz	TIME [s]	Orbit Positions
5.1	4 500/8.33 R	2 1500/25 R	1	1B-2B-3B
5.2	4 500/8.33 R	2 1000/16.66 L	0.5	1B-2B-3B
5.3	4 500/8.33 R	2 1000/16.66 L	3	1B-2B-3B
5.4	4 1000/16.66 R	2 1500/25 L	1	1B-2B-3B
5.5	4 1000/16.66 R	2 1500/25 L	3	1B-2B-3B
5.6	4 1200/20 R	2 1500/25 L	0.25	1B-2B-3B
5.7	9 1200/20 R	25 1500/25 L	1	1B-2B-3B
5.8	9 1200/20 R	25 1500/25 L	0.5	1B-2B-3B
5.9	18 800/13.33 R	16 1600/26.66 R	1	1B-2B-3B
5.10	18 700/11.66 R	16 1400/23.33 L	1	1B-2B-3B
5.11	19 700/11.66 R	15 1400/23.33 L	1	1A-2-3A
5.12	22 1200/20 R	12 1600/26.6	1	1A-2-3A
5.13	22 1200/20 R	12 1600/26.6 L	3	1A-2-3A
5.14	22 1200/20 R	12 1600/26.6 L	5	1A-2-3A

Case 5.1 is shown in Figure 5.3 with orbits and accelerations for 3 accelerometers positions as presented in Figure 5.3. Figure 5.2 presents an orbit in the centre of the mass of the testing rig calculated using the excel spreadsheet which was mentioned already at the beginning of the chapter 5.1. Accelerometer position 2 is in the majority of cases above the centre of mass or very close to it and the strong correlation can be observed.

Table 5.2 presents the Case 5.1 testing parameters.

Both vibrators were running in the same direction with frequencies of 8.33 Hz (left vibrator) and 25 Hz (right vibrator) and the sample was taken over 0.5s. All orbits have different shapes and amplitudes. The analytical and physical testing results correlate well. The vibrators self-sychronised and repeatability of the signal can be observed in Figure 5.3 which presents orbits and acceleration amplitudes in X and Y directions.

Table 5.2 Test parameters of screen test Case 5.1 with vibrators rotating with different frequencies

	Unit	Value
Moment of Inertia	kgm^2	2.699
Vibrator Static Moment (each)	kgm	$1387.8e^{-5}$
Distance of left exciter centre to the centre of mass	m	0.173456
Distance of right exciter centre to the centre of mass	m	0.323026
Left vibrator rotational speed	rpm/Hz	500/8.33
Left vibrator direction of rotation	L/R	R
Right vibrators rotational speed	rpm/Hz	1500/25
Right vibrator direction of rotation	L/R	R
Mass of the setup	kg	24.7

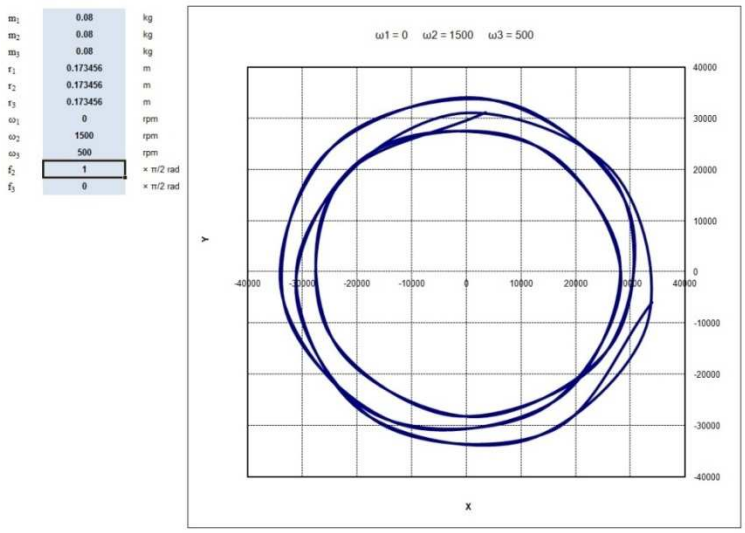

Figure 5.2 Orbit plots and X - Y excel calculated amplitude and stroke shape in the centre of mass of the test rig for case 5.1

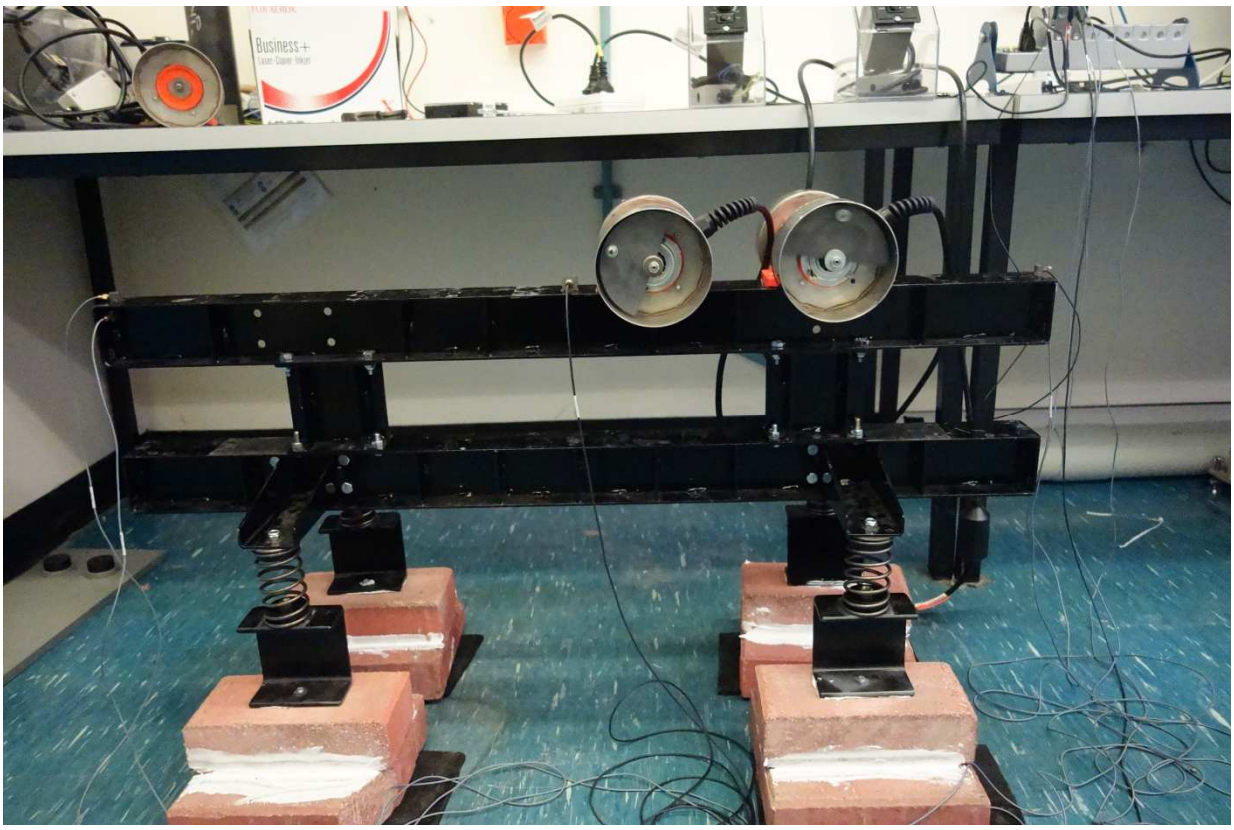

Figure 5.3 Case 5.1 Setup

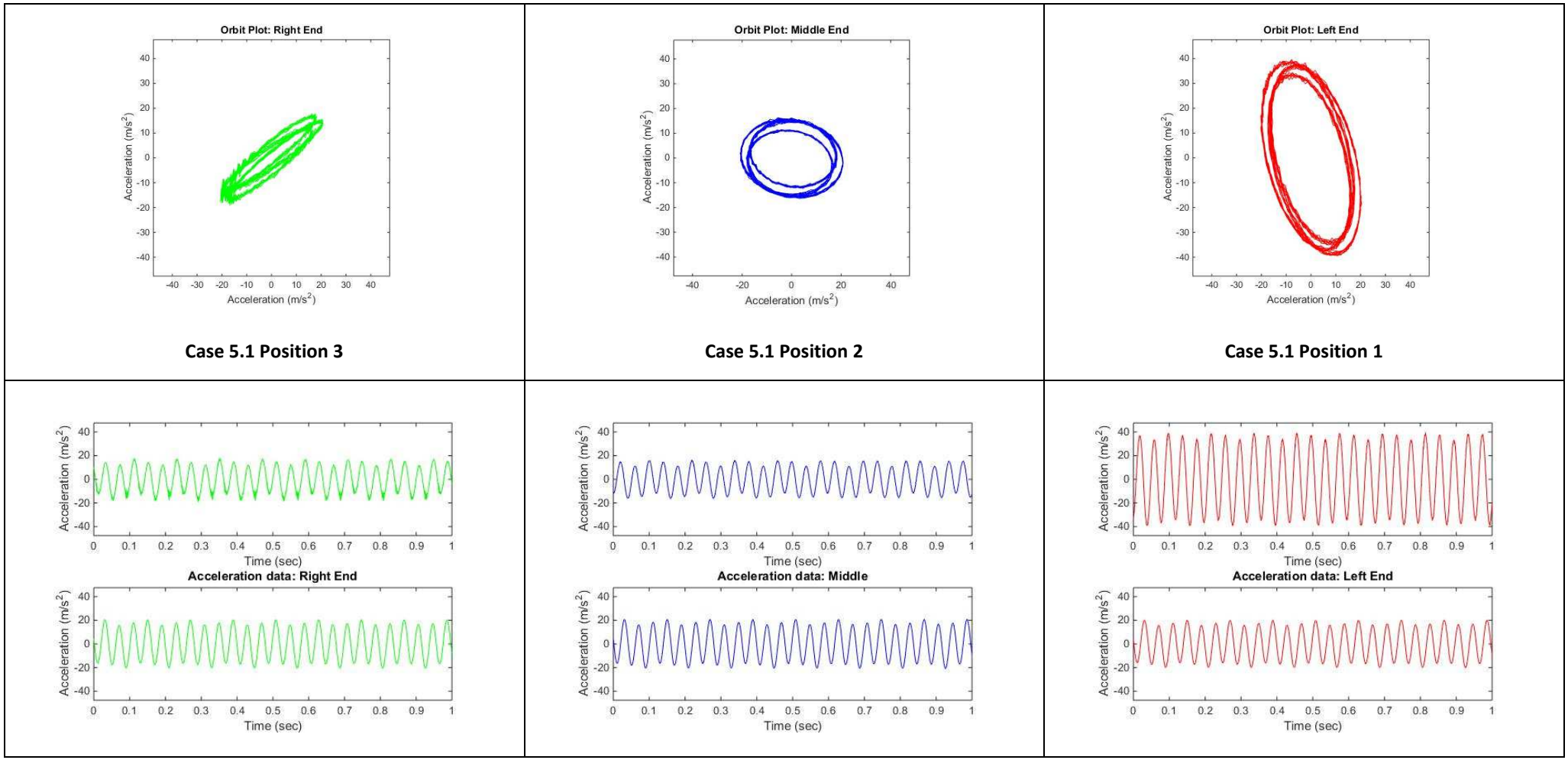

Figure 5.4 Orbit plots and acceleration graphs (X – lower graph, Y-upper graph) for case 5.1

Case 5.2 is shown in Figure 5.6 with orbits and accelerations for 3 accelerometers positions presented in Figure 5.7. Figure 5.5 presents an orbit in the centre of mass of the testing rig calculated using excel spreadsheet. Table 5.3 presents case testing parameters.

Both vibrators were running in the opposite direction with frequencies of 8.33 Hz (left vibrator) and 16.66 Hz (right vibrator) and sample was taken over 0.5s. All orbits have different shapes and amplitudes. The analytical and physical testing results correlate well. The vibrators self-sychronised and repeatability of the signal can be observed in Figure 5.6 which presents orbits and acceleration amplitudes in X and Y directions.

Table 5.3 Test parameters of screen test Case 5.2 with vibrators rotating with different frequencies

	Unit	Value
Moment of Inertia	kgm^2	2.699
Vibrator Static Moment (each)	kgm	$1387.8e^{-5}$
Distance of left exciter centre to the centre of mass	m	0.173456
Distance of right exciter centre to the centre of mass	m	0.323026
Left vibrator rotational speed	rpm/Hz	500/8.33
Left vibrator direction of rotation	L/R	R
Right vibrators rotational speed	rpm/Hz	1000/16.66
Right vibrator direction of rotation	L/R	L
Mass of the setup	kg	24.7

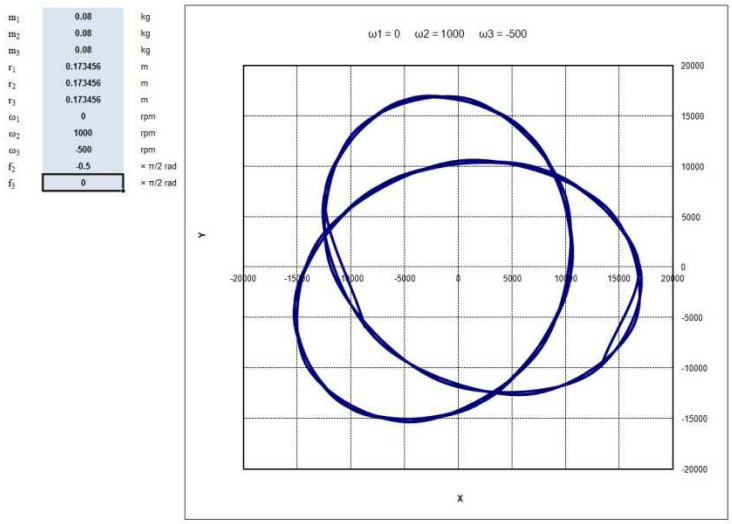

Figure 5.5 Orbit plots and X - Y excel calculated amplitude and stroke shape in the centre of mass of the test rig for case 5.2

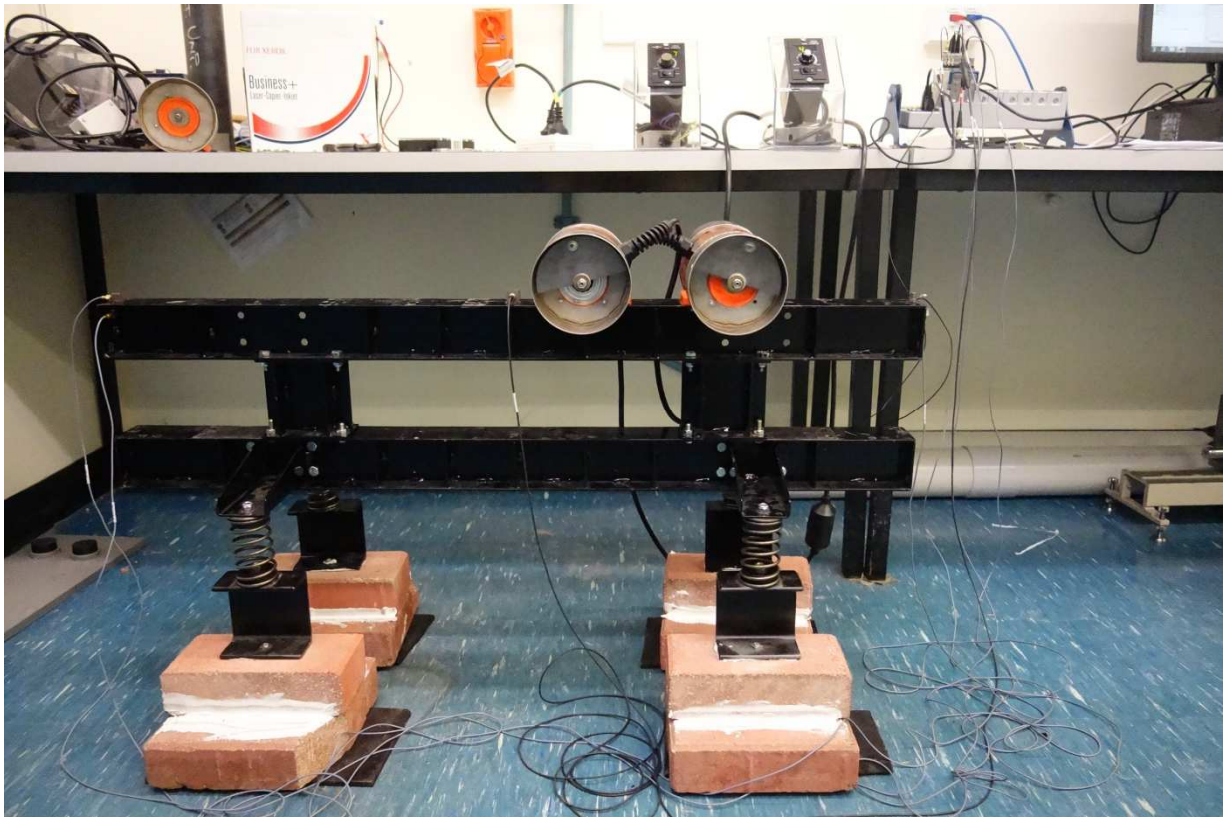

Figure 5.6 Case 5.2 Setup

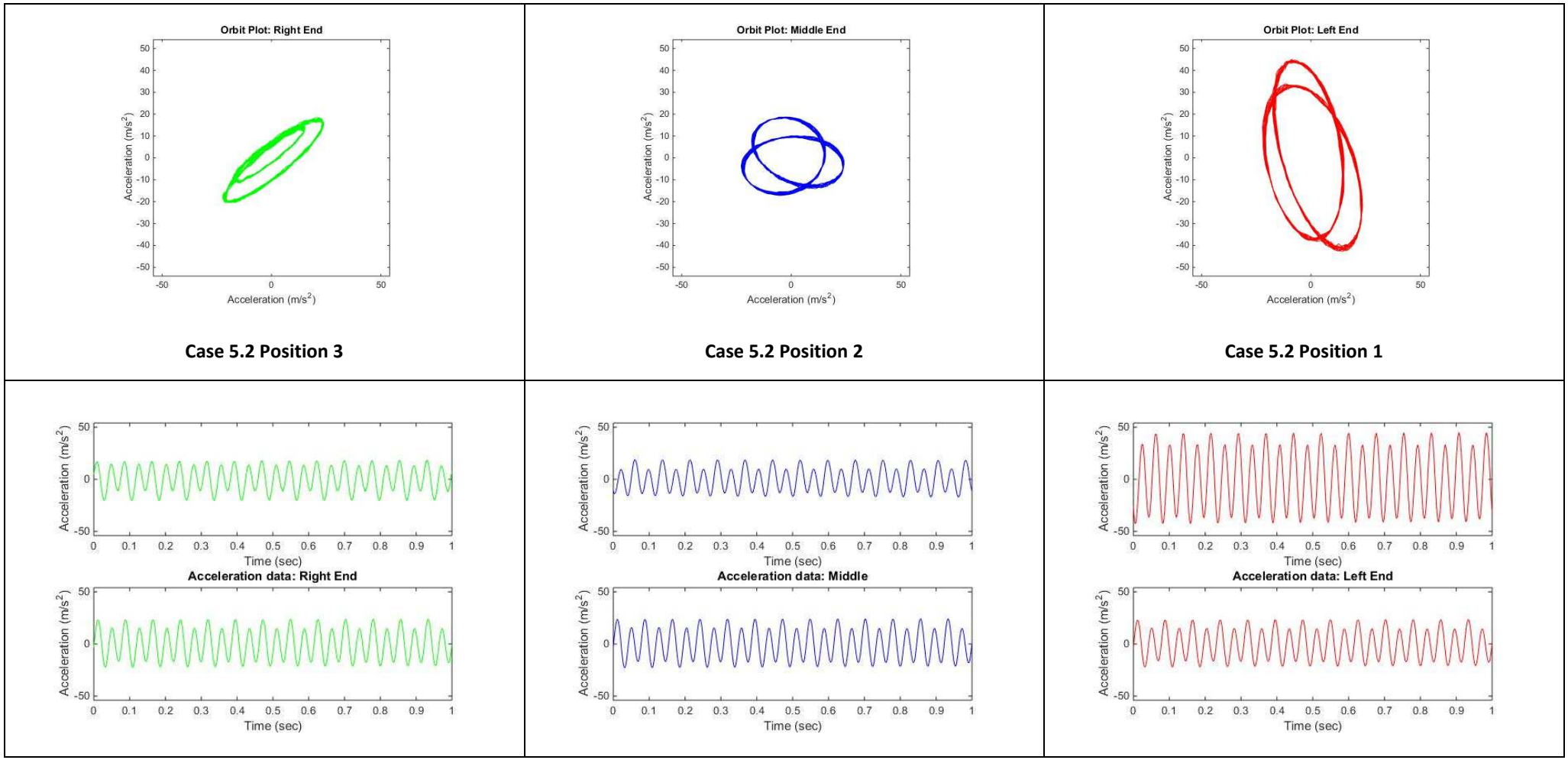

Figure 5.7 Orbit plots and acceleration graphs (X – lower graph, Y-upper graph) for case 5.2

Table 5.4 Test parameters of screen test Case 5.3 with vibrators rotating with different frequencies

	Unit	Value
Moment of Inertia	kgm^2	2.699
Vibrator Static Moment (each)	kgm	$1387.8e^{-5}$
Distance of left exciter centre to the centre of mass	m	0.173456
Distance of right exciter centre to the centre of mass	m	0.323026
Left vibrator rotational speed	rpm/Hz	500/8.33
Left vibrator direction of rotation	L/R	R
Right vibrators rotational speed	rpm/Hz	1000/16.66
Right vibrator direction of rotation	L/R	L
Mass of the setup	kg	24.7

Case 5.3 is shown in the Figure 5.8 with orbits and accelerations for 3 accelerometers positions presented in Figure 5.9. Figure 5.7 presents an orbit in the centre of the mass of the test rig calculated using excel spreadsheet and Table 5.4 presents case testing parameters.

All parameters are as in Case 5.2 but the signal has been recorded over 3s period which represents almost 50 cycles for the exciter on the right side. All orbits have different shapes and amplitudes. The analytical and physical testing results correlate well. The vibrators self-sychronised and repeatability of the signal can be observed in Figure 5.9 which presents orbits amplitudes in X and Y directions.

Figure 5.8 Case 5.3 Setup

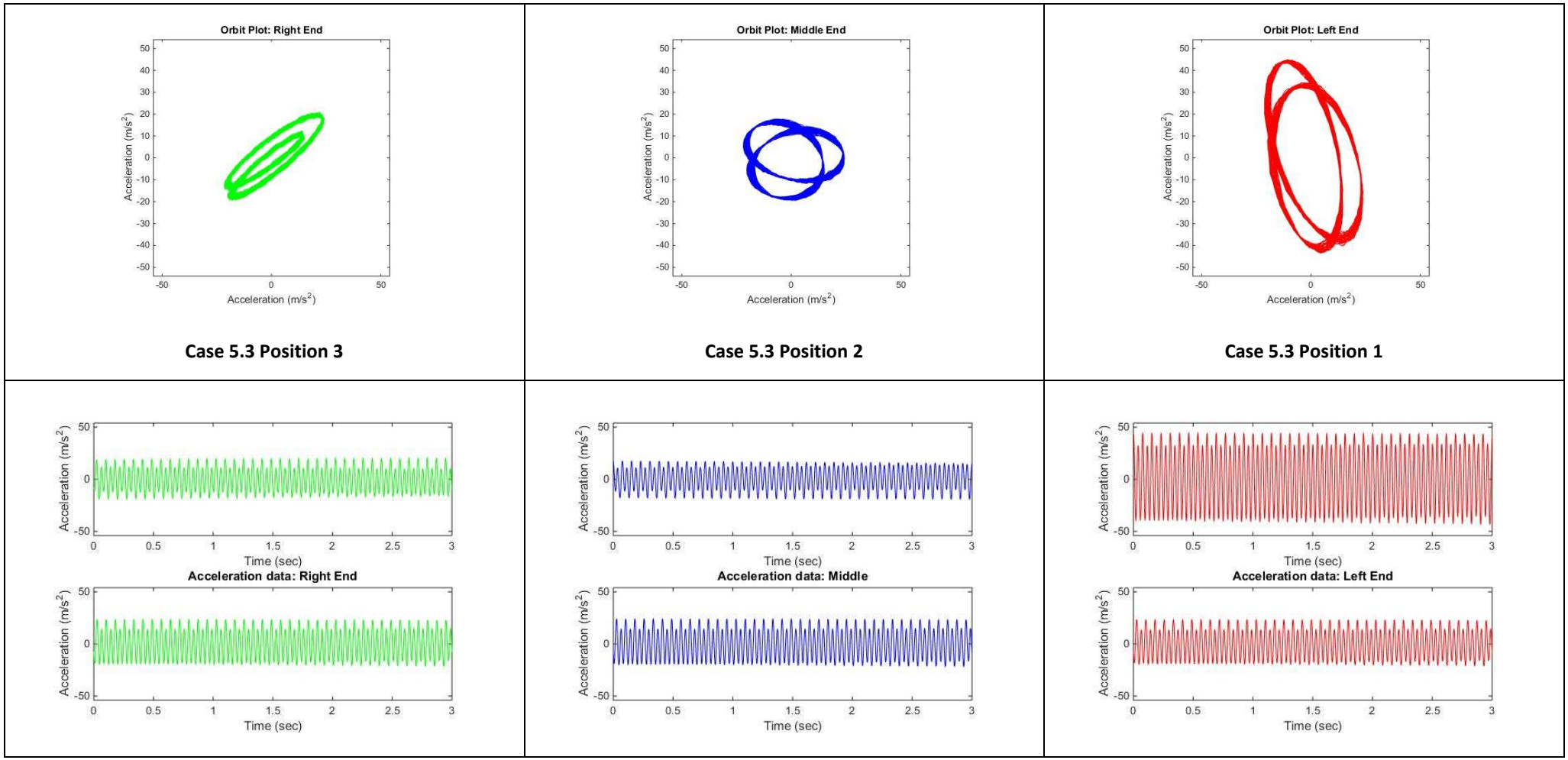

Figure 5.9 Orbit plots and acceleration graphs (X – lower graph, Y-upper graph) for case 5.3

Case 5.4 is shown in the Figure 5.11 with orbits and accelerations for 3 accelerometer positions presented in Figure 5.12. Figure 5.10 presents an orbit in the centre of mass of the testing rig calculated using excel spreadsheet and Table 5.5 presents the case testing parameters.

Both vibrators were running in the opposite direction with frequencies of 16.66 Hz (left vibrator) and 25 Hz (right vibrator). All orbits have different shapes and amplitudes. The analytical and physical testing results correlate well. The vibrators self-sychronised and repeatability of the signal can be observed in Figure 5.12 which presents orbits and acceleration amplitudes in X and Y directions. The recorded period presented was taken over 0.5s and shows the regular time waveform response.

Table 5.5 Test parameters of screen test Case 5.4 with vibrators rotating with different frequencies

	Unit	**Value**
Moment of Inertia	kgm^2	2.699
Vibrator Static Moment (each)	kgm	$1387.8e^{-5}$
Distance of left exciter centre to the centre of mass	m	0.173456
Distance of right exciter centre to the centre of mass	m	0.323026
Left vibrator rotational speed	rpm/Hz	1000/16.66
Left vibrator direction of rotation	L/R	R
Right vibrators rotational speed	rpm/Hz	1500/25
Right vibrator direction of rotation	L/R	L
Mass of the setup	kg	24.7

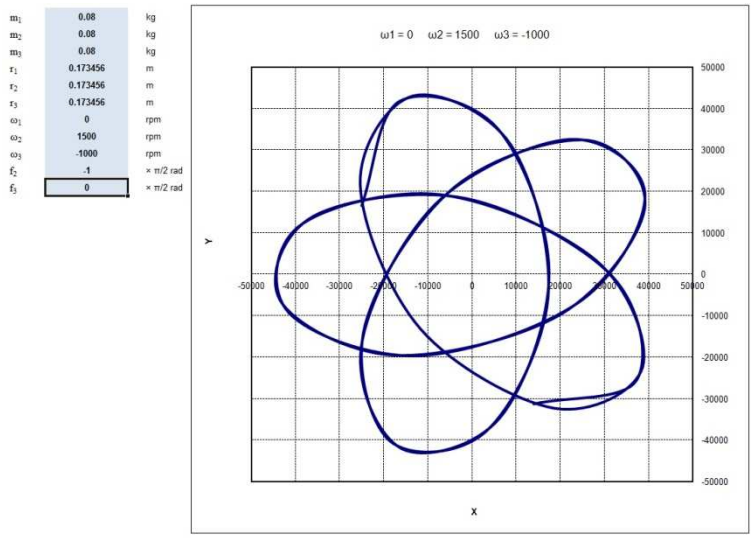

Figure 5.10 Orbit plots and X - Y excel calculated amplitude and stroke shape in the centre of mass of the test rig for case 5.4

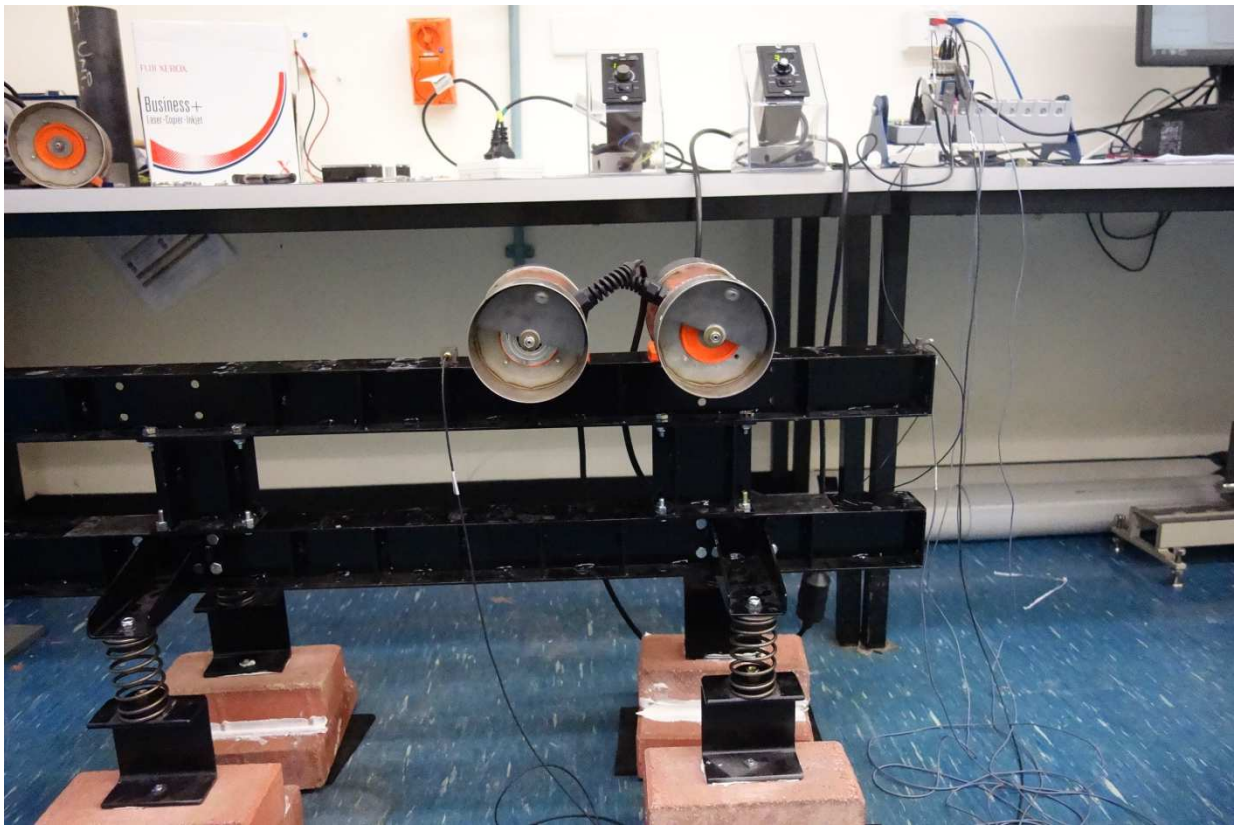

Figure 5.11 Case 5.4 Setup

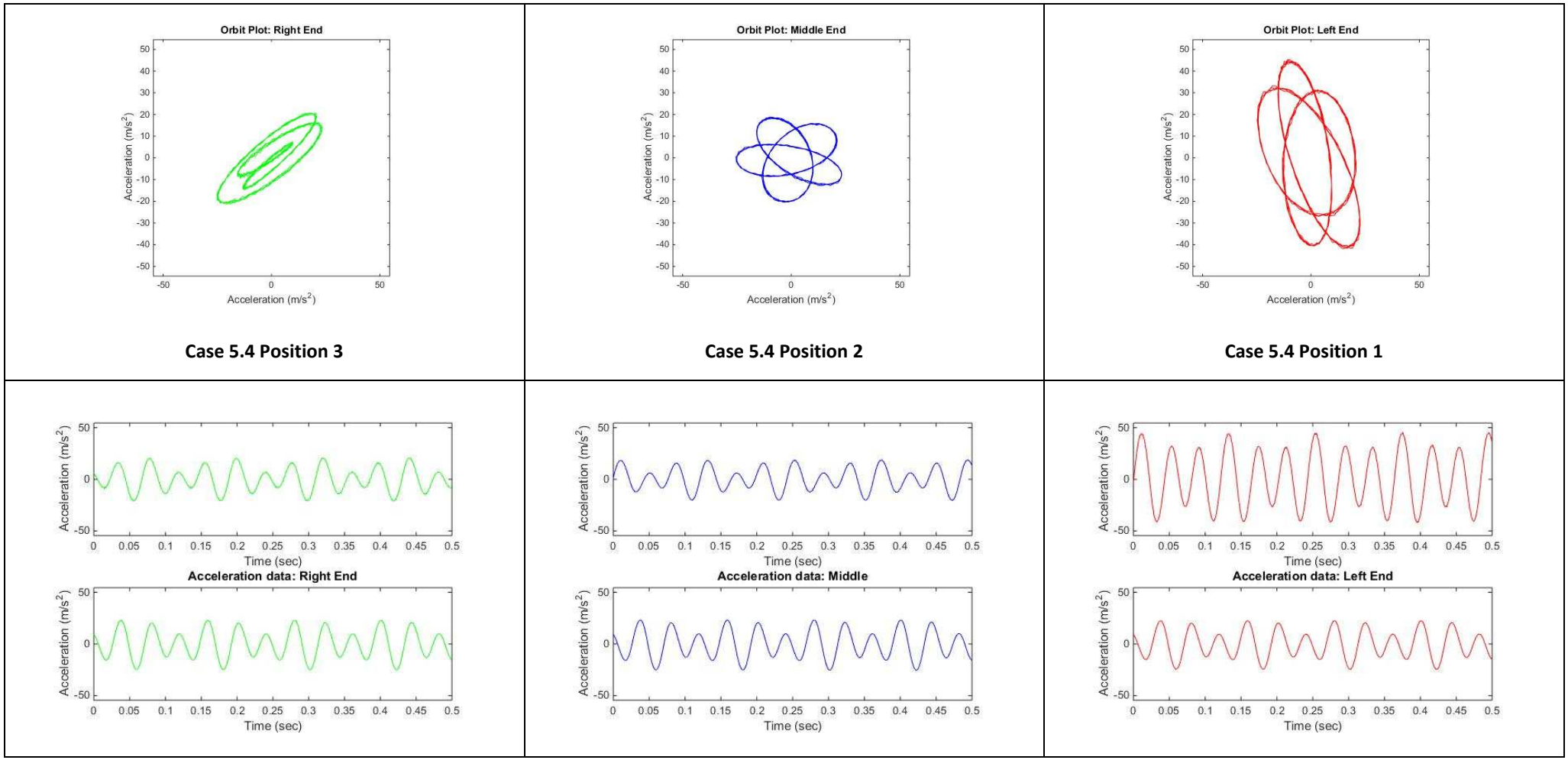

Figure 5.12 Orbit plots and acceleration graphs (X – lower graph, Y-upper graph) for case 5.4

Case 5.5 is shown in the Figure 5.14 with orbits and accelerations for the 3 accelerometer positions presented in Figure 5.15. Figure 5.13 presents an orbit in the centre of mass of the testing rig calculated using the excel spreadsheet. Table 5.6 presents the case testing parameters.

All parameters are as in Case 5.5 but the signal has been recorded over 3s period which for the right exciter represents almost 75 cycles and shows regular time waveform responses.

All orbits have different shapes and amplitudes. The analytical and physical testing results correlate well. The vibrators self-sychronised and repeatability of the signal can be observed in Figure 5.15 which presents orbits and acceleration amplitudes in X and Y directions.

Table 5.6 Test parameters of screen test Case 5.5 with vibrators rotating with different frequencies

	Unit	Value
Moment of Inertia	kgm^2	2.699
Vibrator Static Moment (each)	kgm	$1387.8e^{-5}$
Distance of left exciter centre to the centre of mass	m	0.173456
Distance of right exciter centre to the centre of mass	m	0.323026
Left vibrator rotational speed	rpm/Hz	1000/16.66
Left vibrator direction of rotation	L/R	R
Right vibrators rotational speed	rpm/Hz	1500/25
Right vibrator direction of rotation	L/R	L
Mass of the setup	kg	24.7

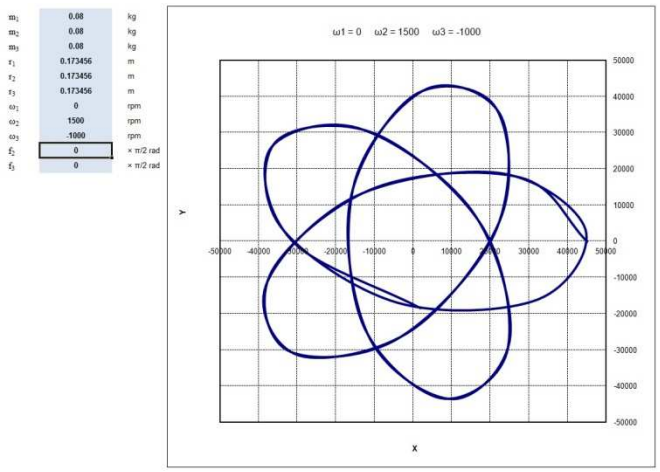

Figure 5.13 Orbit plots and X - Y excel calculated amplitude and stroke in the centre of mass of the test rig for case 5.5

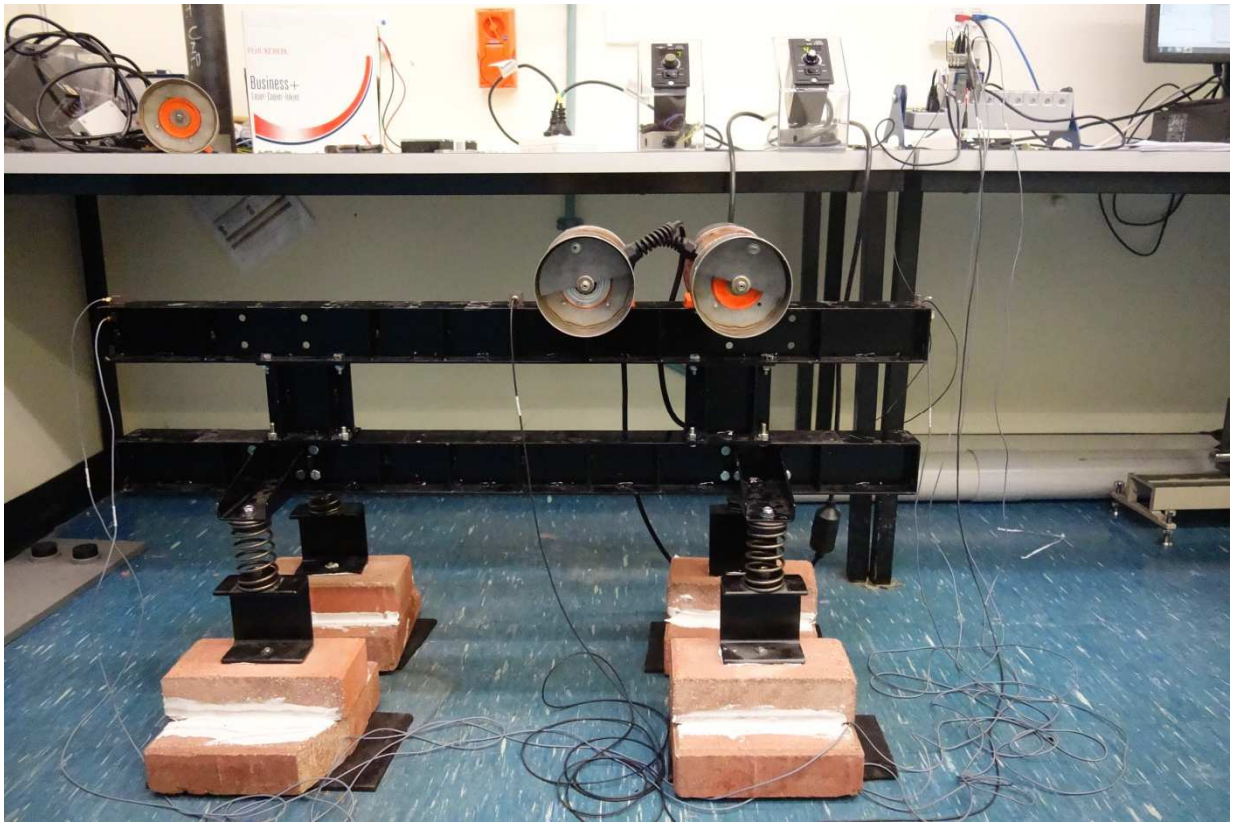

Figure 5.14 Case 5.5 Setup

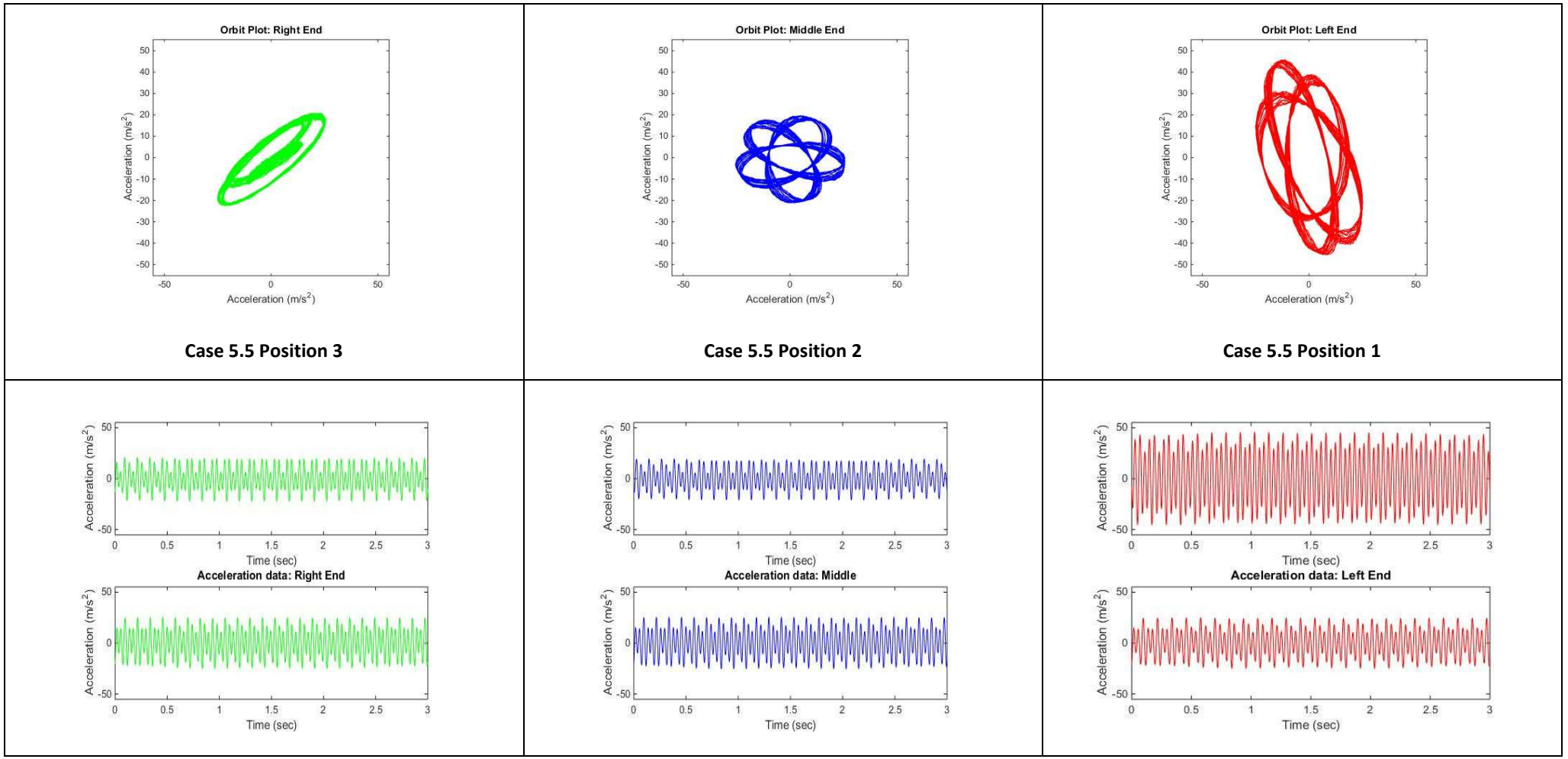

Figure 5.15 Orbit plots and acceleration graphs (X – lower graph, Y-upper graph) for case 5.5

Case 5.6 is shown in the Figure 5.17 with orbits and accelerations for 3 accelerometer positions presented in Figure 5.18. Figure 5.16 presents an orbit in the centre of mass of the testing rig calculated using the excel spreadsheet and Table 5.7 presents the case testing parameters.

Both vibrators were running in the same direction with frequencies of 20 Hz (left vibrator) and 25 Hz (right vibrator) and sample was taken over 0.25s period. All orbits have different shapes and amplitudes. The analytical and testing results correlate well. The vibrators self-sychronised and repeatability of the signal can be observed in Figure 5.18 which presents orbits and acceleration amplitudes in X and Y directions.

Table 5.7 Test parameters of screen test Case 5.6 with vibrators rotating with different frequencies

	Unit	Value
Moment of Inertia	kgm^2	2.699
Vibrator Static Moment (each)	kgm	$1387.8e^{-5}$
Distance of left exciter centre to the centre of mass	m	0.173456
Distance of right exciter centre to the centre of mass	m	0.323026
Left vibrator rotational speed	rpm/Hz	1200/20
Left vibrator direction of rotation	L/R	R
Right vibrators rotational speed	rpm/Hz	1500/25
Right vibrator direction of rotation	L/R	L
Mass of the setup	kg	24.7

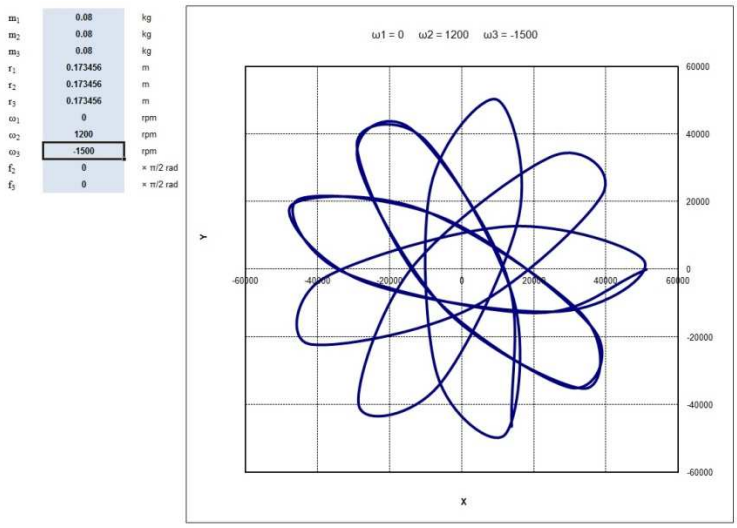

Figure 5.16 Orbit plots and X - Y excel calculated amplitude and stroke in the centre of mass of the test rig for case 5.6

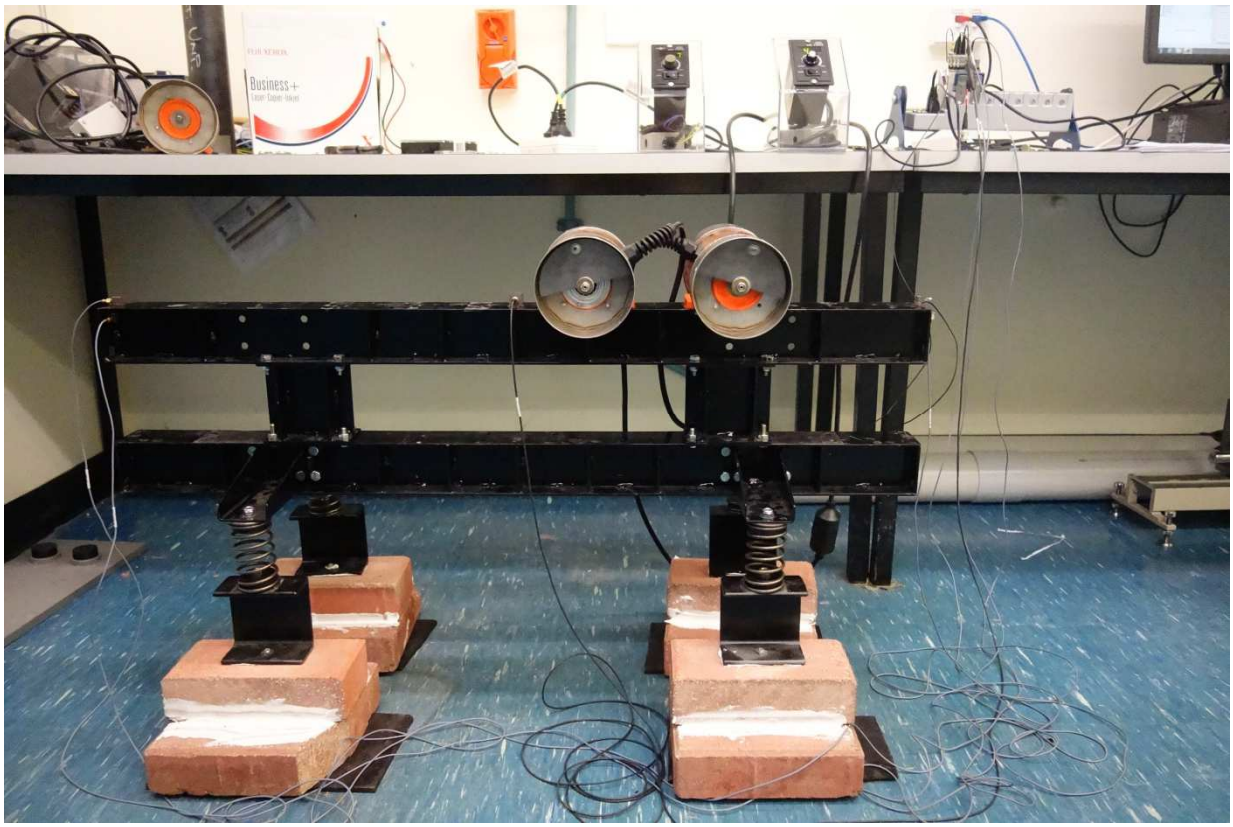

Figure 5.17 Case 5.6 Setup

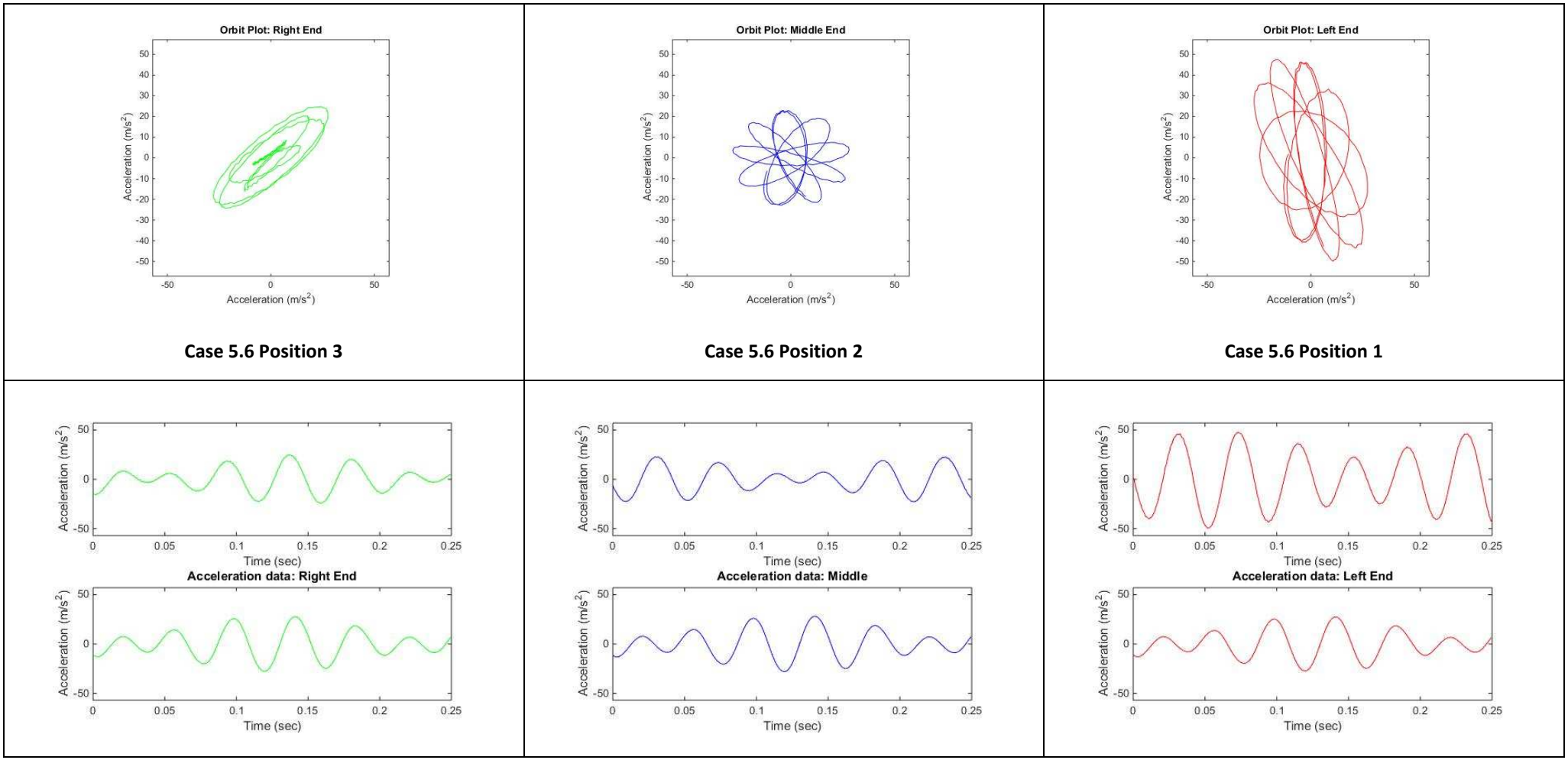

Figure 5.18 Orbit plots and acceleration graphs (X – lower graph, Y-upper graph) for case 5.6

Case 5.7 is presented in Figure 5.20 with orbits and accelerations for the 3 accelerometer positions presented in Figure 5.21. Figure 5.19 presents an orbit in the centre of mass of the testing rig calculated using the excel spreadsheet. Table 5.8 presents the case testing parameters.

Both vibrators were running in the same direction with frequencies of 20Hz (left vibrator) and 25 Hz (right vibrator) and the sample was recorded over 0.5s period. All orbits have different shapes and amplitudes. The analytical and testing results correlate well. The vibrators self-sychronised and repeatability of the signal can be observed in Figure 5.21 which presents orbits and acceleration amplitudes in X and Y directions.

Table 5.8 Test parameters of screen test Case 5.7 with vibrators rotating with different frequencies

	Unit	Value
Moment of Inertia	kgm^2	1.9761
Vibrator Static Moment (each)	kgm	$1387.8e^{-5}$
Distance of left exciter centre to the centre of mass	m	0.327393
Distance of right exciter centre to the centre of mass	m	0.307205
Left vibrator rotational speed	rpm/Hz	1200/20
Left vibrator direction of rotation	L/R	R
Right vibrators rotational speed	rpm/Hz	1500/25
Right vibrator direction of rotation	L/R	R
Mass of the setup	kg	24.7

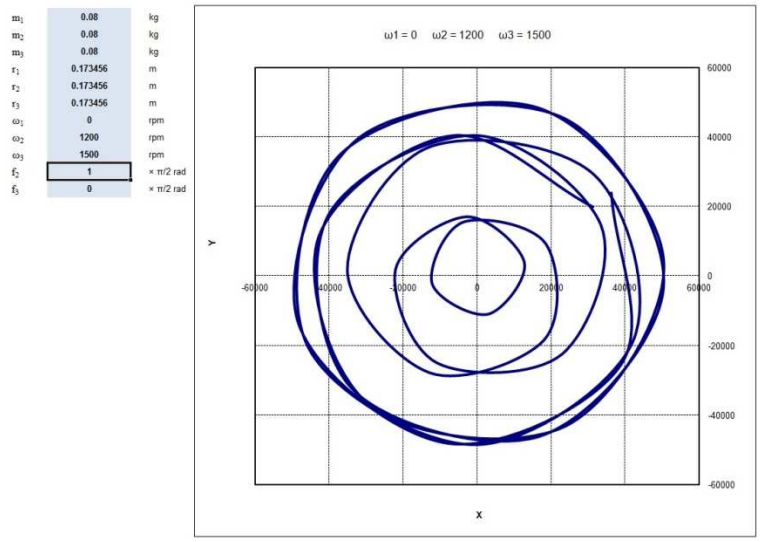

Figure 5.19 Orbit plots and X - Y excel calculated amplitude and stroke in the centre of mass of the test rig for case 5.7

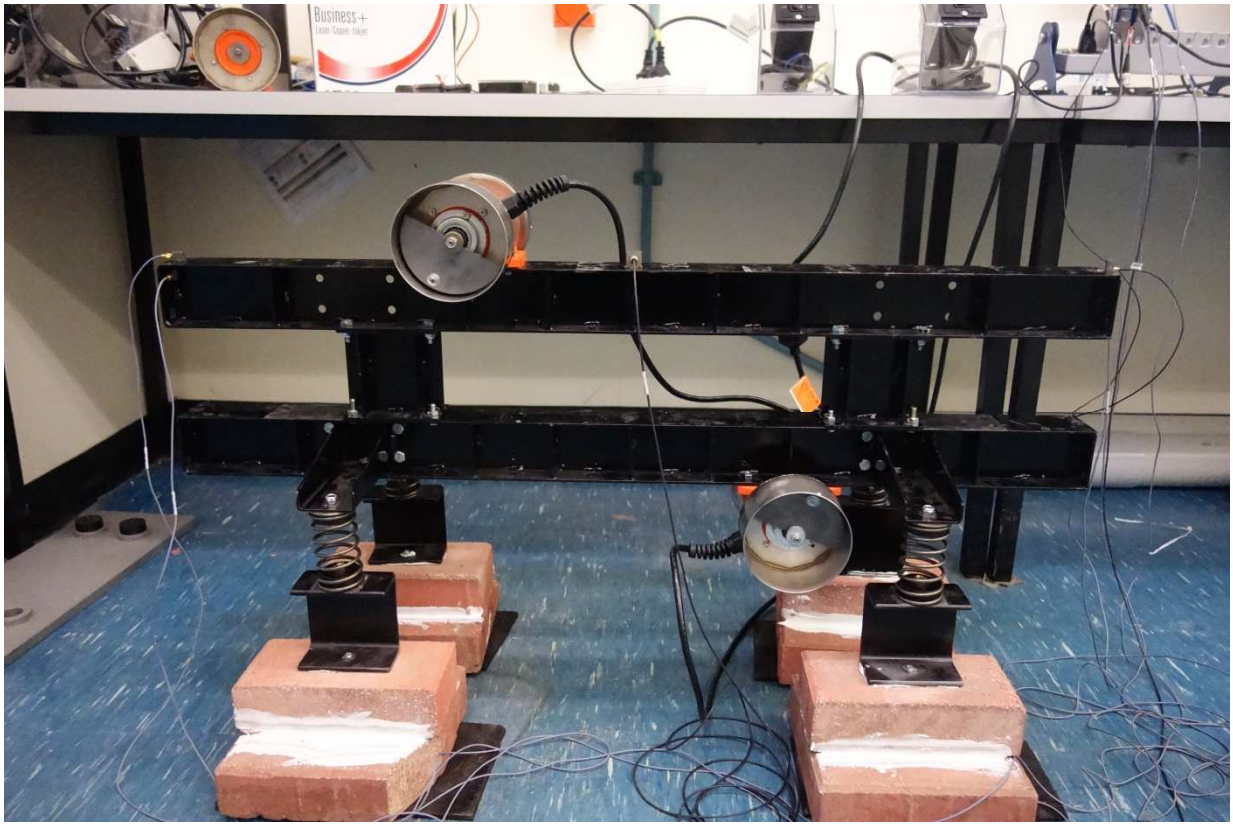

Figure 5.20 Case 5.7 Setup

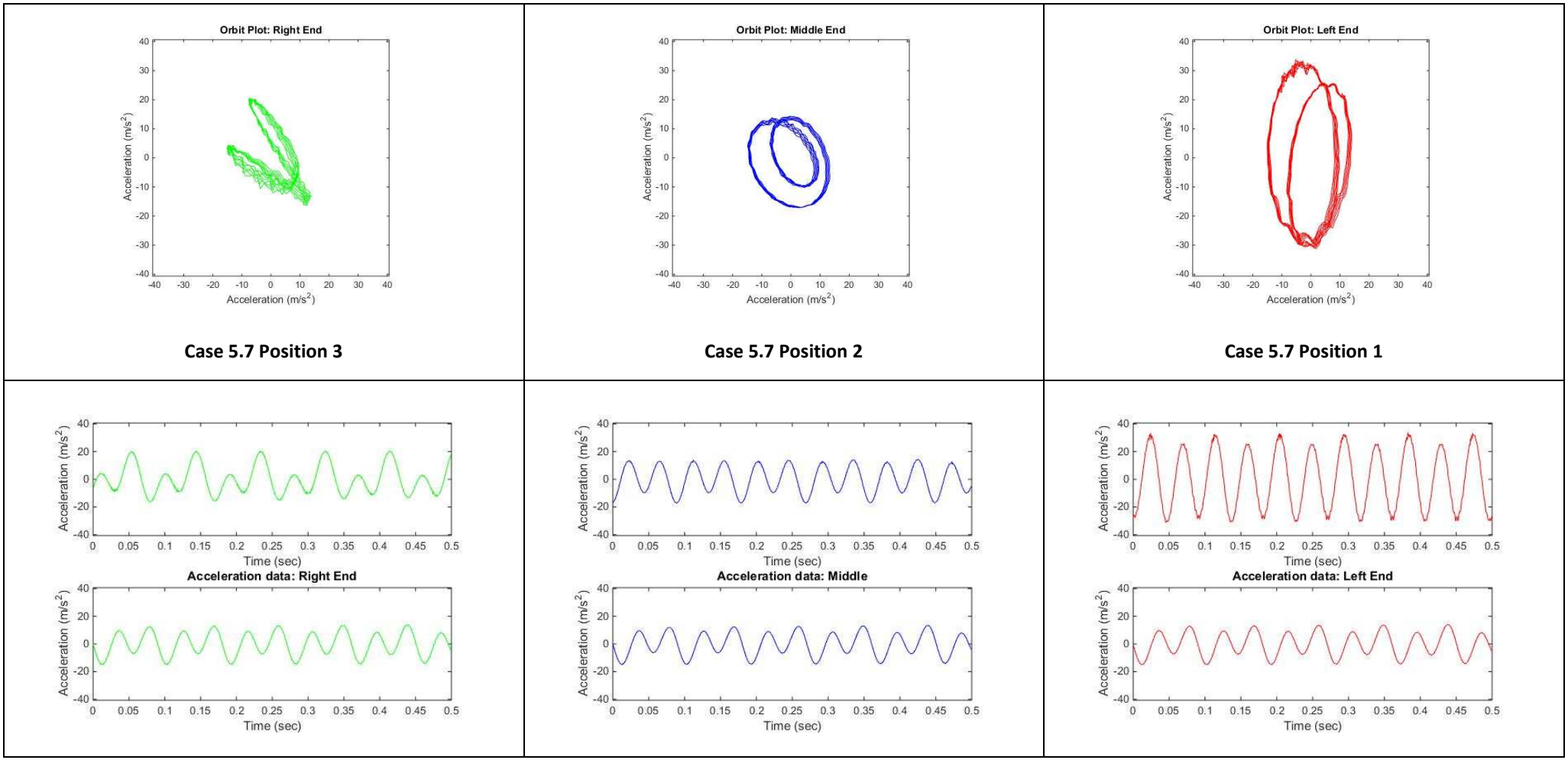

Figure 5.21 Orbit plots and acceleration graphs (X – lower graph, Y-upper graph) for case 5.7

Case 5.8 is presented in Figure 5.23 with orbits and accelerations for 3 accelerometer positions presented in Figure 5.24. Figure 5.22 presents an orbit in the centre of mass of the testing rig calculated using excel spreadsheet and Table 5.9 presents the case testing parameters.

Both vibrators were running in the opposite directions with frequencies of 20 Hz (left vibrator) and 25 Hz (right vibrator) and sample was taken over 0.5s period. All orbits have different shapes and amplitudes. The analytical and testing results correlate well. The vibrators self-sychronised and repeatability of the signal can be observed in Figure 5.24 which presents orbits and acceleration amplitudes in X and Y directions.

The calculated trajectory is the same in the middle of the testing rig as in Case 5.6, the orbits in positions 1 and 3 are however completely different.

Table 5.9 Test parameters of screen test Case 5.8 with vibrators rotating with different frequencies

	Unit	Value
Moment of Inertia	kgm^2	2.0697
Vibrator Static Moment (each)	kgm	$1387.8e^{-5}$
Distance of left exciter centre to the centre of mass	m	0.327399
Distance of right exciter centre to the centre of mass	m	0.307205
Left vibrator rotational speed	rpm/Hz	1200/20
Left vibrator direction of rotation	L/R	R
Right vibrators rotational speed	rpm/Hz	1500/25
Right vibrator direction of rotation	L/R	L
Mass of the setup	kg	24.7

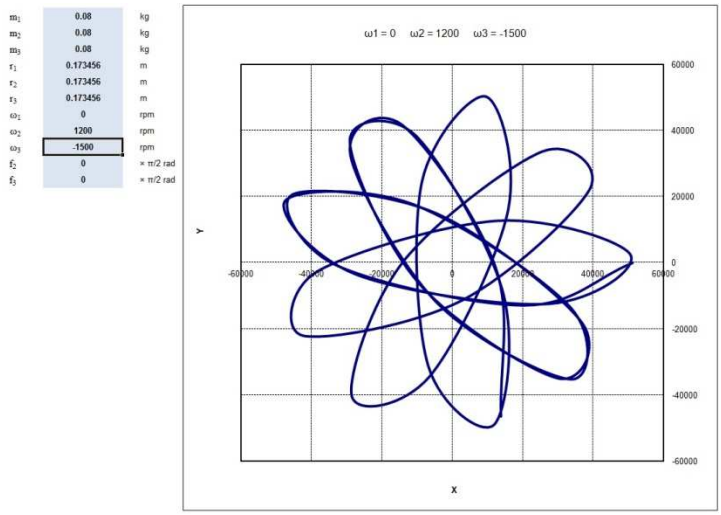

Figure 5.22 Orbit plots and X - Y excel calculated amplitude and stroke in the centre of mass of the test rig for case 5.8

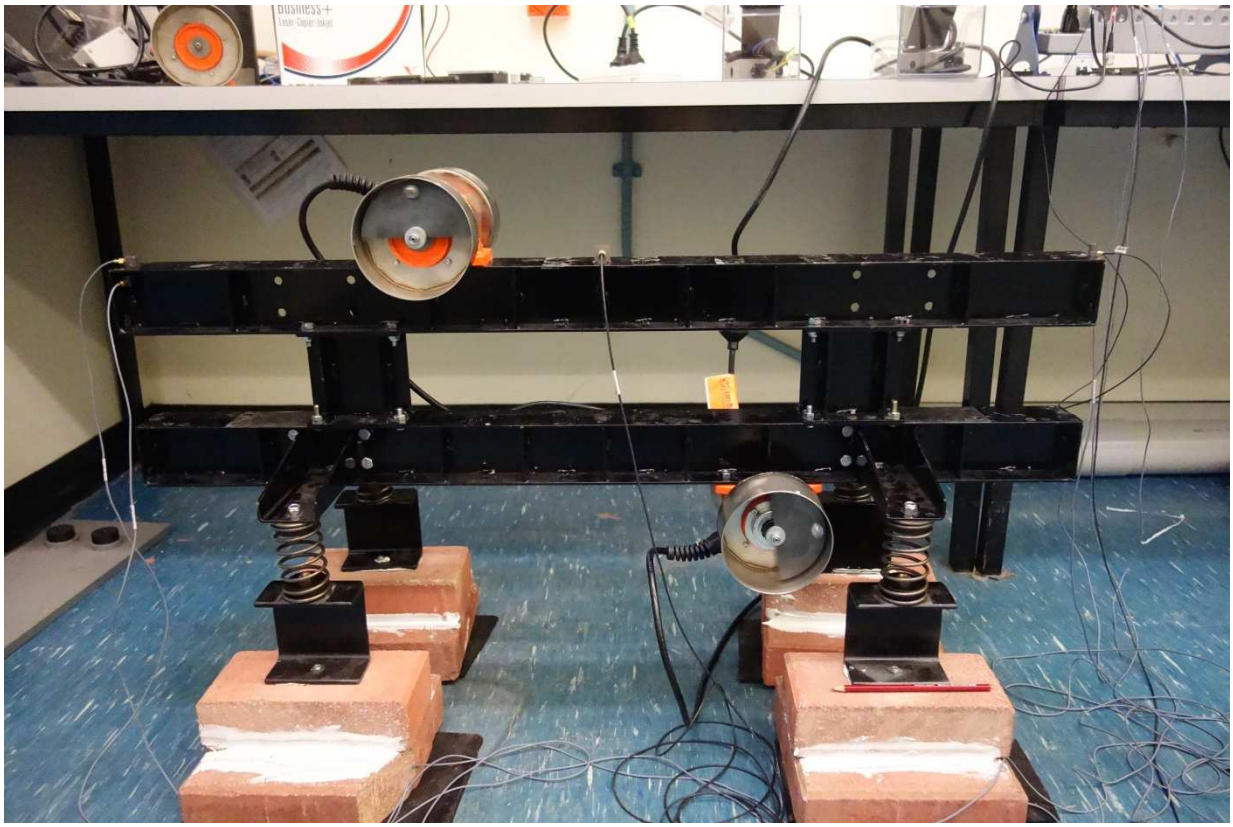

Figure 5.23 Case 5.8 Setup

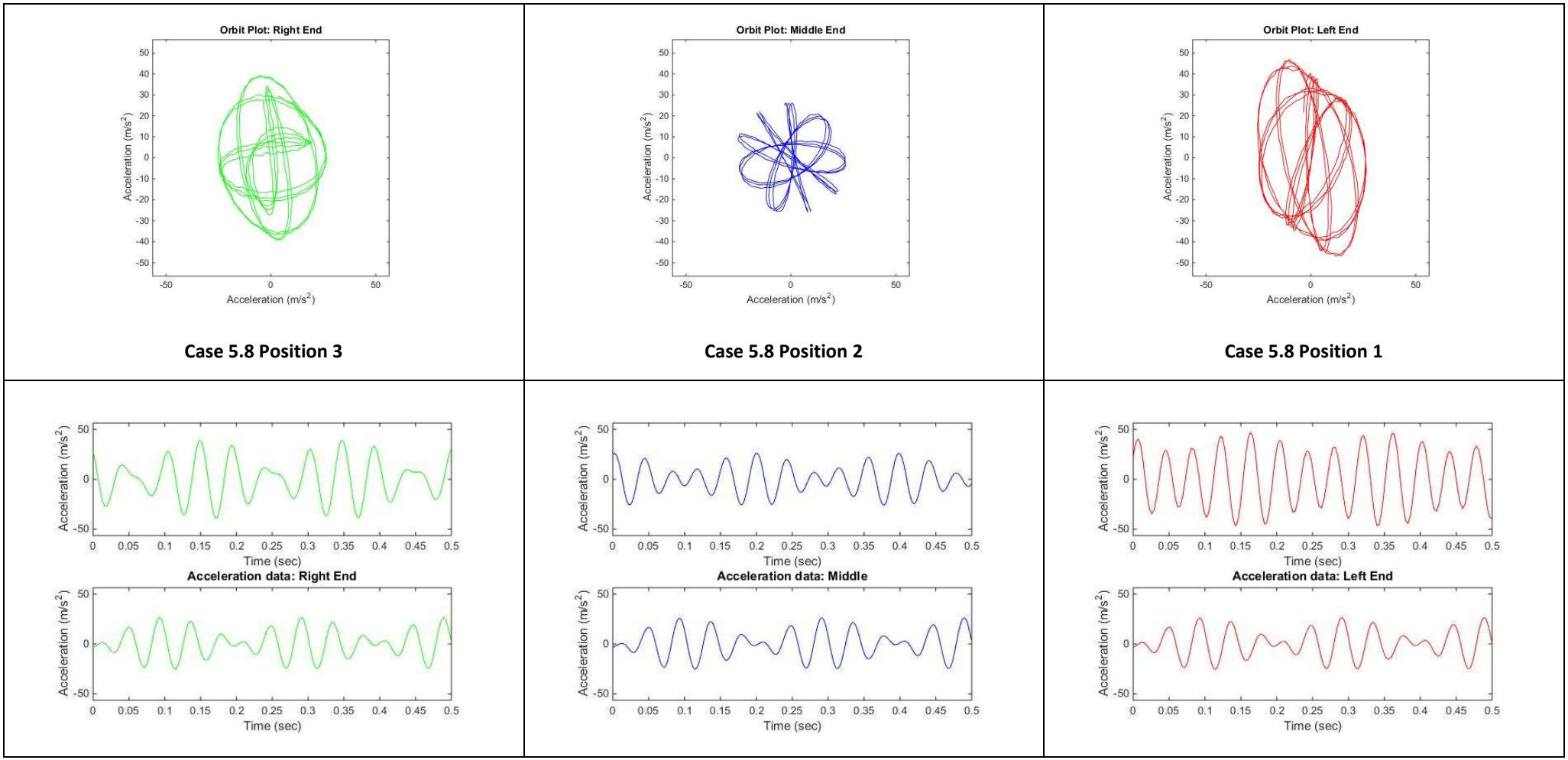

Figure 5.24 Orbit plots and acceleration graphs (X – lower graph, Y-upper graph) for case 5.8

Case 5.9 is shown in the Figure 5.26 with orbits and accelerations for 3 accelerometer positions presented in Figure 5.27. Figure 5.25 presents an orbit in the centre of mass of the testing rig calculated using excel spreadsheet and Table 5.10 presents the case testing parameters.

Both vibrators were running in the same direction with frequencies of 13.33 Hz (left vibrator) and 26.66 Hz (right vibrator) and sample was taken over 1s period. All orbits have different shapes and amplitudes. The analytical and testing results correlate well. The vibrators self-sychronised and repeatability of the signal can be observed in Figure 5.27 which presents orbits and acceleration amplitudes in X and Y directions.

Table 5.10 Test parameters of screen test Case 5.9 with vibrators rotating with different frequencies

	Unit	Value
Moment of Inertia	kgm^2	2.165
Vibrator Static Moment (each)	kgm	$1387.8e^{-5}$
Distance of left exciter centre to the centre of mass	m	0.092465
Distance of right exciter centre to the centre of mass	m	0.092465
Left vibrator rotational speed	rpm/Hz	800/13.33
Left vibrator direction of rotation	L/R	R
Right vibrators rotational speed	rpm/Hz	1600/26.66
Right vibrator direction of rotation	L/R	R
Mass of the setup	kg	24.7

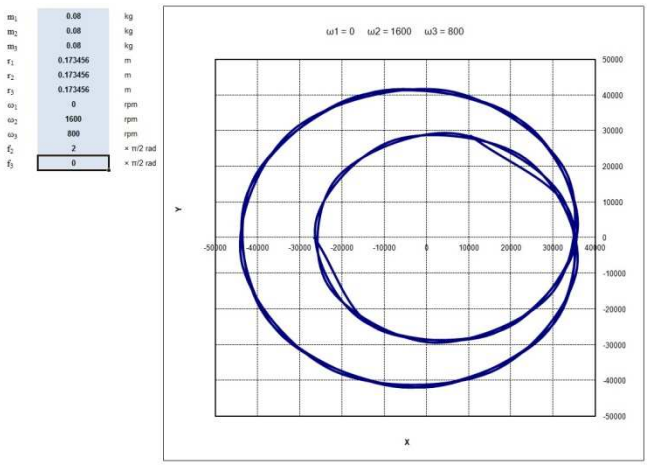

Figure 5.25 Orbit plots and X - Y excel calculated amplitude and stroke in the centre of mass of the test rig for case 5.9

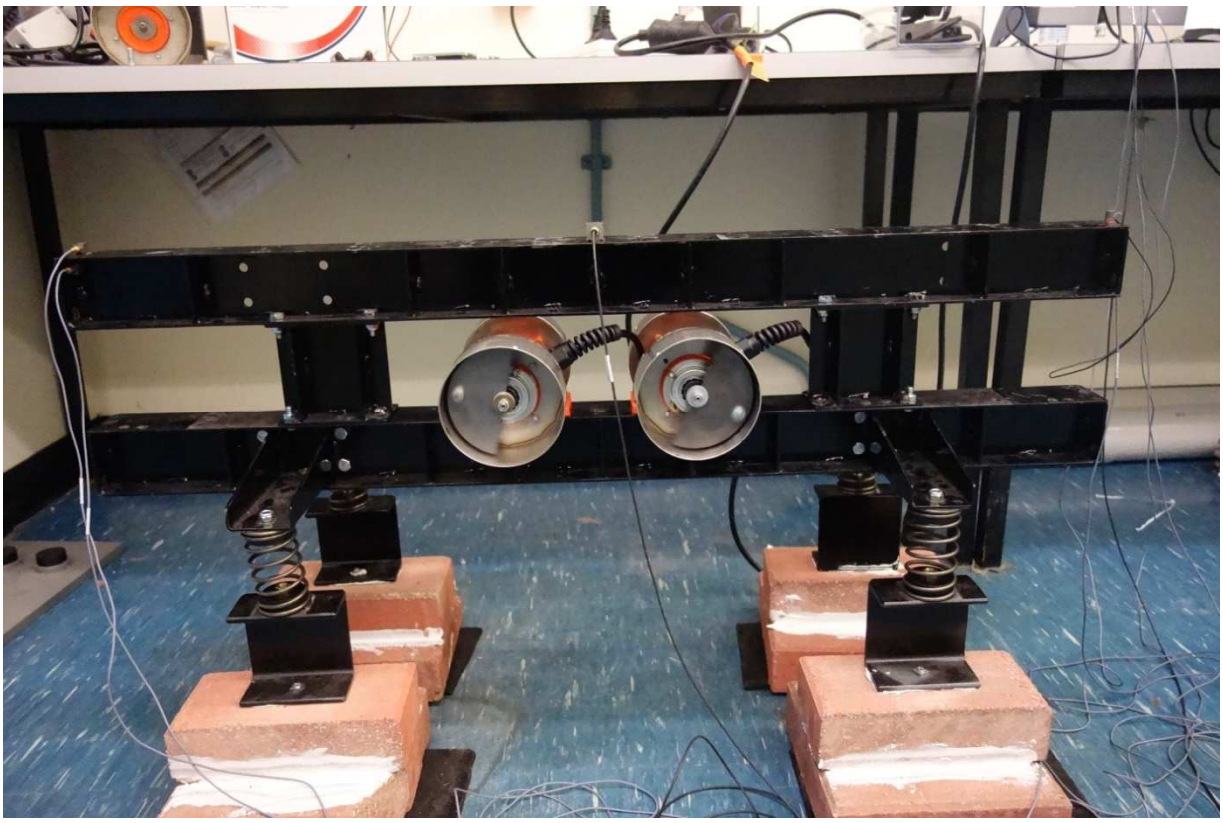

Figure 5.26 Case 5.9 Setup

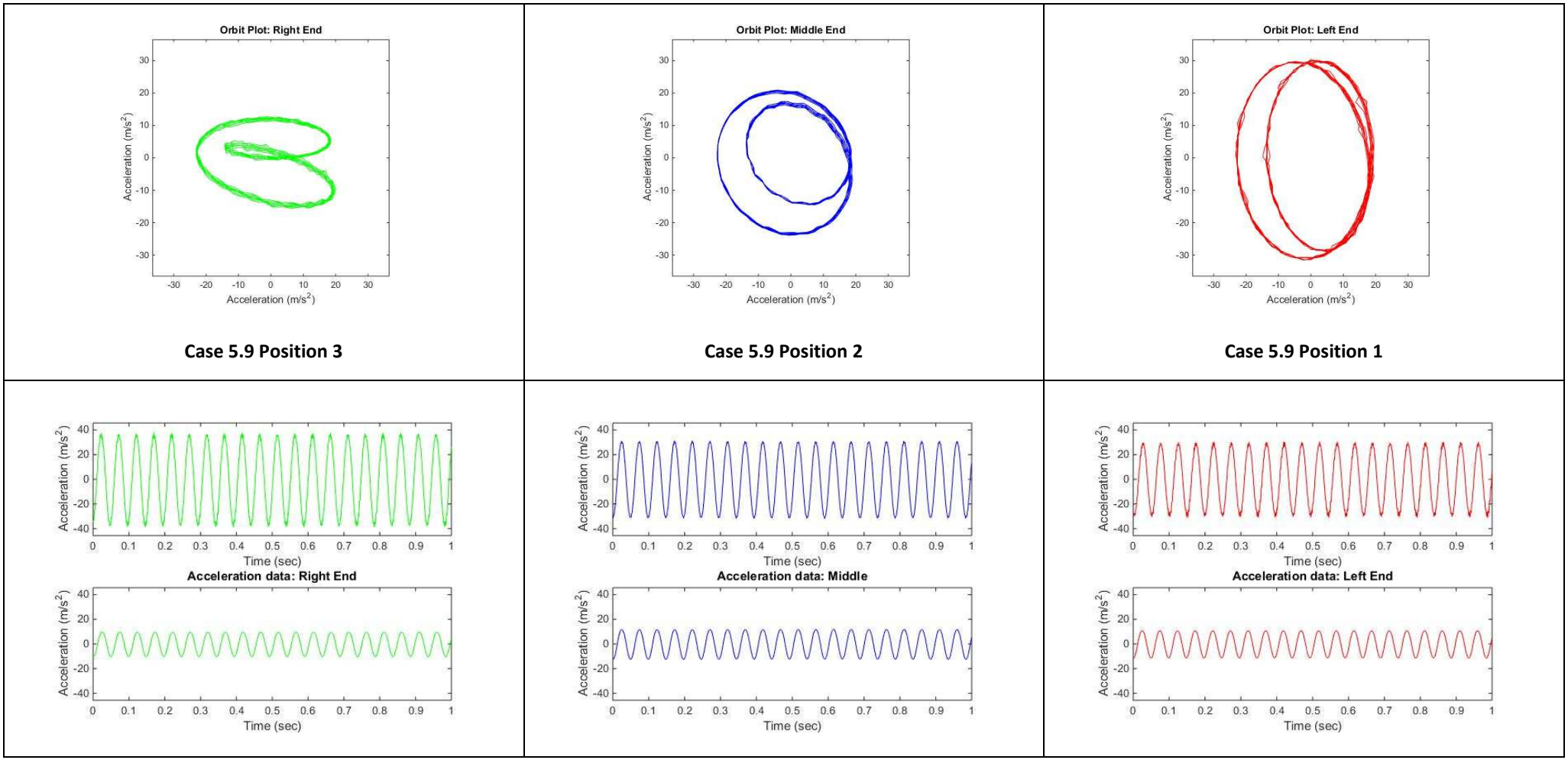

Figure 5.27 Orbit plots and acceleration graphs (X – lower graph, Y-upper graph) for case 5.9

Case 5.10 is shown in the Figure 5.29 with orbits and accelerations for 3 accelerometer positions presented in Figure 5.30. Figure 5.28 presents an orbit in the centre of mass of the testing rig calculated using the excel spreadsheet. Table 5.11 presents the case testing parameters.

Both vibrators were running in the opposite directions with frequencies of 11.66 Hz (left vibrator) and 23.33 Hz (right vibrator) and sample was taken over 0.5s period. All orbits have different shapes and amplitudes. The analytical and testing results correlate well. The vibrators self-sychronised and repeatability of the signal can be observed in Figure 5.30 which presents orbits and acceleration amplitudes in X and Y directions. There are some harmonics showing on the orbit and in the time waveform response at location 3 but it did not affect the self-synchronisation.

Table 5.11 Test parameters of screen test Case 5.10 with vibrators rotating with different frequencies

	Unit	Value
Moment of Inertia	kgm^2	1.365
Vibrator Static Moment (each)	kgm	$1387.8e^{-5}$
Distance of left exciter centre to the centre of mass	m	0.101929
Distance of right exciter centre to the centre of mass	m	0.101929
Left vibrator rotational speed	rpm/Hz	700/11.66
Left vibrator direction of rotation	L/R	R
Right vibrators rotational speed	rpm/Hz	1400/23.33
Right vibrator direction of rotation	L/R	L
Mass of the setup	kg	17.8

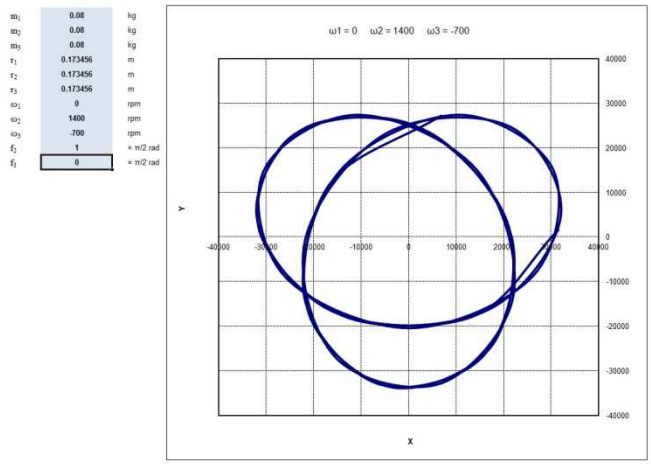

Figure 5.28 Orbit plots and X - Y excel calculated amplitude and stroke in the centre of mass of the test rig for case 5.10

Figure 5.29 Case 5.10 Setup

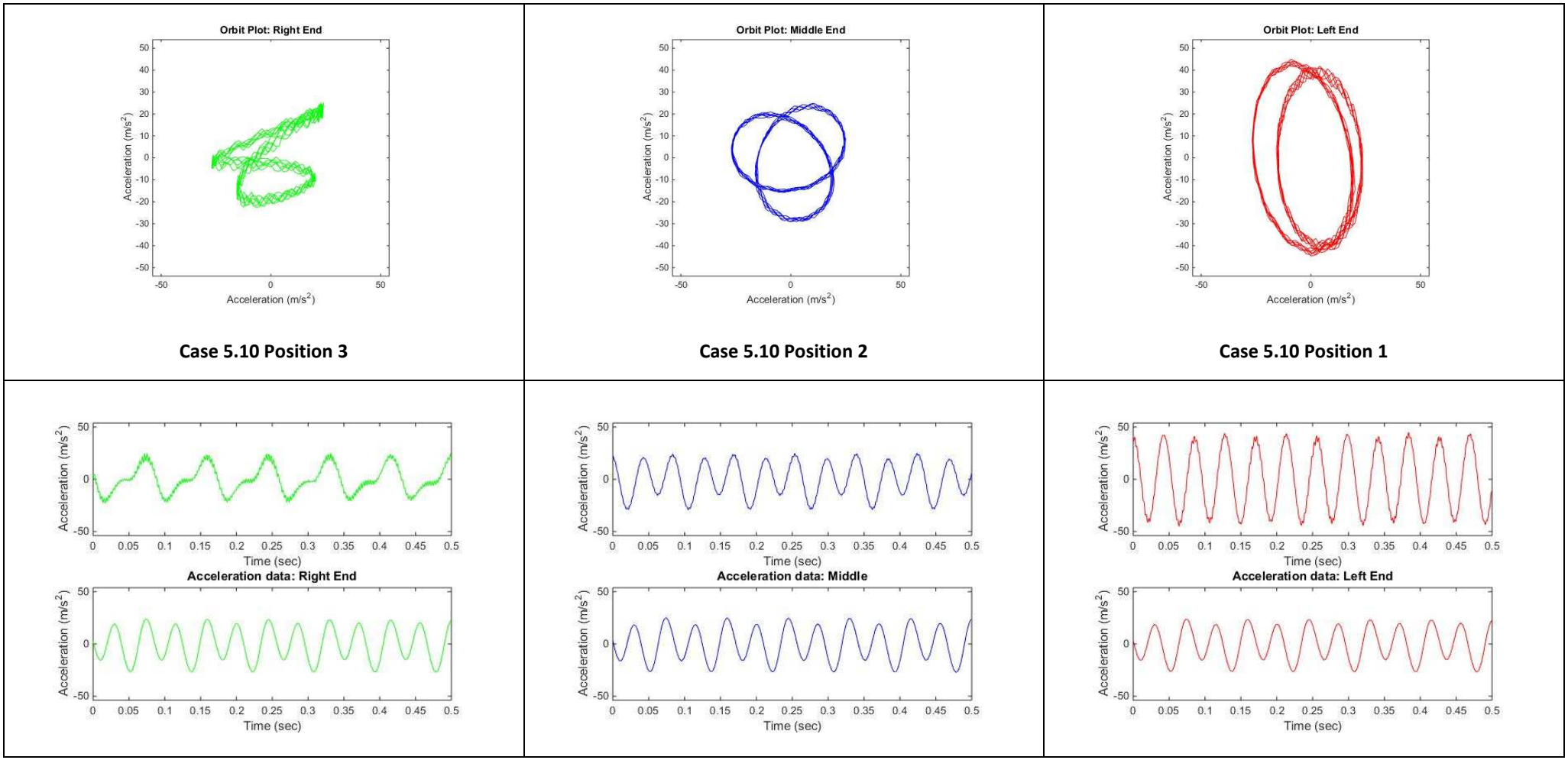

Figure 5.30 Orbit plots and acceleration graphs (X – lower graph, Y-upper graph) for case 5.10

Case 5.11 is shown in the Figure 5.31 with orbits and accelerations for 3 accelerometer positions presented in Figure 5.32. Figure 5.28 presents an orbit in the centre of mass of the testing rig calculated using excel spreadsheet which is the same as in Case 5.10. Table 5.12 presents the case testing parameters.

Both vibrators were running in the opposite directions with frequencies of 11.66 Hz (left vibrator) and 23.33 Hz (right vibrator) and the sample was taken over 0.25s. All orbits have different shapes and amplitudes. The analytical and testing results correlate well. The vibrators self-sychronised and repeatability of the signal can be observed in Figure 5.32 which presents orbits and acceleration amplitudes in X and Y directions. Difference between cases 5.10 and 5.11 was the slightly different positions of vibrators. The orbit at the position 2 was the same, orbits at positions 1 and 3 changed shape slightly and the amplitude in the Y direction increased.

Table 5.12 Test parameters of screen test Case 5.11 with vibrators rotating with different frequencies

	Unit	Value
Moment of Inertia	kgm^2	1.816
Vibrator Static Moment (each)	kgm	$1387.8e^{-5}$
Distance of left exciter centre to the centre of mass	m	0.18916
Distance of right exciter centre to the centre of mass	m	0.18916
Left vibrator rotational speed	rpm/Hz	700/11.66
Left vibrator direction of rotation	L/R	R
Right vibrators rotational speed	rpm/Hz	1400/23.33
Right vibrator direction of rotation	L/R	L
Mass of the setup	kg	17.8

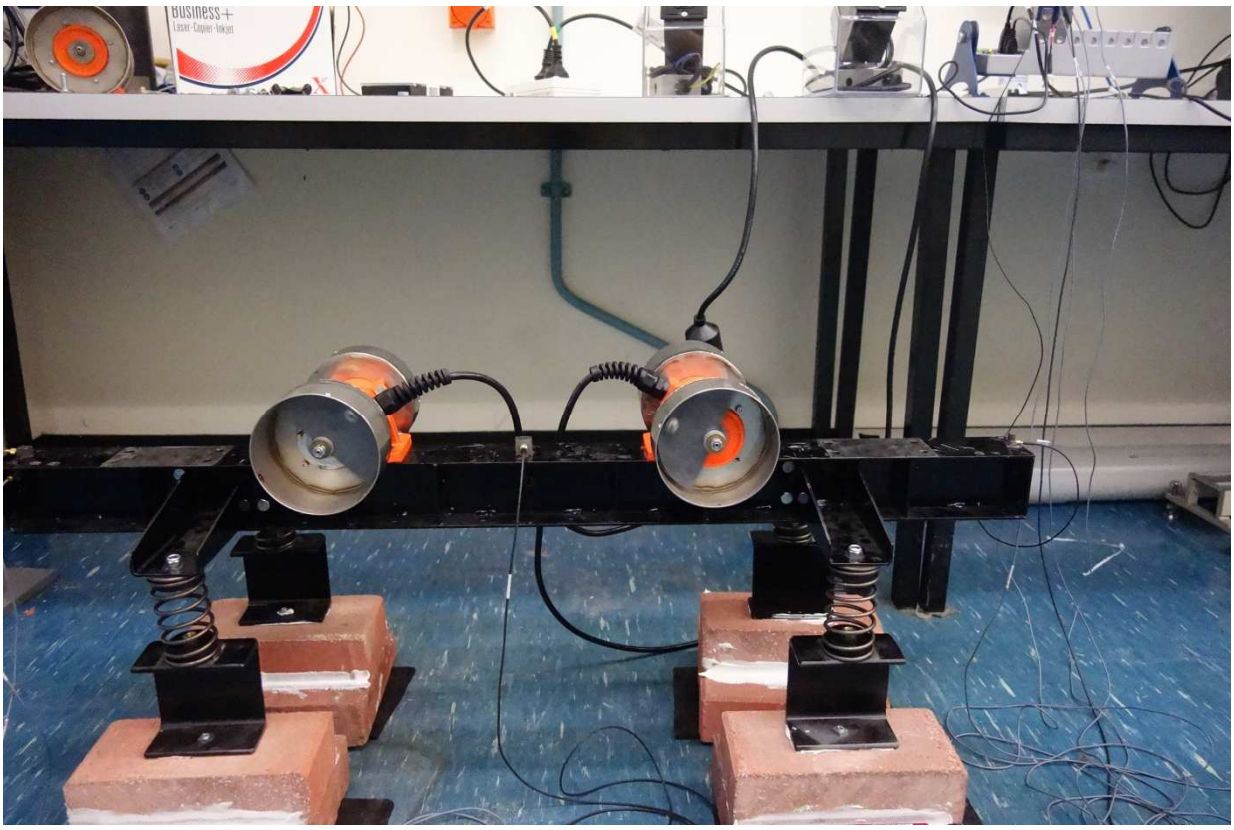

Figure 5.31 Case 5.11 Setup

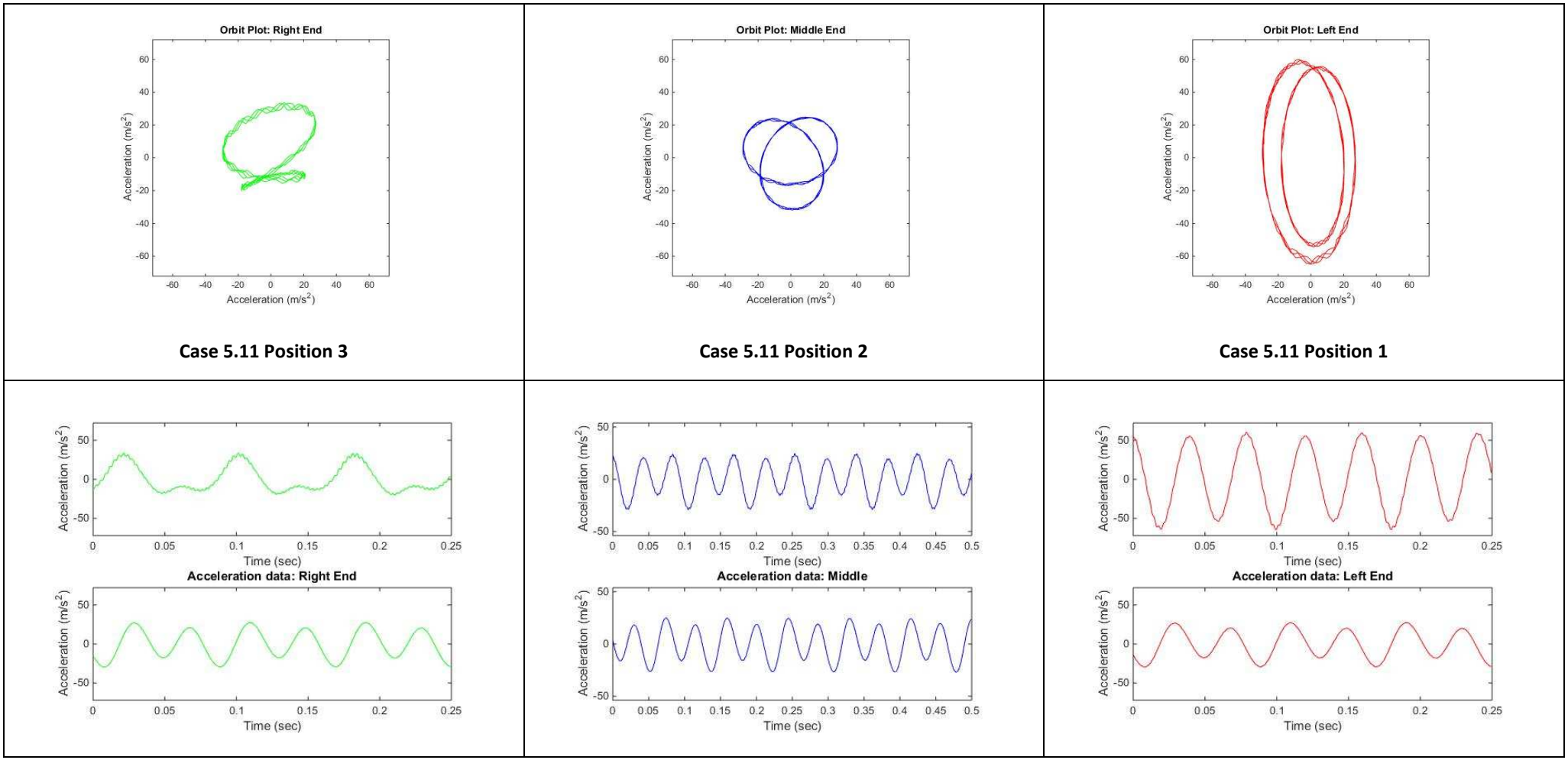

Figure 5.32 Orbit plots and acceleration graphs (X – lower graph, Y-upper graph) for case 5.11

Case 5.12 is shown in the Figure 5.34 with orbits and accelerations for 3 accelerometer positions presented in Figure 5.35. Figure 5.33 presents an orbit in the centre of mass of the testing rig calculated using the excel spreadsheet. Table 5.13 presents the case testing parameters.

Both vibrators were running in the opposite directions with frequencies of 20 Hz (left vibrator) and 26.6 Hz (right vibrator) and sample was taken over 1s period. All orbits have different shapes and amplitudes. The analytical and testing results correlate well. The vibrators self-sychronised and repeatability of the signal can be observed in Figure 5.35 which presents orbits and acceleration amplitudes in X and Y directions.

Table 5.13 Test parameters of screen test Case 5.12 with vibrators rotating with different frequencies

	Unit	Value
Moment of Inertia	kgm^2	3.013
Vibrator Static Moment (each	kgm	$1387.8e^{-5}$
Distance of left exciter centre to the centre of mass	m	0.507899
Distance of right exciter centre to the centre of mass	m	0.507899
Left vibrator rotational speed	rpm/Hz	1200/20
Left vibrator direction of rotation	L/R	R
Right vibrators rotational speed	rpm/Hz	1600/26.6
Right vibrator direction of rotation	L/R	L
Mass of the setup	kg	17.8

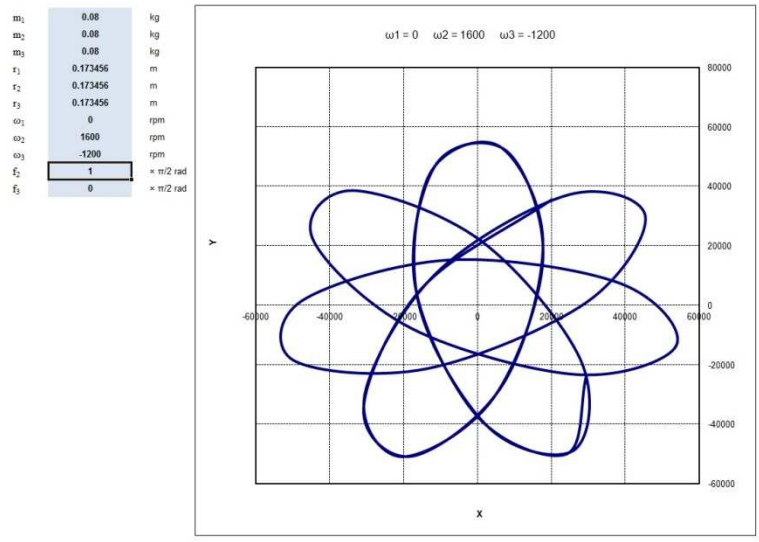

Figure 5.33 Orbit plots and X - Y excel calculated amplitude and stroke in the centre of mass of the test rig for case 5.12

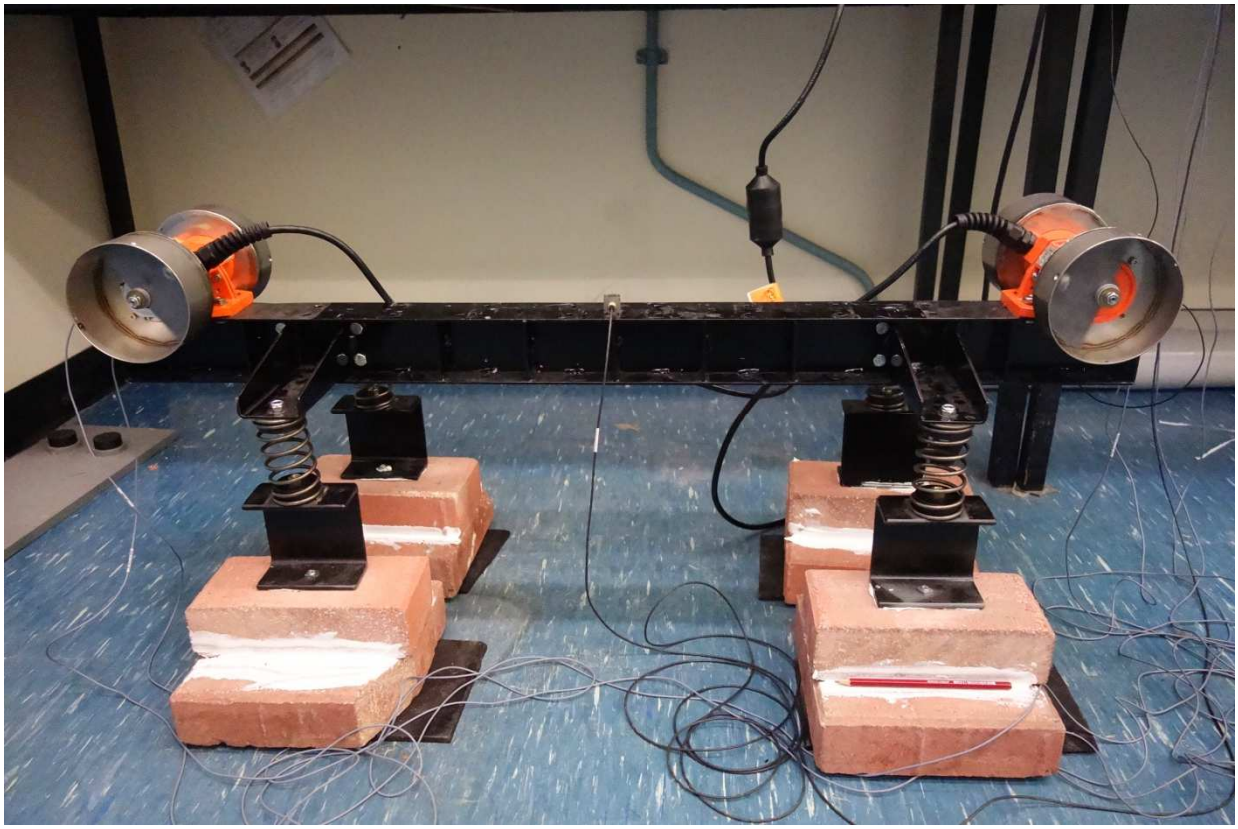

Figure 5.34 Case 5.12 Setup

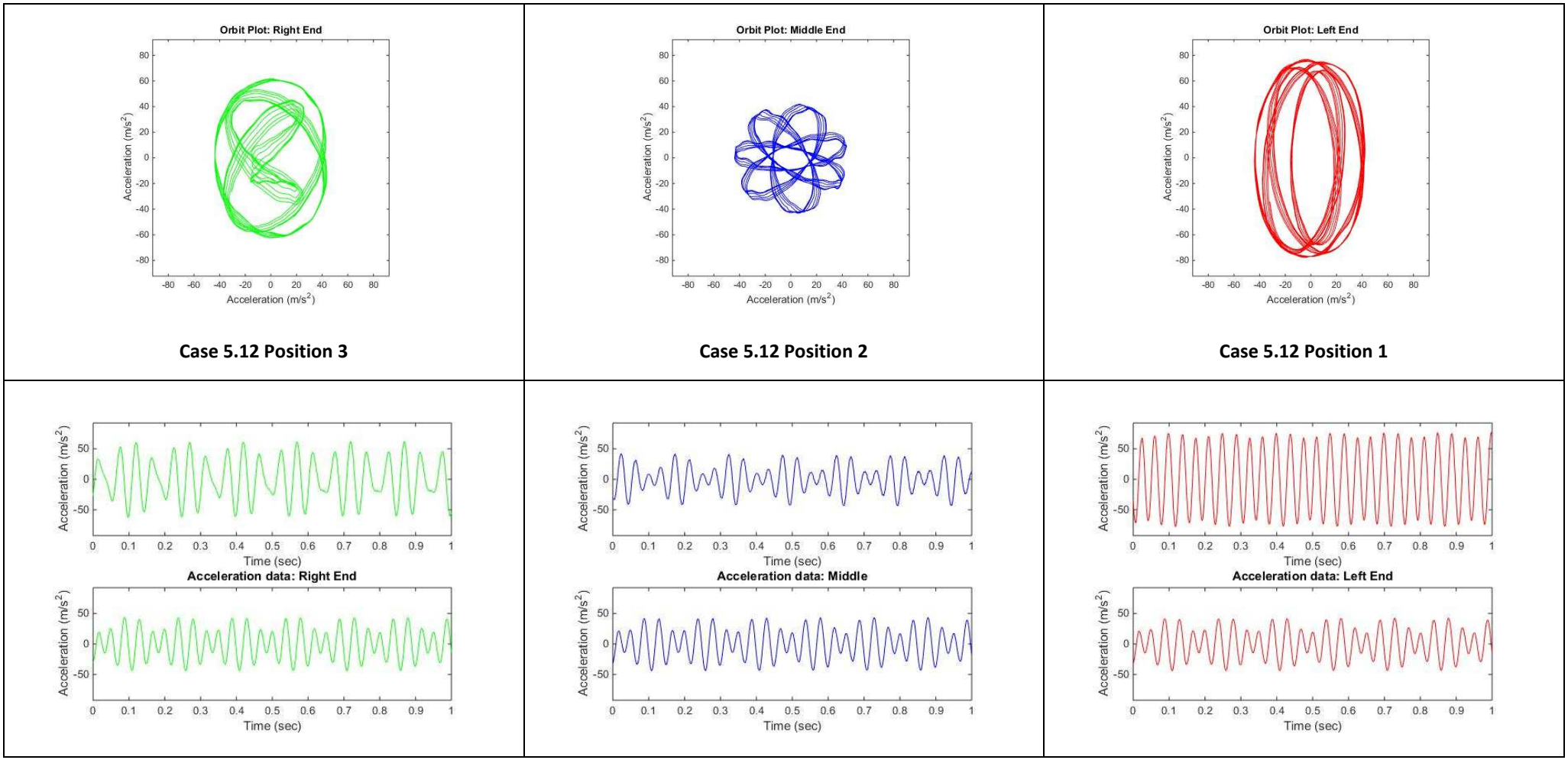

Figure 5.35 Orbit plots and acceleration graphs (X – lower graph, Y-upper graph) for case 5.12

Case 5.13 is shown in the Figure 5.36 with orbits and accelerations for 3 accelerometer positions presented in Figure 5.37. Figure 5.33 presents an orbit in the centre of mass of the testing rig calculated using the excel spreadsheet. Table 5.14 presents the case testing parameters.

All parameters were the same as in case 5.12 but the time waveform response sample has been recorded over a 3s period. The analytic and testing results correlate well. The vibrators self-sychronised and repeatability of the signal can be observed in Figure 5.37 which presents orbits and acceleration amplitudes in X and Y directions.

Table 5.14 Test parameters of screen test Case 5.13 with vibrators rotating with different frequencies

	Unit	Value
Moment of Inertia	kgm^2	3.013
Vibrator Static Moment (each)	kgm	$1387.8e^{-5}$
Distance of left exciter centre to the centre of mass	m	0.507899
Distance of right exciter centre to the centre of mass	m	0.507899
Left vibrator rotational speed	rpm/Hz	1200/20
Left vibrator direction of rotation	L/R	R
Right vibrators rotational speed	rpm/Hz	1600/26.6
Right vibrator direction of rotation	L/R	L
Mass of the setup	kg	17.8

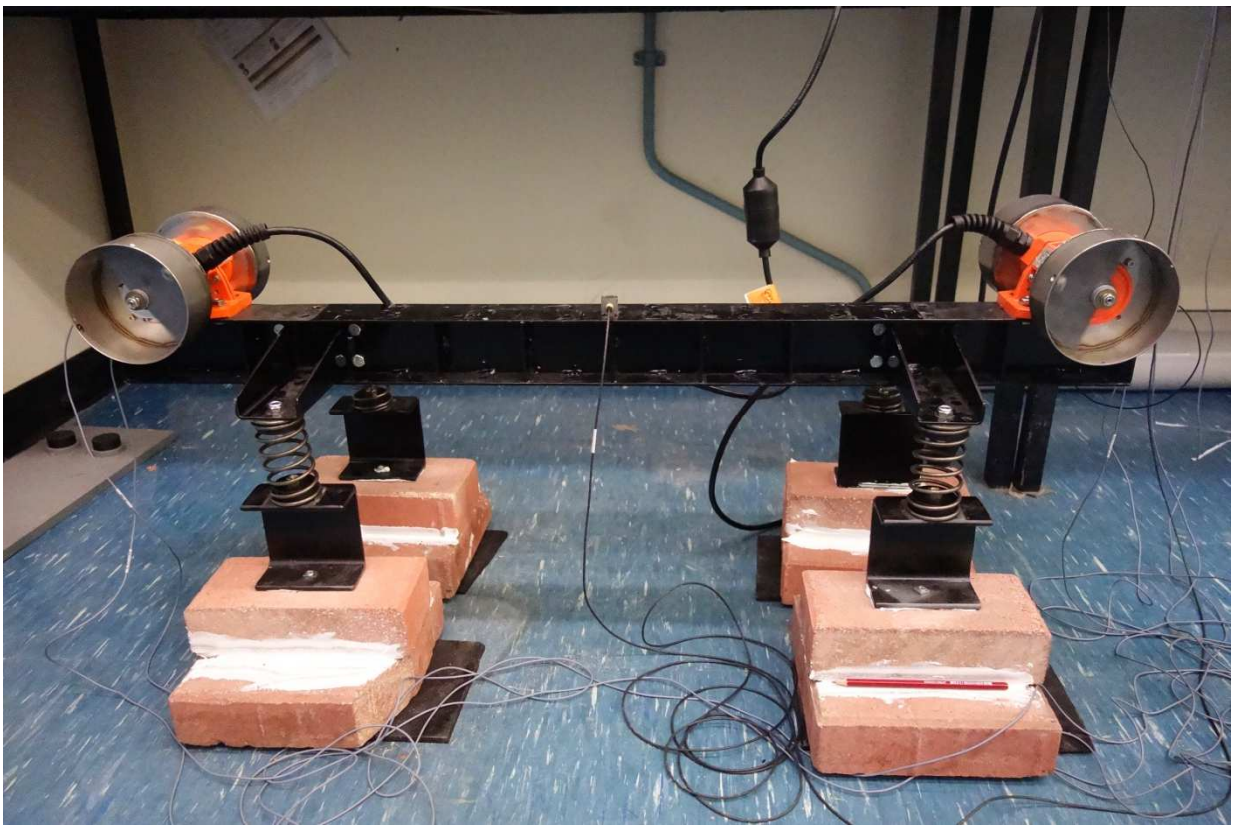

Figure 5.36 Case 5.13 Setup

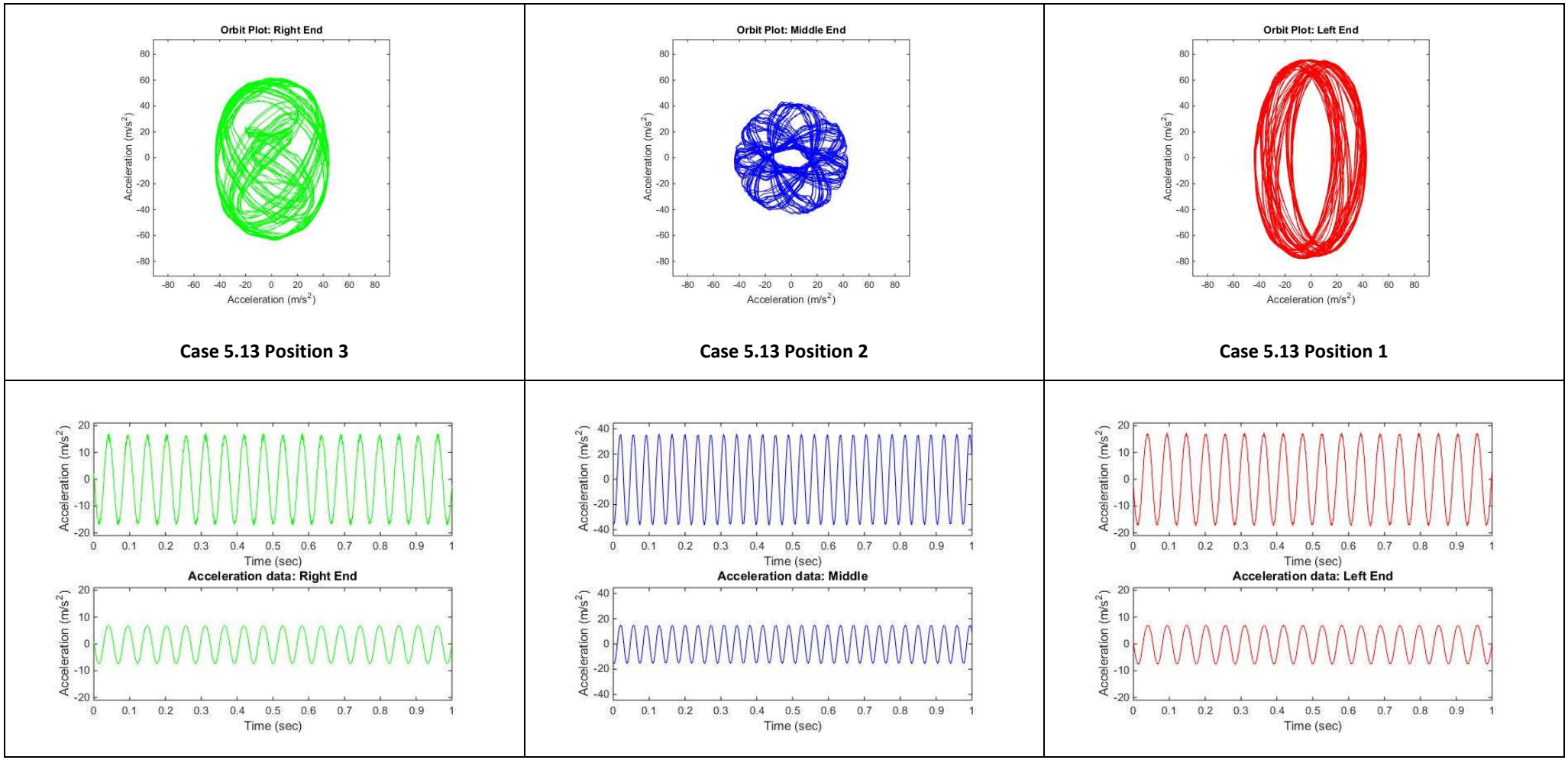

Figure 5.37 Orbit plots and acceleration graphs (X – lower graph, Y-upper graph) for case 5.13

Case 5.14 is presented in the Figure 5.38 with orbit and accelerations for 3 accelerometer positions presented in Figure 5.39. Figure 5.33 presents an orbit in the centre of mass of the testing rig calculated using the excel spreadsheet. Table 5.15 presents the case testing parameters.

All parameters were the same as in Case 5.12 and Case 5.13 but the time waveform sample has been recorded over 5s period which represents 100 cycles for the left vibrator and 133 cycles for the right one. The analytical and testing results correlate well. The vibrators self-sychronised and repeatability of the signal can be observed in Figure 5.39 which presents orbits and acceleration amplitudes in X and Y directions.

Table 5.15 Test parameters of screen test Case 5.14 with vibrators rotating with different frequencies

	Unit	Value
Moment of Inertia	kgm^2	3.013
Vibrator Static Moment (each)	kgm	$1387.8e^{-5}$
Distance of left exciter centre to the centre of mass	m	0.507899
Distance of right exciter centre to the centre of mass	m	0.507899
Left vibrator rotational speed	rpm/Hz	1200/20
Left vibrator direction of rotation	L/R	R
Right vibrators rotational speed	rpm/Hz	1600/26.6
Right vibrator direction of rotation	L/R	L
Mass of the setup	kg	17.8

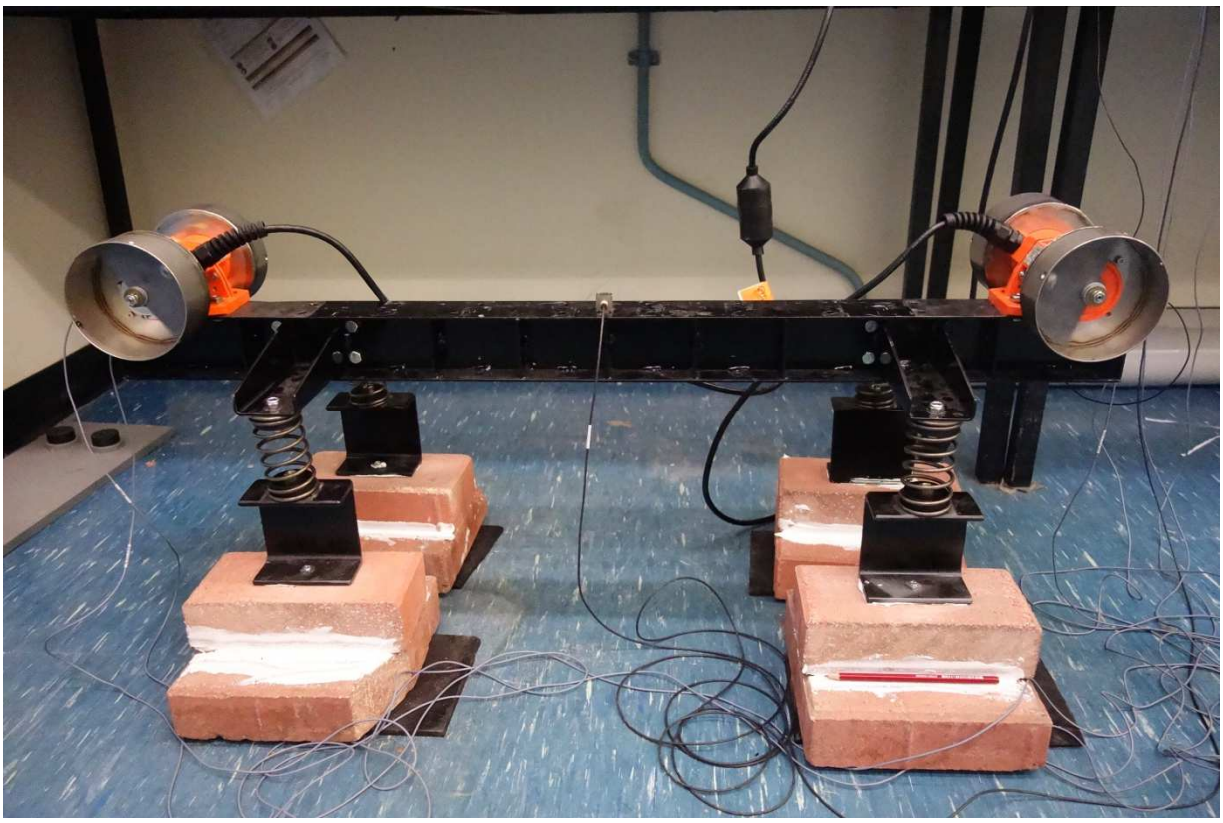

Figure 5.38 Case 5.14 Setup

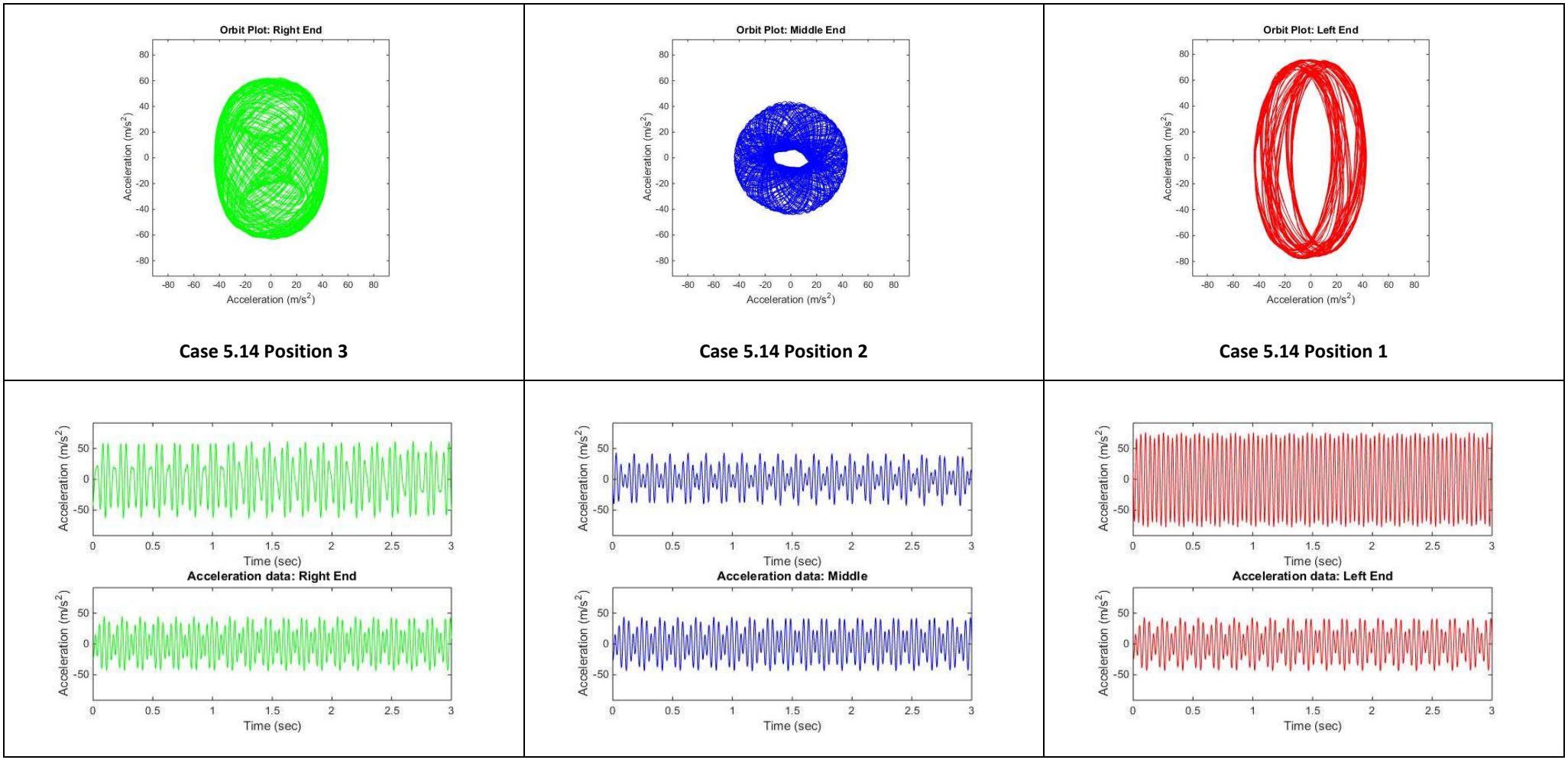

Figure 5.39 Orbit plots and acceleration graphs (X – lower graph, Y-upper graph) for case 5.14

5.2 Critical analysis of experimental results with two different frequencies - results

Several different combinations of ω, moment of inertia (changed by removing the upper part of the rig), and vibrating position were tried with 14 presented cases.

Vibrators self-synchronised with each other regardless of direction of revolutions. The trajectories of the orbit vibrations are cyclical and repeatable but the synchronisation will not be preserved in case of power turned off to one of them like in previous chapters with vibrators running with the same frequency, clockwise or counter clockwise.

If the power was cut off to the faster running vibrator it will slow down to match the slower running vibrator, then they would synchronise with each other. Both vibrators would then run with the same speed regardless of direction of revolution.

If the power was cut off to the slower vibrator, it would then stop.

The vibration is cyclical with the regular shapes. These shapes could be used to improve the operation of vibrating screens by improving the stratification and separation of the material.

Trajectories become more complex when the ratio of running speed gets to a higher value i.e; trajectory for the ratio 3/4 (Case 5.12) is more complex than for ratio 1/2, shown in Figure 5.11. It is also very likely that the strongest self-synchronisation force between operating frequencies is at the ratio of 1/2.

The combination of frequencies to be used for the process will be a function of a screening process and screen design which would determine operating frequency options.

Screening processes would require higher amplitudes for coarse screening and smaller amplitudes for fine particles and that can be achieved by dual frequency screens. Benefits of dual frequency screens have been proven in research (Lawinska et al., 2014) with results showing 24% screening efficiency improvement with the same capacity and test conditions. Paul Cleary (Clearly et al., 2009) simulated screening process on multi-deck banana screens using the Discrete Element Method. One of the conclusions of the research was that higher efficiency can be achieved by modulating the screen frequency and acceleration, it is not

feasible in practice because of high inertia of vibrators but it can be simulated by dual frequency motion.

Design, commission and installation of dual-frequency screens would be more difficult in comparison to ‘standard screens’ though because of the two running frequencies and subharmonics and superharmonics that can affect the natural frequencies of the screen and supporting structure, (Mi Han, S., Benaroya, H.; (2002)), however dual-frequency screens would offer better efficiency of screening processes and more designs should be used in the industry. Dual frequency screens offer options for adjustments to the process which are not possible with single frequency screens. They would however require much higher level of engineering and maintenance capability than currently available in the majority of mineral processing plant facilities.

Chapter 6
Simulation of testing with two vibrators using Finite Element Analysis

The vibrating screen trajectories are in most cases different for each point of the screen body. The exceptions are the linear motion screen with the line of force going through the centre of mass and the circular motion screen when the vibrator is positioned exactly at the centre of mass of the vibrating screen.

It would beneficial to be able to simulate the screen stroke shape, magnitude and angle, for any combination of vibrators because it would help to determine the suitability of these parameters to the required process and also help with structural design of the screen.

Building a small model of the screen or a testing prototype is not practical, and is expensive and time consuming, so several cases of physical tests were simulated using Finite Element Analysis.

Strand7 FEA analysis has been used here with natural frequency and harmonic analysis performed to check the suitability of FEA for stroke magnitude and shape simulation. Two types of models have been used - one built of plates and another built using beams. The results were practically the same with the beam model solving faster and the solution time difference will be obviously bigger with more complex models.

Both solvers are linear and don't take into account non-linearity of the screen structure or spring behavior which means that for example spring closing will not be as shown in the solution but that was not the purpose of the current analysis.

Several different examples have been selected from different cases with vibrators running in the same and opposite direction and also dual-frequency cases were simulated.

For symmetrical location of vibrators about the centre of mass, the load cases and determination of direction and the phase difference of the response is relatively simple. The problem arises with the asymmetrical position of vibrators about the centre of mass and then the testing rig becomes very handy to help to ‘calibrate’ the FEA model. The FEA model

is very helpful when it comes to determine the shape and size of orbits at any point of the vibrating equipment before it will be actually fully designed and fabricated. The acceleration is important to determine and calculate the stresses in the vibrating screen body, to calculate the fatigue life of the equipment and also to determine locations of strain gauges to confirm the FEA calculation. 4 test cases were selected from the previous chapters and the FEA simulation and analysis presented in this section. The results confirm that if the proper setup of the FEA model is done, then the results correlate well with the results from the physical testing.

Figure 6.1 presents the setup of Case 4.1.4 with both vibrators rotating in the same direction at 1450 rpm.

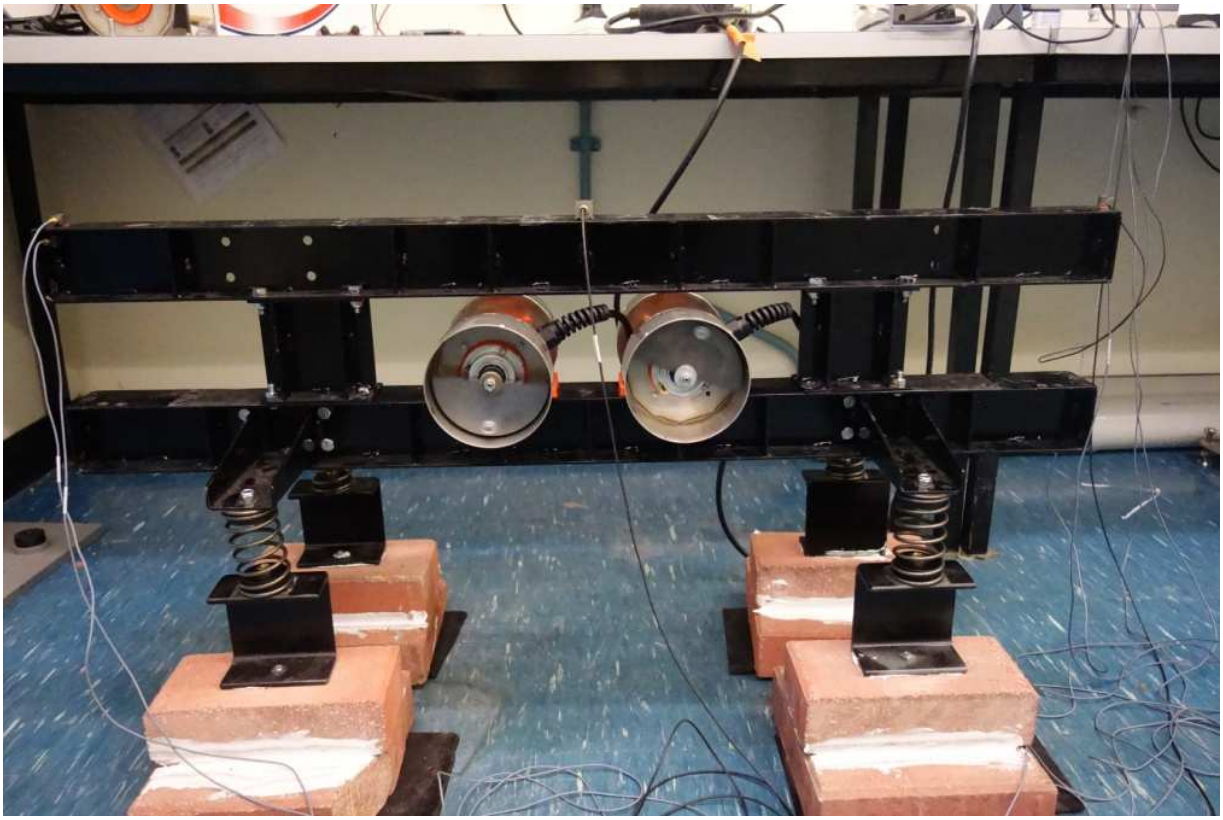

Figure 6.1 Case 4.1.4 Setup

Figure 6.2 shows the physical results from the testing rig (upper row) and the bottom row presents the results obtained from FEA simulation. Both results show similar stroke shape and magnitude with the rig testing results displaying some spring vibration as the vibrating force causes movement of supports and significant spring displacements. Stroke shape and magnitude in the middle of the testing rig is smaller than on the end which represents the rocking motion of the testing rig.

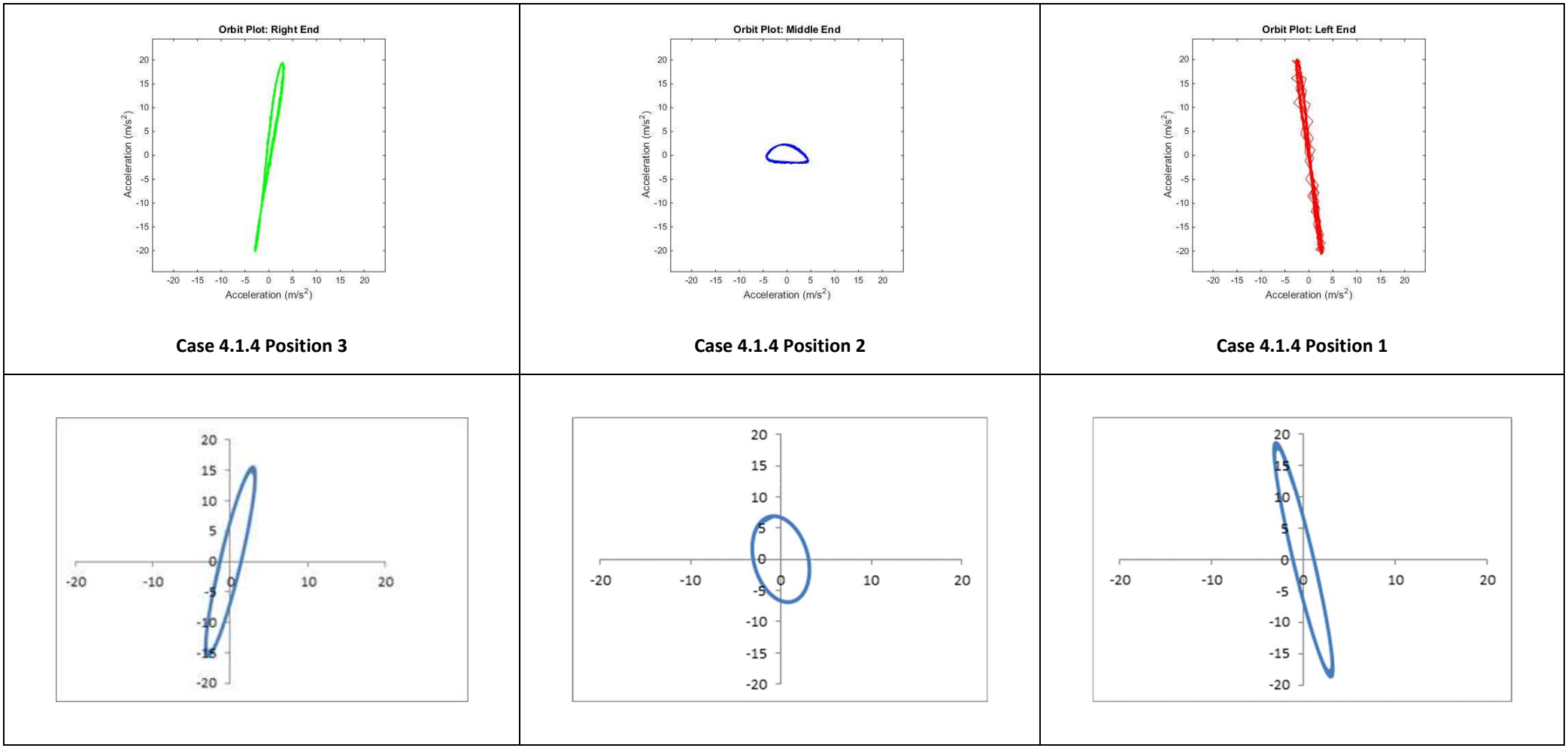

Figure 6.2 Comparison orbits from Case 4.1.7 and Strand 7 simulation

Figure 6.3 presents the setup of Case 4.1.7, with both vibrators rotating in the same direction at 1060 rpm.

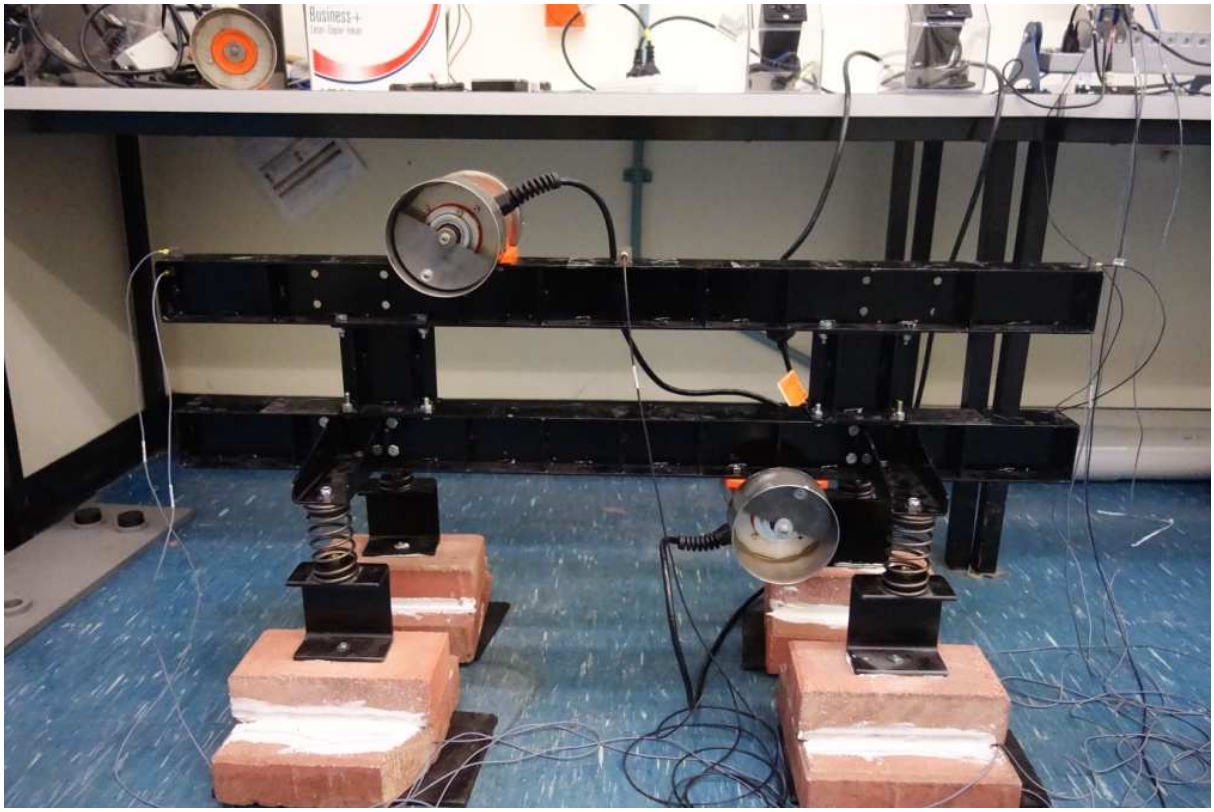

Figure 6.3 Case 4.1.7 Setup

Figure 6.4 shows the accelerometers signal from the testing rig in the upper row and bottom row presents results obtained from the Strand 7 FEA simulation. The result shows similar stroke shape and magnitude. Some differences in stroke in the middle of the testing rig are noticeable, however the results are acceptable.

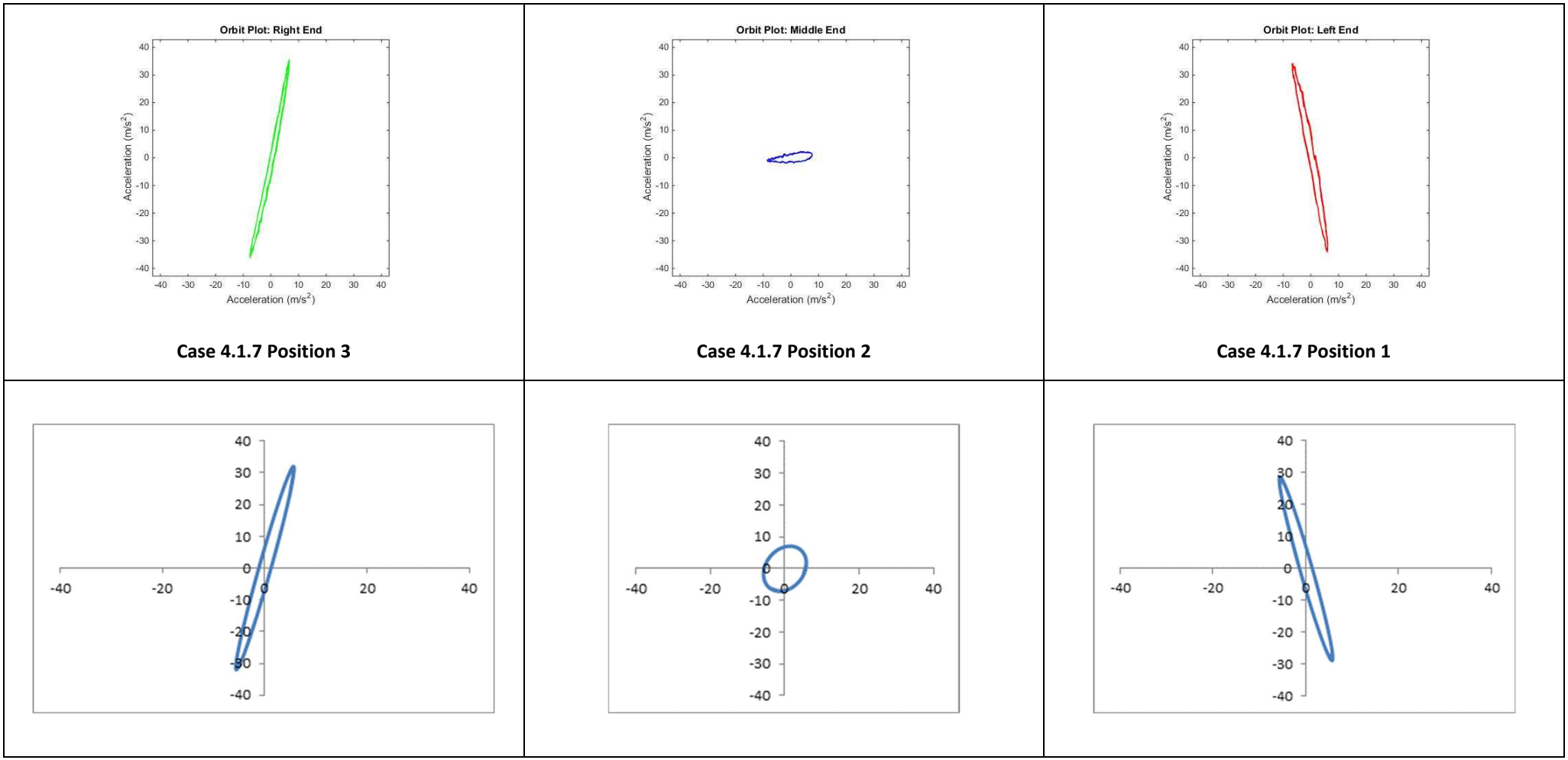

Figure 6.4 Comparison orbits from Case 4.1.7 and Strand 7 simulation

Figure 6.5 presents the setup of Case 4.1.10, with both vibrators rotating in the same direction at 1200 rpm.

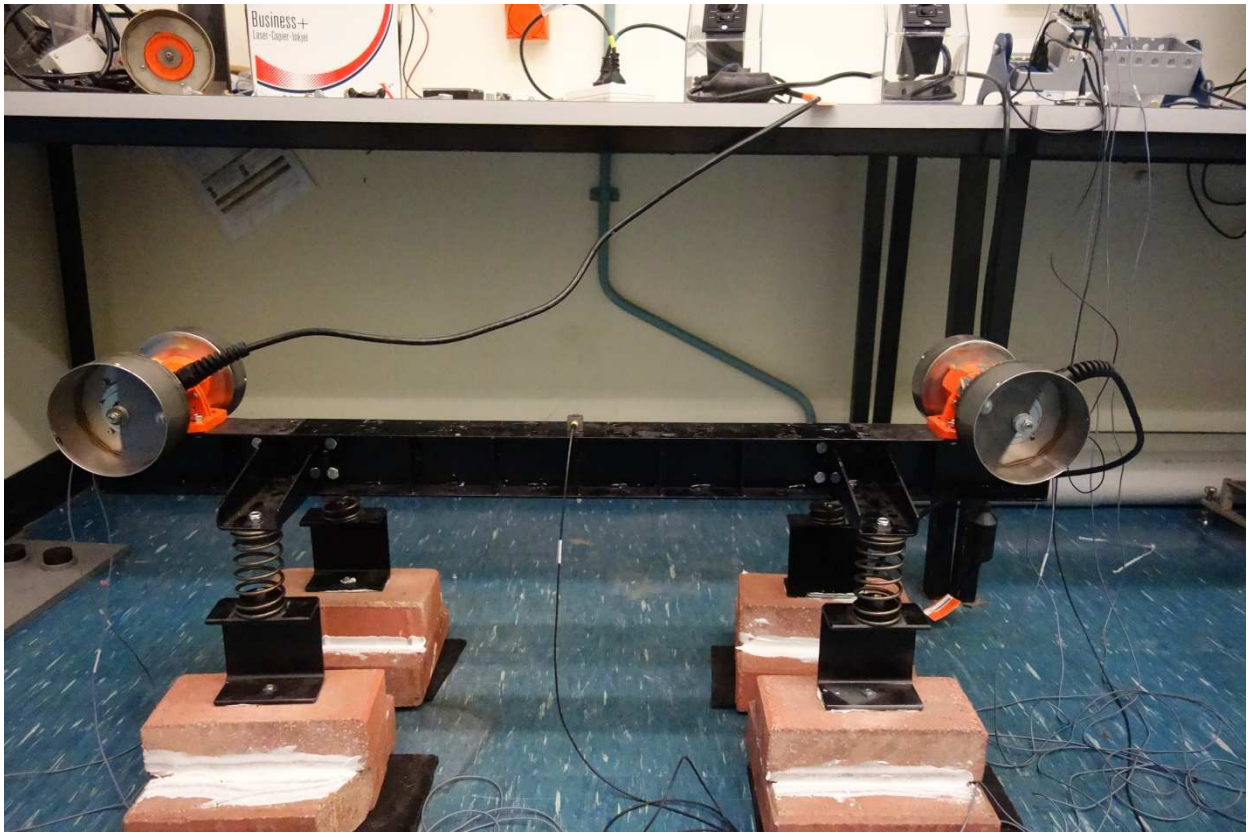

Figure 6.5 Case 4.1.10 Setup

Figure 6.6 shows the physical results from the testing rig in the upper row, where the bottom row presents results obtained from the FEA simulation. Both results are showing similar stroke shape and with slightly smaller amplitude at the ends of the testing rig. Both results show very small stroke magnitude in the middle. It shows very good correlation between physical testing results and mathematical simulation using FEA software.

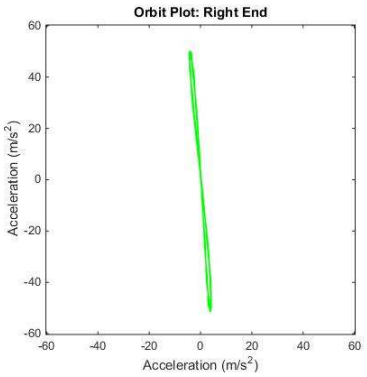

Case 4.1.10 Position 3

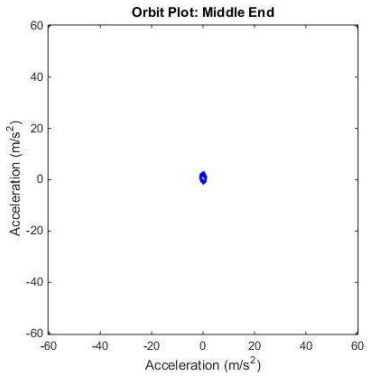

Case 4.1.10 Position 2

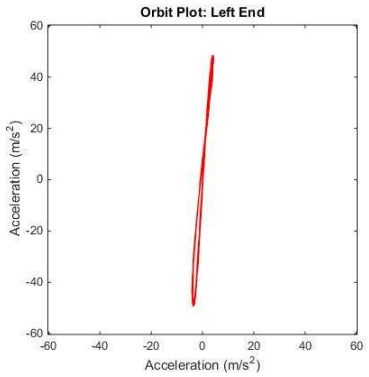

Case 4.1.10 Position 1

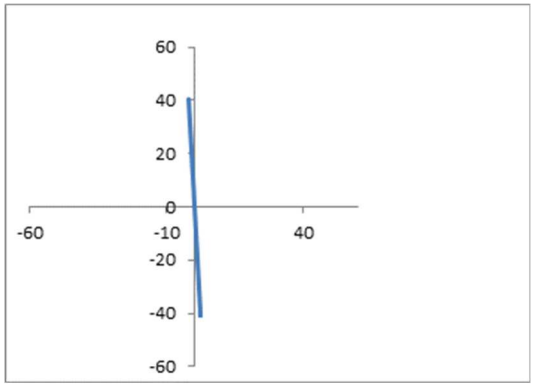

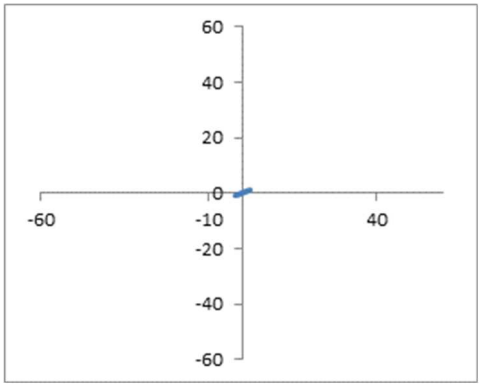

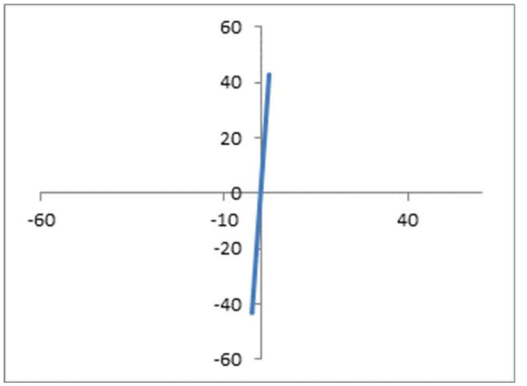

Figure 6.6 Comparison orbits from Case 4.1.10 and Strand 7 simulation

Figure 6.7 presents setup of Case 5.12 vibrators rotating in opposite directions with left vibrator working at 1200 rpm and right operating at 1600 rpm.

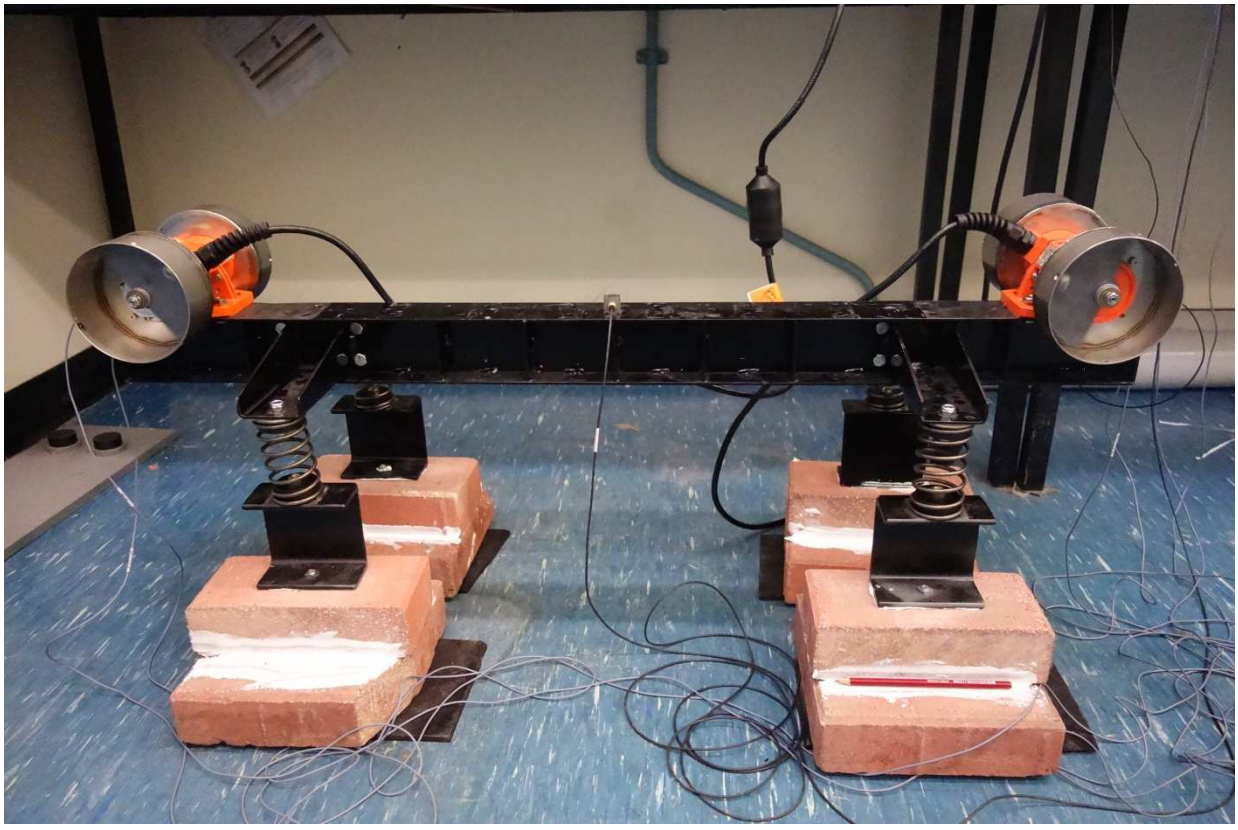

Figure 6.7 Case 5.12 Setup

Figure 6.8 shows the physical results from the testing rig in the upper row, while the bottom row presents results obtained from the FEA simulation. There are some differences in the stroke however if the complexity of the stroke is taken into account the correlation is still close for the case of dual frequency simulation. The moment when self-synchronisation starts, it makes a difference to the stroke shape and therefore the shape difference can be observed in this case. The timing and counterweight positions when self-sychronisation started on the testing rig and in FEA simulation are different. Stroke magnitudes are similar in all cases.

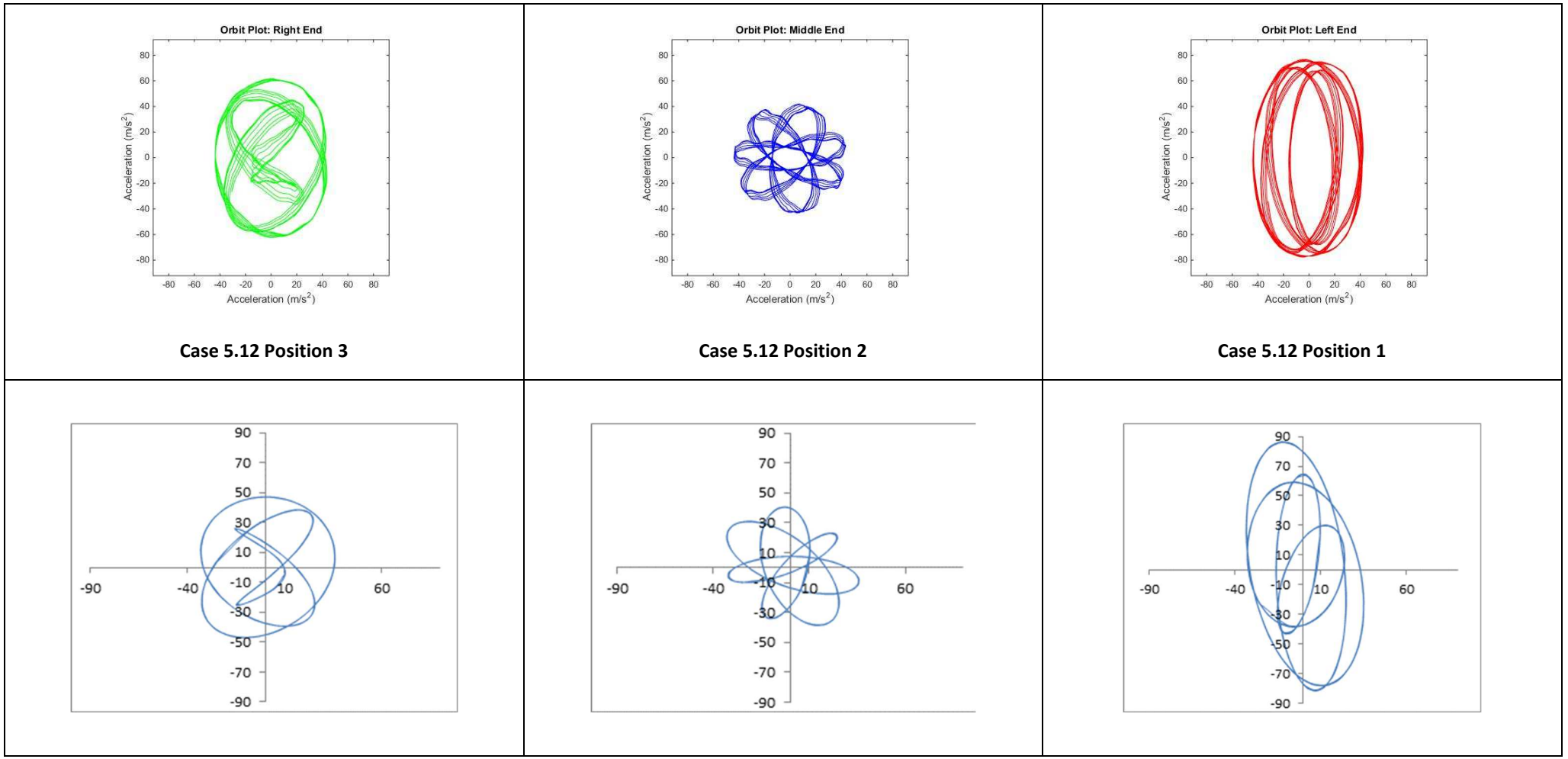

Figure 6.8 Comparison orbits from Case 5.12 and Strand 7 simulation

6.1 Simulation of testing with two vibrators using Finite Element Analysis results

Four cases of two vibrators operating on the testing rig were simulated using Strand 7 Finite Element Analysis software. 3 cases were presented with vibrators operating in the same directions with the test rig moving in a rocking type motion and one case with dual frequency type of movement with two vibrators working in opposite directions with different frequencies. In all cases the correlation between results from physical testing and FEA simulation was seen to be close.

There were some differences in stroke shape in the case of dual frequency setup. It is thought to be related to the moment when the self-synchronisation starts and the position of the centre of mass of the testing rig and synchronization between both vibrators. More important is that the stroke magnitude was very similar in all cases which will allow simulating it and calculating the acceleration on the vibrating screen. Standard screens are designed to operate at maximum 5g, so knowing the stroke magnitude will permit the control of the screen structural stress either by changing the rpm of the vibrators or by modifying the static moment of the vibrator(s) counterweights. It is especially valid for screen modifications at the client site where the time for modifications and changes is very limited and all adjustments have to be planned in advance. Understanding possible changes to stroke shape and amplitude are also very important from the process point of view and options to modify these parameters and different points of a screening deck can significantly improve screening efficiency.

Finite element analysis proved itself to be a very useful tool in simulation of vibrating equipment movement.

Chapter 7
Example of an application of self-synchronisation in the industry on an example of a gearless exciter design

7.1 Introduction

An example for an application of self-synchronisation with vibrating screens can be seen in a modified design of a box exciter which uses the self-synchronisation principle. Currently geared versions are commonly used in the mining industry. The majority of mining screens use a box exciter as a method of forcing vibrations of the screen structure and screening media. A standard box exciter is shown in Figure 7.1, consisting of a housing, 4 bearings, 4 counterweights, 2 shafts and a set of gears that force-synchronise both shafts and keeps the same phase and direction of the centrifugal force independent of the centre of mass of the vibrating screen. Such a screen can be driven with a single electric motor and the shaft between exciters transfers the torque to the other exciter using the same electric motor, as shown in Figure 7.2.

Figure 7.1 Typical example of a geared exciter (VIBFEM).

Figure 7.2 Example of a vibrating screen with 2 exciters connected with a single shaft

7.2 Problems encountered in existing geared exciters

Unbalanced counterweights of the geared exciters are self-synchronising about themselves but also about the centre of gravity of the operating screen. Screen design is never perfect and the centre of gravity is never perfectly aligned with the direction of the unbalanced force created by the exciters and therefore when the counterweights are 'trying' to adjust to the centre of gravity, the gears are preventing that from happening. Additionally, material fed to the screen will move the centre of gravity further. With material feed not being constant, the centre of gravity also constantly moves as represented in Figure 7.3 and Figure 7.4.

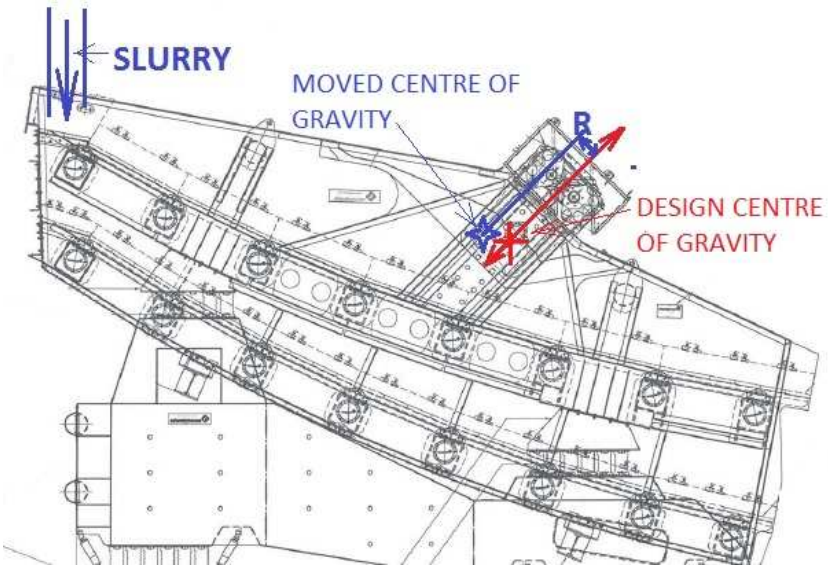

Figure 7.3 'Design' centre of gravity and the 'real' constantly moving CoG

Figure 7.4 High energy feed arrangement.

Constantly moving material load also causes constant movement (vibration) of the centre of mass and results in vibration of the gear teeth impacting against each other and in consequence, pitting of gears or even broken teeth can occur as shown in Figure 7.5. Similar events can occur during screen shut down, when the screen is going through the natural frequency rigid body modes and counterweights will swing in forward and backward directions, with all impacts transferred through the gears. It can also create bearing problems similar to those shown in Figure 7.6.

Figure 7.5 Pitting of the gears

Figure 7.6 Present damage to bearing caused by metal particles in the lubricating oil

Standard working positions of the exciters are with inclined positions of 45 degrees, with the bottom pair of bearings submerged in the oil bath (at the beginning but later both bearings rely on splash lubrication). The upper pair of bearings have to be splash lubricated from the beginning, which with the size and width of the double row cylindrical bearings does create additional problems and very few bearings reach the 20,000 operating hours, even though the standard manufacturers claim is 40,000 hours and even much higher number when you use bearing manufacturers' modified rating life calculations. As an exciter has gears, there is also conflict with what type of oil has to be used i.e; for bearing splash lubrication, a lower viscosity oil should be used than for gear load transfer, where with vibration and impacting, the gears work with extreme pressure. Figure 7.6 presents a condition where 320 cSt oil was used to satisfy gear loading but problems with splash lubrication of upper bearings led to overheating, accelerated oil degradation and damage to the seals. With a box external temperature of 132.8˚C, it could be expected that the internal oil operating temperature could be approximately 150˚C, as shown in Figure 7.7.

	Seal 111.7 Box 118.5	98.4	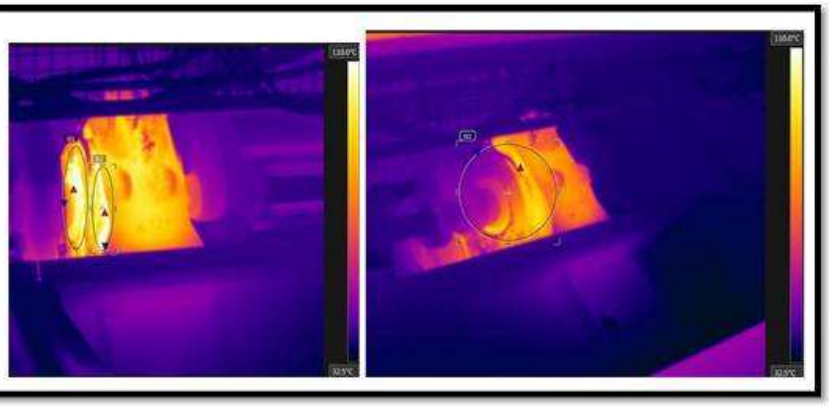

Figure 7.7 Box exciter temperature reading

An additional problem with geared exciters is the extra heat generated by the working gears, where excessive oil splashing, combined with oil foaming can lower the oil level below the acceptable level for the lower bearing pair even though the measured level can be correct during maintenance. The end result can be seized bearings and often gears will look like those shown in Figure 7.8.

Figure 7.8 Damaged gears as a result of seized bearings.

7.3 Gearless exciter design

Using the self-synchronisation principle the gearless exciter has been designed and with gears removed the gear related problems have also disappeared - metal particles contaminating lubricating oil, noise, extra heat generation, etc. Additionally, gear removal made possible modifications to the box and both pairs of bearings have been redesigned working continuously in the oil bath. When using the gearless exciter, there are options to create linear, elliptical and dual frequency type motions. It can also be used for dual frequency screens which makes it very flexible and versatile. Changes to the exciter can be easily done at the industry location to accommodate changes to the process and to improve screening efficiency.

A gearless exciter has to be driven by 2 electric motors which adds some redundancy and if one of the electric motors fails, both exciters will keep working with increased power draw by the working motor. Figure 7.9 presents a commercial gearless exciter, where the exciter has been built, tested and is working in the industry.

Figure 7.9 Gearless exciter on the test stand

7.3.1 Gearless exciter testing

The industrial gearless exciter has been tested on the test rig with different running speeds and directions of revolutions to confirm the results obtained from the lab testing rig experiment results.

Vibration measurement equipment used for the testing was different to that which was used in the University Lab. It consisted of,

- Laptop
- HBM software CATMAN
- 1-MX840B - HBM 8 channel universal amplifier (6 channels used for testing)
- 6 single direction accelerometers - general purpose 100mV/g
- Frequency controller
- Testo 882 Adjustable focus thermal imager was used to check temperature level and heat flow distribution

Figure 7.10 presents the photo of the testing equipment setup used for the gearless exciter workshop testing.

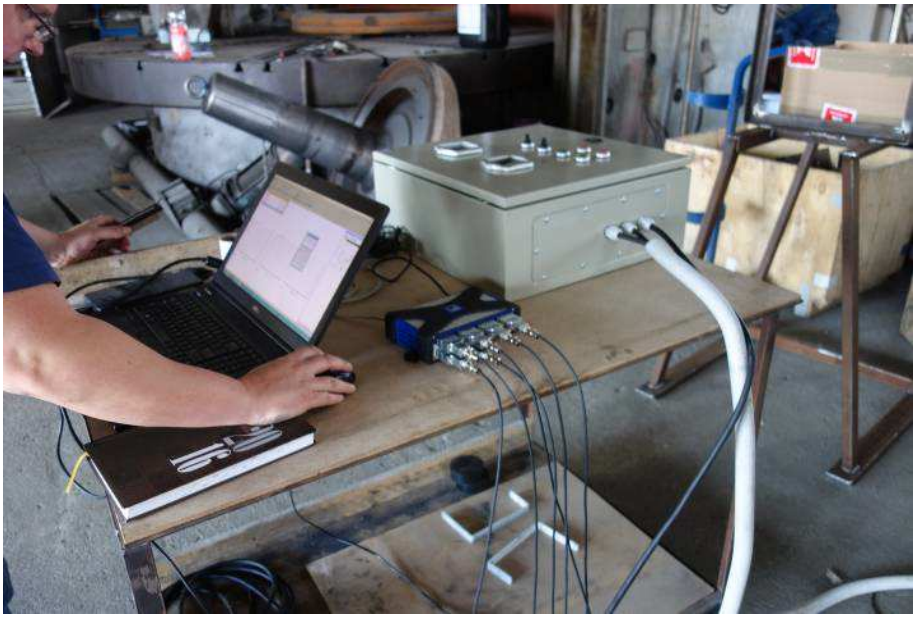

Figure 7.10 Testing setup

Figure 7.11, Figure 7.12 and Figure 7.13 show the location of accelerometers.

Figure 7.11 Front end accelerometers location on the gearless exciter testing rig

Figure 7.12 Accelerometers in the middle on the gearless exciter testing rig

Figure 7.13 Accelerometers at the back location on the gearless exciter testing rig

Table 7.1 presents testing parameters for testing of gearless exciter.

Table 7.1 Testing parameters for gearless exciter

Case No	Lower shaft[rpm]	Upper Shaft[rpm]		Measurement Time
7.1	-1000	+1000		2s
7.2	-1500	0	Only one electric motor working from start	2s
7.3	-1000	-1500		2s
7.4	-1000	-1000		2s
7.5	+1000	-1500		2s
7.6	-1000	-1500		0.25s
7.7	-1000	-1500		0.5s

Channel 1 - Front (red)

Channel 2- Middle (green)

Channel 3 - Back (turquoise)

Figures 7.14 to 7.21 show orbits for the respective cases and Figures 7.22 and 7.23 displays the heat distribution pattern obtain with an infrared camera.

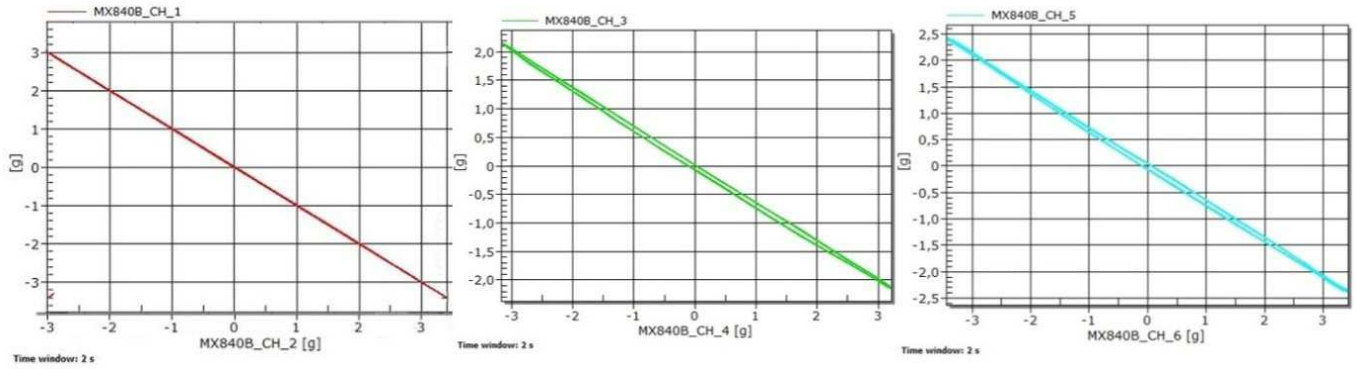

Figure 7.14 Orbits for the Case 7.1

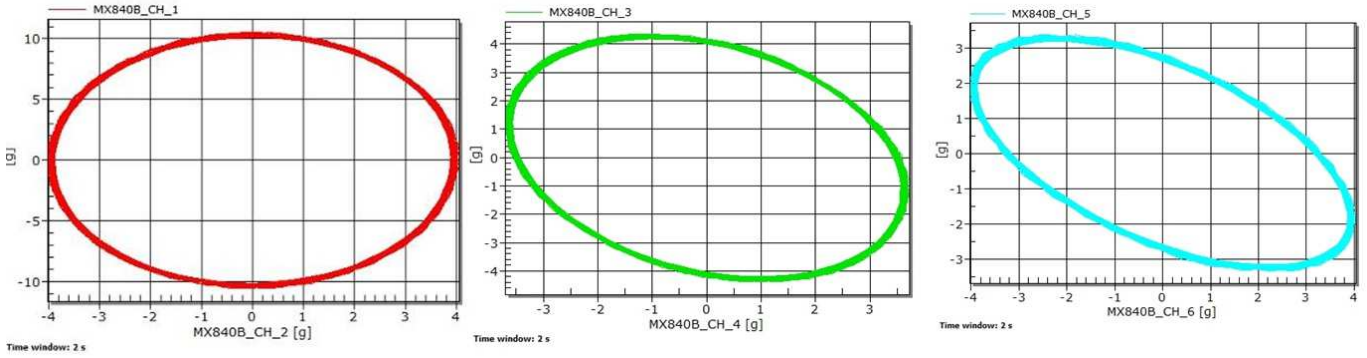

Figure 7.15 Orbits for the Case 7.2

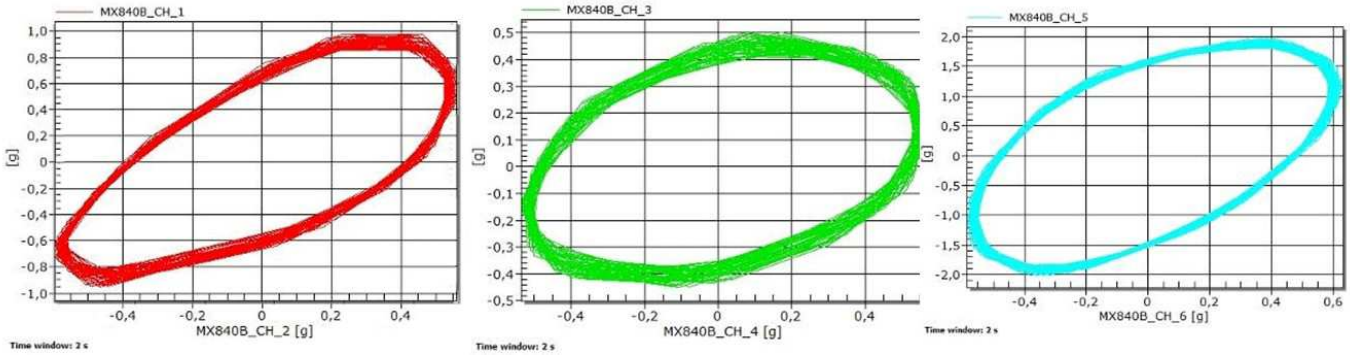

Figure 7.16 Orbits for the Case 7.3

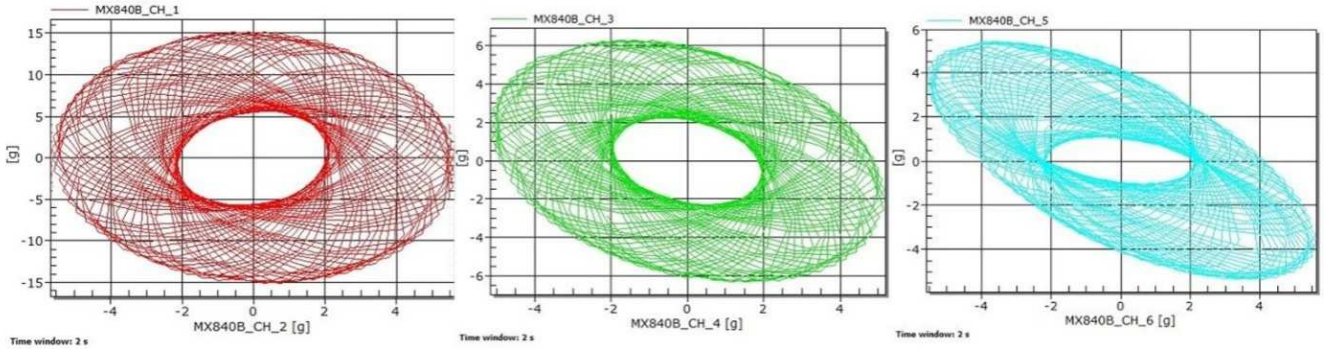

Figure 7.17 Orbits for the Case 7.4

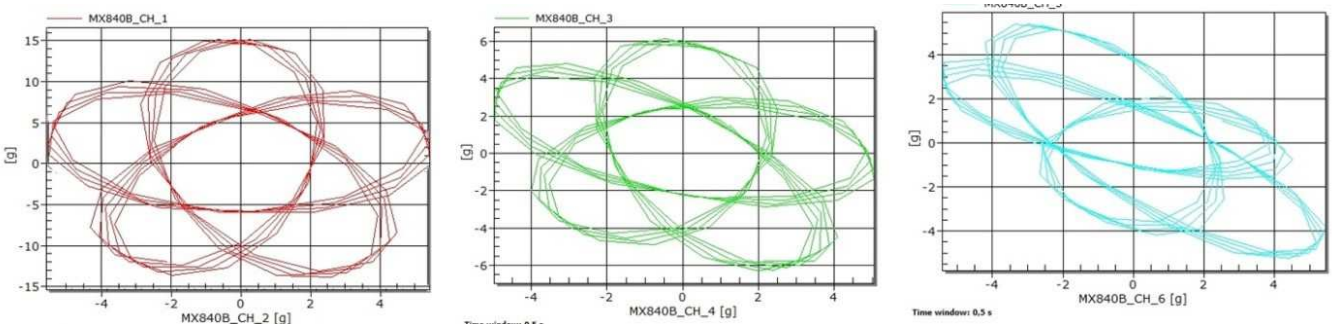

Figure 7.18 Orbits for the Case 7.5

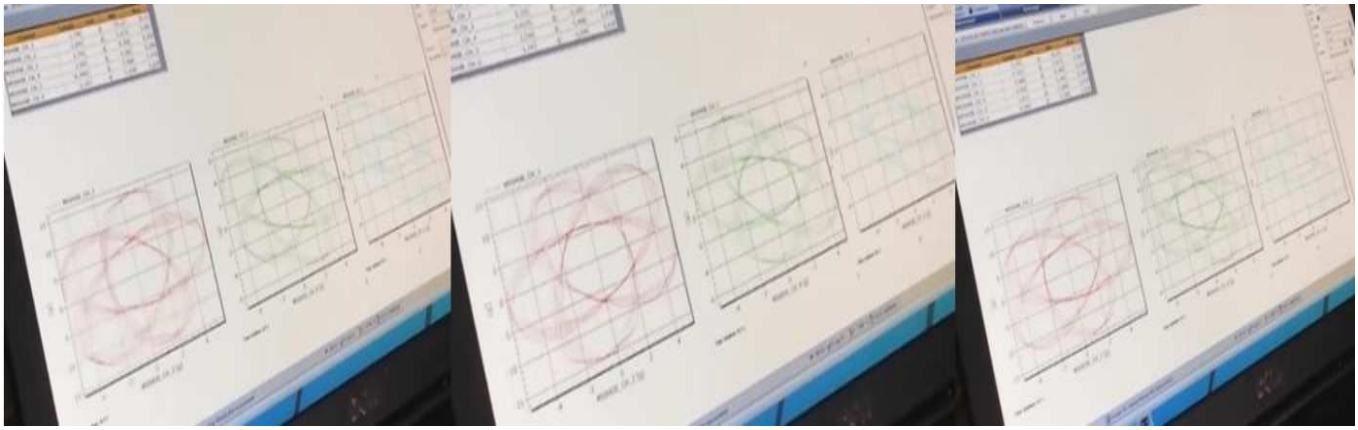

Figure 7.19 Computer screen dump for Case 7.5

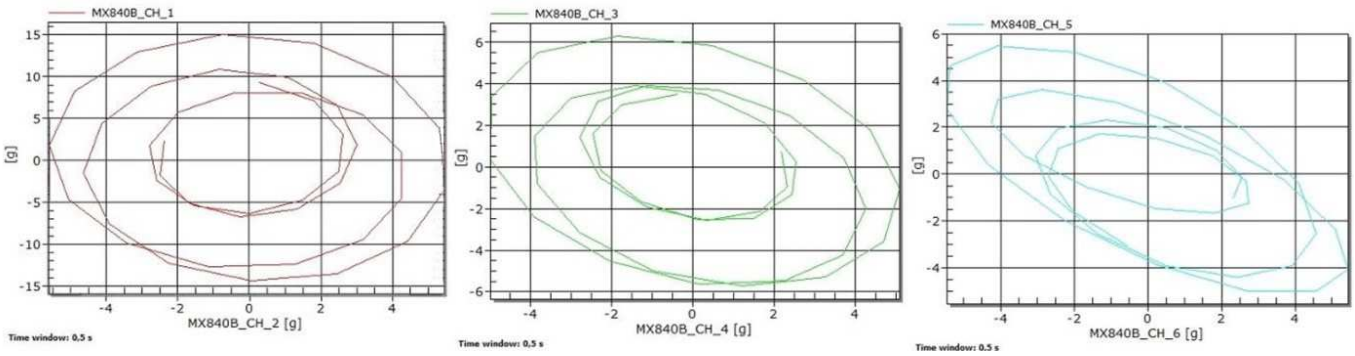

Figure 7.20 Orbits for the Case 7.6

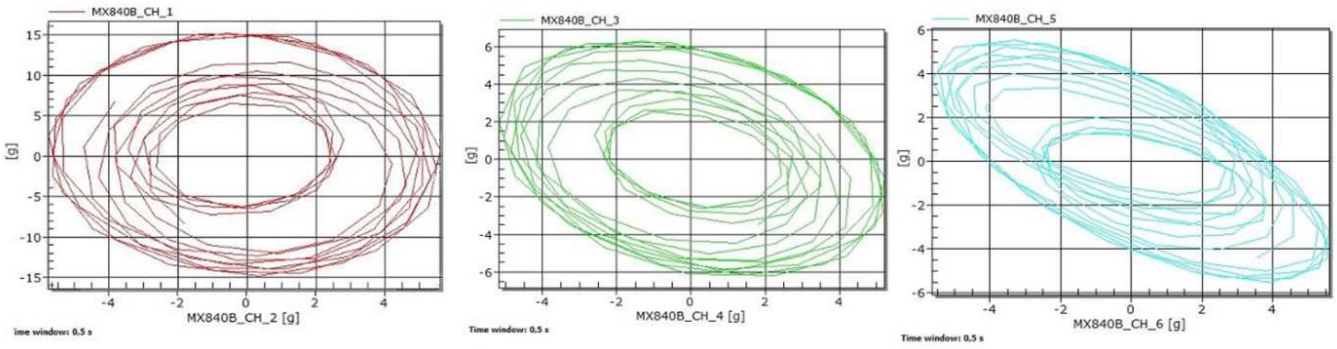

Figure 7.21 Orbits for the Case 7.7

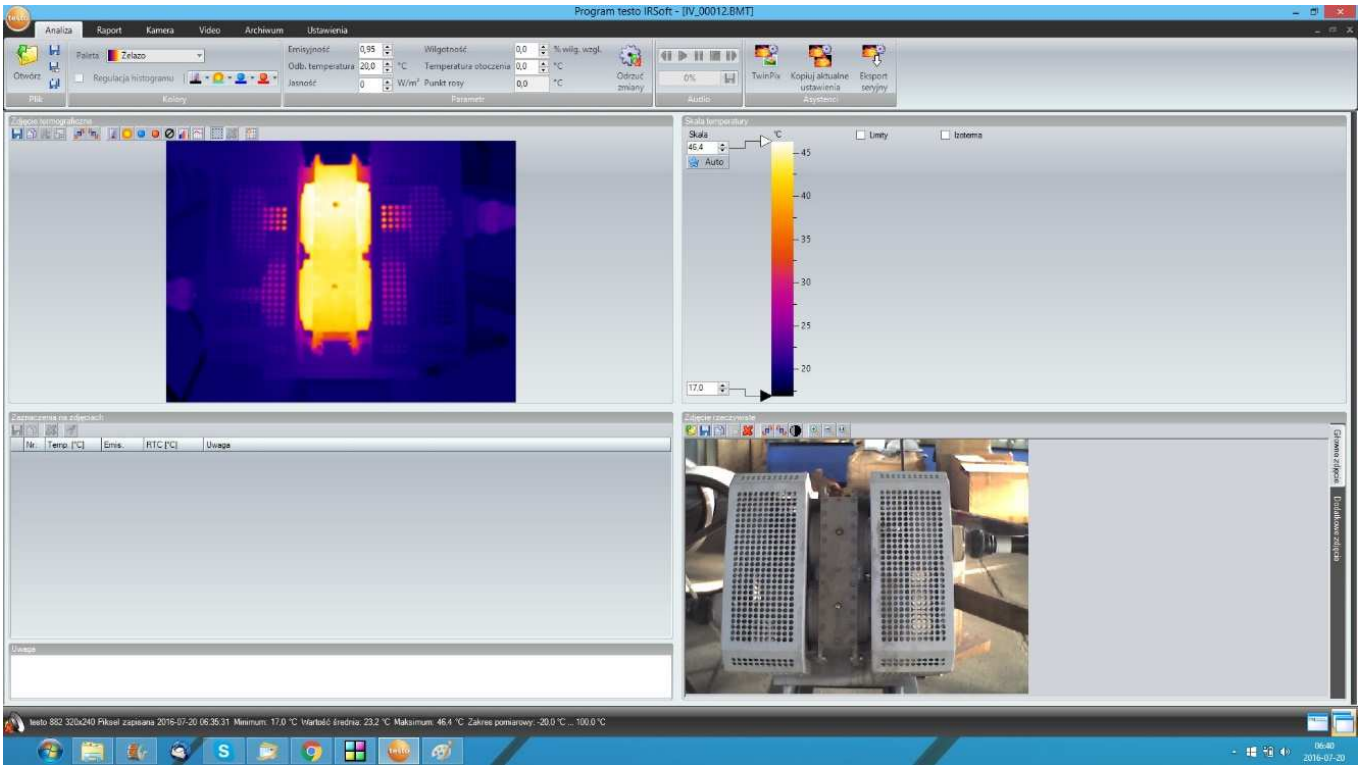

Figure 7.22 Thermal image of a gearless exciter taken after 1 hour of testing

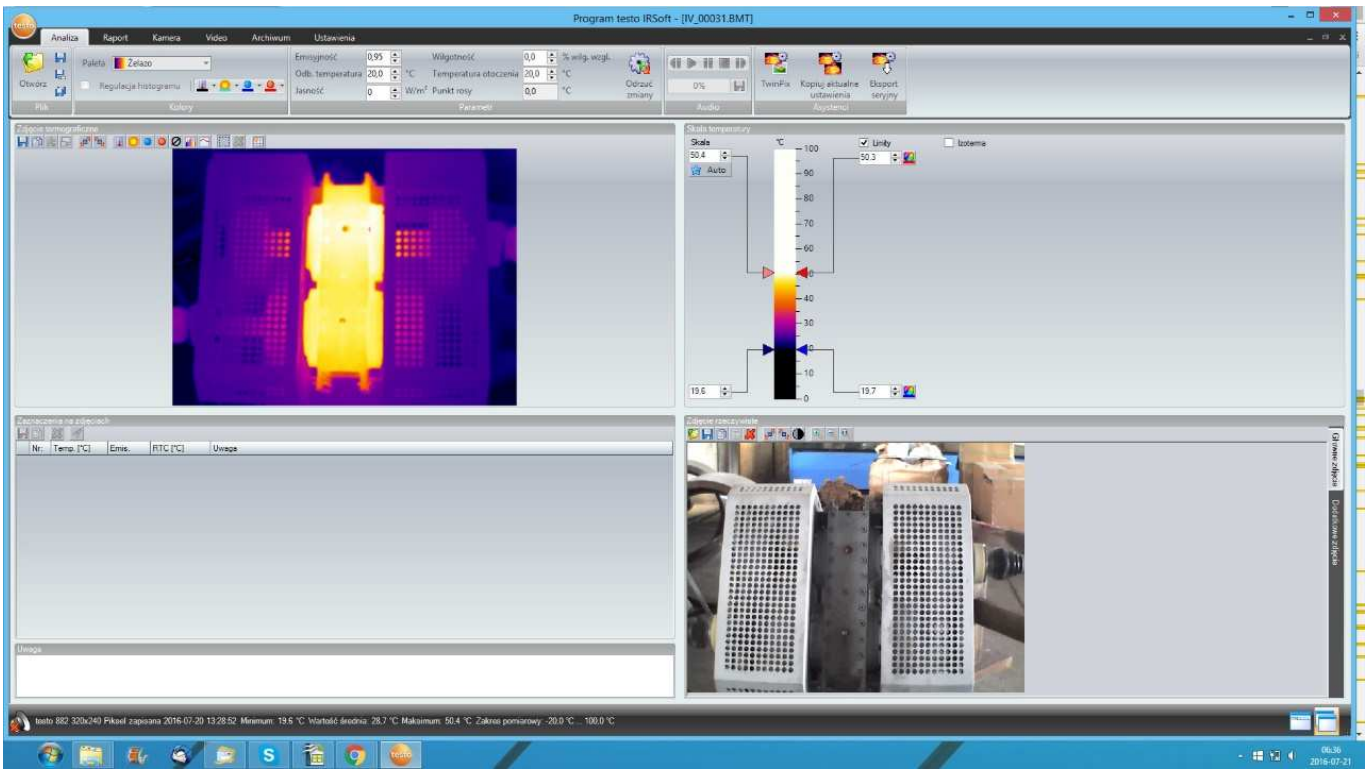

Figure 7.23 Thermal image of a gearless exciter taken after 9 hour of testing

Test results correlate well with the laboratory test results and show the trajectories as expected. The difference between ambient and operating temperature is below 30˚C which was a very good result and confirms that the gear removal and using the self-synchronisation effect instead of forced kinematic coupling does make a difference to the heat balance. Pictures taken with a thermal imager show even temperature distribution, in Figure 7.22 and Figure 7.23, with temperatures well below the recommended temperature of 30 deg above the ambient.

The temperature results are the results of an improved lubrication system which was possible because of application of the self-synchronisation phenomenon instead of gears which allowed for internal modifications to the box. The improved lubrication system is not possible with geared versions of exciters.

Figure 7.24 Two testing rigs with gearless exciters driven with two electric motors (Goster P/L).

Figure 7.24 shows a photograph of the testing of two rigs with two gearless exciters which have counterweights set with a phase difference of 180 degrees. The purpose of this exercise was to check if the exciters will self-synchronise and if they could be run reliably so cancellation of the vibration signal could be achieved. By setting the counterweights in 180 degrees phase difference the neutral balance has been achieved, which means that the starting moment of the exciters is very low and there is no need to use oversize electric motor to overcome the initial starting torque. Additionally, with the testing rigs running in opposite phases, the vibration signal transmitted to the structure will be low in comparison to a case of two running with 0 degree phase difference. The same results can be achieved for screens running as dual frequency screens. The preliminary testing looked very promising and will be implemented into industry to confirm higher screening efficiency and better reliability of exciters by achieving longer life of bearings and lower noise of the installations which is important especially in colder climates when vibrating screens are working in the buildings.

7.3.2 FEA simulation of vibrating screen with gearless exciter

This simulation with a gearless exciter has been done to show the possibilities of self-synchronisation of vibrators and to provide comparison to what can be achieved using 'traditional' methods. The simulation has been done using Strand7 Finite Element Software.

Several options are presented for screen stroke shape and comparison is made with a Metso screen with a single vibrator.

Figure 7.25 shows an elliptical/circular motion, with both shafts rotating in the same direction with the same frequency and it is similar result as per the presented Metso screen. In this specific case the self-synchronisation phenomenon can't be used and both exciter shafts will have to use a kinematic coupling to keep them working with zero degrees phase difference, the simplest way being to use toothed belt.

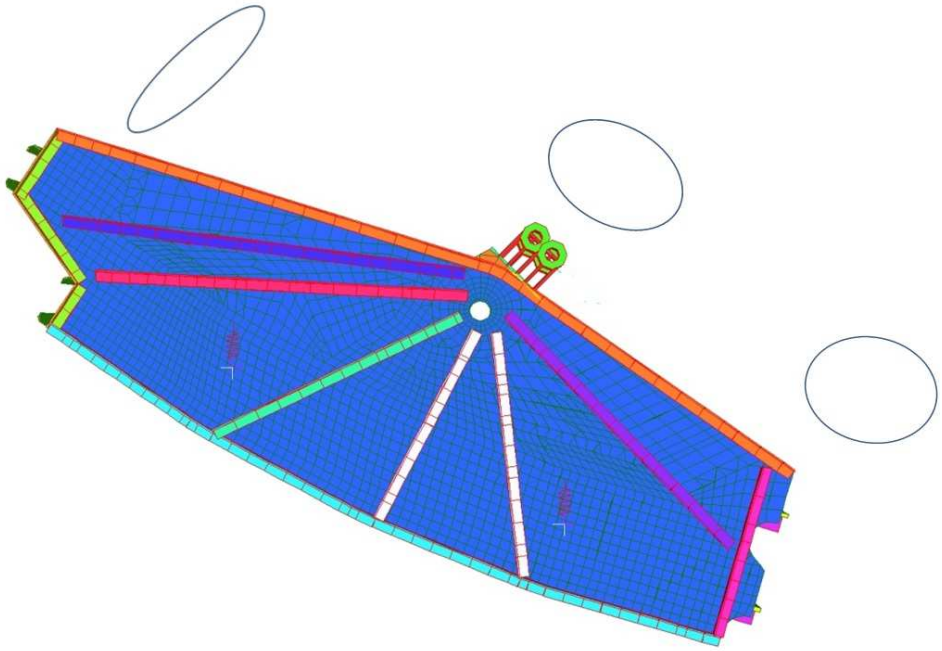

Figure 7.25 FEA simulation of circular/elliptical screen stroke shape using gearless exciter with shafts connected using toothed belt

Figure 7.26 presents a dual frequency solution with both shafts rotating in the opposite directions, with two different frequencies.

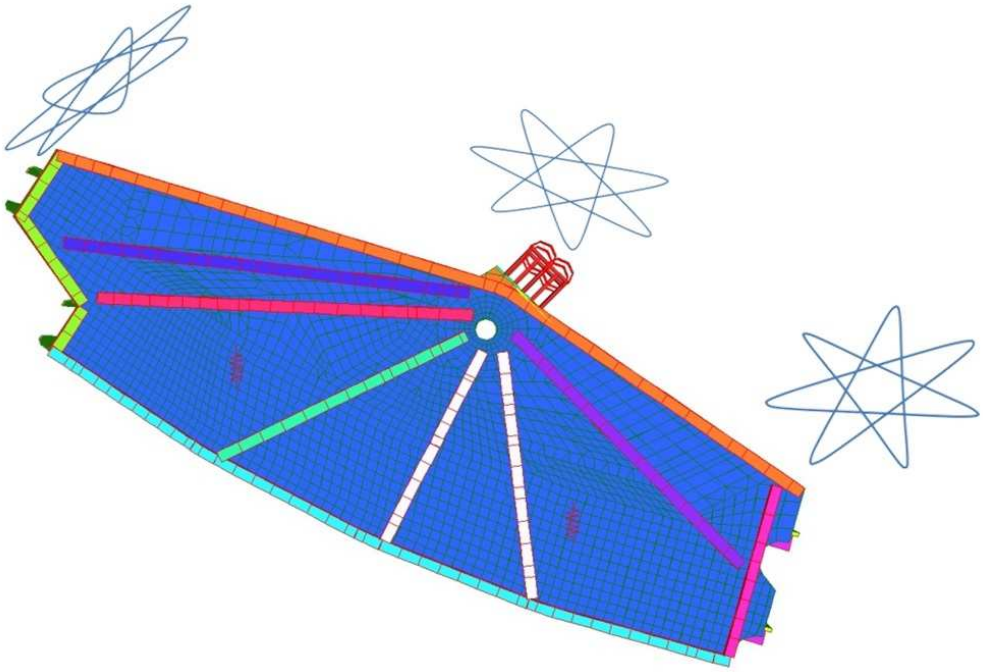

Figure 7.26 FEA simulation of dual-frequency screen stroke shape using gearless exciter

Figure 7.27 presents the simulation from a dual frequency exciter, with both shafts rotating in the same direction with two different frequencies.

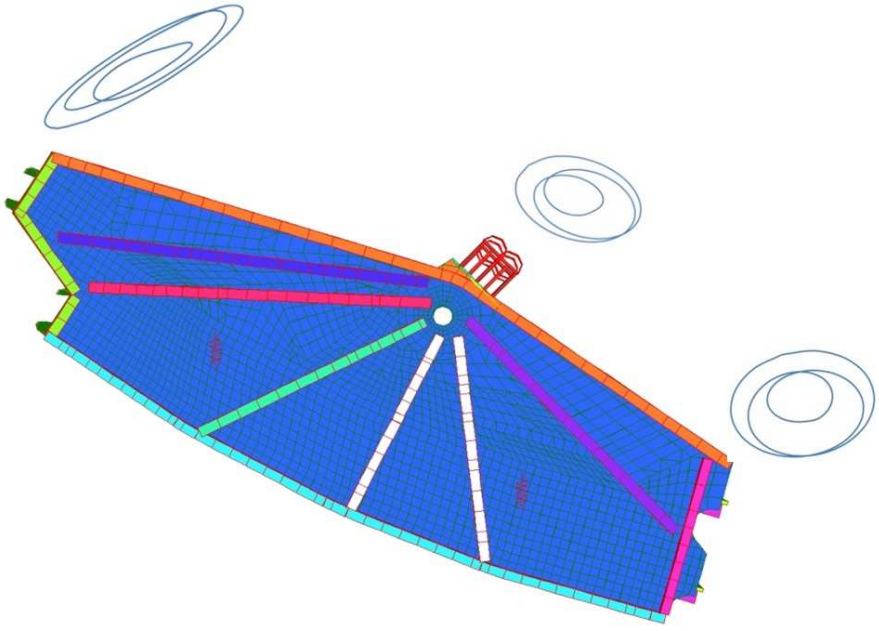

Figure 7.27 FEA simulation of dual-frequency screen stroke shape using gearless exciters

Figure 7.28 illustrates an option for a linear motion, with both shafts rotating in the opposite directions, having the same frequency.

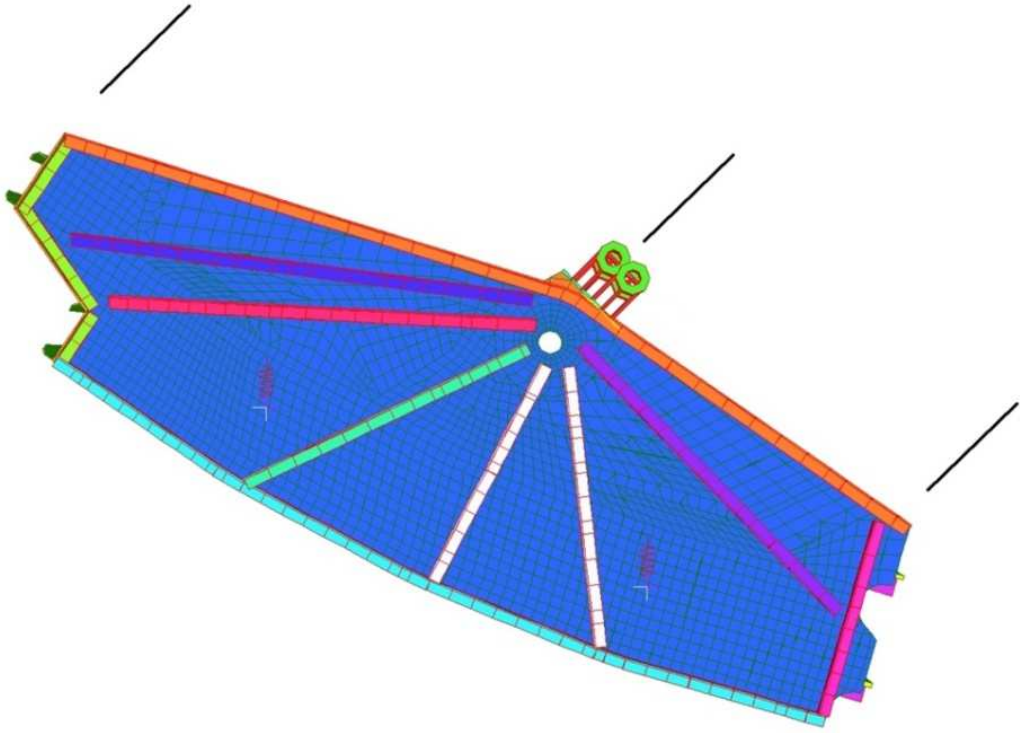

Figure 7.28 FEA simulation of screen linear stroke shape using gearless exciter

All changes can be done easily at the client site and real testing with material would determine the best screen parameters for the specific process.

It means that several screens of the same type can work in the same mine or quarry with different stroke shape and frequency which will be determined by the process requirements.

It would require high standards from the commissioning engineers but the outcome will be increased efficiency which is important not only in better profitability but because all mineral resources are finite.

Figure 7.29 shows a Metso screen which the gearless exciter screens have been compared to.

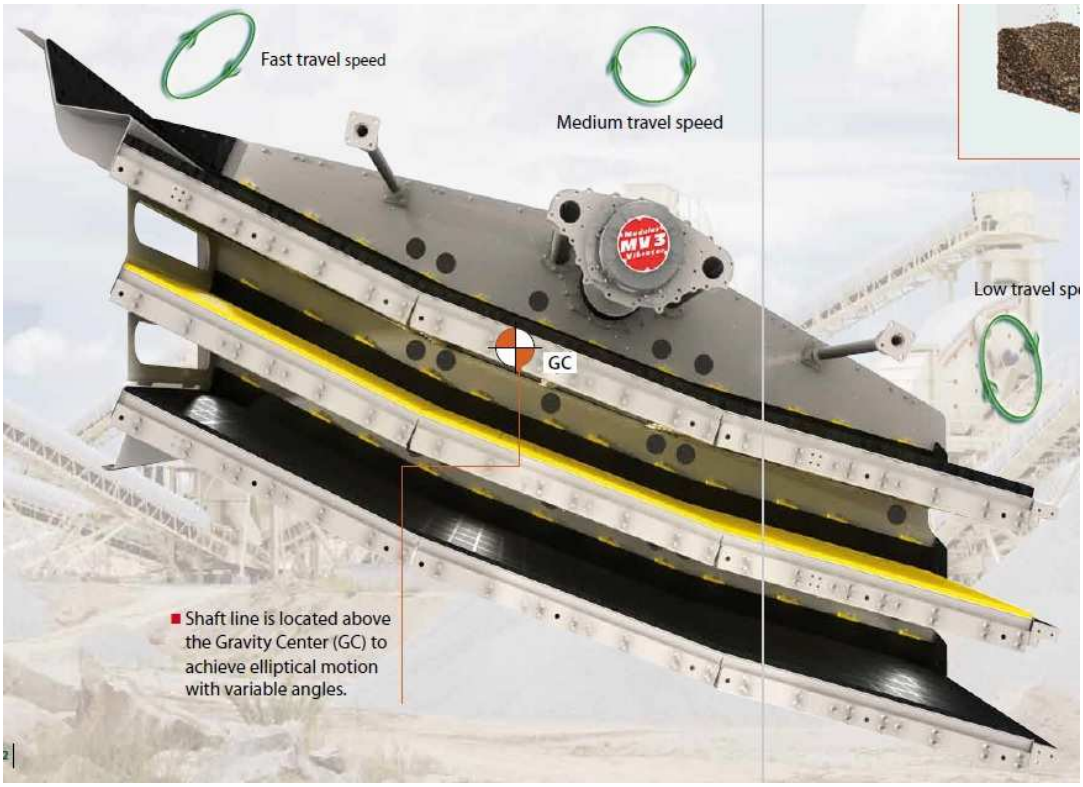

Figure 7.29 Metso TS screen with circular exciter - stroke shape (Metso catalogue)

7.3.3 FEA simulation of vibrating screen with gearless exciter results

The purpose of the research investigated the self-synchronisation phenomenon of vibrators and confirmed the stability and conditions of it happening.

The self-synchronisation can be used in the practical applications and bring the benefits but it also can be expensive or detrimental if the unique features and response behaviours are not taken into account. In the field of vibrating screens an example of geared box type exciter can be used as a case of a design where the self-synchronisation was not taken into consideration. With counterweights self-synchronising about themselves and about the centre of mass, wear is created on a gear set, that generates extra heat as the centre of mass is never stationary, because of the material moving on the screen deck and also because of the feed material impacting on the vibrating screen. Geared exciters all rely on splash lubrication which is not very reliable especially when the vibrating screen experiences frequent starts and stops. With bearings operating with mixed lubrication regimes, (at best) few bearings last for more than 8000 hours even though they are theoretically designed for 40,000 hours bearing life operation. More work into vibrators counter and synch rotation using self-synchronisation would create simpler, better, cheaper and more reliable designs.

Chapter 8
Discussion Chapter

There has been some research study done in the self-synchronisation though the majority of the research has been theoretical and has not been confirmed on physical models. As the phenomenon is still not fully understood there can be 'surprises' when the technology is implemented into industry. More testing should be done to understand relationships between mass, static moment, moment of inertia and operating frequency as it can benefit in development of new technologies and applications.

To further the research, collaborative research between universities and industry can offer investigations and solutions to problems with vibrating screens that occur in the field. Screens can be made lighter, which in many cases also means stronger and with better distribution of natural frequencies that is important especially with dual frequency screens. Lighter screens also mean lighter supporting structures and better energy efficiency. Combining self-synchronisation phenomena and resonance effect would create new types of screens which would be cost and energy effective.

Testing of vibrators operating in the same direction showed that they will always self-synchronise and the bond between the vibrators is very strong. The results always included rocking motion, with the centre of mass being a pivot point. The circular movement of the testing rigs was never achieved because there was no option to set operating parameters of the testing rig to fulfill theoretical conditions required to obtain the phase difference of 0 degrees and to prove or disapprove the calculations.

Dual-frequency testing is a relatively new field but there are already several companies manufacturing this type of vibrating screens. Vibrators self-sychronised and the bond was higher for higher values of speed ratios i.e. ratio 1:2 has stronger bond than ratio 1:3. Data recording was done over a time span of several seconds to confirm the stability and repeatability of movement. In all cases the vibrators synchronized and the frequencies adjusted to the full integer ratio of frequencies.

Testing of vibrators operating in the opposite directions was different as there are already several screen designs that use the self-synchronisation of vibrators operating in the opposite directions. Theoretical work has been done by Blekhman (1988) but there has also been work done by several other researches including Banaszewski (2000), who presented calculations and testing results from a physical testing rig which proved that his calculations correlate well with tests results for the vibrator position as illustrated in Figure 8.1.

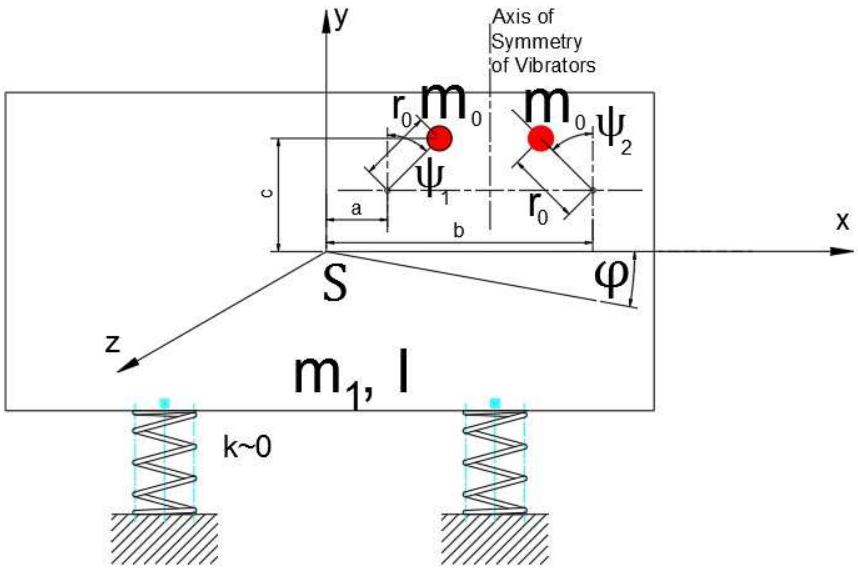

Figure 8.1 Diagram for experiment and calculations

The shape of the ellipsis is a function of the moment of inertia and the location of the vibrators, centre of gravity and screen design and that is the reason that the ratios between minor and major axis change with the location of the measuring points. Stroke shape, angle of inclination and amplitude calculated correlated well with physical testing results and also with testing results from vibrating screens presented in Figure 8.2, and Figure 8.3 presenting results taken from a high speed camera.

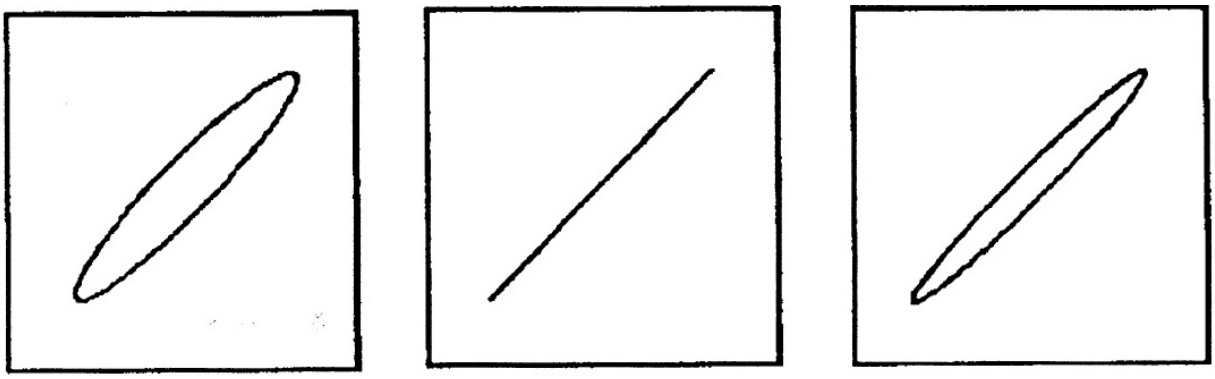

Figure 8.2 Stroke shape results obtained in calculations (Banaszewski)

Figure 8.3 Stroke shape obtained using high speed camera (Banaszewski)

Cheng Da Xian (2000) analysed conditions for synchronization and the related orbit shapes are presented in Table 8.1. Calculations of the angle and orbit shapes would yield similar results to obtained by Banaszewski (2000), but the theoretical results were not confirmed by physical testing.

Table 8.1 Conditions of synchronization for vibrators as per Test Case 4.2.1 with vibrators rotating in the opposite directions (Cheng Da Xian (2000) Mechanical Vibration)

Item	Self-synchronization	Exciter self-synchronous deflection
The exciter position diagram	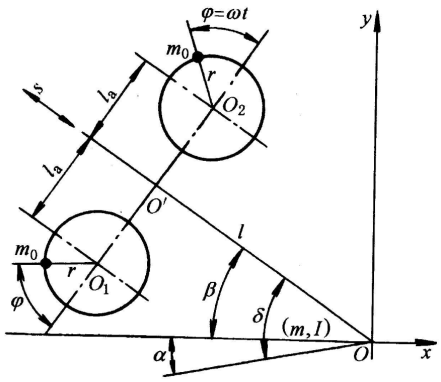	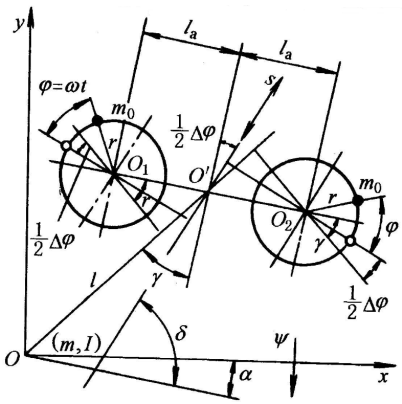
	O is the mass centre, O_1, O_2 is the rotation centre of the exciter, *O′* is the middle point between O_1 and O_2, l_a is the distance of O_1O' and $O'O_2$, *α* is the inclination angle, *m* is the mass for the machine and *I* is the moment of inertia about *O*.	In order to reduce the height of the machine and improve the stress state, O_1O_2 can be rotated around *O′*, parallel with the bottom surface of the machine, which is the inclination angle *γ*.
Condition for Synchronization	Condition for Synchronization: $\left\|\frac{m_0^2 r^2 \omega^2 W}{\Delta M_g - \Delta M_f}\right\| \geq 1$ For stability conditions that far from the resonance: $W \approx \frac{l_a}{I + \sum I_0} > 0$ From the synchronization condition and stability condition, it shows that the larger of l_a, the smaller of the difference of the driving force between the two motorsΔM_g, and the smaller of the difference of the friction resistance moment generated by the exciter, and therefore, it is more easily to be synchronization.	
Vibration angle	$\delta = \beta + \alpha$	$\delta = 90° - \gamma + \frac{1}{2}\Delta\varphi$ $\Delta\varphi = -\cot\frac{l^2 + l_a^2 \cos 2\gamma}{l_a \sin 2\gamma}$
The locus of the machine motion	The machine moves in a straight line.	Because of the moment and the swing, the whole machine except the mass centre moves along an oval locus, this is very close to a straight line.

Figure 8.4 presents a working vibrating screen with vibrators setup as in the diagram used by Banaszewski (Figure 8.1) and manual stroke test cards taken during operation of the vibrating screen are shown in Figure 8.5.

Figure 8.4 Vibrating screen with two unbalanced shafts driven by two separate electric motors (Sand Mine, Mosznica).

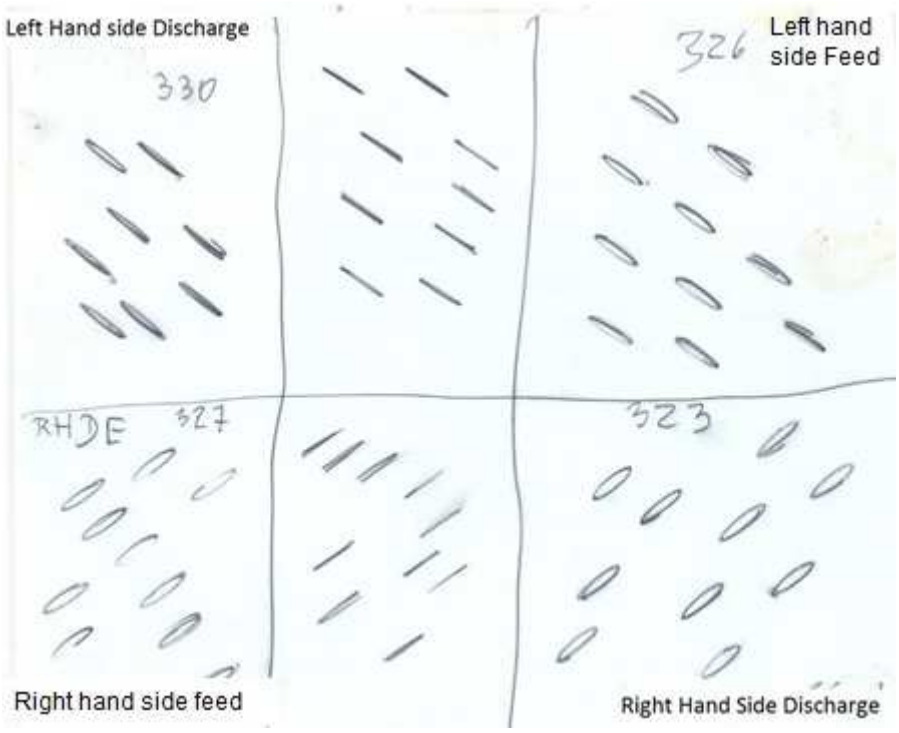

Figure 8.5 Test card taken from a screen operating with two self-synchronised vibrators

The test results confirmed the calculation done by Banaszewski and they also correlated well with the results obtained from the testing rig. Differences in shapes presented in the test card, shown in Figure 8.5 are the results of the screen operating close to the natural frequency and uneven screen supports. Differences between the left hand side and right hand side feed end was 1 mm, while similar measurements at the feed end showed a larger 7 mm difference, which is more than double of the recommended tolerance in this case of 3mm, presuming that the steel structure is leveled properly. Both factors i.e. operating close to the natural frequency and uneven spring support caused differences between stroke shapes on the left and right hand side of the screen but have no effect on self-synchronisation. In principle though they look as predicted in calculations and experiments.

Chapter 9
Conclusion

The purpose of the research was to investigate the self-synchronisation phenomenon of vibrators and to confirm the stability and conditions of it happening and the suitability of its application in the vibrating equipment field. Physical testing confirmed the theoretical calculations. Small variation of movement and of stroke was a response of the testing rig becoming nonlinear when the higher load was causing large deflection of the springs. Most researches do not take nonlinearity into account to simplify the process and the calculations outcomes are close to the physical testing results with an acceptable error.

When the results of the vibrators operating in the same direction are considered, then the theoretical calculations have been partially confirmed as there was no option to fulfill conditions for self-sychronisation as specified by Blekhman (2000);

$$\frac{\mathrm{Mr}^2}{\mathrm{I}} < 2 \; conditions \; for \; sy\text{chronised motion of two vibrators for circular motion}$$

As the mass is also related to moment of inertia the only option really is to increase the ‘r’ which would make the rig very long and impractical for the purpose of the research and practical application in the field of vibrating screens. The self-synchronisation phenomenon strength of the bond and stability has been confirmed. Application of two vibrators in the field of vibrating screens using the synchronization phenomenon with the same direction of rotation is not practicable.

The part of the thesis related to two vibrators operating in the opposite direction confirmed synchronization in all conditions and very strong bond between both unbalanced motors. The synchronization was not affected by the testing rig operating close to the natural frequency, similarly as in the case of vibrators rotating in the same direction.

The third testing mode involved vibrators operating with different frequencies and rotating in the same and different directions. The resulting screen movement increases the randomization of particles travelling over the screening deck and this way increasing screening efficiency without increasing structural stress on the vibrating screen structure.

The novelty of the research is that it confirmed the self-synchronisation for two vibrators and provides the possibility of applications in vibrating equipment and other industries. It has also confirmed that properly built mathematical models using Finite Element Analysis software can be used to simulate the behavior of a vibrating screen and therefore eliminate the need for physical prototypes, reducing time and cost requirements for development.

The self-synchronisation can be used in the practical applications and bring the benefits but it also can be expensive or detrimental if not taken into account or not understood. In the field of vibrating screens an example of geared box type exciter can be used as a case in which self-synchronisation was not taken into consideration, resulting in significant lost time and production. More work into vibrators counter and synch rotation using self-synchronisation would create simpler, better and more reliable designs and reduce cost of drive arrangements.

Unfortunately in the case of vibrating screens, most research has taking into account mechanical movement only and there are very few studies where it has been done in combination of screening efficiency studies which is why the testing of two vibrators operating with two different frequencies were performed.

This research confirmed that the self-sychronisation can be successfully used in the field of vibrating equipment which will make the vibrators more reliable and easier to maintain. Currently used box type vibrators are designed and built without taking the self-synchronisation effect into account and this has a detrimental effect on the life of the bearings. The self-sychronisation is present in all test cases with very strong connection when the vibrators are working at the same operating speed, regardless of the direction of revolutions. The research confirmed that the self-synchronisation effect can be used for its intended purpose.

Chapter 10
Future research

As per the Nicola Tesla quote; 'If you want to find the secrets of the universe, think in terms of energy, frequency and vibration'. This research has provided significant motivation to further develop self-synchronisation for vibrating screens and to pursue further research developments for maximizing its applicability in the field.

Preliminary testing of three vibrating motors has been done and it has shown that the self-synchronisation phenomenon also takes place. It was noticed that two vibrators running in the same direction did self-synchronise and then they synchronized with a single vibrator running in the opposite direction. Figure 10.1 presents a testing rig result with three vibrators and frequency controllers.

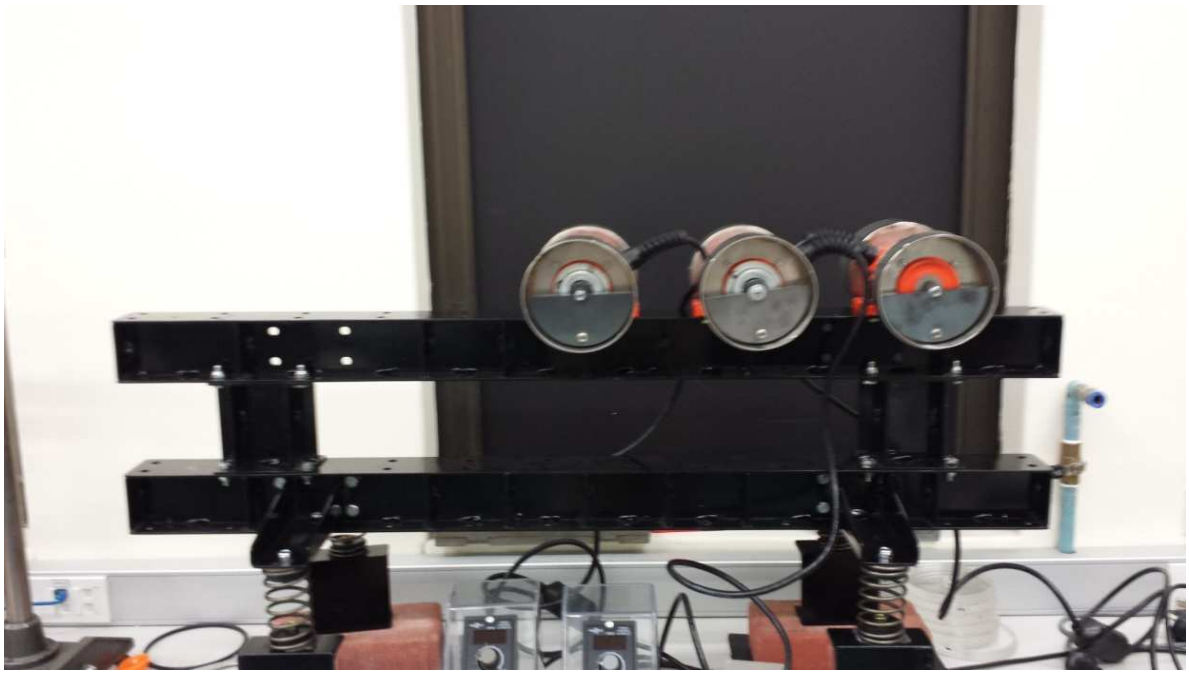

Figure 10.1 Testing rig with three vibrators

Vibrators on Figures 10.2 and 10.3 rotate in directions right, right, left (from left to right) and Figures 10.4 and 10.5 show the phase between vibrators operating in opposite directions for comparison of phase purposes.

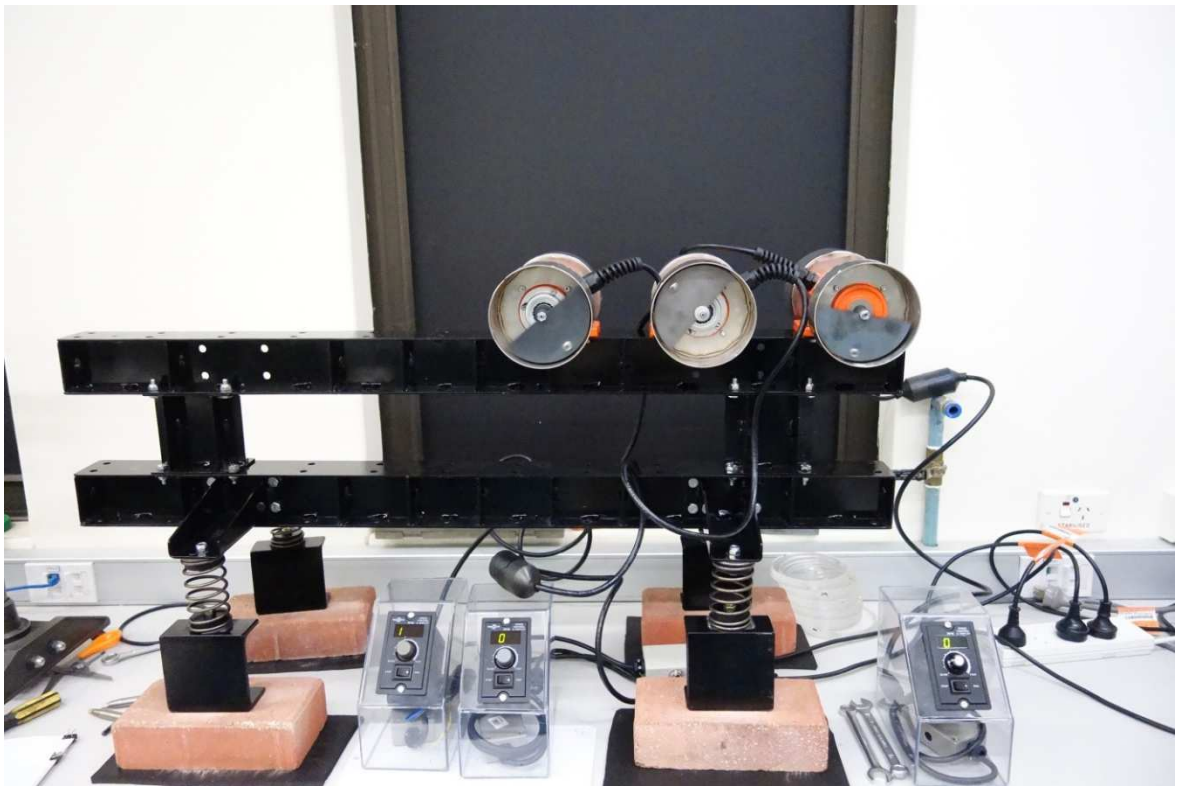

Figure 10.2 Testing rig operating with three vibrators

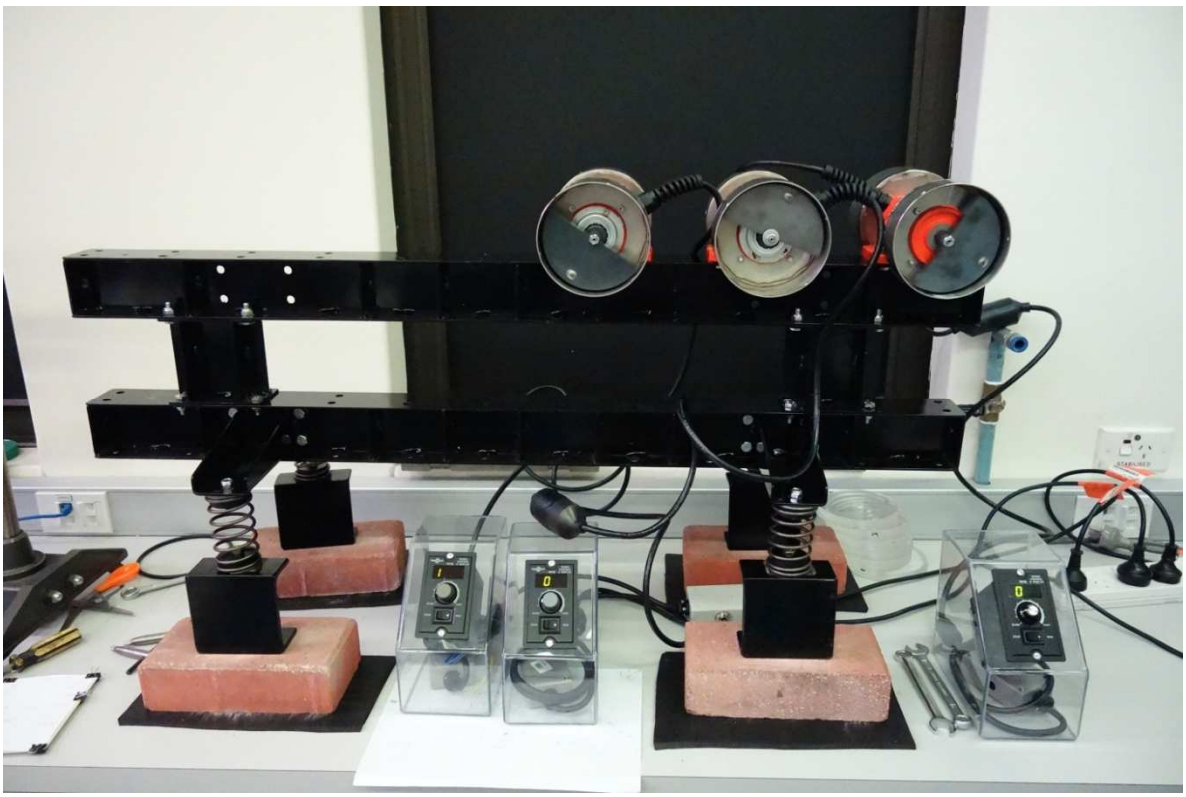

Figure 10.3 Testing rig operating with three vibrators

There are obvious similarities in the presented figures to the cases with two vibrators operating in the same and opposite directions. The exciters synchronised about each other with 180 degrees phase difference for rotation in opposite direction of operation and also at 180 degrees for vibrators rotating in the same direction. Proper testing has to be done to confirm this claim but if correct it would imply that synchronization will happen to an unlimited number of vibrators in the same way as it happens between two vibrators. Analytical calculation confirmed self-synchronisation of three (Rumiancev at al.) and four exciters (Zhao at al., 2010).

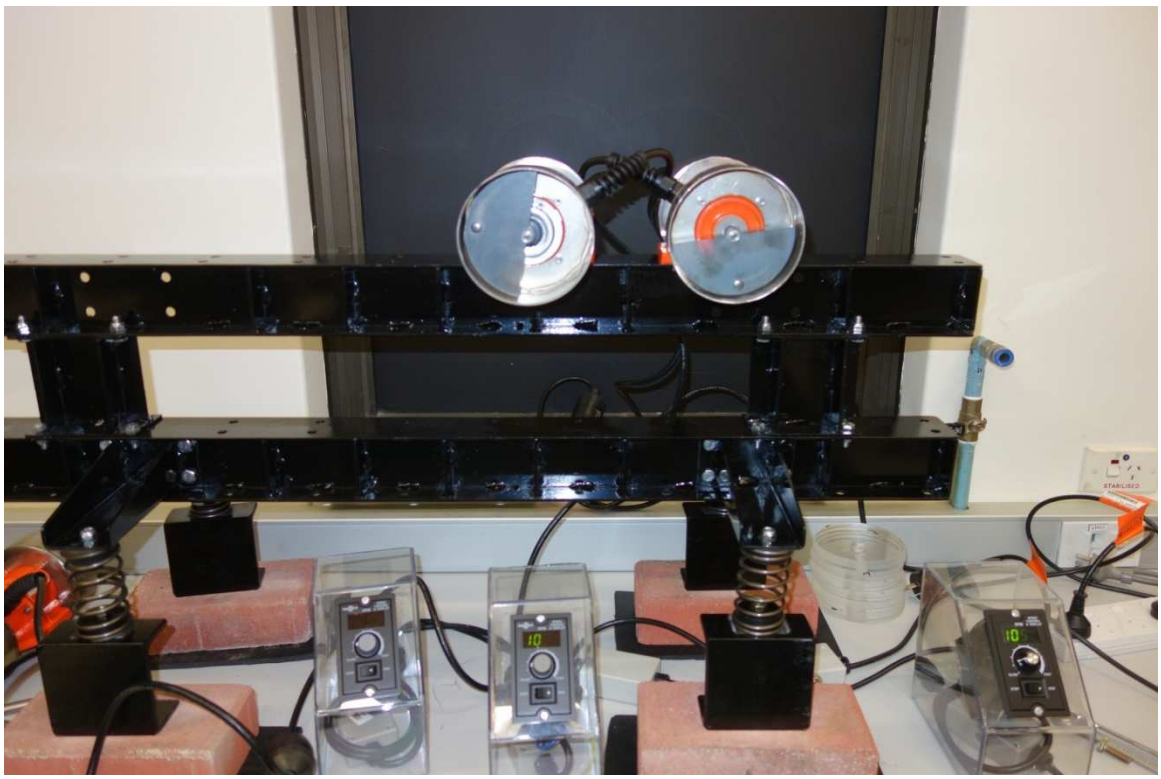

Figure 10.4 Two vibrators operating in opposite directions

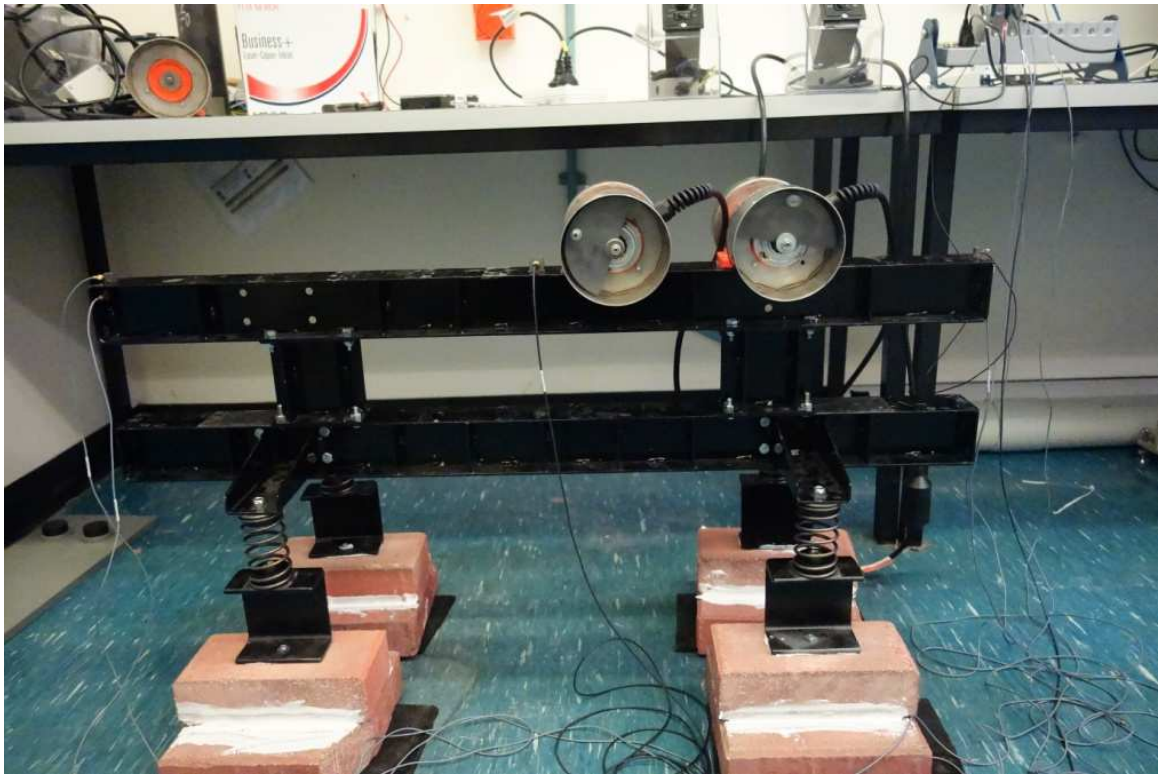

Figure 10.5 Two vibrators operating in opposite directions

In 1909 Frahm invented a dynamic vibration absorber which can be used to reduce or eliminate periodic sinusoidal vibrations, shown in Figure 10.6. The principle can be used to reduce or completely eliminate vibrations on machine foundations or the vibration of isolating frames and therefore eliminate vibration of the screening plants.

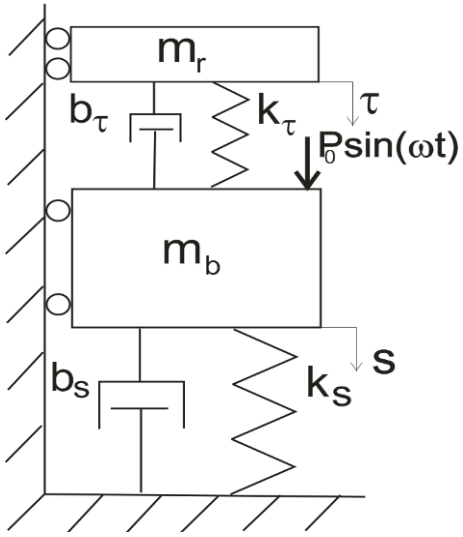

Figure 10.6 Frahm's Dynamic Vibration Absorber (Giergiel, 1986)

The current testing rig can be redesigned to enable testing of several different arrangements to check for optimal solutions to build a vibration absorber operating on Frahm's principle.

In theory the Frahm's absorber should have a minimal damping and following this principle the leaf springs are the best for the purpose but using rubber would make the device simpler and more reliable to build and operate.

Presented in Figure 10.7 is a testing rig setup to test Frahm's principle for application as a dynamic vibration absorber but instead of using mass, the self-synchronisation principle and proper size vibrators would be used to reduce or eliminate vibrations. The drawback is that it will not be effective in transients but can be relatively easily applied to existing installation or structures.

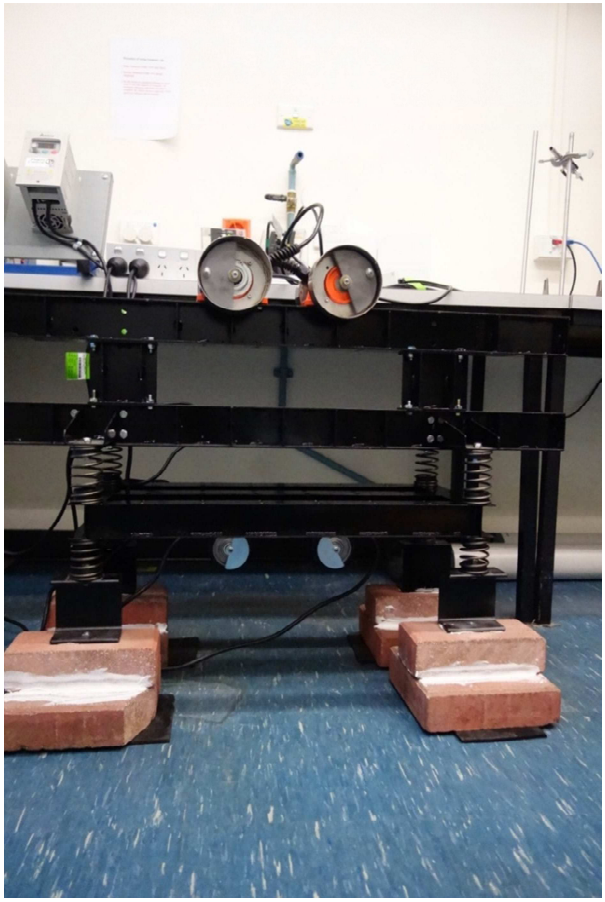

Figure 10.7 Rig setup for testing Frahm's principle

The idea is that using rubber with some damping, as shown in Figure 10.8, the system would still operate and that would make the resonance curve 'flatter' as presented in Figure 10.9.

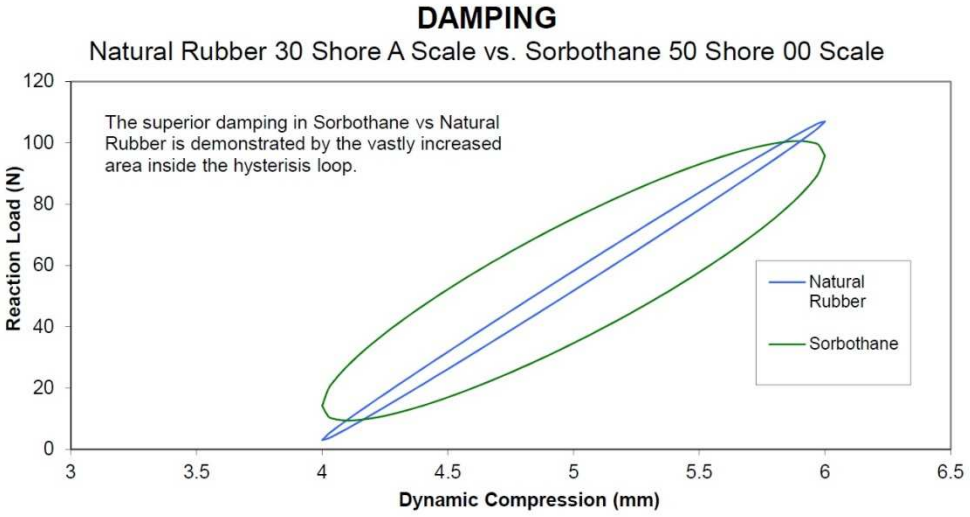

Figure 10.8 Rheotane versus Rubber damping (Mackay Rubber, catalogue)

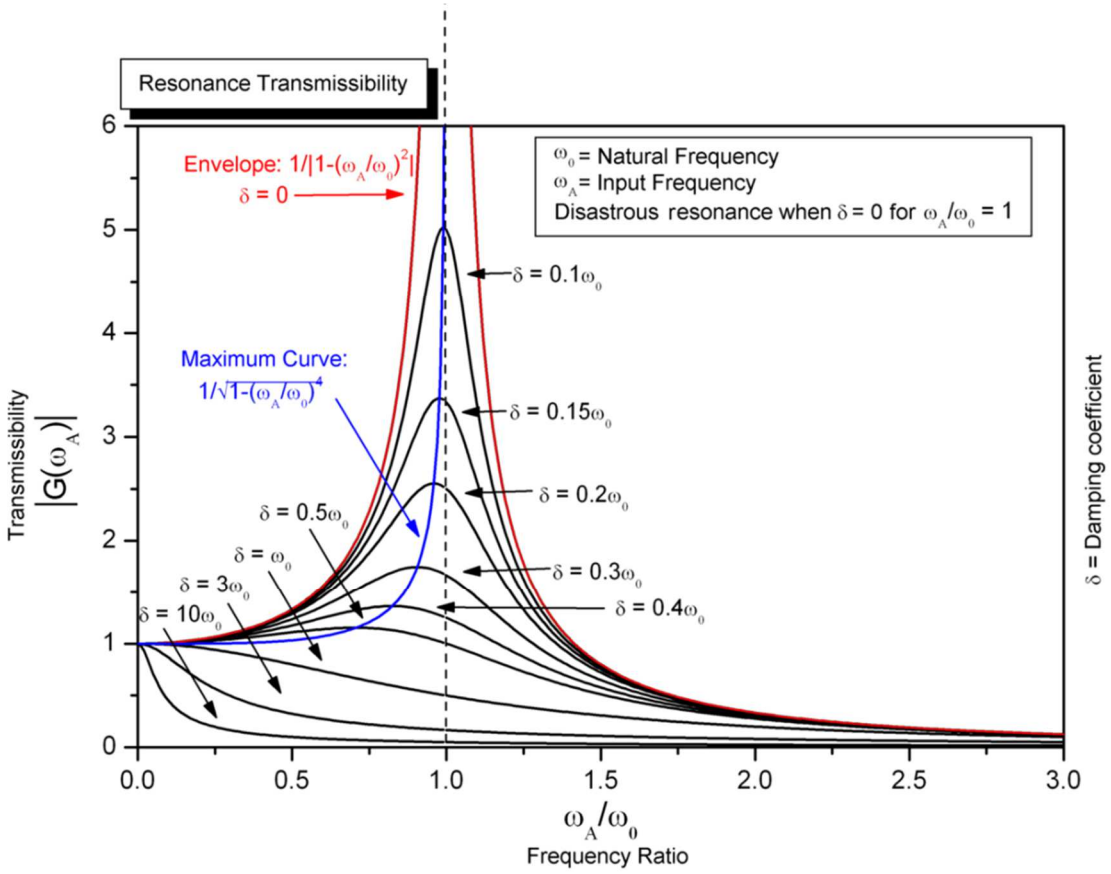

Figure 10.9 Typical magnification factor curves for a tuned two-mass system (Ogata, 2005)

Another direction for the research is synchronisation of vibrators in planes intersecting at different angles. Probably the most common would be 90 degrees, which could be for example some vibrating screen manufacturers which combine linear, vertical and horizontal circular motions. It would be necessary to check the conditions of self-synchronisation under these conditions, and if it can happen and what would be the resultant movement with advantages and disadvantages of it.

Another field of research is in resonance screens. There has been a drop in interest in these types of screens in recent years even though they offer significant savings of energy required to operate this type of screen in comparison to the brute force screens. They also offer some tolerance to increased material load by increasing the amplitude of vibrations. Vibrating screen operating frequency is usually about 0.8-0.9 of the natural frequency determined during static impact testing. During operation of the screen with an added material load (mass increase) the natural frequency decreases and the response moves to the right on the 'X' axis. With fixed operating frequency screens, this increases the magnifying factor and therefore increases the amplitude of vibrations, as shown in Figure 10.9.

Based on the work of Rademacher [1979] comments may be made that with the trough mass to be 2.5 to 3 times of the exciter mass. Subresonant feeders operate below the resonance frequency with ω_a/ω_0 between 0.8 to 0.9 where ω_a - input frequency and ω_0 - natural frequency of the tuned system. There are claims that the 'tuned' feeder maintains its feed rate when the head load varies but with the increased head load and therefore effectively increased pan mass the natural frequency ω_0 with decrease and the frequency ratio ω_a/ω_0 will increase. It is correct to some extent until the natural frequency will move over the 'peak' and then the amplitude will drop and the feeder will be buried under the material load. It also depends heavily on the conveyed material dumping properties as it will determine the dumping of the tuned system.

Figure 10.10 Double Deck Resonance Screen (AMB Engineering)

Figure 10.11 Vibrating screen feeder (Vibroflow)

Figure 10.12 Resonant vibrating feeder for recycling of green waste (Vibroflow)

Figure 10.13 Double deck two mass vibrating screen (General Kinematics)

As mentioned before resonance screens offer better energy efficiency and in a big mine that would account for several million dollars in annual energy savings. Examples of this type of screens are presented in Figures 10.10 to 10.13. The drawback of this type of screen though is they require better maintenance and a higher engineering culture to operate successfully. Figure 10.12 demonstrates an example of a high stroke feeder to transport a high volume, low specific density material in an efficient and cost effective way. A standard solution used by the majority of recycling plants is an apron feeder with a big roll at the discharge to compress the conveyed material and provide friction between material and apron feeder pans. The solution with the apron feeder is at least three times more expensive in capital than a simple vibratory feeder. The cost is further growing during operation and maintenance in comparison with a vibrating feeder that requires very little maintenance.

References

Banaszewski, T. (1988) *Przesiewacze*. Śląsk

Banaszewski, T. (1990) *Przyczyny nieprawidlowej samo-synchronizacji wibratorow w przesiewaczach*. IX Sympozjum Techniki Wibracyjnej i Wibroalustyki, Krakow 1990

Banaszewski, T. (2000) *Wpływ położenia samosynchronizujacych się wibratorów na drgania przesiewacza*, Zeszyty naukowe Politechniki Ślaskiej, Seria; Górnictwo z. 245 Nr kol. 1479

Bangchun, W., Jian, F., Chunyu, Z., Wanli, X. *Vibratory and Controlled Synchronization Engineering*. Alpha Science Intl Ltd 2012.

Blekhman, I. I. (1988) *Synchronisation in Science and Technology*. New York: ASME Press

Blekhman, I. I. (author), Perelman (translator), (1999) *Vibrational Mechanics: Nonlinear Dynamic Effects, General Approach, Applications*, World Scientific Pub Co Inc

Blekhman, I. I. (2015) *Sinhronizatsiya w prirode i tehnike*. Moscow: URSS

Chunyu Zhao, Hongtao Zhu, Yimin Zhang, Bangchun Wen (2010) *Synchronization of two coupled exciters in a vibrating system of spatial motion*. Acta Mechanica Sinica 2010) 26:477-493

Cleary, Paul, W., Sinnott, Matthew, D., Morrison, Rob. D. (2009) *Separation performance of double deck banana screens – Part 1: Flow and separation for different accelerations*. Minerals Engineering 22 (2009) 1218–1229

Cleary, Paul, W., Sinnott, Matthew, D., Morrison, Rob. D. (2009) *Separation performance of double deck banana screens – Part 2: Quantitative predictions*. Minerals Engineering 22 (2009) 1230–1244

Clough, R.W., Penzien, J. (1995) *Dynamics of Structures*, Third Edition, Computers & Strutures, Inc

Czubak, P. (2012) *Dobor czestosci wymuszenia przenosnika dzialajacego na zasadzie eliminatora Frahma z warunku minimalizacji sil przekazywanych na podloze*. Modelowanie Inzynierskie 43, Gliwice 2012, 27-34

Czubak P., (2013) *Analysis of the new solution of the vibratory conveyor*. Archives of Metallurgy and Materials, Vol. 58, No 4.

Fischer M., (1982) *Doppel-Frequenz-Siebmaschinen in der Bewahrung*, Aufbereitungs Technik., 12, 687-693

Giergiel, J, (1986) *Drgania ukladow mechanicznych*. Krakow, Wydawnictwo AGH

Huygens, C. *Horologuium Oscillatorium*, Paris 1673

Lawinska, K., Remigiusz Modrzewski, R., Wodzinski, P. (2014) *Wyniki badan kruszyw mineralnych na przesiewaczu dwuczestosciowym*. Mining Science – Mineral Aggregates, vol. 21(1), 2014, 129–138

Michalczyk J., Cieplok G., (2014) *Disturbances in self-synchronisation of vibrators in vibratory machines*. Arch. Min.Sci. Vol. 59, No 1, 225-237

Michalczyk, J. *Maszyny wibracyjne, obliczenia dynamiczne, drgania, hałas*. (1995). Wydawnictwa Naukowo - Techniczne

Michalczyk, J., Banaszewski, T. *Oddziaływanie dynamiczne maszyn stosowanych w przeróbce surowców mineralnych*. (2006) Wydawnictwa AGH

Michalczyk, J., (2012) *Inaccuracy in self-synchronisation of vibrators of two-drive vibratory machines caused by insufficient stiffness of vibrators mounting*. Archives of Metallurgy and Materials 57, 3

Mi Han, S., Benaroya, H.; (2002) *Nonlinear and stochastic dynamics of compliant offshore structures*. Springer - Science + Business Media, B.V.

Modrzewski, R, Wodzinski, P (2010) *Ruch Drgajacy rzeszota przesiewacza dwuczęstościowego*, Górnictwo i Inżynieria Zeszyt 4/1 2010

Ogata, Katsuhiko (2005) *System Dynamics* (4th ed.). University of Minnesota.

Rademacher, F.J.C. (1979) *Feeders and vibratory conveyors*. Bulk Solids Handling Research Associates (TUNRA) Limited

Rumyantsev, S., Shihov, A., Tarasov, D. *Optimization of start-up processes of vibration transport machines with three unbalanced vibration exciters*. ISBN: 978-1-61804-165-4

Yang, J.H., Sanjuánb, Miguel, A.F., Liua, H.G. *Vibrational subharmonic and superharmonic resonances*. Commun Nonlinear Sci Numer Simulat 30 (2016) 362–372

Zhao, C.Y, Chun Yu, WEN Bang Chun, ZHANG Xue Liang.(2009) *Synchronisation of the four identical unbalanced rotors in a vibrating system of plane motion*. Science China, Technological Sciences, Vol.53 No 2, 405-422

Appendixes

Appendix A

A.1 Script to run data acquisition using National Instrument NI 9234

```
%Script to run data acquisition using National Instrument NI 9234

 s = daq.createSession('ni');
 s.DurationInSeconds = 1 ;
 Dur = s.DurationInSeconds;
 s.Rate = 256; % sample rate Hz
 s.addAnalogInputChannel('cDAQ1Mod1', 'ai0', 'Accelerometer');
 s.addAnalogInputChannel('cDAQ1Mod1', 'ai1', 'Accelerometer');
 s.addAnalogInputChannel('cDAQ1Mod1', 'ai2', 'Accelerometer');
 s.addAnalogInputChannel('cDAQ1Mod1', 'ai3', 'Accelerometer');
 s.addAnalogInputChannel('cDAQ1Mod2', 'ai0', 'Accelerometer');
 s.addAnalogInputChannel('cDAQ1Mod2', 'ai1', 'Accelerometer');
 dt = 1/s.Rate;
 % Setting Accelerometer Sensitivities
 s.Channels(1).Sensitivity = 0.9998E-3;
 s.Channels(2).Sensitivity = 9.772E-3;
 s.Channels(3).Sensitivity = 10.78E-3;
 s.Channels(4).Sensitivity = 10.01E-3;
 s.Channels(5).Sensitivity = 10.15E-3;
 s.Channels(6).Sensitivity = 9.63E-3;
% Start Acquisition
 data = s.startForeground();
 data_ch1 = data(:,1);
 data_ch2 = data(:,2);
 data_ch3 = data(:,3);
 data_ch4 = data(:,4);
 data_ch5 = data(:,5);
 data_ch6 = data(:,6);
 N = length(data_ch1);
 t = 0:dt:(N-1)*dt;
 m_amp = 1.2*max(max(data));
 % Acceleration Time Plots
 %Left end
 figure(1)
 subplot(2,1,1)
 plot(t,data_ch1,'r-');
 xlabel('Time (sec)');
 ylabel('Acceleration (m/s^2)');
 axis([0 Dur -m_amp m_amp]);
 subplot(2,1,2)
 plot(t,data_ch2,'r-');
 xlabel('Time (sec)');
 ylabel('Acceleration (m/s^2)');
 title('Acceleration data: Left End');
 axis([0 Dur -m_amp m_amp]);

 % Middle
 figure(2)
 subplot(2,1,1)
 plot(t,data_ch3,'b-');
 xlabel('Time (sec)');
 ylabel('Acceleration (m/s^2)');
 axis([0 Dur -m_amp m_amp]);
```

```
subplot(2,1,2)
plot(t,data_ch4,'b-');
xlabel('Time (sec)');
ylabel('Acceleration (m/s^2)');
title('Acceleration data: Middle');
axis([0 Dur -m_amp m_amp]);
% Right End
figure(3)
subplot(2,1,1)
plot(t,data_ch5,'g-');
xlabel('Time (sec)');
ylabel('Acceleration (m/s^2)');
axis([0 Dur -m_amp m_amp]);

subplot(2,1,2)
plot(t,data_ch6,'g-');
xlabel('Time (sec)');
ylabel('Acceleration (m/s^2)');
title('Acceleration data: Right End');
axis([0 Dur -m_amp m_amp]);

% Orbit Plots
figure(4)
plot(data_ch2,data_ch1,'r-');
xlabel('Acceleration (m/s^2)');
ylabel('Acceleration (m/s^2)');
title('Orbit Plot: Left End');
axis([-m_amp m_amp -m_amp m_amp]); axis 'square';
figure(5)
plot(data_ch4,data_ch3,'b-');
xlabel('Acceleration (m/s^2)');
ylabel('Acceleration (m/s^2)');
title('Orbit Plot: Middle End');
axis([-m_amp m_amp -m_amp m_amp]); axis 'square';
figure(6)
plot(data_ch6,data_ch5,'g-');
xlabel('Acceleration (m/s^2)');
ylabel('Acceleration (m/s^2)');
title('Orbit Plot: Right End');
axis([-m_amp m_amp -m_amp m_amp]); axis 'square';
```